

Copyright is owned by the Author of the thesis. Permission is given for a copy to be downloaded by an individual for the purpose of research and private study only. The thesis may not be reproduced elsewhere without the permission of the Author.

# Modular Functionalization of Engineered Polyhydroxyalkanoate Scaffolds

A Thesis Presented in Partial Fulfilment of the Requirements for Degree

Doctor of Philosophy

In

Microbiology at

Massey University, New Zealand

Jin Xiang, Wong

2019

## Abstract

Microbial polyhydroxyalkanoates (PHAs) are spherical polyesters that are naturally synthesized *in vivo* by a variety of microorganisms as carbon and energy reserves under imbalanced nutrition environments. Notably, PHA particles can be functionalized by the genetic modification of surface-exposed PHA-associated proteins, *e.g.* PHA synthase (PhaC), and this approach has led to multiple successful proof-of-concept demonstrations for biotechnology applications. However, current recombinant methods to functionalize PHAs require a certain biological complexity, such as simultaneous polyester and protein synthesis within a single cell. The less defined nature of this technology means limited control over particle morphology and surface functionalization. Seeking to overcome these limitations, the work presented in this thesis is to introduce the concept of modularity to the PHA particle technology, by merging the PHA particle technology with Tag/Catcher protein ligation systems. The Catcher domain can rapidly form a covalent bond with its pairing short peptide tag in a site-specific manner, without the need of additional reagents nor enzymes at broad ligation conditions. The SpyTag/SpyCatcher pair was merged recombinantly with PHA particle technology, where the resulting SpyCatcher-coated PHA particles were able to immobilize various SpyTagged proteins *in vitro* in a tunable manner and remained functional. This thesis further demonstrates several functionalization processes to streamline this modular strategy by assessing the possibility of whether non-purified SpyTagged proteins could ligate with the PHA particles in complex environments. The results demonstrated that SpyCatcher-coated PHA particles could be functionalized adequately using two

of the proposed methods. To further expand the design space of this generic modular platform towards programmable multi-functionalization, various bimodular PHA particles utilizing alternative Tag/Catcher pairs (*e.g.* SdyTag/SdyCatcher and SnoopTag/SnoopCatcher pairs) were designed and studied. One of the constructs resulted in the simultaneous multi-functionalization of plain PHA particles in one-step with two differently tagged proteins in *in vivo* and *ex vivo* reaction conditions. This work presents the modular design of PHA scaffolds and several streamlined manufacturing processes to the production of task-specific designer PHAs. Introducing the concept of modularity to the PHA particle technology enabled better control of particle uniformity, reproducibility, and immobilized protein density while remaining functional. These concepts should be broadly applicable to the design and manufacture of advanced functional materials for industrial applications.

## **Acknowledgements**

First of all, I would like to express my gratitude to all my Ph. D. supervisors, Professor Bernd Rehm, Professor Dave Harding, and Associate Professor Andrew Sutherland-Smith for their guidance and continuous encouragement throughout my studies.

Many thanks to all the current and former members of the Rehm Lab at Massey University, particularly Dr. Shuxiong Chen, Dr. Jinping Du, Kampachiro Ogura, and Dr. Majela González Miró, Dr. Wankuson Chanasit for being very helpful. It has been a pleasure to work with them.

Special thanks to Dr. Natisha Magan, Dr. Zoe Jordens, and technicians in the School of Fundamental Sciences, Massey University, for actively engaging with me in dealing with laboratory management.

I am also thankful to Trevor Loo from the Massey University Mass Spectrometry laboratory for his help with mass spectrometry, the Manawatū Microscopy Imaging Centre (MMIC) for their microscopy services, and the Massey Genome Service for DNA sequencing.

Lastly, but not least, I would like to thank my wife, Chen Zhao, and my family for their unconditional love, support, and understanding throughout my studies.

## **Preface**

This thesis is written in accordance with the guidelines on “PhD thesis with Publications” published by the Graduate Research School, Massey University (December 2015). The publication status of each chapter is listed below.

### **Chapter 1**

#### **Introduction**

This chapter of this thesis was prepared by Jin Xiang Wong and is not for publication purposes.

### **Chapter 2**

#### **Bioengineered Polyhydroxyalkanoates as Immobilized Enzyme Scaffolds for Industrial Applications**

Published: **Wong, J. X.**, Ogura, K., Chen, S. and Rehm, B. H. A. (2020). Bioengineered Polyhydroxyalkanoates as Immobilized Enzyme Scaffolds for Industrial Applications. *Frontiers in Bioengineering and Biotechnology*, 8:156.

Contributions: Ogura, K. wrote section “Enzyme Immobilization for Industrial Applications” of the manuscript, Chen, S. wrote section “Utilization of Various Supramolecular

Assemblies as Enzyme Immobilization Supports” of the manuscript, and **Wong, J. X.** wrote Sections “Utilization of Various Supramolecular Assemblies as Enzyme Immobilization Supports”, “Biological Supramolecular Assemblies as Biocatalyst Supports” and “Comparative Analysis of *In Vivo* Immobilization Strategies” of the manuscript. Rehm, B. H. A. provided critical input in regard to structure, content, and language of the manuscript. All authors provided critical feedback and approved the final version of the manuscript.

### **Chapter 3**

#### **Design of Modular Polyhydroxyalkanoate Scaffolds for Protein Immobilization by Directed Ligation**

Published: **Wong, J. X.** and Rehm, B. H. A. (2018). Design of Modular Polyhydroxyalkanoate Scaffolds for Protein Immobilization by Directed Ligation. *Biomacromolecules*, 19 (10), 4098-4112.

Contributions: **Wong, J. X.** and Rehm, B. H. A. conceived the main conceptual ideas of this study. **Wong, J. X.** designed the study and performed all the experiments. **Wong, J. X.** prepared the manuscript in consultation with Rehm, B. H. A. All authors provided critical feedback and approved to the final version of the manuscript.

## **Chapter 4**

### **Covalent Functionalization of Bioengineered Polyhydroxyalkanoate Particles directed by Specific Protein-Protein Interactions**

Published: **Wong, J. X.**, Gonzalez-Miro, M., Sutherland-Smith, A. J., and Rehm, B. H. A. (2020). Covalent Functionalization of Bioengineered Polyhydroxyalkanoate Particles Directed by Specific Protein-Protein Interactions. *Frontiers in Bioengineering and Biotechnology*, 8:44.

Contributions: **Wong, J. X.** and Rehm, B. H. A. conceived the main conceptual ideas of this study. **Wong, J. X.** and Rehm, B. H. A. designed the study and **Wong, J. X.** performed all the experiments except part of the DNA cloning work. Gonzalez-Miro, M. performed part of the cloning work. Rehm, B. H. A. and Sutherland-Smith, A. J. provided technical feedback. **Wong, J. X.** took the lead in writing the paper in consultation with Rehm, B. H. A., Sutherland-Smith, A. J., and Gonzalez-Miro, M. All authors have given approval to the final version of the manuscript.

## **Chapter 5**

### **General Discussion and Future Works**

This chapter of this thesis was prepared by Jin Xiang Wong and is not for publication purposes.

## Table of Contents

Abstract.....	ii
Acknowledgements .....	iv
Preface .....	v
List of Tables .....	xiv
List of Figures .....	xvi
List of Abbreviations .....	xxii
Chapter 1. General Introduction .....	1
1.1 Introduction to Polyhydroxyalkanoate Particle Technology .....	1
1.2 Thesis Aims .....	5
1.3 Thesis Findings.....	6
1.4 References .....	7
Chapter 2. Bioengineered Polyhydroxyalkanoates as Immobilized Enzyme Scaffolds for Industrial Applications .....	12
2.1 Abstract.....	13
2.2 Enzyme Immobilization for Industrial Applications .....	14
2.3 Utilization of Various Supramolecular Assemblies as Enzyme Immobilization Supports .....	19
2.3.1 Polyhydroxyalkanoates (PHAs) .....	19
2.3.2 Virus-Like Particles (VLPs) .....	22

2.3.3 Enzyme-Derived Nanoparticles (EZPs) .....	23
2.3.4 Extracellular Membrane Vesicles (EMVs) .....	24
2.3.5 Magnetosomes .....	25
2.4 Biological Supramolecular Assemblies as Biocatalyst Supports .....	26
2.5 Comparative Analysis of <i>In Vivo</i> Immobilization Strategies .....	53
2.5.1 Advantages and Current Limitations of the Recombinant PHA Particle Technology .....	53
2.5.2 Use of Enzyme-coated PHA Particles in Continuous-Flow Bioprocessing .....	58
2.5.3 Potential Industrial Applications of the PHA Particle Technology ..	59
2.6 Conclusions and Future Perspectives .....	61
2.7 References .....	64
Preface to Chapter 3 .....	86
Chapter 3. Design of Modular Polyhydroxyalkanoate Scaffolds for Protein Immobilization by Directed Ligation.....	87
3.1 Abstract.....	88
3.2 Introduction .....	88
3.3 Experimental Section.....	92
3.3.1 Bacterial Strains, Genetic Manipulation, and Growth Conditions ...	92
3.3.2 Polyhydroxyalkanoate (PHA) Particle Production and Isolation .....	93
3.3.3 Production and Purification of Soluble Protein .....	94
3.3.4 Protein Analysis.....	95
3.3.5 Protein Quantification .....	95

3.3.6 Proteomic analysis .....	96
3.3.7 Immobilization of SpyTagged Proteins onto SpyCatcher-PHA Particles .....	96
3.3.8 Optimization of SpyTag/SpyCatcher Chemistry .....	97
3.3.9 Assembly of the Immobilized Multiprotein Complex using SpyCatcher-PHA Particles.....	97
3.3.10 Compositional Analysis of PHA Particles .....	98
3.3.11 Zeta Potential Measurement .....	98
3.3.12 PHA Particle Size Distribution Measurement .....	99
3.3.13 Fluorescence Screening, Microscopy Analysis, and Fluorescence Intensity Measurement .....	99
3.3.14 Starch Degradation Screen and Colorimetric Assay for $\alpha$ -Amylase .....	100
3.3.15 Organophosphohydrolase Functionality Assay .....	100
3.3.16 Thermal Stability .....	101
3.3.17 pH Stability.....	101
3.3.18 Recycling .....	102
3.4 Results and Discussion .....	102
3.4.1 Design and Production of SpyCatcher-Displaying PHA Particles. ....	102
3.4.2 Immobilization of SpyTagged Proteins to SpyCatcher-PHA Particles: Confirmation and Optimization of Ligation Reactions towards Single and Multiprotein Display.....	104
3.4.3 Enzyme Immobilization Using SpyCatcher-PHA Particles .....	116

3.4.4 Thermal Stability .....	120
3.4.5 pH Stability .....	124
3.4.6 Recycling .....	127
3.5 Conclusions .....	129
3.6 References .....	131
3.7 Supporting Information .....	145
Preface to Chapter 4 .....	184
Chapter 4. Covalent Functionalization of Bioengineered Polyhydroxyalkanoate Particles directed by Specific Protein-Protein Interactions .....	185
4.1 Abstract .....	186
4.2 Introduction .....	187
4.3 Materials and Methods .....	191
4.3.1 Bacterial Strains, Genetic Manipulation, and Culture Conditions .	191
4.3.2 Polyhydroxyalkanoate (PHA) Particle and Soluble Protein Produc- tion .....	192
4.3.3 Protein Analysis .....	193
4.3.4 Protein Quantification .....	193
4.3.5 Proteomic analysis .....	194
4.3.6 Isolation of Plain Catcher-coated PHA Particles and <i>In Vivo</i> Func- tionalized of Catcher-coated PHA Particles (Process 1) .....	194
4.3.7 Isolation and <i>Ex Vivo</i> Functionalization of Catcher-coated PHA Par- ticles (Process 2) .....	195

4.3.8 Isolation and <i>Ex Vivo</i> Functionalization of Catcher-coated PHA Particles (Process 3).....	195
4.3.9 Isolation and Purification of Tagged Soluble Protein .....	196
4.3.10 <i>In Vitro</i> Functionalization of Various Catcher-coated PHA Particles .....	197
4.3.11 Compositional Analysis of PHA Particles .....	197
4.3.12 Scanning Electron Microscopy (SEM) and Transmission Electron Microscopy (TEM) Analysis .....	198
4.3.13 Particle Size Distribution (PSD) Measurement .....	198
4.3.14 Fluorescence Microscopy Analysis .....	198
4.3.15 Qualitative Starch Degradation Screen .....	199
4.3.16 Organophosphohydrolase Functionality Assay .....	199
4.3.17 Heat–Cooling Cycle Stability.....	200
4.3.18 Freeze–Thaw Cycle Stability .....	200
4.4 Results .....	201
4.4.1 Production and Characterization of SpyCatcher-coated PHA Particles .....	201
4.4.2 Surface Functionalization of SpyCatcher-coated PHA Particles using Processes 1–3 .....	204
4.4.3 Enzymatic Performance of Functionalized SpyCatcher-coated PHA Particles using the Proposed Processes .....	211
4.4.4 Design and Production of Bimodular PHA Particles .....	214

4.4.5 Screening of Bimodular PHA Particles Suitable for Efficient Simul- taneous Dual-Functionalization .....	217
4.4.6 Structural Characterization of Selected Bimodular PHA Particles	220
4.4.7 Robustness of Functionalized Bimodular PHA Particles .....	222
4.4.8 Functional Performance of Functionalized Bimodular PHA Particles .....	224
4.5 Discussion.....	226
4.6 References .....	233
4.7 Supporting Information .....	243
Chapter 5. General Discussion and Future Works .....	311
Appendix .....	322

## List of Tables

### Chapter 2

Table 1. Biological supramolecular assemblies engineered for <i>in vivo</i> immobilization of industrially relevant enzymes. ....	26
Table 2. Comparison of PHA particle technology with other biological supramolecular assemblies.....	54

### Chapter 3

Table S1. Bacterial strains used in the current study.....	145
Table S2. Plasmids constructed and used in the current study.....	145
Table S3. Primers constructed and used in the current study.....	148
Table S4. LC–MS/MS analysis of fusion proteins.....	159
Table S5. Particle size distribution statistics of various PHA particles used in this study. .....	173

### Chapter 4

Table S1. Bacterial strains used in the current study.....	243
Table S2. Plasmids constructed and used in the current study.....	243
Table S3. Primers constructed and used in the current study.....	247
Table S4. Amino acid sequence of fusion proteins .....	251

Table S5. Protein identification by liquid chromatography-tandem mass spectrometry (LC-MS/MS). .....	273
---	-----

## List of Figures

### Chapter 2

Figure 1. Enzyme immobilization <i>via</i> various biological supramolecular assemblies.....	18
Figure 2. Composition, structure, and assembly of PHA particles .....	21
Figure 3. Innovative strategies to overcome the limitations of PHA particle technology.	57

### Chapter 3

Figure 1. Design, production, and modular functionalization of SpyCatcher-PhaC PHA particles.....	107
Figure 2. Physicochemical characterization of SpyCatcher-PhaC PHA particles.....	112
Figure 3. Fluorescence of SpGFP immobilized to SpyCatcher-PhaC PHA particles .....	115
Figure 4. OpdA and BLA enzymatic functionality assays. ....	118
Figure 5. Stability and recycling of SpyTagged proteins immobilized to SpyCatcher-PhaC PHA particles .....	123
Figure S1. Densitometric protein quantification of SP fusion protein on PHA particles using BSA standard.....	162
Figure S2. Densitometric protein quantification of SpGFP-H6 using BSA standard .....	163
Figure S3. Densitometric protein quantification of SpOpdA-H6 using BSA standard...	164
Figure S4. Densitometric protein quantification of SpBLA-H6 using BSA standard ....	165

Figure S5. Optimization of ligation reactant ratio of SP-P over soluble SpGFP-H6 at total reactant concentration of 10 $\mu$ M at 4°C in 50 mM Tris-HCl for 24 hours.....	166
Figure S6. Optimization of ligation reactant ratio of SP-P over soluble SpOpdA-H6 at total reactant concentration of 10 $\mu$ M at 4°C in 50 mM Tris-HCl for 24 hours.....	167
Figure S7. Optimization of ligation reactant ratio of SP-P over soluble SpBLA-H6 at total reactant concentration of 10 $\mu$ M at 4°C in 50 mM Tris-HCl for 24 hours.....	168
Figure S8. Optimization of ligation time of SP-P with SpGFP-H6 at reactant ratio of 2:1 (SpyCatcher:SpyTag) at 4°C in 50 mM Tris-HCl.....	169
Figure S9. Optimization of ligation time of SP-P with SpOpdA-H6 at reactant ratio of 2:1 (SpyCatcher:SpyTag) at 4°C in 50 mM Tris-HCl.....	170
Figure S10. Optimization of ligation time of SP-P with SpBLA-H6 at reactant ratio of 2:1 (SpyCatcher:SpyTag) at 4°C in 50 mM Tris-HCl.....	171
Figure S11. Step-wise fabrication of multifunctional SpyCatcher-PhaC PHA particles (MF-SP-P). .....	172
Figure S12. Validation of the reproducibility of modular functionalization of SpyCatcher-PhaC PHA particles ( $n=9$ ).....	175
Figure S13. Densitometric protein quantification of SpGFP-SP-L on PHA particles using BSA standard.....	176
Figure S14. Densitometric protein quantification of immobilized multi-proteins (MF-SP-L) on PHA particles using BSA standard.....	177
Figure S15. Densitometric protein quantification of SpOpdA-SP-L on PHA particles using BSA standard.....	178

Figure S16. Densitometric protein quantification of SpBLA-SP-L on PHA particles using BSA standard.....	179
Figure S17. Fluorescence can be detected on SpGFP-SP-P.....	180
Figure S18. Fluorescence intensity of the SpGFP-SP-P at varying ligation time. ....	180
Figure S19. Starch degradation screen .....	182
Figure S20. Recycling of soluble free SpyTagged proteins as positive control.....	183

## Chapter 4

Figure 1. Schematic of modular functionalization of PHA particles .....	190
Figure 2. Production and characterization of SpyCatcher-coated PHA particles.....	203
Figure 3. Modular functionalization of SpyCatcher-coated PHA particles with various SpyTagged proteins implementing processes 1–3 using different plain SpyCatcher-coated PHA particles as negative controls.....	207
Figure 4. Particle size distribution of various functionalized SpyCatcher-coated PHA particles produced using processes 1–3 by DLS analysis (mean, n = 3).....	211
Figure 5. Enzymatic assay of SpBLA and SpOpdA functionalized SpyCatcher-coated PHA particles.....	212
Figure 6. Production and functionalization of various Catcher domain-coated PHA particles <i>in vitro</i> .....	215
Figure 7. Structural characterization of various NPP-Ps.....	221
Figure 8. Exposure of plain NPP-P to extreme conditions prior functionalization as visualized by SDS–PAGE analysis and screening of samples under blue light. ....	223

Figure 9. Fluorescence microscopy analysis of SpGFP-H6 and SnGFP-H6 functionalized NPP-Ps with appropriate positive and negative controls .....	225
Figure 10. Qualitative starch degradation assay hydrolyzed by SpBLA-H6 and SnBLA-H6 functionalized NPP-Ps with appropriate positive and negative controls.....	226
Figure S1. Flowchart of <i>in vivo</i> functionalization of SpyCatcher-coated PHA particles using process 1 .....	290
Figure S2. Flowchart of <i>ex vivo</i> functionalization of SpyCatcher-coated PHA particles using process 2 .....	291
Figure S3. Flowchart of <i>ex vivo</i> functionalization of SpyCatcher-coated PHA particles using process 3 .....	292
Figure S4. Three possible ligated products from functionalized SPS fusion protein-displaying PHA particles (SPS-P) (orange/brown) using SpyTagged proteins .....	293
Figure S5. Poly( <i>R</i> )-3-hydroxybutyric acid (PHB) standard curve obtained from GC–MS. ....	293
Figure S6. Whole cell lysate (WCL) of <i>E. coli</i> BL21(DE3) containing modular <i>in vivo</i> functionalized SpyCatcher-coated PHA particles (Process 1) .....	294
Figure S7. Chlorferon standard curve obtained from fluorescence spectroscopy for the OpdA activity assay.....	295
Figure S8. Densitometric protein quantification of wild-type PhaC (WT) on PHA particles relative to BSA standards .....	295
Figure S9. Densitometric protein quantification of SpyCatcher-PhaC (SP) fusion protein on PHA particles relative to BSA standards.....	296

Figure S10. Densitometric protein quantification of SpyCatcher-PhaC-SpyCatcher (SPS) fusion protein on PHA particles relative to BSA standards .....	297
Figure S11. Densitometric protein quantification of PhaC-OpdA fusion protein on PHA particles relative to BSA standards.....	298
Figure S12. Densitometric protein quantification of SpOpdA-SP ligated protein (SpOpdA-SP-L) on PHA particles relative to BSA standards (Process 1) .....	299
Figure S13. Densitometric protein quantification of SpOpdA-SPS ligated protein (SpOpdA-SPS-L) on PHA particles relative to BSA standards (Process 1). ....	300
Figure S14. Densitometric protein quantification of SpOpdA-SP ligated protein (SpOpdA-SP-L) on PHA particles relative to BSA standards (Process 2) .....	301
Figure S15. Densitometric protein quantification of SpOpdA-SPS ligated protein (SpOpdA-SPS-L) on PHA particles relative to BSA standards (Process 2). ....	302
Figure S16. Densitometric protein quantification of N-terminally SpyTagged and C-terminally hexahistidine-tagged soluble OpdA (SpOpdA-H6) .....	303
Figure S17. Densitometric protein quantification of various combinations of Catcher domains fused PhaC fusion proteins relative to BSA standards. ....	304
Figure S18. Densitometric protein quantification of various tagged GFP fusion proteins relative to BSA standards .....	305
Figure S19. Densitometric protein quantification of different tagged BLA fusion proteins relative to BSA standards .....	306
Figure S20. Modular functionalization of DPN fusion protein displaying PHA particles (DPN-P) <i>in vitro</i> using various tagged GFPs .....	307

Figure S21. Modular functionalization of NPD fusion protein displaying PHA particles (NPD-P) <i>in vitro</i> using various tagged GFPs. ....	308
Figure S22. Modular functionalization of PPN fusion protein displaying PHA particles (PPN-P) <i>in vitro</i> using various tagged GFPs .....	309
Figure S23. NPP fusion protein displaying PHA particles (NPP-P) could react with tagged proteins individually and simultaneously in complex environments <i>ex vivo</i> (Pro- cess 2) .....	310

## List of Abbreviations

Ap<sup>r</sup> Ampicillin resistance  
Asp Aspartic acid  
BSA Bovine serum albumin  
BLA *Bacillus licheniformis*  $\alpha$ -amylase  
BLA-PhaC-P BLA-PhaC fusion protein displayed on PHA particles  
CoA Coenzyme A  
Cm<sup>r</sup> Chloramphenicol resistance  
CP Capsid protein  
D [3,2] Surface area moment mean/Sauter mean diameter  
D [4,3] Volume moment mean/De Brouckere mean diameter  
DETP Dietlythiophosphate  
DLS Dynamic light scattering  
DNA Deoxyribonucleic acid  
DPN SdyCatcher- PhaC-SnoopCatcher fusion protein  
DPN-P DPN fusion protein displaying PHA particles  
Dx (10) Particle size corresponding to 10% cumulative size distribution  
Dx (50) Particle size corresponding to 50% cumulative size distribution  
Dx (90) Particle size corresponding to 90% cumulative size distribution  
ELS Electrophoretic light scattering  
EMV Extracellular membrane vesicle  
EZP Enzyme-derived nanoparticle  
fg Femtogram  
g Gravitational force equivalent  
GC-MS Gas chromatography-mass spectroscopy  
GFP *Aequorea victoria* green fluorescent protein  
h Hour  
HCl Hydrochloric acid  
He-Ne Helium-Neon  
IPTG Isopropyl  $\beta$ -D-1-thiogalactopyranoside  
kDa Kilo Dalton  
Km<sup>r</sup> Kanamycin resistance  
LB Luria-Bertani  
LB-Lennox Luria-Bertani, Lennox  
LC-MS/MS liquid chromatography-tandem mass spectrometry  
Lys Lysine

$\text{m}^2/\text{kg}$  Specific surface  
 MF-SP-P Multifunctional SP-P  
 $\text{m}^2/\text{kg}$  Square meter per kilogram  
 min Minute  
 mL Milliliter  
 mL/min Milliliter per minute (Flowrate)  
 mM Millimolar  
 mV Millivolt  
 $n$  Number of replicates  
 NaCl Sodium chloride  
 ng Nanogram  
 Ni-NTA Nickel-nitrilotriacetic acid  
 nm Nanometer  
 NPD SnoopCatcher-PhaC-SdyCatcher fusion protein  
 NPD-P NPD fusion protein-displaying PHA particles  
 NPP SnoopCatcher-PhaC-SpyCatcher fusion protein  
 NPP-SpGFP-L NPP-SpGFP ligated protein  
 NPP-SpGFP-P NPP-SpGFP-L-displaying PHA particles  
 NPP-SpBLA-L NPP-SpBLA ligated protein  
 NPP-SpBLA-P NPP-SpBLA-L-displaying PHA particles  
 NPP-P NPP fusion protein displaying PHA particles  
 $\text{OD}_{600}$  Optical density at a wavelength of 600 nm  
 OpdA *Agrobacterium radiobacter* organophosphohydrolase  
 PALS Phase analysis light scattering  
 pH Potential of hydrogen  
 PAPs Polyhydroxyalkanoate-associated proteins  
 PHA Polyhydroxyalkanoate  
 PhaC-GFP-P PhaC-GFP fusion protein displaying PHA particles  
 PhaC PHA synthase  
 PhaC-OpdA-P PhaC-OpdA fusion protein displayed on PHA particles  
 PHB Poly-(*R*)-3-hydroxybutyrate  
 pI Isoelectric point  
 $\text{pm}^2$  Square picometer  
 ppm parts per million  
 PPN SpyCatcher-PhaC-SnoopCatcher fusion protein  
 PPN-P PPN fusion protein displaying PHA particles  
 PPN-SnGFP-P PPN-SnGFP ligated protein displaying PHA particles  
 PS PhaC- SpyCatcher fusion proteins  
 PS-P PS fusion proteins displayed on PHA particles  
 $R^2$  Coefficient of determination

RNA Ribonucleic acid  
 rpm Revolutions per minute  
 s Second  
 ScP Scaffold protein  
 SD Standard Deviation  
 SDS–PAGE sodium dodecyl sulfate–polyacrylamide gel electrophoresis  
 SEM Scanning electron microscopy  
 SP SpyCatcher-PhaC fusion protein  
 SP-P SP fusion protein displayed on PHA particles  
 SdBLA-H6 SdyTagged BLA bearing His<sub>6</sub> tag  
 SnBLA-H6 SnoopTagged BLA bearing His<sub>6</sub> tag  
 SnBLA-NPP-L SnBLA-NPP ligated protein  
 SnBLA-NPP-P SnBLA-NPP-L-displaying PHA particles  
 SnBLA-NPP-SpBLA-L SnBLA-NPP-SnBLA ligated protein  
 SnBLA-NPP-SpBLA-P SnBLA-NPP-SnBLA-L-displaying PHA particles  
 SnBLA-NPP-SpGFP-L SnBLA-NPP-SpGFP ligated protein  
 SnBLA-NPP-SpGFP-P SnBLA-NPP-SpGFP-L-displaying PHA particles  
 SpBLA SpyTagged BLA  
 SpBLA-H6 SpyTagged BLA bearing His<sub>6</sub> tag  
 SpBLA-SP-L SpBLA-SP-ligated protein  
 SpBLA-SP-P SpBLA-immobilized SP-P  
 SdGFP-H6 SdyTagged GFP bearing His<sub>6</sub> tag  
 SdGFP-DPN-L SdGFP-DPN ligated proteins  
 SdGFP-DPN-P SdGFP-DPN-L-displaying PHA particles  
 SdGFP-PPN-P SdGFP-PPN ligated protein displaying PHA particles  
 SnGFP-H6 SnoopTagged GFP bearing His<sub>6</sub> tag  
 SnGFP-NPD-L SnGFP-NPD ligated protein  
 SnGFP-NPD-P SnGFP-NPD-L-displaying PHA particles  
 SnGFP-NPP-L SnGFP-NPP ligated protein  
 SnGFP-NPP-P SnGFP-NPP-L-displaying PHA particles  
 SnGFP-NPP-SpBLA-L SnGFP-NPP-SpBLA ligated protein  
 SnGFP-NPP-SpBLA-P SnGFP-NPP-SpBLA-L displaying PHA particles  
 SnGFP-NPP-SpGFP-L SnGFP-NPP-SpGFP ligated protein  
 SnGFP-NPP-SpGFP-P SnGFP-NPP-SpGFP-L-displaying PHA particles  
 SpGFP SpyTagged GFP  
 SpGFP-H6 SpyTagged GFP bearing His<sub>6</sub> tag  
 SpGFP-PPN-L SpGFP-PPN ligated protein  
 SpGFP-PPN-P SpGFP-PPN-L displaying PHA particles  
 SpGFP-SP-L SpGFP-SP-ligated protein  
 SpGFP-SP-P SpGFP-immobilized SP-P

SpOpdA- SpyTagged OpdA  
 SpOpdA-H6 SpyTagged OpdA bearing His<sub>6</sub> tag  
 SpOpdA-SP-L SpOpdA-SP-ligated protein  
 SpOpdA-SP-P SpOpdA-immobilized SP-P  
 SPS SpyCatcher-PhaC-SpyCatcher fusion protein  
 SPS-P SPS fusion protein displayed on PHA particles  
 SpBLA-SPS-L SpBLA-SPS-ligated protein  
 SpBLA-SPS-P SpBLA-immobilized SPS-P  
 SpGFP-SPS-L SpGFP-SPS-ligated protein  
 SpGFP-SPS-P SpGFP-immobilized SPS-P  
 SpOpdA-SPS-L SpOpdA-SPS-ligated protein  
 SpOpdA-SPS-P SpOpdA-immobilized SPS-P  
 TEM Transmission electron microscopy  
 Tet<sup>r</sup> Tetracycline resistance  
 Tris-HCl Trisaminomethane hydrochloride  
 U/mg Specific activity  
 v/v Volume per volume  
 VLP Virus-like particle  
 w/v Weight per volume  
 WT Wild-type PhaC  
 WT-P Wild-type PHA particles  
 µm micrometer  
 µM micromolar  
 µm micrometer  
 °C Degree Celsius  
 λ Wavelength

# Chapter 1

## General Introduction

### 1.1 Introduction to Polyhydroxyalkanoate Particle Technology

Microbial polyhydroxyalkanoates (PHAs) are a class of linear polyesters manufactured inside bacterial cells in nature as storage compounds to deposit surplus carbon supplies under limiting oxygen, nitrogen, and phosphorus conditions (1). PHAs can be broadly classified into three major classes, namely short-chain length PHAs, medium-chain length PHAs, and long-chain length PHAs, which consist of 3–5, 6–14, and more than 14 carbon atoms respectively. To date, over 150 PHA monomers (*e.g.* (*R*)-3-hydroxy fatty acids) have been identified, ranging from PHA monomers with saturated, unsaturated, branched, and various functionalized side groups embedded polymer chains (2-4). The length and composition of these PHA monomers, as well as the combinations of their arrangement in the form of homopolymers or copolymers, can influence the parameters (*e.g.* glass transition temperature, degree of crystallinity, and melting point) that dictate the mechanical and elastomeric properties of the material (4-6).

These core-shell like spherical polyesters have an amorphous hydrophobic core covered by a protein coating, with diameter sizes in the range of 100–500 nm and molecular weights of 200–3000 kDa (4, 7). Typically, a single bacterial cell can synthesis and store

approximately 5–10 PHA particles in their cytosol contributing up to 90% of the dry cell weight (8, 9). More than 10 PHA biosynthesis pathways have been described that lead to the formation of a wide range of PHAs with different properties (10). Particularly, biosynthesis of PHAs mediated by *Cupriavidus necator* PhaC is one of the most established pathways to catalyze the polymerization of PHAs (11). The biosynthesis of PHAs via this pathway is largely influenced by the availability of three major enzymes, PHA synthase (PhaC),  $\beta$ -ketothiolase (PhaA), and acetoacetyl-CoA reductase (PhaB) (12-14). Briefly, active PhaC dimers polymerize (*R*)-3-hydroxyacyl-CoA thioesters, synthesized by PhaA and PhaB enzymes, to PHA chains (15, 16). PhaC dimers remain covalently attached to growing PHA chains and thus convert the hydrophobic PHA chains into amphipathic molecules, enabling self-assembly into PHA particles (6, 17).

Microbial PHAs have been considered as a promising next-generation scaffolding platform for protein immobilization. The surface of the PHA particles can be modified to append a diverse range of functional handles by synthesizing chemically reactive PHAs (*e.g.* using metabolic engineering and chemical means) and recombinant PHAs (*e.g.* by genetic engineering of PHA-associated proteins) (13). Sizable efforts have been devoted to the synthesis of chemically reactive PHAs, for instance, the addition of a variety of functional handles appended to the PHA polymer structures (18). Extensive work on incorporating various functional moieties onto the backbone of PHAs, including adding double bonds, hydroxylation, carboxylation, and various click chemistry enabled sidechains have been demonstrated to produce a range of chemically reactive PHAs (19-21). The attachment of these desired functional moieties onto the backbone of PHAs allows further covalent coupling

of biological macromolecules (*e.g.* proteins and DNA) to the PHAs. A range of surface-exposed functional groups present on the amino acid residues of proteins can be exploited to facilitate bioconjugation, *e.g.* carboxyl groups of aspartic acid and glutamic acid residues, amine groups of glutamine and lysine residues, and thiol groups of cysteine residues (22, 23).

Meanwhile, recombinant PHAs incorporated with desired functions can be achieved by the direct genetic manipulation of PHA-associated proteins that naturally coated on the PHA particles using recombinant DNA technology. PHA particles are coated by a diverse range of PHA-associated proteins comprising of PHA synthase (PhaC), PHA depolymerase (PhaZ), Phasins (PhaF and PhaP), and other regulatory and structural proteins (13). These PHA-associated proteins anchored on the PHA particles often take part in several critical roles in regulating the PHA particle production, structural integrity, and particle distribution *in vivo* (24, 25). Particularly, the PHA-binding properties of PhaC and phasins via covalent interactions and physisorption respectively to anchor on the surface of PHA particles have been of interest in recent years for protein immobilization and purification for industrial applications, which will be reviewed thoroughly and compared with other biological supramolecular assemblies in chapter 2.

The target proteins of interest can be recombinantly fused to these PHA-associated proteins to allow the functionalization of PHA particles *in vivo* in one-step (3). This method permits the one-step production of functionalized PHA particles without the need for purification

and extra conjugation steps to immobilize proteins. Moreover, the genetic engineering of PHA-associated proteins (PAPs) enables spatial arrangement and oriented protein immobilization (26). When comparing the chemically-synthesized PHAs to their recombinant counterparts, it becomes clear that the latter are able to avoid the laborious crosslinking reaction optimization and the harsh reaction conditions that could lead to potential disruption, or suboptimal performance of native protein function (27, 28). However, the biological complexity of the recombinant functionalization of PHA particles *in vivo* makes control over a few aspects of the technology difficult (3). Critical analysis of the recombinant PHA particle technology, such as the advantages and the limitations of the PHA particle technology, and the feasibility of this technology in the industrial environments will be reviewed in chapter 2.

Therefore, to address these issues, the concept of modularity is proposed to merge the recombinant PHA particle technology with Tag/Catcher protein ligation systems (29-31). In chapter 3 of this thesis, the utilization of SpyTag/SpyCatcher chemistry proved successful in rendering specificity *in vitro* when merged with the PHA particle technology. The modular approach offers more control, such as the orientation of the attached proteins and surface coverage when compared to the conventional method of functionalizing recombinant PHA particles. Then, to streamline the modular functionalization strategy, several innovative processes were designed to append functional proteins directly from complex mixtures to recombinant PHA particles without the need of laborious soluble protein purification, which will be covered in chapter 4. Chapter 4 also details the design of various bimodular

PHA scaffolds by making use of multiple combinations of alternative Tag/Catcher systems on the same PHA scaffold.

## 1.2 Thesis Aims

The overall aims of the work presented in this thesis are:

- To provide insights into the advances in utilizing the PHA particle technology as an enzyme immobilization platform and a critical perspective of this technology for industrial applications.
- To demonstrate the modular design and preparation of SpyCatcher-coated PHA particles and the modular assembly of various SpyTagged proteins onto the surface of SpyCatcher-coated PHA particles *in vitro*.
- To investigate the feasibility of several innovative streamlined approaches to add functional proteins from complex mixtures to bioengineered modular PHA particles avoiding target protein purification.
- To present the construction of bimodular PHA scaffolds harnessing the specificity of various combinations of alternative Tag/Catcher mediated protein ligation systems.

### 1.3 Thesis Findings

Chapter 2 of this thesis presents a literature review based on the recent progress in the *in vivo* production of self-assembled PHA particles and their use as scaffolds for immobilizing biocatalysts in comparison with other biological supramolecular assemblies used for *in vivo* enzyme immobilization. This chapter also critically analyzes several aspects of the practical implementation of PHA particle technology and refers to some examples of industrial applications that could use this technology. This chapter was accepted for publication in *Frontiers in Bioengineering and Biotechnology*.

Chapter 3 of this thesis demonstrates a modular approach toward the functionalization of PHA particles using the SpyTag/SpyCatcher protein ligation system. The results suggested that the current modular strategy offers more control, such as tunable surface coverage and orientation of immobilized proteins, as well as improved particle uniformity. In general, the immobilization of the SpyTagged proteins onto the SpyCatcher-coated PHA particles resulted in either retained or enhanced functionality and stability when compared to the soluble forms. This chapter was accepted for publication in *Biomacromolecules*.

Chapter 4 of this thesis further investigates some of the extensions of utilizing the modular design approach to functionalize PHA particles. The first part of this chapter expands the modular functionalization concept presented in Chapter 3 to *in vivo* and *ex vivo* complex ligation environments. Several streamlined processes were implemented to enable covalent surface functionalization of PHA particles while avoiding target protein purification.

Meanwhile, the second part of this chapter presents the design of a bimodular PHA scaffolding platform by harnessing the specificity of various combinations of alternative Tag/Catcher mediated protein ligation systems (*e.g.* SdyTag/SdyCatcher and SnoopTag/SnoopCatcher pairs), followed by the successful demonstration of simultaneous functionalization of the selected bimodular PHA scaffold. This chapter was accepted for publication in *Frontiers in Bioengineering and Biotechnology*.

#### **1.4 References**

1. Escapa IF, García JL, Bühler B, Blank LM, Prieto MA. The polyhydroxyalkanoate metabolism controls carbon and energy spillage in *Pseudomonas putida*. *Environ. Microbiol.* 2012;14(4):1049-63.
2. Keshavarz T, Roy I. Polyhydroxyalkanoates: bioplastics with a green agenda. *Curr. Opin. Microbiol.* 2010;13(3):321-6.
3. Gonzalez-Miro M, Chen S, Gonzaga ZJ, Evert B, Wibowo D, Rehm BHA. Polyester as antigen carrier toward particulate vaccines. *Biomacromolecules.* 2019;20(9):3213-32.
4. Zinn M, Witholt B, Egli T. Occurrence, synthesis and medical application of bacterial polyhydroxyalkanoate. *Adv. Drug. Delivery Rev.* 2001;53(1):5-21.

5. Rehm BH. Polyester synthases: natural catalysts for plastics. *Biochem. J.* 2003;376(1):15-33.
6. Rehm BH. Biogenesis of microbial polyhydroxyalkanoate granules: a platform technology for the production of tailor-made bioparticles. *Curr. Issues Mol. Biol.* 2007;9(1):41.
7. Bhatt R, Patel K, Trivedi U. *A Handbook of Applied Biopolymer Technology: Synthesis, Degradation and Applications: The Royal Society of Chemistry; 2011. p. 311-31.*
8. Koller M, Salerno A, Dias M, Reiterer A, Braunegg G. Modern biotechnological polymer synthesis: a review. *Food Technol. Biotechnol.* 2010;48(3):255-69.
9. Mathuriya AS, Yakhmi J. Polyhydroxyalkanoates: Biodegradable plastics and their applications. *Handbook of Ecomaterials.* 2017:1-29.
10. Meng D-C, Shen R, Yao H, Chen J-C, Wu Q, Chen G-Q. Engineering the diversity of polyesters. *Curr. Opin. Biotechnol.* 2014;29:24-33.
11. Sudesh K, Abe H, Doi Y. Synthesis, structure and properties of polyhydroxyalkanoates: biological polyesters. *Prog. Polym. Sci.* 2000;25(10):1503-55.

12. Draper JL, Rehm BH. Engineering bacteria to manufacture functionalized polyester beads. *Bioengineered*. 2012;3(4):203-8.
13. Parlane NA, Gupta SK, Rubio-Reyes P, Chen S, Gonzalez-Miro M, Wedlock DN, et al. Self-assembled protein-coated polyhydroxyalkanoate beads: properties and biomedical applications. *ACS Biomater. Sci. Eng.* 2016;3(12):3043-57.
14. Lee JW, Parlane NA, Wedlock DN, Rehm BH. Bioengineering a bacterial pathogen to assemble its own particulate vaccine capable of inducing cellular immunity. *Sci. Rep.* 2017;7:41607.
15. Peoples OP, Sinskey AJ. Poly-beta-hydroxybutyrate (PHB) biosynthesis in *Alcaligenes eutrophus* H16. Identification and characterization of the PHB polymerase gene (phbC). *J. Biol. Chem.* 1989;264(26):15298-303.
16. Peoples OP, Sinskey AJ. Poly-beta-hydroxybutyrate biosynthesis in *Alcaligenes eutrophus* H16. Characterization of the genes encoding beta-ketothiolase and acetoacetyl-CoA reductase. *J. Biol. Chem.* 1989;264(26):15293-7.
17. Taguchi S, Doi Y. Evolution of polyhydroxyalkanoate (PHA) production system by “enzyme evolution”: successful case studies of directed evolution. *Macromol. Biosci.* 2004;4(3):145-56.

18. Li Z, Yang J, Loh XJ. Polyhydroxyalkanoates: opening doors for a sustainable future. *NPG Asia Mater.* 2016;8(4):e265-e.
19. Nigmatullin R, Thomas P, Lukasiewicz B, Puthussery H, Roy I. Polyhydroxyalkanoates, a family of natural polymers, and their applications in drug delivery. *J. Chem. Technol. Biotechnol.* 2015;90(7):1209-21.
20. Hazer B, Steinbüchel A. Increased diversification of polyhydroxyalkanoates by modification reactions for industrial and medical applications. *Appl. Microbiol. Biotechnol.* 2007;74(1):1-12.
21. Kai D, Loh XJ. Polyhydroxyalkanoates: Chemical Modifications Toward Biomedical Applications. *ACS Sustain. Chem. Eng.* 2014;2(2):106-19.
22. Faccio G. From protein features to sensing surfaces. *Sensors.* 2018;18(4):1204.
23. Sletten EM, Bertozzi CR. Bioorthogonal chemistry: Fishing for Selectivity in a Sea of Functionality. *Angew. Chem., Int. Ed.* 2009;48(38):6974-98.
24. Mezzina MP, Pettinari MJ. Phasins, Multifaceted Polyhydroxyalkanoate Granule-Associated Proteins. *Appl. Environ. Microbiol.* 2016;82(17):5060-7.
25. Grage K, Jahns AC, Parlane N, Palanisamy R, Rasiah IA, Atwood JA, et al. Bacterial Polyhydroxyalkanoate Granules: Biogenesis, Structure, and Potential Use as Nano-

- /Micro-Beads in Biotechnological and Biomedical Applications. *Biomacromolecules* 2009;10(4):660-9.
26. Hooks DO, Venning-Slater M, Du J, Rehm B. Polyhydroxyalkanoate synthase fusions as a strategy for oriented enzyme immobilisation. *Molecules* 2014;19(6):8629-43.
  27. Hess GT, Cragolini JJ, Popp MW, Allen MA, Dougan SK, Spooner E, et al. M13 bacteriophage display framework that allows sortase-mediated modification of surface-accessible phage proteins. *Bioconjugate Chem.* 2012;23(7):1478-87.
  28. Brune KD, Leneghan DB, Brian IJ, Ishizuka AS, Bachmann MF, Draper SJ, et al. Plug-and-Display: decoration of virus-like particles via isopeptide bonds for modular immunization. *Sci. Rep.* 2016;6:19234.
  29. Zakeri B, Fierer JO, Celik E, Chittock EC, Schwarz-Linek U, Moy VT, et al. Peptide tag forming a rapid covalent bond to a protein, through engineering a bacterial adhesin. *Proc. Natl. Acad. Sci. USA.* 2012;109(12):E690-E7.
  30. Tan LL, Hoon SS, Wong FT. Kinetic controlled Tag-Catcher interactions for directed covalent protein assembly. *PloS One* 2016;11(10):e0165074.
  31. Veggiani G, Nakamura T, Brenner MD, Gayet RV, Yan J, Robinson CV, et al. Programmable polyproteins built using twin peptide superglues. *Proc. Natl. Acad. Sci. USA.* 2016;113(5):1202-7.

## Chapter 2

### Bioengineered Polyhydroxyalkanoates as Immobilized Enzyme Scaffolds for Industrial Applications

Jin Xiang Wong<sup>1,2</sup>, Kampachiro Ogura<sup>1</sup>, Shuxiong Chen<sup>3</sup> and Bernd H. A. Rehm<sup>3\*</sup>

<sup>1</sup> School of Fundamental Sciences, Massey University, Private Bag, 11222 Palmerston North, New Zealand.

<sup>2</sup> MacDiarmid Institute of Advanced Materials and Nanotechnology, Victoria University of Wellington, Wellington 6140, New Zealand.

<sup>3</sup> Centre for Cell Factories and Biopolymers, Griffith Institute for Drug Discovery, Griffith University, Don Young Road, Nathan, 4111 Queensland, Australia.

**Publication status:** published in *Frontiers in Bioengineering and Biotechnology* (Wong, J. X., Ogura, K., Chen, S., and Rehm, B. H. A. (2020). Bioengineered Polyhydroxyalkanoates as Immobilized Enzyme Scaffolds for Industrial Applications. *Frontiers in Bioengineering and Biotechnology*, 8: 156.)

## 2.1 Abstract

Enzymes function as biocatalysts and are extensively exploited in industrial applications. Immobilization of enzymes using support materials has been shown to improve enzyme properties, including stability and functionality in extreme conditions and recyclability in biocatalytic processing. This review focuses on the recent advances utilizing the design space of *in vivo* self-assembled polyhydroxyalkanoate (PHA) particles as scaffolds to immobilize biocatalysts. Self-assembly of biologically active enzyme-coated PHA particles is a one-step *in vivo* production process, which avoids the costly and laborious *in vitro* chemical cross-linking of purified enzymes to separately produced support materials. The homogeneous orientation of enzymes densely coating PHA particles enhances the accessibility of catalytic sites, improving enzyme function. The PHA particle technology has been developed into a remarkable scaffolding platform for the design of cost-effective designer biocatalysts amenable toward robust industrial bioprocessing. In this review, PHA particle technology will be compared to other biological supramolecular assembly-based technologies suitable for *in vivo* enzyme immobilization. Recent progress in the fabrication of biological particulate scaffolds using enzymes of industrial interest will be summarized. Additionally, we outline innovative approaches to overcome limitations of *in vivo* assembled PHA particles to enable fine-tuned immobilization of multiple enzymes to enhance performance in multi-step cascade reactions, such as those used in continuous flow bioprocessing.

## **2.2. Enzyme Immobilization for Industrial Applications**

Enzymes are capable of accelerating chemical reactions with high substrate specificity, stereoselectivity, and energy-efficient conversion properties (1). These enzyme properties attract interest from the biotechnology sector and are considered as a substitute to chemical catalysts in various applications, such as biomass conversion, food processing, and the production of pharmaceuticals (2). Despite the excellent catalytic properties of enzymes, utilization of natural enzymes at industrial scales is often hampered by their general protein characteristics (3). For example, enzymes are prone to denaturation/unfolding when removed from their native environments. Specifically, enzymes are sensitive to changes in their environments and are unstable in extreme conditions, such as high temperatures, high pressures, extreme pH, detergents, and organic solvents (1). Furthermore, it is challenging to separate soluble enzymes and their respective products from the reaction mixture. Hence, enzymes are often rendered inactive and removed after a single use (1). From an economic point of view, the poor recycling and difficulty in the recovery of enzymes are drawbacks, which severely limit the use of enzymes in industrial processes.

To overcome the shortcomings mentioned above, various enzyme immobilization techniques, especially scaffolding-based approaches, have been developed in the past decades (4, 5). Immobilization of enzymes results in the confinement of enzymes to a particular space, such as either displayed on, or encapsulated within, solid support materials, creating a heterogeneous biocatalyst system while retaining enzyme specificity and activity (6). Interestingly, densely localizing enzymes on the scaffolding carriers can significantly

improve the catalytic performance and structural stability of enzymes in certain scenarios due to macromolecular crowding (7, 8). The nonspecific interactions between the immobilized enzymes and solid support materials could also further enhance the overall function and stability of immobilized enzymes (9-11). The crowding of globular proteins could also create an artificial environment improving the protein stability against chaotropic agents and temperature stress (12).

Immobilized enzyme-based catalytic systems facilitate separation of the enzyme from the reaction mixture. This strategy enables the repeated use of the immobilized enzymes and rapid termination of a catalytic reaction by physically removing the immobilized enzyme-bearing carriers from the reaction mixture (3, 13). This approach also prevents contamination of the product by the carried-over enzyme, thus reducing downstream process complexity and operational costs. Moreover, immobilized enzyme-based biocatalysts allow the implementation of flow-through formats in continuous bioprocessing approaches (14, 15). Nevertheless, in some cases, enzyme immobilization can impair the functionality of enzymes, as a result of unfavorable conformational changes in enzymes and restricted substrate access in comparison to their soluble counterparts (16-18). However, the advantages of enzyme immobilization outweigh their unfavorable impact and enhance the efficient implementation of biocatalysts in industrial processes.

Therefore, it is paramount to develop cost-effective and pragmatic enzyme immobilization approaches for potential industrial applications (19-21). In general, scaffolding-based

enzyme immobilization strategies can be categorized into *in vitro* and *in vivo* approaches. The *in vitro* approaches can offer excellent controllability by tuning the physicochemical properties of carriers (e.g. particle size and distribution, or surface charge) as well as by controlling the density of the immobilized enzymes (22, 23). However, the *in vitro* methods often require harsh reaction conditions, such as the presence of toxic cross-linking agents, solvents, extreme temperature, and pH, for successful enzyme immobilization, and these conditions can potentially compromise enzyme function (24). Furthermore, most *in vitro* immobilization methods (e.g. chemical modifications and physical adsorption) are not able to control the enzyme orientation on the solid supports, which directly influences the accessibility of substrates to the catalytic sites of enzymes (25, 26). Also, due to the inherent structural complexity of enzymes, localizing them onto support materials using existing *in vitro* conjugation technologies often necessitates labor-intensive reactions and process optimization steps (21, 27). In addition, multiple separate manufacturing schemes are necessary for large-scale manufacturing of biocatalysts using *in vitro* cross-linking technologies (e.g. manufacturing lines for both enzyme and support materials, and subsequent conjugation steps), which increases production cost (14, 21, 27).

Recently developed *in vivo* immobilization strategies offer an exciting new concept for enzyme immobilization that holds promise for cost-effective production of improved industrial biocatalysts (21). Recent progress in understanding the underlying self-assembly mechanism of a diverse range of naturally occurring supramolecular nanostructures has led to the possibility of constructing task-specific designer scaffolding platforms *in vivo*. Industrially relevant enzymes of interest can easily be covalently displayed on the surface

and/or incorporated within a variety of bio-nanostructures *in vivo* using genetic engineering of the self-assembling subunits (19, 28, 29). In contrast to the *in vitro* methods, the *in vivo* approaches can display enzymes in a homogeneous and oriented manner on solid supports. These *in vivo* approaches enable to bypass the harsh and time-consuming immobilization procedures that are often encountered in the *in vitro* methods. The *in vivo* formation of solid supports displaying enzymes is implemented intracellularly in bacterial cells by one-step production and, thus, additional cross-linking between the enzymes and solid materials is not needed. This one-pot approach is convenient, efficient, and ultimately enables the low-cost production of robust biocatalysts at a large scale (19).

Several promising biological supramolecular assemblies, such as polyhydroxyalkanoate (PHA) particles (30, 31), virus-like particles (VLPs) (29, 32), enzyme-derived nanoparticles (EZPs) (28, 33, 34), membrane vesicles (19, 35), and magnetosomes (36, 37) have been studied to immobilize a variety of functional proteins, including industrially relevant enzymes using recombinant fusion technology (**Figure 1**). Briefly, genetically amenable components of these scaffolds are translationally fused with proteins of interest, such as *e.g.* enzymes, and are produced in a range of recombinant expression systems, like various prokaryotic and eukaryotic organisms. These recombinant host cells allow simultaneous protein and scaffold synthesis and subsequent self-assembly of these components. Such methods have been used to produce immobilized enzymes with improved functionality, presenting a promising means for cost-effective and one-step *in vivo* enzyme immobilization. Here, we will first review the most promising supramolecular assemblies suitable for *in vivo* enzyme immobilization and recent proof-of-concept demonstrations. Then, we will

compare the advantages and limitations of PHA particle technology with other biological scaffold-based *in vivo* enzyme immobilization methods focusing on immobilization of industrially relevant enzymes. Finally, we will discuss innovative methods to expand the utility of the PHA particle technology, including its implementation into continuous-flow catalytic conversions.

Biological supramolecular assemblies suitable for enzyme immobilization

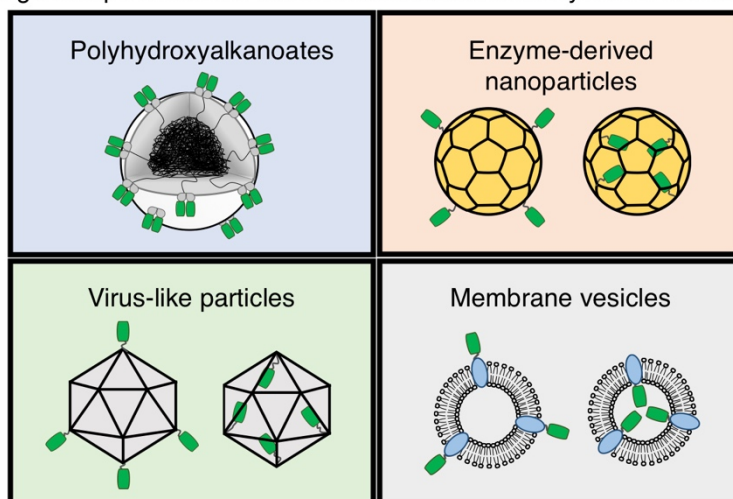


**Figure 1.** Enzyme (shown in green) immobilization *via* various biological supramolecular assemblies.

## 2.3 Utilization of Various Supramolecular Assemblies as Enzyme Immobilization

### Supports

#### 2.3.1 Polyhydroxyalkanoates

PHAs are natural biopolyesters, composed of (*R*)-3-hydroxy fatty acids, and are produced by various bacteria in the presence of an excess carbon source, such as glucose (23, 38). PHAs are synthesized by PHA synthases and are deposited as spherical polyester inclusions that serve as an energy and carbon source (39, 40). PHA particles vary in size and range between 100 and 500 nm (23, 30, 41). Poly-(*R*)-3-hydroxybutyrate (PHB) was the first PHA polymer identified by Lemoigne in 1926 in *Bacillus megaterium* and is the most common form of PHA (42, 43). Generally, each bacterial cell can produce 5–10 PHA particles, the mass of which can contribute up to 90% of cellular dry weight (44–46). The physicochemical properties of PHA particles are significantly influenced by the length and composition of the hydroxyl fatty acids (23, 46). Over 150 different PHA constituents are known (23, 47, 48). The PHAs are classified into three main classes, dependent on their chemical structure and the chain length of the fatty acid monomers: short-chain length PHAs (3–5 carbon atoms); medium-chain length PHAs (6–14 carbon atoms); and long-chain length PHAs (>14 carbon atoms) (46, 49). Short-chain length PHAs generally have a high level of crystallinity and, thus, are hard and brittle. Medium-chain length PHAs usually have a low melting temperature and crystallinity and, therefore, they are more elastic (30, 46, 50).

PHA particles are comprised of an amorphous hydrophobic PHA core surrounded by PHA-associated proteins (PAPs), including PHA synthase (PhaC), phasins (*e.g.* PhaP and PhaF), structural proteins, PHA depolymerase, structural proteins, and other regulatory proteins (**Figure 2A**) (30). Numerous metabolic pathways can provide an array of (*R*)-3-hydroxy fatty acids for the production of PHAs with varying structures and properties as reviewed elsewhere (51). PhaC dimers can polymerize these monomer precursors to PHA chains while PhaC itself remains attached to nascent PHA chains *via* a covalent thioester bond involving the active site cysteine residue of the PhaC (52, 53). The covalent link between these two components, namely the growing hydrophobic PHA chains and the soluble PhaC, eventually leads to amphipathic molecules self-assembling into the spherical PHA particles as shown in scanning electron microscopy (SEM) and transmission electron microscopy (TEM) micrographs (**Figure 2B**) (48, 54). Another interesting class of PAPs, the phasins, are a type of amphipathic protein that has several roles in controlling the structure and surface properties of PHA particles (55, 56). Notably, phasins have a high binding affinity to the outer surface of PHA particles *in vivo* and *in vitro* mediated by physical adsorption (57).

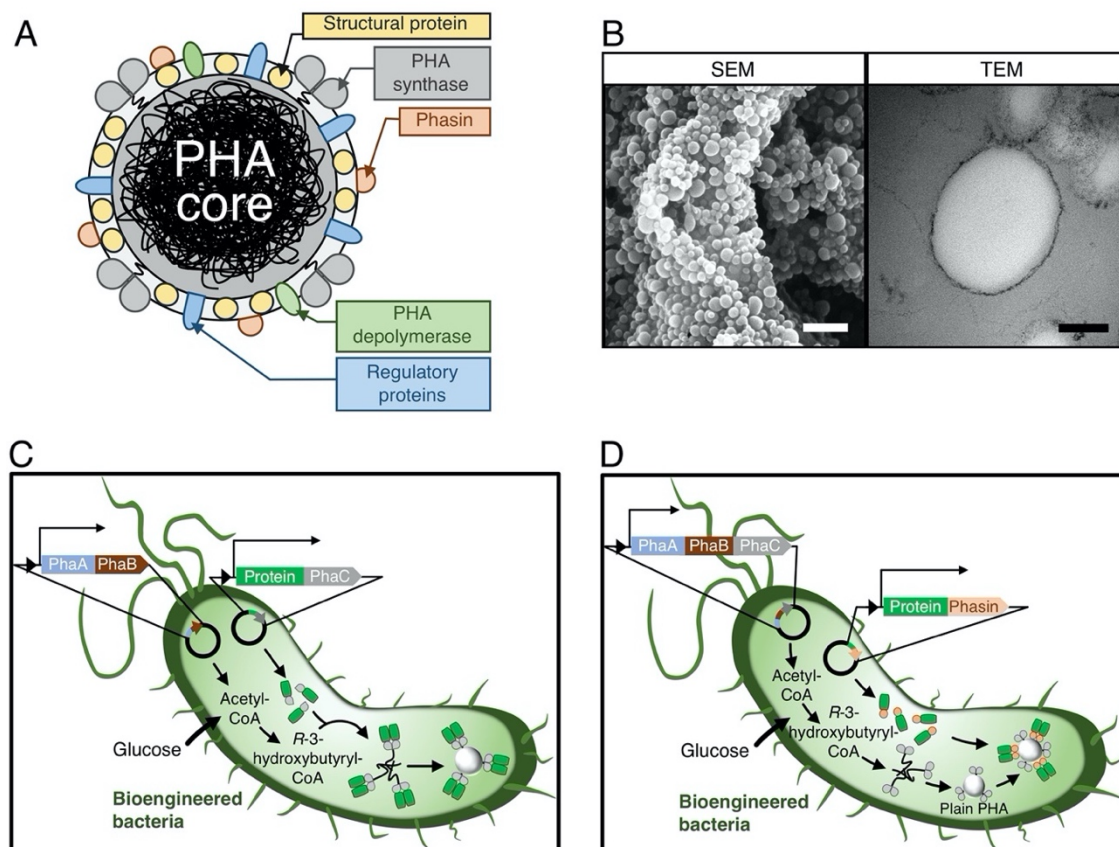


**Figure 2.** Composition, structure, and assembly of PHA particles. **(A)** Schematic of a wild-type PHA particle coated by PAPs. **(B)** SEM and TEM micrographs of PHA particles. White scale bar, 1  $\mu\text{m}$ ; black scale bar, 100 nm. **(C)** Self-assembly and functionalization of PHA particles using a PhaC-based gene fusion approach. **(D)** Self-assembly and functionalization of PHA particles using a phasin-based translational fusion approach.

The PHA-anchoring characteristics of these PAPs *via* both covalent interactions (PhaC) and physical adsorption (PhaF and PhaP) to the surface of PHA particles have been exploited to fabricate task-specific designer PHA particles using recombinant DNA technology (58-62). PAPs can be translationally fused to target proteins, including industrially relevant enzymes, to enable the recombinant production of functionalized PHA particles

*in vivo* (**Figures 2C and 2D**). This approach allows the cost-effective oriented display of immobilized enzymes on the polymeric particulate carrier in one step, ultimately avoiding the laborious chemical cross-linking between enzymes and particles *in vitro* after isolation (30, 31, 63).

### **2.3.2 Virus-Like Particles (VLPs)**

Virus-like particles (VLPs) consist of the viral capsid proteins (64). The formation of VLPs is a self-assembling process of the viral capsid, which potentially mimics the general structure of the parental virus. However, VLPs do not contain nucleic acids, and, thus, there is no risk of causing infection (64, 65). The capsid protein (CP) subunits can be genetically modified for bioconjugation, enabling molecules of interest to be densely displayed or encapsulated in homogeneous spatial orientation (64, 66). VLPs have made significant advances in various fields, from vaccinology to industrial uses due to their promising characteristics, including monodispersed particle size distribution, defined geometric surfaces, biosafety, and functional programmability (65, 67). Additionally, the viral capsids are stable over a wide range of environmental conditions, such as temperature and pH, which make them suitable for different applications, including industrial biocatalysis (68-71). Nevertheless, abundant production of VLPs on an industrial scale is challenging (66, 67). A significant drawback of the VLP platform is that the size of the protein attached to, or accommodated within, the particles is limited. This disadvantage precludes the presentation of large functional moieties (64).

### 2.3.3 Enzyme-Derived Nanoparticles (EZPs)

Enzyme-derived nanoparticles (EZPs) are highly organized cage-like nanostructures that can be found in both prokaryotic and eukaryotic cells. These naturally evolved protein assemblies can often comprise biomacromolecules such as *e.g.* enzymes or inorganic moieties (*e.g.* iron) that are involved in a range of metabolic and biochemical pathways (peroxidase catalyzed processes (encapsulin), production of vitamin B2 (lumazine synthase), and iron homeostasis (ferritin)) (72-74). These spherical nanostructures are highly attractive owing to their particle uniformity, biocompatibility, and precise controllability. Being able to fine-tune the morphological architecture and functions of these particulate scaffolds has made them excellent candidates for the design of biocatalytic nanoreactors (28, 34, 75). EZPs can be reprogrammed to incorporate various foreign biological functions such as *e.g.* enzymes of industrial interest. Both chemical and bioengineering methods can be utilized to modify the scaffold protein (ScP) subunits of EZPs to enable spatial organization of enzymes within and/or on the surface of the EZPs. This design space enables the fabrication of various artificial multienzyme complexes for industrial uses (28). Although these scaffolds have been manufactured in numerous recombinant expression systems (*e.g.* various prokaryotic and eukaryotic organisms), they have been mainly assembled in *E. coli* strains (33). Advances in protein engineering in recent years has allowed the development of unique structural assemblies of EZPs using *de novo* and *in silico* design of novel EZPs (76-80).

#### 2.3.4 Extracellular membrane vesicles (EMVs)

Extracellular membrane vesicles (EMVs) are lipid membrane-derived compartments and are found in all domains of life (81-83). Their sizes are in the range of 20–1000 nm in diameter (83, 84), and they mainly serve as carrier vehicles to mediate cell-to-cell communication by transporting biological cargo as, for example, DNA, RNA, and proteins (85, 86). The classification of these functionally and structurally diverse EMVs, including the bacterial outer membrane vesicles, microvesicles, and exosomes, has been thoroughly reviewed (83, 84, 87, 88). Although the exact underlying mechanism on how different EMVs are formed is still unknown, recent studies show that various recombinantly modified protein production cell lines, including well-established *E. coli* production strains, can produce task-specific EMVs. It was shown that foreign proteins of interest, such as enzymes, could be incorporated into the outer surface or within the inner surface of the EMVs *via* membrane-anchoring motifs, such as transmembrane domains, using genetic engineering to create respective translational fusions (89, 90). This approach led to numerous pharmaceutical and bioremediation applications (91-94). In addition, EMVs are relatively stable in ambient environments and can be manufactured cost-effectively (95). However, isolation and purification of EMVs still require expensive and laborious ultracentrifugation steps, which potentially impact the structural integrity of EMVs and which prohibit industrial scale production (85, 89, 96).

### 2.3.5 Magnetosomes

Bacterial magnetosomes are inclusions (20–60 nm) present in magnetotactic bacteria comprised of magnetic mineral crystals (iron oxide or iron sulfide nanoparticle) surrounded by a phospholipid double-layered membrane (97). The magnetosome membrane is derived from the cytoplasmic membrane and can protect the iron crystal from oxidation (97). Many magnetosome membrane proteins (*e.g.* MamB, MamM, MamH, and MamZ) are involved in magnetosome formation and dictate the iron uptake into the vesicle (97-99). Meanwhile, the size and morphology of the magnetosomes are controlled by another set of magnetosome membrane proteins as, for example, MamC/Mms13, MamD, MamF, MamG, MamR, MamS, Mms6, and MmsF (97, 98, 100). Interestingly, magnetosomes can be functionalized *in vivo* by fusing foreign proteins of interest to the magnetosome membrane proteins, such as MamC/Mms13, MagA, and Mms16 (101, 102). The translational fusion of functional proteins to these transmembrane proteins of magnetosomes has led to numerous successful prototypes in a wide range of applications, including industrial uses (103-108). The inherent magnetic characteristics of magnetosomes make them very useful in some situations, especially for implementation in magnetic-field-related technologies, such as magneto-immunoassays and biomedical imaging (102). The implementation of magnetosomes also allows rapid magnetic separation of the functionalized particulate scaffolds from the bulk fluids (21). However, several technical issues encountered in manipulating and cultivating magnetosomes represent some of the main hurdles in expanding the use of this exciting technology (109).

## 2.4. Biological Supramolecular Assemblies as Biocatalyst Supports

**Table 1** summarizes recent studies describing *in vivo* immobilization approaches for a range of industrially relevant enzymes, detailing their functional performance and robustness in various experimented conditions.

**Table 1.** Biological supramolecular assemblies engineered for *in vivo* immobilization of industrially relevant enzymes

Type of biological scaffolds and their anchoring motifs.	Target enzyme (Origin) (Gene fusion site) (Production host)	Catalytic performance	Stability	Ref.
<b>Polyhydroxyalkanoates (PHAs)</b>				
PHAs via <i>Cupriavidus necator</i> PHA synthase PhaC	$\alpha$ -amylase ( <i>Bacillus licheniformis</i> ) (C-terminus) ( <i>E. coli</i> Origami B (DE3))	<ul style="list-style-type: none"> <li>Consistent with the reported activity of soluble counterpart.</li> <li>Michaelis-Menten constant (<math>K_m</math>) of immobilized <math>\alpha</math>-amylase catalyzing starch degradation: 5 <math>\mu</math>M</li> <li><math>K_m</math> of soluble <math>\alpha</math>-amylase reported in the literature catalyzing starch degradation: 9.6 <math>\mu</math>M</li> </ul>	<ul style="list-style-type: none"> <li>Tolerant to extreme pH and temperature.</li> </ul>	(110)

		<ul style="list-style-type: none"> <li>Specific activity of immobilized <math>\alpha</math>-amylase catalyzing starch degradation: 506 mU/mg of fusion protein.</li> </ul>		
	Hexavalent chromium reductase, NemA ( <i>E. coli</i> ) (N-terminus) ( <i>E. coli</i> BL21(DE3))	<ul style="list-style-type: none"> <li>Showed activity to their substrate but at varying efficiencies.</li> <li><math>K_m</math> of immobilized NemA for the reduction of Cr(VI): <math>94 \pm 26 \mu\text{M}</math>.</li> <li><math>K_m</math> of soluble NemA for the reduction of Cr(VI): <math>16 \pm 8.6 \mu\text{M}</math>.</li> <li><math>K_m</math> of immobilized NemA for the reduction of NADH: <math>490 \pm 30 \mu\text{M}</math>.</li> <li><math>K_m</math> of soluble NemA for the reduction of NADH: <math>450 \pm 30 \mu\text{M}</math></li> </ul>	<ul style="list-style-type: none"> <li>No observable reduction in activity after 36 weeks of storage at <math>4^\circ\text{C}</math>.</li> </ul>	(111) ^
	<i>N</i> -acetylglucosamine 2-epimerase, Slr1975 ( <i>Synechocystis</i> sp. PCC 6803) (N-terminus) ( <i>E. coli</i> BL21(DE3))	<ul style="list-style-type: none"> <li>Artificial enzyme cascading system had overall conversion yield of ~22%, compared to that of traditional method at ~33% catalyzing <i>N</i>-acetyl-D-glucosamine conversion to <i>N</i>-acetylneuraminic acid.</li> <li>Specific activity of immobilized Slr1975 catalyzing <i>N</i>-acetyl-D-</li> </ul>	<ul style="list-style-type: none"> <li>Retained ~80% of its initial activity after five reaction cycles.</li> </ul>	(112) *

	<p><i>N</i>-acetylneuraminic acid aldolase, NanA (<i>E. coli</i>) (C-terminus) (<i>E. coli</i> BL21(DE3))</p>	<p>glucosamine conversion to <i>N</i>-acetyl-D-mannosamine: <math>1.76 \pm 0.38</math> U/mg fusion protein.</p> <ul style="list-style-type: none"> <li>Specific activity of immobilized Slr1975 catalyzing <i>N</i>-acetyl-D-glucosamine conversion to <i>N</i>-acetyl-D-mannosamine when co-immobilized with NanA: <math>0.58 \pm 0.07</math> U/mg of fusion protein.</li> <li>Specific activity of immobilized NanA catalyzing <i>N</i>-acetyl-D-mannosamine conversion to <i>N</i>-acetylneuraminic acid: <math>42.6 \pm 6.9</math> U/mg of fusion protein.</li> <li>Specific activity of immobilized NanA catalyzing <i>N</i>-acetyl-D-mannosamine conversion to <i>N</i>-acetylneuraminic acid when co-immobilized with Slr1975: <math>81.9 \pm 19</math> U/mg of fusion protein.</li> </ul>		
	<p>Lipase B (<i>Candida antarctica</i>) (N-terminus) (<i>E. coli</i> BL21 (DE3))</p>	<ul style="list-style-type: none"> <li>Retained but exhibited lower activity (~30-40%) catalyzing glycerol tributyrates hydrolysis when compared to the commercially available immobilized lipase (Novozyme 435).</li> </ul>	<ul style="list-style-type: none"> <li>Retained initial activity after seven weeks of storage at 4°C.</li> </ul>	(60) ^*

	<p>Carbonic anhydrase</p> <p>(<i>Desulfovibrio vulgaris</i> str. “Miyazaki F”),</p> <p>DvCA</p> <p>(C-terminus)</p> <p>(<i>E. coli</i> BL21(DE3))</p>	<ul style="list-style-type: none"> <li>Retained but exhibited lower activity when compared to the commercially available soluble counterpart.</li> <li>Specific activity of immobilized DvCA catalyzing the hydration of carbon dioxide: 114 U/mg of enzyme (highest at 211 U/mg of enzyme).</li> </ul>	<ul style="list-style-type: none"> <li>Tolerant to alkaline and elevated temperature environments.</li> </ul>	(61) *
	<p>Lipase M37</p> <p>(<i>Photobacterium lipolyticum</i>)</p> <p>(C-terminus)</p> <p>(<i>E. coli</i> XL1-Blue)</p>	<ul style="list-style-type: none"> <li>Consistent with the reported activity of soluble counterpart but exhibited narrow substrate chain length specificity.</li> <li>Specific activity of immobilized lipase M37 catalyzing <i>p</i>-nitrophenyl esters conversion to <i>p</i>-nitrophenol: <math>108.4 \pm 2.5</math> U/g of dry weight PHA particles.</li> </ul>	<ul style="list-style-type: none"> <li>Enhanced thermal stability and retained initial activity after four weeks of storage at 4°C.</li> </ul>	(113) *
	<p>Alkaline polygalacturonate lyase, PGL</p> <p>(<i>Bacillus subtilis</i>)</p> <p>(C-terminus)</p>	<ul style="list-style-type: none"> <li>Retained ~85% of the catalytic activity of soluble counterpart.</li> <li>Specific activity of immobilized PGL catalyzing polygalacturonic acid conversion to unsaturated</li> </ul>	<ul style="list-style-type: none"> <li>Retained ~60% of its initial activity after eight reaction cycles.</li> </ul>	(114) *

	<p>(<i>E. coli</i> BL21(DE3))</p>	<p>oligo-galacturonic acid: <math>184.67 \pm 11.53</math> U/mg of enzyme.</p> <ul style="list-style-type: none"> <li>Specific activity of soluble PGL catalyzing polygalacturonic acid conversion to unsaturated oligo-galacturonic acid: <math>215.93 \pm 8.95</math> U/mg of enzyme.</li> </ul>	<ul style="list-style-type: none"> <li>Moderately enhanced thermal and pH stability.</li> </ul>	
	<p>Tyrosinase (<i>Verrucomicrobium spinosum</i>) (C-terminus) (<i>E. coli</i> BL21(DE3))</p>	<ul style="list-style-type: none"> <li>Immobilized tyrosinase showed enhanced specific activity catalyzing L-tyrosine conversion to L-dopaquinone when compared to its soluble counterpart.</li> <li>Monophenolase activity of immobilized tyrosinase catalyzing L-tyrosine conversion to 3,4-dihydroxyphenyl-L-alanine: <math>9155.88 \pm 312.57</math> U/g of enzyme.</li> <li>Monophenolase activity of soluble tyrosinase catalyzing L-tyrosine conversion to 3,4-dihydroxyphenyl-L-alanine: <math>2185.50 \pm 74.61</math> U/g of enzyme.</li> <li>Diphenolase activity of immobilized tyrosinase catalyzing 3,4-dihydroxyphenyl-L-alanine conversion to L-</li> </ul>	<ul style="list-style-type: none"> <li>Retained its initial activity up to six reaction cycles.</li> <li>Widened optimal operating temperature range.</li> </ul>	(115) *

		<p>dopaquinone: <math>297.27 \pm 21.25</math> U/g of enzyme.</p> <ul style="list-style-type: none"> <li>▪ Diphenolase activity of soluble tyrosinase catalyzing 3,4-dihydroxyphenyl-L-alanine conversion to L-dopaquinone: <math>32.10 \pm 3.10</math> U/g of enzyme.</li> </ul>		
	<p>D-tagatose-3-epimerase, DTE (<i>Pseudomonas cichorii</i>) (C-terminus) (<i>E. coli</i> ClearColi BL21 (DE3))</p>	<ul style="list-style-type: none"> <li>▪ Had overall conversion yield of ~33% catalyzing D-fructose conversion to D-allulose.</li> <li>▪ Specific activity of immobilized DTE catalyzing D-fructose conversion to D-allulose: <math>357.77 \pm 16.66</math> U/mg of enzyme.</li> <li>▪ Specific activity of soluble DTE catalyzing D-fructose conversion to D-allulose: <math>531.29 \pm 31.87</math> U/mg of enzyme.</li> </ul>	<ul style="list-style-type: none"> <li>▪ Retained ~80% of its initial activity after eight reaction cycles.</li> <li>▪ Exhibited similar thermal and pH stability when compared to its soluble counterpart.</li> </ul>	(116) *
<p>PHAs via <i>Pseudomonas putida</i> phasin PhaF</p>	<p><math>\beta</math>-galactosidase, <math>\beta</math>-gal (<i>E. coli</i>) (N-terminus) (<i>Pseudomonas putida</i> GPG-Tc6)</p>	<ul style="list-style-type: none"> <li>▪ Showed specific activity to its substrate.</li> <li>▪ Specific activity of immobilized <math>\beta</math>-gal catalyzing the hydrolysis of <i>o</i>-nitro-phenyl-<math>\beta</math>-D-galactopyranoside: <math>2.8 \times 10^5</math> U/mg of enzyme.</li> </ul>	<ul style="list-style-type: none"> <li>▪ N/A</li> </ul>	(117) *

		<ul style="list-style-type: none"> <li>Specific activity of soluble <math>\beta</math>-gal catalyzing the hydrolysis of <i>o</i>-nitro-phenyl-<math>\beta</math>-D-galactopyranoside cleaved from <math>\beta</math>-gal displaying PHA particles: <math>2.2 \times 10^5</math> U/mg of enzyme.</li> </ul>		
	Cry1Ab toxin ( <i>Bacillus thuringiensis</i> ) (N-terminus) ( <i>Pseudomonas putida</i> GPG-Tc6)	<ul style="list-style-type: none"> <li>Immobilized Cry1Ab showed 7.2-fold less insecticidal activity against the larvae of <i>Sesamia nonagrioides</i> when compared with its soluble counterpart.</li> </ul>	<ul style="list-style-type: none"> <li>N/A</li> </ul>	(118) ^*
PHAs via <i>Cu-priavidus ne-cator</i> phasin PhaP	D-hydantoinase, D-HDT ( <i>Agrobacterium radiobacter</i> NRRL B11291) (N-terminus) ( <i>E. coli</i> DH5 $\alpha$ )	<ul style="list-style-type: none"> <li>Immobilized D-HDT showed similar specific activity in catalyzing D,L-hydroxyphenyl hydantoin conversion to <i>N</i>-carbamoyl-L-<i>p</i>-hydroxy phenylglycine with its soluble counterpart.</li> <li>Ranged between 80–107 U due to varying biosynthesis conditions of <i>in vivo</i> functionalized PHA particles.</li> </ul>	<ul style="list-style-type: none"> <li>Stable up to seven reaction cycles. Enhanced stability at elevated temperatures.</li> </ul>	(119) *

	Lysine decarboxylase, CadA ( <i>E. coli</i> ) (N-terminus) ( <i>E. coli</i> BL21(DE3))	<ul style="list-style-type: none"> <li>Consistent with its soluble counterpart.</li> <li>Specific activity of immobilized CadA catalyzing lysine conversion to cadaverine: <math>179.5 \pm 1.8</math> U/mg of enzyme.</li> <li>Specific activity of soluble CadA catalyzing lysine conversion to cadaverine: <math>95.15 \pm 9.5</math> U/mg of enzyme.</li> </ul>	<ul style="list-style-type: none"> <li>Retained its initial activity up to five reaction cycles.</li> <li>Moderately enhanced thermal and pH stability.</li> </ul>	(120) *
PHAs via <i>Cu-priavidus necator</i> PHA synthase PhaC and PHAs via <i>Cu-priavidus necator</i> phasin PhaP	Organophosphorus hydrolase, OpdA ( <i>Pseudoalteromonas</i> sp. SCSIO 04301) (N-terminus) ( <i>E. coli</i> BL21(DE3))	<ul style="list-style-type: none"> <li><math>K_m</math> of OpdA immobilized using PhaC catalyzing paraoxon hydrolysis: <math>6.188 \pm 2.490</math> mM.</li> <li><math>K_m</math> of OpdA immobilized using PhaP catalyzing paraoxon hydrolysis: <math>6.116 \pm 1.299</math> mM.</li> <li><math>K_m</math> of soluble OpdA catalyzing paraoxon hydrolysis: <math>3.203 \pm 0.929</math> mM.</li> <li><math>k_{cat}</math> of OpdA immobilized using PhaC catalyzing paraoxon hydrolysis: <math>11.904 \pm 3.893</math> s<sup>-1</sup>.</li> <li><math>k_{cat}</math> of OpdA immobilized using PhaP catalyzing paraoxon hydrolysis: <math>11.223 \pm 1.752</math> s<sup>-1</sup>.</li> </ul>	<ul style="list-style-type: none"> <li>Enhanced stability particularly under acidic conditions.</li> <li>Retained ~80% of its initial activity after 10 repeated use cycles.</li> </ul>	(121)

		<ul style="list-style-type: none"> <li>▪ <math>k_{cat}</math> of soluble OpdA catalyzing paraoxon hydrolysis: <math>3.0 \pm 0.526 \text{ s}^{-1}</math>.</li> <li>▪ <math>k_{cat}/K_m</math> of OpdA immobilized using PhaC catalyzing paraoxon hydrolysis: <math>1961 \pm 138 \text{ M}^{-1}\text{s}^{-1}</math>.</li> <li>▪ <math>k_{cat}/K_m</math> of OpdA immobilized using PhaP catalyzing paraoxon hydrolysis: <math>1850 \pm 104 \text{ M}^{-1}\text{s}^{-1}</math>.</li> <li>▪ <math>k_{cat}/K_m</math> of soluble OpdA catalyzing paraoxon hydrolysis: <math>935 \pm 89 \text{ M}^{-1}\text{s}^{-1}</math>.</li> <li>▪ Specific activity of OpdA immobilized using PhaC catalyzing paraoxon hydrolysis: <math>0.096 \pm 0.0047 \text{ U/mg}</math> of enzyme.</li> <li>▪ Specific activity of OpdA immobilized using PhaP catalyzing paraoxon hydrolysis: <math>0.109 \pm 0.0014 \text{ U/mg}</math> of enzyme.</li> <li>▪ Specific activity of OpdA immobilized using PhaC and PhaP catalyzing paraoxon hydrolysis: <math>0.112 \pm 0.0044 \text{ U/mg}</math> of enzyme.</li> <li>▪ Specific activity of soluble OpdA catalyzing paraoxon hydrolysis: <math>1.648 \pm 0.222 \text{ U/mg}</math> of enzyme.</li> </ul>		
--	--	---	--	--

<b>Virus-like particles (VLPs)</b>				
Bacteriophage MS2 CP subunit	Pyridoxal phosphate dependent tryptophanase, TnaA ( <i>E. coli</i> (N- and C-terminal) ( <i>E. coli</i> BL21(DE3) Star)	<ul style="list-style-type: none"> <li>Artificial enzyme cascading system comprised of covalently immobilized TnaA and FMO showed enhanced overall conversion yield catalyzing L-tryptophan conversion to indigo when compared to the soluble controls.</li> </ul>	<ul style="list-style-type: none"> <li>Retained ~95% of its initial activity after one week of storage at 25°C, compared to its soluble counterpart (~5%).</li> </ul>	(122) ^*
	Flavin- mononucleotide and nicotinamide adenine dinucleotide phosphate dependent containing monooxygenase, FMO ( <i>Methylophaga</i> sp. Strain SK1) (N- and C-terminal) ( <i>E. coli</i> BL21(DE3) Star)			

Bacteriophage P22 CP subunit	Alcohol dehydrogenase D ( <i>Pyrococcus furiosus</i> ) (C-terminus) ( <i>E. coli</i> BL21(DE3))	<ul style="list-style-type: none"> <li>▪ Showed specific activity for the reduction of 3-hydroxy-2-butanone to 2,3-butanediol.</li> </ul>	<ul style="list-style-type: none"> <li>▪ No loss in activity at 25°C was observed.</li> </ul>	(123) ^*
	Hydrogenase 1 subunit A and subunit B, HyaA and HyaB ( <i>E. coli</i> ) (C-terminus) ( <i>E. coli</i> BL21(DE3))	<ul style="list-style-type: none"> <li>▪ ~80–270-fold higher than the reported activity of soluble counterpart for hydrogen production.</li> <li>▪ Catalytic activity of immobilized hydrogenase for hydrogen production: 3218 ± 394 nmol H<sub>2</sub> /mg min.</li> <li>▪ Catalytic activity of the soluble hydrogenase for hydrogen production reported in the literature: 12–38 nmol H<sub>2</sub> /mg min.</li> </ul>	<ul style="list-style-type: none"> <li>▪ Showed resistance against proteolytic and thermal inactivation.</li> </ul>	(124) *
Parvovirus B19 CP subunit	Lipase, Bp1A ( <i>Bacillus pumilus</i> ) (N- and C-termini)	<ul style="list-style-type: none"> <li>▪ Showed specific activity catalyzing the hydrolysis of 4-nitrophenyl acetate but lower when compared to its soluble counterpart.</li> </ul>	<ul style="list-style-type: none"> <li>▪ Enhanced thermal stability.</li> <li>▪ First-order rate constant of degradation of immobilized lipase at</li> </ul>	(125) *

	<p>(<i>E. coli</i> BL21(DE3))</p> <ul style="list-style-type: none"> <li>▪ Specific activity of immobilized Bp1A catalyzing the hydrolysis of 4-nitrophenyl acetate: <math>9.5 \pm 1.4</math> U/<math>\mu</math>mol of enzyme.</li> <li>▪ Specific activity of soluble Bp1A catalyzing the hydrolysis of 4-nitrophenyl acetate: <math>202 \pm 0.4</math> U/<math>\mu</math>mol enzyme.</li> </ul>	<p>40°C: <math>0.68 \pm 0.11</math> h<sup>-1</sup>.</p> <ul style="list-style-type: none"> <li>▪ First-order rate constant of degradation of soluble lipase at 40°C: <math>4.82 \pm 0.37</math> h<sup>-1</sup>.</li> </ul>	
	<p><math>\alpha</math>-glucosidase, Ima1p (<i>Saccharomyces cerevisiae</i>) (C-terminus) (<i>E. coli</i> BL21(DE3))</p> <ul style="list-style-type: none"> <li>▪ ~3-fold increase in catalytic activity when compared to its soluble counterpart.</li> <li>▪ Catalytic activity of immobilized Ima1p catalyzing 4-nitrophenyl-<math>\alpha</math>-D-glucopyranoside hydrolysis: <math>2.1 \pm 0.05</math> mM/min/mg.</li> <li>▪ Catalytic activity of soluble Ima1p catalyzing 4-nitrophenyl-<math>\alpha</math>-D-glucopyranoside hydrolysis: <math>0.67 \pm 0.02</math> mM/min/mg.</li> <li>▪ <math>K_m</math> of immobilized Ima1p catalyzing 4-nitrophenyl-<math>\alpha</math>-D-glucopyranoside hydrolysis: <math>1.92 \pm 0.13</math> mM.</li> <li>▪ <math>K_m</math> of soluble Ima1p catalyzing 4-nitrophenyl-<math>\alpha</math>-D-glucopyranoside hydrolysis: <math>1.72 \pm 0.16</math> mM.</li> </ul>	<ul style="list-style-type: none"> <li>▪ Impaired thermal stability.</li> </ul>	(126)

Cowpea chlorotic mottle virus CP subunit	Lysozyme (Enterobacteriophage T4) (C-terminus) ( <i>E. coli</i> BLR(DE3) pLysS)	<ul style="list-style-type: none"> <li>▪ Showed catalytic activity catalyzing the degradation of fluorescently labelled <i>M. luteus</i> cell walls but ~7-fold less active than its soluble counterpart.</li> <li>▪ Catalytic activity of immobilized lysozyme catalyzing the degradation of fluorescently labelled <i>M. luteus</i> cell walls: ~400 arbitrary unit (AU)/min.</li> <li>▪ Catalytic activity of soluble lysozyme catalyzing the degradation of fluorescently labelled <i>M. luteus</i> cell walls: ~2800 AU/min.</li> </ul>	▪ N/A	(127) *
<b>Enzyme-derived nanoparticles (EZPs)</b>				
<i>Bacillus stearothermophilus</i> pyruvate dehydrogenase multienzyme complex E2 core ScP subunit functionalized with elastin-like	Endoglucanase CelA ( <i>Clostridium thermocellum</i> ) (C-terminus) ( <i>E. coli</i> BL21(DE3))	<ul style="list-style-type: none"> <li>▪ Immobilized CelA on ELP-E2 nanoparticles increased the amount of reduced sugar compared to its soluble counterpart.</li> <li>▪ Catalytic activity of immobilized CelA catalyzing cellulose hydrolysis: ~17 <math>\mu\text{mol/h}</math>.</li> <li>▪ Catalytic activity of soluble CelA catalyzing cellulose hydrolysis: ~14 <math>\mu\text{mol/h}</math>.</li> </ul>	▪ Immobilized CelA on ELP-E2 nanoparticles remained functional up to 70°C.	(128) *

peptide (ELP-E2)				
	$\beta$ -galactosidase, $\beta$ -gal ( <i>E. coli</i> ) (C-terminus) ( <i>E. coli</i> BL21(DE3))	<ul style="list-style-type: none"> <li>▪ Immobilized <math>\beta</math>-gal on ELP-E2 nanoparticles showed catalytic activity visualized by the change in the color of substrate into yellow due to the release of <i>o</i>-nitrophenol.</li> </ul>	<ul style="list-style-type: none"> <li>▪ N/A</li> </ul>	
<i>Citrobacter freundii</i> Pdu bacterial microcompartment ScP subunit (D18 or P18)	Glycerol dehydrogenase, GldA ( <i>E. coli</i> ) (N-terminus) ( <i>E. coli</i> BL21(DE3) pLysS)	<ul style="list-style-type: none"> <li>▪ Co-immobilization or aggregation of tagged enzymes catalyzing glycerol conversion to 1,2-propanediol resulted in enhanced conversion yield <i>in vivo</i> compared to the soluble counterpart.</li> <li>▪ A reduction of 90% in the specific activity of GldA bearing D18 when compared to the untagged control catalyzing glycerol conversion to dihydroacetone.</li> </ul>	<ul style="list-style-type: none"> <li>▪ N/A</li> </ul>	(129) *
	Dihydroxyacetone kinase, DhaK ( <i>E. coli</i> ) (N-terminus) ( <i>E. coli</i> BL21(DE3) pLysS)	<ul style="list-style-type: none"> <li>▪ A reduction of 55% in the specific activity of GldA bearing P18 when compared to the untagged control catalyzing glycerol conversion to dihydroacetone.</li> </ul>		
	Methylglyoxal synthase, MgsA	<ul style="list-style-type: none"> <li>▪ Specific activity of immobilized DhaK bearing D18 catalyzing</li> </ul>		

	<p>(<i>E. coli</i>)</p> <p>(N-terminus)</p> <p>(<i>E. coli</i></p> <p>BL21(DE3)</p> <p>pLysS)</p>	<p>dihydroacetone conversion to dihydroacetone phosphate: ~5.5 <math>\mu\text{mol}/\text{min}/\text{mg}</math>.</p> <ul style="list-style-type: none"> <li>Specific activity of immobilized DhaK bearing P18 catalyzing dihydroacetone conversion to dihydroacetone phosphate: ~5.0 <math>\mu\text{mol}/\text{min}/\text{mg}</math>.</li> </ul>		
	<p>1,2-propanediol</p> <p>oxidoreductase,</p> <p>FucO</p> <p>(<i>E. coli</i>)</p> <p>(N-terminus)</p> <p>(<i>E. coli</i></p> <p>BL21(DE3)</p> <p>pLysS)</p>	<ul style="list-style-type: none"> <li>Specific activity of untagged DhaK catalyzing dihydroacetone conversion to dihydroacetone phosphate: ~5.1 <math>\mu\text{mol}/\text{min}/\text{mg}</math>.</li> <li>Specific activity of immobilized MgsA bearing D18 catalyzing dihydroacetone phosphate conversion to methylglyoxal: ~14 <math>\mu\text{mol}/\text{min}/\text{mg}</math>.</li> <li>Specific activity of immobilized MgsA bearing P18 catalyzing dihydroacetone phosphate conversion to methylglyoxal: ~13 <math>\mu\text{mol}/\text{min}/\text{mg}</math>.</li> <li>Specific activity of untagged Mgs catalyzing dihydroacetone phosphate conversion to methylglyoxal: ~16 <math>\mu\text{mol}/\text{min}/\text{mg}</math>.</li> <li>Specific activity of immobilized GldA bearing D18 catalyzing</li> </ul>		

		<p>methylglyoxal conversion to lactaldehyde: <math>\sim 0.4 \mu\text{mol/min/mg}</math>.</p> <ul style="list-style-type: none"> <li>▪ Specific activity of immobilized GldA bearing P1 catalyzing methylglyoxal conversion to lactaldehyde: <math>\sim 0.9 \mu\text{mol/min/mg}</math>.</li> <li>▪ Specific activity of untagged GldA catalyzing methylglyoxal conversion to lactaldehyde: <math>\sim 2.1 \mu\text{mol/min/mg}</math>.</li> <li>▪ Specific activity of immobilized FucO bearing D18 catalyzing lactaldehyde conversion to 1,2-propanediol: <math>\sim 6.0 \mu\text{mol/min/mg}</math>.</li> <li>▪ Specific activity of immobilized FucO bearing P18 catalyzing lactaldehyde conversion to 1,2-propanediol: <math>\sim 2.5 \mu\text{mol/min/mg}</math>.</li> <li>▪ Specific activity of untagged FucO catalyzing lactaldehyde conversion to 1,2-propanediol: <math>\sim 10.0 \mu\text{mol/min/mg}</math>.</li> </ul>		
<i>Salmonella enterica</i> Pdu bacterial	$\beta$ -galactosidase, $\beta$ -gal ( <i>E. coli</i> ) (N-terminus)	<ul style="list-style-type: none"> <li>▪ Showed specific activity to their respective substrates but at varying efficiencies.</li> </ul>	<ul style="list-style-type: none"> <li>▪ Enhanced pH stability but not against thermal stress.</li> </ul>	(130, 131) *

microcompartment ScP subunit	( <i>Salmonella enterica</i> )	<ul style="list-style-type: none"> <li>▪ Catalytic activity of immobilized <math>\beta</math>-gal catalyzing lactose conversion: <math>62 \pm 7</math> <math>\mu\text{mol/h/mg}</math> of protein.</li> </ul>		
	Glycerol dehydrogenase, GldA ( <i>E. coli</i> ) (N-terminus) ( <i>Salmonella enterica</i> )	<ul style="list-style-type: none"> <li>▪ Catalytic activity of soluble <math>\beta</math>-gal catalyzing lactose conversion: <math>82 \pm 7</math> <math>\mu\text{mol/h/mg}</math> of protein.</li> <li>▪ Catalytic activity of immobilized <math>\beta</math>-gal catalyzing o-nitrophenyl-<math>\beta</math>-galactoside (oNPG) conversion: <math>4.2 \pm 0.17</math> <math>\mu\text{mol/h/mg}</math> of protein.</li> </ul>		
	Esterase, Est5 (soil metagenome) (N-terminus) ( <i>Salmonella enterica</i> )	<ul style="list-style-type: none"> <li>▪ Catalytic activity of soluble <math>\beta</math>-gal catalyzing oNPG conversion: <math>3.9 \pm 0.11</math> <math>\mu\text{mol/h/mg}</math> of protein.</li> <li>▪ Catalytic activity of immobilized <math>\beta</math>-gal catalyzing 4-methylumbelliferyl <math>\beta</math>-D-galactopyranoside (MUG) conversion: <math>3.2 \times 10^6 \pm 1.8 \times 10^5</math> relative fluorescence unit (rfu)/min/mg of protein.</li> <li>▪ Catalytic activity of soluble <math>\beta</math>-gal catalyzing MUG conversion: <math>5.0 \times 10^6 \pm 1.7 \times 10^4</math> rfu/min/mg of protein.</li> <li>▪ Catalytic activity of immobilized GldA catalyzing acetol conversion: <math>1.1 \pm 0.2</math> <math>\mu\text{mol/h/mg}</math>.</li> </ul>		

		<ul style="list-style-type: none"> <li>▪ Catalytic activity of soluble GldA catalyzing acetol conversion: <math>1.4 \pm 0.2 \mu\text{mol/h/mg}</math>.</li> <li>▪ Catalytic activity of immobilized GldA catalyzing methylglyoxal conversion: <math>1.0 \pm 0.1 \mu\text{mol/h/mg}</math>.</li> <li>▪ Catalytic activity of soluble GldA catalyzing methylglyoxal conversion: <math>2.1 \pm 0.4 \mu\text{mol/h/mg}</math>.</li> <li>▪ Catalytic activity of immobilized Est5 catalyzing 4-nitrophenyl butyrate (<i>p</i>NP-butyrate) conversion: <math>0.5 \pm 0.0 \mu\text{mol/h/mg}</math>.</li> <li>▪ Catalytic activity of soluble Est5 catalyzing <i>p</i>NP-butyrate conversion: <math>4.3 \pm 0.3 \mu\text{mol/h/mg}</math>.</li> </ul>		
<i>Salmonella enterica</i> Pdu bacterial microcompartment mutant ScP subunit O3-33	Alcohol dehydrogenase D, AdhD ( <i>Pyrococcus furiosus</i> ) (N-terminus) ( <i>E. coli</i> BL21(DE3))	<ul style="list-style-type: none"> <li>▪ Retained function but at decreased enzyme kinetic activity.</li> <li>▪ <math>K_m</math> of immobilized AdhD for cofactor <math>\text{NAD}^+</math>: <math>140 \pm 20 \mu\text{M}</math>.</li> <li>▪ <math>K_m</math> of soluble AdhD for cofactor <math>\text{NAD}^+</math>: <math>20 \pm 7 \mu\text{M}</math>.</li> <li>▪ <math>K_m</math> of immobilized AdhD for substrate 2,3-butanediol: <math>140 \pm 10 \text{ mM}</math>.</li> </ul>	<ul style="list-style-type: none"> <li>▪ Doubled electrochemical operational stability.</li> </ul>	(132) ^

		<ul style="list-style-type: none"> <li>▪ <math>K_m</math> of soluble AdhD for substrate 2,3-butanediol: <math>38 \pm 8</math> mM.</li> <li>▪ Turnover number (<math>k_{cat}</math>) of immobilized AdhD: <math>0.046 \pm 0.002</math> s<sup>-1</sup>.</li> <li>▪ <math>k_{cat}</math> of soluble AdhD: <math>0.088 \pm 0.009</math> s<sup>-1</sup>.</li> <li>▪ Apparent <math>K_m</math> of immobilized AdhD for the electrochemical activity: <math>28 \pm 4</math> mM.</li> <li>▪ Apparent <math>K_m</math> of soluble AdhD for the electrochemical activity: <math>27 \pm 3</math> mM.</li> <li>▪ Apparent <math>k_{cat}</math> of immobilized AdhD for the electrochemical activity: <math>0.0084 \pm 0.0001</math> s<sup>-1</sup>.</li> <li>▪ Apparent <math>k_{cat}</math> of soluble AdhD for the electrochemical activity: <math>0.0086 \pm 0.0002</math> s<sup>-1</sup>.</li> </ul>		
<i>Aquifex aeolicus</i> Lumazine syn- thase ScP subu- nit	β-lactamase ( <i>E. coli</i> ) (C-terminus) ( <i>E. coli</i> BL21(DE3))	<ul style="list-style-type: none"> <li>▪ Enhanced catalytic activity catalyzing nitrocefin hydrolysis at specific configuration.</li> </ul>	▪ N/A	(133) ^*

<i>Thermotoga maritima</i> Ketohydroxy-glutarate aldolase ScP subunit	(+)– $\gamma$ -lactamase ( <i>Microbacterium hydrocarbonoxydans</i> ) (N-terminus) ( <i>E. coli</i> BL21(DE3))	<ul style="list-style-type: none"> <li>▪ <math>K_m</math> of immobilized (+)-<math>\gamma</math>-lactamase catalyzing Vince lactam hydrolysis: <math>86 \pm 2.6</math> mM.</li> <li>▪ <math>K_m</math> of soluble (+)-<math>\gamma</math>-lactamase catalyzing Vince lactam hydrolysis: <math>120.4 \pm 7.2</math> mM.</li> <li>▪ <math>k_{cat}</math> of immobilized (+)-<math>\gamma</math>-lactamase catalyzing Vince lactam hydrolysis: <math>12,830 \pm 164.5</math> s<sup>-1</sup>.</li> <li>▪ <math>k_{cat}</math> of soluble (+)-<math>\gamma</math>-lactamase catalyzing Vince lactam hydrolysis: <math>20088 \pm 718</math> s<sup>-1</sup></li> </ul>	<ul style="list-style-type: none"> <li>▪ Enhanced thermal stability, higher tolerance against organic solvents, proteolysis and high substrate concentrations.</li> </ul>	(134) ^
<i>Archaeoglobus fulgidus</i> Ferritin ScP subunit	Kemp eliminase HG3.17 ( <i>Thermoascus aurantiacus</i> ) (N-terminus) ( <i>E. coli</i> BL21-Gold (DE3))	<ul style="list-style-type: none"> <li>▪ <math>K_m</math> of immobilized HG3.17 catalyzing 5-nitro benzisoxazole degradation: <math>1400 \pm 100</math> <math>\mu</math>M.</li> <li>▪ <math>K_m</math> of soluble HG3.17 catalyzing 5-nitro benzisoxazole degradation: <math>1700 \pm 200</math> <math>\mu</math>M.</li> <li>▪ <math>k_{cat}</math> of immobilized HG3.17 catalyzing 5-nitro benzisoxazole degradation: <math>150 \pm 30</math> s<sup>-1</sup>.</li> <li>▪ <math>k_{cat}</math> of soluble HG3.17 catalyzing 5-nitro benzisoxazole degradation: <math>170 \pm 10</math> s<sup>-1</sup>.</li> <li>▪ Specificity constant (<math>k_{cat}/K_m</math>) of immobilized HG3.17 catalyzing</li> </ul>	<ul style="list-style-type: none"> <li>▪ Showed only partial proteolytic protection after incubation with the blood plasma protease factor Xa.</li> <li>▪ Immobilized RA95.5-8F showed enhanced thermal stability.</li> </ul>	(135) ^

		<p>5-nitro benzisoxazole</p> <p>degradation: <math>(11.2 \pm 2.5) \times 10^4 \text{ M}^{-1} \text{ s}^{-1}</math>.</p> <p>▪ <math>k_{cat}/K_m</math> of soluble HG3.17 catalyzing 5-nitro benzisoxazole degradation: <math>(9.9 \pm 1.0) \times 10^4 \text{ M}^{-1} \text{ s}^{-1}</math>.</p>		
	<p>Artificial retro-aldolase</p> <p>RA95.5-8F</p> <p>(<i>Saccharolobus solfataricus</i> P2)</p> <p>(C-terminus)</p> <p>(<i>E. coli</i> BL21-Gold (DE3))</p>	<p>▪ <math>K_m</math> of immobilized RA95.5-8F catalyzing (<i>R</i>)-4-hydroxy-4-(6-methoxy-2-naphthyl)-2-butanone degradation: <math>280 \pm 30 \text{ } \mu\text{M}</math>.</p> <p>▪ <math>K_m</math> of soluble RA95.5-8F catalyzing (<i>R</i>)-4-hydroxy-4-(6-methoxy-2-naphthyl)-2-butanone degradation: <math>300 \pm 20 \text{ } \mu\text{M}</math>.</p> <p>▪ <math>k_{cat}</math> of immobilized RA95.5-8F catalyzing (<i>R</i>)-4-hydroxy-4-(6-methoxy-2-naphthyl)-2-butanone degradation: <math>6.2 \pm 0.4 \text{ s}^{-1}</math>.</p> <p>▪ <math>k_{cat}</math> of soluble RA95.5-8F catalyzing (<i>R</i>)-4-hydroxy-4-(6-methoxy-2-naphthyl)-2-butanone degradation: <math>4.3 \pm 0.1 \text{ s}^{-1}</math>.</p> <p>▪ <math>k_{cat}/K_m</math> of immobilized RA95.5-8F catalyzing (<i>R</i>)-4-hydroxy-4-(6-methoxy-2-naphthyl)-2-</p>		

		<p>butanone degradation: <math>(2.2 \pm 0.2) \times 10^4 \text{ M}^{-1}\text{s}^{-1}</math>.</p> <ul style="list-style-type: none"> <li>▪ <math>k_{cat}/K_m</math> of soluble RA95.5-8F catalyzing (R)-4-hydroxy-4-(6-methoxy-2-naphthyl)-2-butanone degradation: <math>(1.4 \pm 0.2) \times 10^4 \text{ M}^{-1}\text{s}^{-1}</math>.</li> </ul>		
	<p>Carbonic anhydrase 2 (<i>Homo sapiens</i>) (N-terminus) (<i>E. coli</i> BL21-Gold (DE3))</p>	<ul style="list-style-type: none"> <li>▪ <math>k_{cat}/K_m</math> of immobilized carbonic anhydrase 2 catalyzing 4-nitrophenyl acetate degradation: <math>(1.2 \pm 0.3) \times 10^4 \text{ M}^{-1}\text{s}^{-1}</math>.</li> <li>▪ <math>k_{cat}/K_m</math> of soluble carbonic anhydrase 2 catalyzing 4-nitrophenyl acetate degradation: <math>(1.4 \pm 0.4) \times 10^3 \text{ M}^{-1}\text{s}^{-1}</math>.</li> </ul>		
<p><i>Myxococcus xanthus</i> Encapsulin ScP subunit</p>	<p>Pyruvate decarboxylase, Aro10p (<i>Saccharomyces cerevisiae</i>) (C-terminus) (<i>Saccharomyces cerevisiae</i> PK2-1D)</p>	<ul style="list-style-type: none"> <li>▪ Decarboxylation activity of immobilized Aro10p catalyzing 4-hydroxyphenylpyruvate conversion to 4-hydroxyphenylacetaldehyde is consistent with its non-immobilized counterpart.</li> </ul>	<ul style="list-style-type: none"> <li>▪ Enhanced protection against proteolytic degradation.</li> </ul>	(136) ^*

Extracellular membrane vesicles (EMVs)				
Outer membrane vesicles (OMV) via <i>Pseudomonas syringae</i> INA5 ice nucleation protein InaV	Endoglucanase CelA <i>(Clostridium thermocellum)</i> (N-terminus) <i>(E. coli</i> JC8031)	▪ Artificial enzyme cascading system comprised of immobilized CelA, CelE, and CelG had enhanced glucose production (~23-fold higher) compared to its soluble counterpart.	▪ N/A	(137) ^*
	Exoglucanase CelE <i>(Candida cellulytica)</i> (N-terminus) <i>(E. coli</i> JC8031)			
	Endoglucanase CelG <i>(Candida cellulytica)</i> (N-terminus) <i>(E. coli</i> JC8031)			
	Organophosphorus hydrolase, OpdA <i>(Flavobacterium</i> sp. strain ATCC 27551)	▪ Enhanced paraoxon degradation rate with notable improvement in overall enzyme kinetics upon immobilization.	▪ Enhanced thermal and pH stability. ▪ Retained at least ~83% of its initial activity	(89) ^

	<p>(N-terminus)</p> <p>(<i>E. coli</i> JC8031)</p>	<ul style="list-style-type: none"> <li>▪ <math>K_m</math> of immobilized OpdA on OMV catalyzing paraoxon hydrolysis: <math>42.14 \pm 5.22 \mu\text{M}</math>.</li> <li>▪ <math>K_m</math> of OpdA-OMV immobilized on microcrystalline cellulose catalyzing paraoxon hydrolysis: <math>51.27 \pm 8.14 \mu\text{M}</math>.</li> <li>▪ <math>K_m</math> of soluble OpdA catalyzing paraoxon hydrolysis: <math>47.95 \pm 9.36 \mu\text{M}</math>.</li> <li>▪ <math>k_{cat}</math> of immobilized OpdA on OMV catalyzing paraoxon hydrolysis: <math>5716 \pm 379 \text{ s}^{-1}</math>.</li> <li>▪ <math>k_{cat}</math> of OpdA-OMV immobilized on microcrystalline cellulose catalyzing paraoxon hydrolysis: <math>5579 \pm 336 \text{ s}^{-1}</math>.</li> <li>▪ <math>k_{cat}</math> of soluble OpdA catalyzing paraoxon hydrolysis: <math>3513 \pm 216 \text{ s}^{-1}</math>.</li> <li>▪ <math>k_{cat}/K_m</math> of immobilized OpdA on OMV catalyzing paraoxon hydrolysis: <math>135.64 \pm 63.86 \mu\text{M}^{-1} \text{ s}^{-1}</math>.</li> <li>▪ <math>k_{cat}/K_m</math> of OpdA-OMV immobilized on microcrystalline cellulose catalyzing paraoxon</li> </ul>	<p>after fifteen reaction cycles. Retained ~20-30% of its initial activity after 40 days of storage.</p>	
--	--	---	--	--

		<p>hydrolysis: <math>108.82 \pm 18.48 \mu\text{M}^{-1}\text{s}^{-1}</math>.</p> <ul style="list-style-type: none"> <li>▪ <math>k_{cat}/K_m</math> of soluble OpdA catalyzing paraoxon hydrolysis: <math>73.26 \pm 19.28 \mu\text{M}^{-1}\text{s}^{-1}</math>.</li> </ul>		
<p>Outer membrane vesicles via <i>E. coli</i> outer membrane porin protein OmpA</p>	<p>Phosphotriesterase (<i>Brevundimonas diminuta</i>) (C-terminus) (<i>E. coli</i> BL21(DE3))</p>	<ul style="list-style-type: none"> <li>▪ Consistent with its soluble counterpart but showed enhanced activity under certain conditions.</li> <li>▪ <math>K_m</math> of immobilized phosphotriesterase catalyzing paraoxon hydrolysis: <math>47.3 \pm 3.1 \mu\text{M}</math>.</li> <li>▪ <math>K_m</math> of soluble phosphotriesterase reported in the literature catalyzing paraoxon hydrolysis: <math>90 \mu\text{M}</math>.</li> <li>▪ <math>k_{cat}</math> of immobilized phosphotriesterase catalyzing paraoxon hydrolysis: <math>2088.7 \pm 47.8 \text{ s}^{-1}</math>.</li> <li>▪ <math>k_{cat}</math> of soluble phosphotriesterase reported in the literature catalyzing paraoxon hydrolysis: <math>2,400 \text{ s}^{-1}</math>.</li> <li>▪ <math>k_{cat}/K_m</math> of immobilized phosphotriesterase catalyzing</li> </ul>	<ul style="list-style-type: none"> <li>▪ Less prone to enzyme inactivation by freezing, lyophilization.</li> <li>▪ Challenging long-term storage and environment conditions.</li> </ul>	<p>(90, 93, 94) ^</p>

		<p>paraoxon hydrolysis: <math>(4.42 \pm 0.23) \times 10^7 \text{ M}^{-1} \text{ s}^{-1}</math>.</p> <ul style="list-style-type: none"> <li>▪ <math>k_{cat}/K_m</math> of soluble phosphotriesterase reported in the literature catalyzing paraoxon hydrolysis: <math>2.7 \times 10^7 \text{ M}^{-1} \text{ s}^{-1}</math>.</li> </ul>		
<b>Magnetosomes</b>				
Magnetosome membrane protein MamC	<p>Organophospho hydrolase, OpdA (<i>Flavobacterium</i> sp. ATCC 27551) (<i>Magnetospirillum magneticum</i> AMB-1)</p>	<ul style="list-style-type: none"> <li>▪ <math>K_m</math> of immobilized OpdA catalyzing ethyl-paraoxon hydrolysis: <math>58 \pm 2.5 \text{ } \mu\text{M}</math>.</li> <li>▪ <math>K_m</math> of soluble OpdA catalyzing ethyl-paraoxon hydrolysis: <math>43 \pm 1.8 \text{ } \mu\text{M}</math>.</li> <li>▪ <math>k_{cat}</math> of immobilized OpdA catalyzing ethyl-paraoxon hydrolysis: <math>151 \pm 6 \text{ s}^{-1}</math>.</li> <li>▪ <math>k_{cat}</math> of soluble OpdA catalyzing ethyl-paraoxon hydrolysis: <math>314 \pm 13 \text{ s}^{-1}</math>.</li> </ul>	<ul style="list-style-type: none"> <li>▪ Stable over six reaction cycles.</li> </ul>	(106) ^
	<p><math>\beta</math>-glucuronidase (<i>E. coli</i>) (C-terminus) (<i>Magnetospirillum</i>)</p>	<ul style="list-style-type: none"> <li>▪ <math>K_m</math> of immobilized <math>\beta</math>-glucuronidase catalyzing <i>p</i>-nitrophenyl-<math>\beta</math>-D-glucuronide hydrolysis: <math>0.17 \times 10^{-3}</math>– <math>0.18 \times 10^{-3} \text{ M}</math>.</li> </ul>	<ul style="list-style-type: none"> <li>▪ Retained at least ~75% of its initial activity after ten reaction cycles.</li> </ul>	(107)

	<i>gryphiswaldens</i> e)	<ul style="list-style-type: none"> <li>▪ <math>K_m</math> of soluble <math>\beta</math>-glucuronidase catalyzing <i>p</i>-nitrophenyl-<math>\beta</math>-D-glucuronide hydrolysis: <math>0.28 \times 10^{-3}</math> M.</li> <li>▪ Specific activity of immobilized <math>\beta</math>-glucuronidase catalyzing <i>p</i>-nitrophenyl-<math>\beta</math>-D-glucuronide hydrolysis: 15.1–16.3 U/mg of enzyme.</li> <li>▪ Specific activity of soluble <math>\beta</math>-glucuronidase catalyzing <i>p</i>-nitrophenyl-<math>\beta</math>-D-glucuronide hydrolysis: 12.7 U/mg of enzyme.</li> </ul>		
Magnetosome membrane protein Mms13	Endoglucanase A <i>(Clostridium thermocellum)</i> (C-terminus) <i>(Magnetospirillum magneticum AMB-1)</i>  $\beta$ -glucosidase <i>(Clostridium thermocellum)</i>	<ul style="list-style-type: none"> <li>▪ Artificial enzyme cascading system comprised of these two enzymes showed catalytic activity catalyzing the hydrolysis of carboxymethyl cellulose and Avicel.</li> <li>▪ Co-immobilization of endoglucanase A and <math>\beta</math>-glucosidase on magnetosomes showed enhanced catalytic activity catalyzing the hydrolysis of carboxymethyl cellulose when</li> </ul>	<ul style="list-style-type: none"> <li>▪ Retained at least ~70% of its initial activity after five reaction cycles.</li> </ul>	(108) ^*

	(C-terminus) <i>(Magnetospirillum magneticum AMB-1)</i>	compared to the suspension mixture of endoglucanase A immobilized magnetosomes and $\beta$ -glucosidase immobilized magnetosomes.		
--	--	---	--	--

<sup>^</sup> Specific and/or catalytic activities are not mentioned in the reference.

\* Kinetic parameters are not mentioned in the reference.

## 2.5. Comparative Analysis of *In Vivo* Immobilization Strategies

### 2.5.1 Advantages and current limitations of the recombinant PHA particle technology

Genetic engineering of PAPs represents an interesting approach for enzyme immobilization on PHA particles. Foreign proteins of interest can be translationally fused to the N- or C-terminus, or both termini of PAPs. The broad applicability and versatility of this approach also allows for the attachment of more than one enzyme to the PHA particle surface (62, 138, 139). Assembly of immobilized multiprotein complexes enables multi-enzymatic cascade systems with superior catalytic performance as recently reviewed (140). Flexible, rigid, and cleavable peptide linkers, such as intein peptide pairs (141) and LPXTG cleavage sites (sortase A-mediated hydrolysis/ligation) (142), can be incorporated between the protein functions and PAPs to mediate release of pure target protein (21, 143). However, underlying molecular mechanisms of PHA particle formation still remain unknown, which intrinsically limits control of their physicochemical properties. For example, a few studies reported that fusing different proteins to PhaC influences the PHA production yield over

biomass, particle size distribution, surface charges, and purity of the target protein (144-147). Decorating PHA particles with proteins using PhaC synthase as an anchoring domain can also cause varying distribution and density of respective proteins on the PHA particles (62, 147). Hooks et al. (2013) also pointed out that displaying *N*-acetylneuraminic acid aldolase (NanA) from *E. coli* on PHA particles through N- and C-terminal fusion of PhaC resulted in varying catalytic performance (112). Moreover, similar findings were reported for phasins where fusion of different foreign polypeptides to the BioF tag (PHA-binding domain of PhaF) might have contributed to inconsistency of the physical adsorption function of the BioF-tagged enzyme to the PHA particle surface (58). A brief comparison of the PHA particle technology with other biological assemblies, detailing their advantages and limitations, is provided in **Table 2**.

**Table 2.** Comparison of PHA particle technology with other biological supramolecular assemblies.

	Advantages	Limitations
Polyhydroxyalkanoates (PHAs)	<ul style="list-style-type: none"> <li>▪ Scalable particle production and able to offer better production yields over biomass</li> <li>▪ Facile particle functionalization and isolation steps</li> <li>▪ Structurally very stable</li> <li>▪ Can be manufactured in a range of recombinant expression systems</li> <li>▪ Biodegradable</li> </ul>	<ul style="list-style-type: none"> <li>▪ Poor controllability on the physico-chemical properties of the particles (<i>e.g.</i> particle size, size distribution, surface charge)–polydisperse and tend to aggregate</li> <li>▪ Concentration and the function of enzymes localized on the particles, and particle production yield</li> </ul>

	<ul style="list-style-type: none"> <li>▪ Enhanced shelf-life</li> </ul>	dependent on the folding status of the recombinant fusion proteins
<p>Protein-based particles</p> <ul style="list-style-type: none"> <li>• Virus-like particles (VLPs)</li> <li>• Enzyme-derived nanoparticles (EZPs)</li> </ul>	<ul style="list-style-type: none"> <li>▪ Highly programmable physico-chemical properties of particles (<i>e.g.</i> particle size, size distribution, surface charge)</li> <li>▪ Multiple modes of immobilization—tethered within and/or on the surface of particles, and between the CP/ScP subunits</li> <li>▪ Can be manufactured in a range of recombinant expression systems</li> <li>▪ Biodegradable</li> </ul>	<ul style="list-style-type: none"> <li>▪ Genetic alteration of CP/ScP subunits could trigger structural instability of these scaffolding platforms</li> <li>▪ Could lead to misfolding of the genetically fused enzymes, especially large domains due to steric hindrance</li> <li>▪ Labor intensive fabrication processes</li> <li>▪ Scalability issues</li> <li>▪ Space available to immobilize functional moieties is limited by the size of the scaffold itself</li> </ul>
<p>Extracellular membrane vesicles (EMVs)</p>	<ul style="list-style-type: none"> <li>▪ Easy decoration of vesicles</li> <li>▪ Enzymes of interest can be appended on the surface or within the vesicles</li> <li>▪ Can be manufactured in a range of recombinant expression systems</li> <li>▪ Biodegradable</li> </ul>	<ul style="list-style-type: none"> <li>▪ Poor particle programmability due to the lack of knowledge on the exact assembly mechanism of membrane vesicles</li> <li>▪ Large-scale consistent production could be difficult</li> <li>▪ Laborious and expensive isolation procedures</li> </ul>
<p>Magnetosomes</p>	<ul style="list-style-type: none"> <li>▪ Unique magnetic properties of magnetosomes could be advantageous in</li> </ul>	<ul style="list-style-type: none"> <li>▪ Tedious cloning steps and limited design space available for extensive</li> </ul>

	<p>some applications (<i>e.g.</i> magnetically-driven solid-liquid separation for re-use)</p> <ul style="list-style-type: none"> <li>▪ Consistent particle size, particle distribution, and architecture</li> </ul>	<p>alterations <i>in vivo</i> due to potential cell toxicity</p> <ul style="list-style-type: none"> <li>▪ Poor controllability in altering the magnetic properties—influenced by the specificity of magnetotactic bacteria</li> <li>▪ Magnetotactic bacteria are difficult to grow—prolonged production time and low production yields</li> </ul>
--	---	---

To circumvent these drawbacks regarding the utilization of the PHA particle technology, PhaC fusion technology is merged with the SpyTag/SpyCatcher chemistry (148), which enable better control over production yields and physicochemical properties (**Figure 3A**) (147). We successfully showed that the SpyTagged proteins could ligate to the SpyCatcher-PhaC coated PHA particles *in vitro*, and controlled multifunctionality of PHA particles could be achieved using a sequential immobilization strategy. This approach requires separate and more laborious production of enzymes and scaffold but offers more control over surface coverage and orientation/ratios of the attached proteins. Consistency of the particle size and surface charge of functionalized SpyCatcher-coated PHA particles were observed. Function and conformational stability of the ligated proteins were retained or enhanced (147). Recently this approach was expanded by developing streamlined processes exploiting the specificity of the SpyTag/SpyCatcher mediated ligation for efficient and cost-effective modular functionalization (149). Overall, PHA particles seem to provide a versatile platform for *in vivo* enzyme immobilization, providing competitive advantages over other

biological scaffolds (**Table 2**). The recent crystal structures, 3D-reconstructed, and homology models of several key PAPs, including *Cupriavidus necator* PhaC and some PhaPs will further inform protein engineering for efficient immobilization of enzymes (150-154).

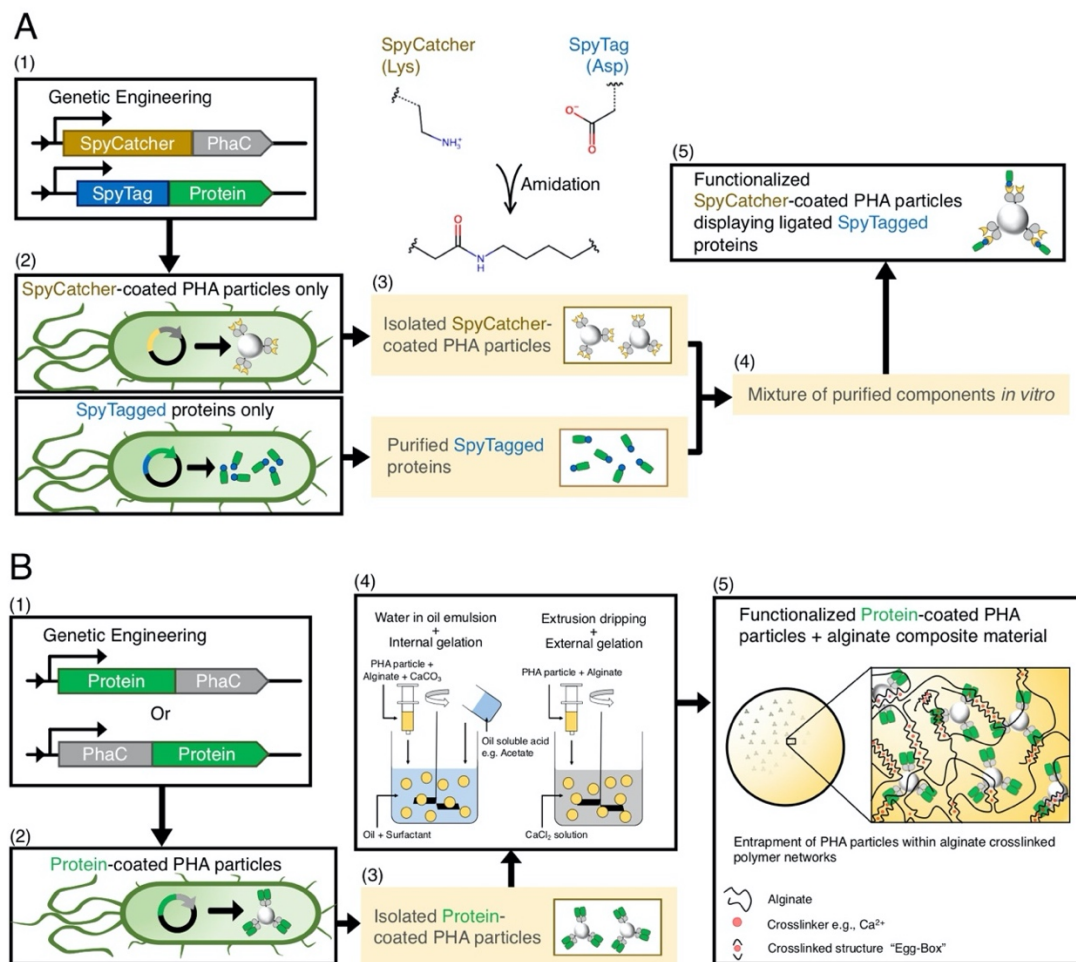


**Figure 3.** Innovative strategies to overcome the limitations of PHA particle technology. **(A)** Schematic overview of biosynthesis and modular functionalization of SpyCatcher-coated PHA particles. **(B)** Schematic illustration of manufacturing of functionalized PHA particles and subsequent fabrication of alginate-PHA composite materials.

### 2.5.2 Use of enzyme-coated PHA particles in continuous-flow bioprocessing

Immobilized enzymes are widely considered for continuous flow processing toward the synthesis of high-value chemicals (155-159). Continuous production of fine chemicals has the potential to accelerate biocatalytic transformations due to enhanced heat and mass transfer between immobilized enzymes and their substrates under flow conditions. The improvement in mass transfer allows the cost-effective miniaturized design of process equipment that ultimately could lead to precise process control and better production yield. Continuous bioprocessing could simplify downstream processing and permit the constant removal of products, such as processes limited by a thermodynamic equilibrium (160, 161). The physical format of the immobilized enzymes needs to be compatible with the continuous-flow process, such as tangential-flow filtration and packed bed/fluidized bed systems (162).

The lack of uniformity and/or the non-porous properties may restrict the utility of enzyme-coated PHA particles for industrial continuous bioprocesses. Apart from the inherent inconsistency of the PHA particles as outlined above, particulate carriers ( $< 1 \mu\text{m}$ ) are often prone to aggregation under various environmental conditions (*e.g.* pH, temperature, and ionic strength), which impairs substrate access to the enzymes (163, 164) and which could adversely affect their performance in continuous flow processes. The non-porous nature of PHA particles (31) and their tendency to aggregate has the potential to cause extensive backpressure in flow-through applications (165). One innovative solution to overcome these issues is to encapsulate the functionalized PHA particles into a porous hydrogel

matrix for efficient integration of enzyme-coated PHA particles into continuous-flow bioprocesses. We recently described an innovative approach that encapsulates functionalized PHA particles within a highly amenable anionic polysaccharide, alginate. The particle–hydrogel composite material was fabricated using the ionotropic gelation method with calcium ion as the cross-linker (**Figure 3B**) (165). Interestingly, the porosity of the alginate microsphere encapsulating functional protein-coated PHA particles could be controlled by pH during the fabrication process, showing the flexibility of this approach. The various functional protein-coated PHA particles encapsulated within alginate microspheres showed either retained (*e.g.* organophosphorus hydrolase) or enhanced (*e.g.* immunoglobulin G-binding ZZ domain) activities in both batch and flow-through mode suggesting suitability for industrial applications (165).

### 2.5.3 Potential industrial applications of the PHA particle technology

There is a widespread agreement that enzyme mediated bioprocesses are environmentally benign as, for example, they reduce consumption of raw materials and energy, while generally able to maintain low levels of waste generation than the traditional non-enzymatic processes (166). The use of enzymes in large-scale manufacturing could reduce the greenhouse gas emissions when compared to the traditional non-enzymatic processes (167). Therefore, due to the disadvantages in using industrially relevant enzymes in soluble form as mentioned, direct attachment of these enzymes to solid scaffolds, including PHAs, has emerged as one of the commercially viable solutions. The advent of PHA particle technology as a generic scaffolding platform for immobilization of enzymes has opened up new

routes to developing next-generation catalytic materials for sustainable bioprocessing. We have summarized the recent proof-of-concept demonstrations of the PHA particle technology for industrial applications reported by our group and others (**Table 1**). Task-specific designer PHA particles can be biosynthesized to serve different industrial applications including the manufacture of commodity chemicals, food products, active pharmaceutical ingredients, and cosmetic chemicals (168). Furthermore, the PHA particle technology can be implemented as a bioremediation tool for the treatment of industrial waste effluents and agricultural pollutants (35).

Since bulk chemicals, such as *e.g.* commodity chemicals and food products, are produced at ton scale, high catalytic turnover and ease of recycling of biocatalysts are required for economic feasibility (166, 169). Biocatalysts also need to be very stable and available at low cost (169). In contrast, production of fine chemicals, such as *e.g.* active pharmaceutical ingredients, and cosmetic chemicals, is often associated with lower unit production volumes (*e.g.* hundreds of kilograms) but higher production yields (169). As the synthesis of these high-value products requires a certain degree of regioselectivity, enantioselectivity, and chemoselectivity (170, 171), these requirements also need to be considered. Because of the stringent need for precise process control to achieve the target product quality, successful implementation of continuous manufacture in bioprocessing will benefit from the use of enzyme-coated PHA particles for fine-chemical production (161). For bioremediation application the PHA particle technology offers advantages such as biodegradability of the non-toxic natural PHA scaffold (172, 173). In recent years, the release of nanoparticles into the environment has sparked some concerns by the research community (174, 175).

Given the encouraging proof-of-concept results that have been reported for the adaptation of PHA particle technology for development of immobilized enzymes for uses in the food industry (110, 114, 116, 117), production of commodity chemicals (60, 113, 120), production of fine chemicals (112, 115, 119), and bioremediation (61, 111, 121), it is anticipated that research prototypes will be developed into industrial products.

## 2.6 Conclusions and Future Perspectives

Advances in the development of several promising biological supramolecular assemblies suitable for *in vivo* enzyme immobilization have been reviewed and a comparison of PHA particle technology with the other scaffolding platforms made. Innovative strategies to address the challenges associated with developing enzyme-coated PHA particles for industrial applications of the technology in industry have been discussed. Immobilized enzymes exhibit distinct advantages over soluble enzymes, including enhanced stability, improved catalytic performance, recycling, and facilitated product purification. The emergence of biologically inspired particulate carriers has been shown to offer promising scaffolding platforms for one-pot *in vivo* enzyme immobilization. Though significant progress has already been made to date, numerous challenges, such as high production costs and lack of control over a range of physicochemical properties, still remain in order for this technology to be advanced beyond proof-of-concept.

As the field of synthetic biology continues to expand rapidly, a more profound understanding of the underlying molecular mechanisms of *in vivo* particle assembly will further

inform the rational design of assembled enzyme-carrier systems. The elucidation of such biological processes will inform strategies to control several aspects as, for instance, simultaneous PHA particle production and functionalization rational molecular engineering approaches. Such customizable features would allow the creation of, for example, application-specific designer PHA particles for a variety of operating environments. These remarkable advances will lay the foundation for the development of monodisperse PHA particles of controllable and reproducible structure and size. Also, it will be equally attractive to develop recombinant PHA particles with programmable surface properties, such as enzyme density/exposure and surface charge. One remaining challenge is control of the spatial organization and density of immobilized enzymes on PHA particles. Furthermore, implementing innovative strategies, such as the concept of modularity, fabrication of particle-hydrogel composite materials, and integrated multifunctionality, should increasingly enable implementation of industrial flow-through processes. The development of robust enzyme-carrier systems with porous structures will be critical to ensure implementation for cost-effective continuous biocatalytic conversion and synthesis reactions.

The versatile PHA particle technology offers avenues to immobilize a range of industrially relevant enzymes for development of the next generation biocatalytic processes. However, the successful "bench-to-factory" translation still requires rigorous optimization and validation to meet industry standards. Additionally, perception barriers as, for instance, the traditional way of thinking and the limited understanding of sustainable bioprocessing, especially among the manufacturers and regulatory authorities, could hinder their application. Therefore, bridging interdisciplinary boundaries between researchers from the field

of molecular biology, chemical engineering, chemistry, and material science should be encouraged. It is critical to integrate diverse methodologies and strategies to further advance *in vivo* enzyme immobilization technologies such as PHA particle technology.

### **Author Contributions**

Ogura, K. wrote section “Enzyme Immobilization for Industrial Applications” of the manuscript, Chen, S. wrote section “Utilization of Various Supramolecular Assemblies as Enzyme Immobilization Supports” of the manuscript, and **Wong, J. X.** wrote Sections “Utilization of Various Supramolecular Assemblies as Enzyme Immobilization Supports”, “Biological Supramolecular Assemblies as Biocatalyst Supports” and “Comparative Analysis of *In Vivo* Immobilization Strategies” of the manuscript. Rehm, B. H. A. provided critical input in regard to structure, content, and language of the manuscript. All authors provided critical feedback and approved the final version of the manuscript.

### **Funding**

This work was supported by the MacDiarmid Institute of Advanced Materials and Nanotechnology (New Zealand) and School of Fundamental Sciences, Massey University (New Zealand) and Griffith Institute for Drug Discovery, Griffith University (Australia).

## Conflict of Interest Statement

B. H. A. Rehm is co-founder and shareholder of PolyBatics Ltd that commercializes veterinary TB diagnostic products related to the PHA particle technology.

## 2.7 References

1. Robinson PK. Enzymes: principles and biotechnological applications. *Essays Biochem.* 2015;59:1-41.
2. Chapman J, Ismail A, Dinu C. Industrial applications of enzymes: Recent advances, techniques, and outlooks. *Catalysts.* 2018;8(6):238.
3. Mohamad NR, Marzuki NHC, Buang NA, Huyop F, Wahab RA. An overview of technologies for immobilization of enzymes and surface analysis techniques for immobilized enzymes. *Biotechnol. Biotechnol. Equip.* 2015;29(2):205-20.
4. Cipolatti EP, Manoel EA, Fernandez-Lafuente R, Freire DMG. Support engineering: relation between development of new supports for immobilization of lipases and their applications. *Biotech. Res. Innov.* 2017;1(1):26-34.
5. Ren S, Li C, Jiao X, Jia S, Jiang Y, Bilal M, et al. Recent progress in multienzymes co-immobilization and multienzyme system applications. *Chem. Eng. J.* 2019;373:1254-78.
6. Hartmeier W. Immobilized biocatalysts: An introduction: Springer Science & Business Media; 2012.

7. Yang Q, Wang B, Zhang Z, Lou D, Tan J, Zhu L. The effects of macromolecular crowding and surface charge on the properties of an immobilized enzyme: activity, thermal stability, catalytic efficiency and reusability. *RSC Adv.* 2017;7(60):38028-36.
8. Zaak H, Siar E-H, Kornecki JF, Fernandez-Lopez L, Pedrero SG, Virgen-Ortíz JJ, et al. Effect of immobilization rate and enzyme crowding on enzyme stability under different conditions. The case of lipase from *Thermomyces lanuginosus* immobilized on octyl agarose beads. *Process Biochem.* 2017;56:117-23.
9. Jia J, Peng X, Qi W, Su R, He Z. Effects of macromolecular crowding on alkaline phosphatase unfolding, conformation and stability. *Int. J. Biol. Macromol.* 2017;101:373-82.
10. Fu J, Liu M, Liu Y, Woodbury NW, Yan H. Interenzyme substrate diffusion for an enzyme cascade organized on spatially addressable DNA nanostructures. *J. Am. Chem. Soc.* 2012;134(12):5516-9.
11. Rodrigues RC, Ortiz C, Berenguer-Murcia Á, Torres R, Fernández-Lafuente R. Modifying enzyme activity and selectivity by immobilization. *Chem. Soc. Rev.* 2013;42(15):6290-307.
12. Minton AP. Effect of a concentrated “inert” macromolecular cosolute on the stability of a globular protein with respect to denaturation by heat and by chaotropes: a statistical-thermodynamic model. *Biophys. J.* 2000;78(1):101-9.
13. Bernal C, Rodríguez K, Martínez R. Integrating enzyme immobilization and protein engineering: an alternative path for the development of novel and improved industrial biocatalysts. *Biotechnol. Adv.* 2018;36(5):1470-80.

14. Zdarta J, Meyer A, Jesionowski T, Pinelo M. A general overview of support materials for enzyme immobilization: characteristics, properties, practical utility. *Catalysts*. 2018;8(2):92.
15. Homaei AA, Sariri R, Vianello F, Stevanato R. Enzyme immobilization: an update. *J. Chem. Biol.* 2013;6(4):185-205.
16. Guisan JM. Immobilization of enzymes and cells: Springer Science & Business Media; 2006.
17. Cao X, Li Y, Zhang Z, Yu J, Qian J, Liu S. Catalytic activity and stability of glucose oxidase/horseradish peroxidase co-confined in macroporous silica foam. *Analyst*. 2012;137(24):5785-91.
18. Fernandez-Lopez L, Pedrero SG, Lopez-Carrobbles N, Gorines BC, Virgen-Ortíz JJ, Fernandez-Lafuente R. Effect of protein load on stability of immobilized enzymes. *Enzyme Microb. Technol.* 2017;98:18-25.
19. Rehm FB, Chen S, Rehm B. Enzyme engineering for *in situ* immobilization. *Molecules*. 2016;21(10):1370.
20. Nguyen HH, Kim M. An overview of techniques in enzyme immobilization. *Appl. Sci. Conver. Technol.* 2017;26(6):157-63.
21. Rehm FB, Chen S, Rehm BH. Bioengineering toward direct production of immobilized enzymes: a paradigm shift in biocatalyst design. *Bioengineered*. 2018;9(1):6-11.
22. Faccio G. From protein features to sensing surfaces. *Sensors*. 2018;18(4):1204.

23. Gonzalez-Miro M, Chen S, Gonzaga ZJ, Evert B, Wibowo D, Rehm BHA. Polyester as antigen carrier toward particulate vaccines. *Biomacromolecules*. 2019;20(9):3213-32.
24. Sletten EM, Bertozzi CR. Bioorthogonal chemistry: Fishing for Selectivity in a Sea of Functionality. *Angew. Chem., Int. Ed.* 2009;48(38):6974-98.
25. Hess GT, Cragnolini JJ, Popp MW, Allen MA, Dougan SK, Spooner E, et al. M13 bacteriophage display framework that allows sortase-mediated modification of surface-accessible phage proteins. *Bioconjugate Chem.* 2012;23(7):1478-87.
26. Brune KD, Leneghan DB, Brian IJ, Ishizuka AS, Bachmann MF, Draper SJ, et al. Plug-and-Display: decoration of virus-like particles via isopeptide bonds for modular immunization. *Sci. Rep.* 2016;6:19234.
27. Krauss U, Jäger VD, Diener M, Pohl M, Jaeger K-E. Catalytically-active inclusion bodies—carrier-free protein immobilizates for application in biotechnology and biomedicine. *J. Biotechnol.* 2017;258:136-47.
28. Schmid-Dannert C, López-Gallego F. Advances and opportunities for the design of self-sufficient and spatially organized cell-free biocatalytic systems. *Curr. Opin. Chem. Biol.* 2019;49:97-104.
29. Wilkerson JW, Yang S-O, Funk PJ, Stanley SK, Bundy BC. Nanoreactors: strategies to encapsulate enzyme biocatalysts in virus-like particles. *New Biotechnol.* 2018;44:59-63.
30. Parlane NA, Gupta SK, Rubio-Reyes P, Chen S, Gonzalez-Miro M, Wedlock DN, et al. Self-assembled protein-coated polyhydroxyalkanoate beads: properties and biomedical applications. *ACS Biomater. Sci. Eng.* 2016;3(12):3043-57.

31. Hooks DO, Venning-Slater M, Du J, Rehm B. Polyhydroxyalkanoate synthase fusions as a strategy for oriented enzyme immobilisation. *Molecules*. 2014;19(6):8629-43.
32. Schwarz B, Uchida M, Douglas T. Biomedical and catalytic opportunities of virus-like particles in nanotechnology. In: Kielian M, Mettenleiter TC, Roossinck MJ, editors. *Advances in Virus Research*. 97: Academic Press; 2017. p. 1-60.
33. Diaz D, Care A, Sunna A. Bioengineering strategies for protein-based nanoparticles. *Genes*. 2018;9(7):370.
34. Raeeszadeh-Sarmazdeh M, Hartzell E, Price JV, Chen W. Protein nanoparticles as multifunctional biocatalysts and health assessment sensors. *Curr. Opin. Chem. Eng.* 2016;13:109-18.
35. Sharma B, Dangi AK, Shukla P. Contemporary enzyme based technologies for bioremediation: A review. *J. Environ. Manage.* 2018;210:10-22.
36. Yan L, Da H, Zhang S, López VM, Wang W. Bacterial magnetosome and its potential application. *Microbiol. Res.* 2017;203:19-28.
37. Jacob JJ, Suthindhiran K. Magnetotactic bacteria and magnetosomes – Scope and challenges. *Mater. Sci. Eng. C*. 2016;68:919-28.
38. Moradali MF, Rehm BHA. Bacterial biopolymers: from pathogenesis to advanced materials. *Nat. Rev. Microbiol.* 2020;In press:In press.
39. Rehm BH. Polyester synthases: natural catalysts for plastics. *Biochem. J.* 2003;376(1):15-33.
40. Rehm BH. Bacterial polymers: biosynthesis, modifications and applications. *Nat. Rev. Microbiol.* 2010;8(8):578.

41. Steinmann B, Christmann A, Heiseler T, Fritz J, Kolmar H. *In vivo* enzyme immobilization by inclusion body display. *Appl. Environ. Microbiol.* 2010;76(16):5563-9.
42. Kikkawa Y, Narike M, Hiraishi T, Kanesato M, Sudesh K, Doi Y, et al. Organization of polyhydroxyalkanoate synthase for *in vitro* polymerization as revealed by atomic force microscopy. *Macromol. Biosci.* 2005;5(10):929-35.
43. Campisano A, Overhage J, Rehm BH. The polyhydroxyalkanoate biosynthesis genes are differentially regulated in planktonic-and biofilm-grown *Pseudomonas aeruginosa*. *J. Biotechnol.* 2008;133(4):442-52.
44. Koller M, Salerno A, Dias M, Reiterer A, Braunegg G. Modern biotechnological polymer synthesis: a review. *Food Technol. Biotechnol.* 2010;48(3):255-69.
45. Lee SY. High cell-density culture of *Escherichia coli*. *Trends Biotechnol.* 1996;14(3):98-105.
46. Mathuriya AS, Yakhmi J. Polyhydroxyalkanoates: Biodegradable plastics and their applications. *Handbook of Ecomaterials.* 2017:1-29.
47. Keshavarz T, Roy I. Polyhydroxyalkanoates: bioplastics with a green agenda. *Curr. Opin. Microbiol.* 2010;13(3):321-6.
48. Rehm BH. Biogenesis of microbial polyhydroxyalkanoate granules: a platform technology for the production of tailor-made bioparticles. *Curr. Issues Mol. Biol.* 2007;9(1):41.
49. Ross G, Ross S, Tighe BJ. Bioplastics: new routes, new products. *Brydson's Plastics Materials: Elsevier;* 2017. p. 631-52.

50. Philip S, Keshavarz T, Roy I. Polyhydroxyalkanoates: biodegradable polymers with a range of applications. *J. Chem. Technol. Biotechnol.* 2007;82(3):233-47.
51. Meng D-C, Shen R, Yao H, Chen J-C, Wu Q, Chen G-Q. Engineering the diversity of polyesters. *Curr. Opin. Biotechnol.* 2014;29:24-33.
52. Peoples OP, Sinskey AJ. Poly-beta-hydroxybutyrate (PHB) biosynthesis in *Alcaligenes eutrophus* H16. Identification and characterization of the PHB polymerase gene (phbC). *J. Biol. Chem.* 1989;264(26):15298-303.
53. Peoples OP, Sinskey AJ. Poly-beta-hydroxybutyrate biosynthesis in *Alcaligenes eutrophus* H16. Characterization of the genes encoding beta-ketothiolase and acetoacetyl-CoA reductase. *J. Biol. Chem.* 1989;264(26):15293-7.
54. Taguchi S, Doi Y. Evolution of polyhydroxyalkanoate (PHA) production system by “enzyme evolution”: successful case studies of directed evolution. *Macromol. Biosci.* 2004;4(3):145-56.
55. Pieper-Fürst U, Madkour MH, Mayer F, Steinbüchel A. Purification and characterization of a 14-kilodalton protein that is bound to the surface of polyhydroxyalkanoic acid granules in *Rhodococcus ruber*. *J. Bacteriol.* 1994;176(14):4328-37.
56. Wieczorek R, Pries A, Steinbüchel A, Mayer F. Analysis of a 24-kilodalton protein associated with the polyhydroxyalkanoic acid granules in *Alcaligenes eutrophus*. *J. Bacteriol.* 1995;177(9):2425-35.
57. Tarazona NA, Machatschek R, Schulz B, Prieto MA, Lendlein A. Molecular insights into the physical adsorption of amphiphilic protein PhaF onto copolyester surfaces. *Biomacromolecules.* 2019;20(9):3242-52.

58. Bello-Gil D, Maestro B, Fonseca J, Dinjaski N, Prieto MA, Sanz JM. Poly-3-hydroxybutyrate functionalization with BioF-tagged recombinant proteins. *Appl. Environ. Microbiol.* 2018;84(4):e02595-17.
59. Bello-Gil D, Roig-Molina E, Fonseca J, Sarmiento-Ferrández MD, Ferrándiz M, Franco E, et al. An enzymatic system for decolorization of wastewater dyes using immobilized CueO laccase-like multicopper oxidase on poly-3-hydroxybutyrate. *Microb. Biotechnol.* 2018;11(5):881-92.
60. Jahns AC, Rehm BH. Immobilization of active lipase B from *Candida antarctica* on the surface of polyhydroxyalkanoate inclusions. *Biotechnol. Lett.* 2015;37(4):831-5.
61. Hooks DO, Rehm BH. Surface display of highly-stable *Desulfovibrio vulgaris* carbonic anhydrase on polyester beads for CO<sub>2</sub> capture. *Biotechnol. Lett.* 2015;37(7):1415-20.
62. Hay ID, Du J, Burr N, Rehm BH. Bioengineering of bacteria to assemble custom-made polyester affinity resins. *Appl. Environ. Microbiol.* 2015;81(1):282-91.
63. Grage K, Jahns AC, Parlane N, Palanisamy R, Rasiah IA, Atwood JA, et al. Bacterial Polyhydroxyalkanoate Granules: Biogenesis, Structure, and Potential Use as Nano-/Micro-Beads in Biotechnological and Biomedical Applications. *Biomacromolecules.* 2009;10(4):660-9.
64. Charlton Hume HK, Vidigal J, Carrondo MJ, Middelberg AP, Roldão A, Lua LH. Synthetic biology for bioengineering virus-like particle vaccines. *Biotechnol. Bioeng.* 2019;116(4):919-35.

65. Janitzek CM, Peabody J, Thrane S, Carlsen PH, Theander TG, Salanti A, et al. A proof-of-concept study for the design of a VLP-based combinatorial HPV and placental malaria vaccine. *Sci. Rep.* 2019;9(1):5260.
66. Tan M, Jiang X. Recent advancements in combination subunit vaccine development. *Hum. Vaccin. Immunother.* 2017;13(1):180-5.
67. Mohsen MO, Zha L, Cabral-Miranda G, Bachmann MF, editors. Major findings and recent advances in virus-like particle (VLP)-based vaccines. *Seminars in immunology*; 2017: Elsevier.
68. Torbensen K, Patel A, Anne A, Chovin A, Demaille C, Bataille L, et al. Immuno-based molecular scaffolding of glucose dehydrogenase and ferrocene mediator on fd viral particles yields enhanced bioelectrocatalysis. *ACS Catal.* 2019;9(6):5783-96.
69. Stanley S. Biological nanoparticles and their influence on organisms. *Curr. Opin. Biotechnol.* 2014;28:69-74.
70. Brasch M, Putri RM, de Ruiter MV, Luque D, Koay MS, Castón JR, et al. Assembling enzymatic cascade pathways inside virus-based nanocages using dual-tasking nucleic acid tags. *J. Am. Chem. Soc.* 2017;139(4):1512-9.
71. Koch C, Wabbel K, Eber FJ, Krolla-Sidenstein P, Azucena C, Gliemann H, et al. Modified TMV particles as beneficial scaffolds to present sensor enzymes. *Front. Plant Sci.* 2015;6:1137.
72. Giessen TW, Silver PA. Widespread distribution of encapsulin nanocompartments reveals functional diversity. *Nat. Microbiol.* 2017;2(6):17029.
73. Azuma Y, Edwardson TG, Hilvert D. Tailoring lumazine synthase assemblies for bionanotechnology. *Chem. Soc. Rev.* 2018;47(10):3543-57.

74. Arosio P, Ingrassia R, Cavadini P. Ferritins: a family of molecules for iron storage, antioxidation and more. *Biochim. Biophys. Acta.* 2009;1790(7):589-99.
75. Lee EJ. Recent advances in protein-based nanoparticles. *Korean J. Chem. Eng.* 2018;35(9):1765-78.
76. Hsia Y, Bale JB, Gonen S, Shi D, Sheffler W, Fong KK, et al. Design of a hyperstable 60-subunit protein icosahedron. *Nature.* 2016;535(7610):136.
77. Xu Y, Jiang S, Simmons CR, Narayanan RP, Zhang F, Aziz A-M, et al. Tunable nanoscale cages from self-assembling DNA and protein building blocks. *ACS Nano.* 2019;13(3):3545-54.
78. King NP, Bale JB, Sheffler W, McNamara DE, Gonen S, Gonen T, et al. Accurate design of co-assembling multi-component protein nanomaterials. *Nature.* 2014;510(7503):103.
79. Bale JB, Gonen S, Liu Y, Sheffler W, Ellis D, Thomas C, et al. Accurate design of megadalton-scale two-component icosahedral protein complexes. *Science.* 2016;353(6297):389-94.
80. Jakobson CM, Slininger Lee MF, Tullman-Ercek D. *De novo* design of signal sequences to localize cargo to the 1, 2-propanediol utilization microcompartment. *Protein Sci.* 2017;26(5):1086-92.
81. Raposo G, Stoorvogel W. Extracellular vesicles: exosomes, microvesicles, and friends. *J. Cell Biol.* 2013;200(4):373-83.
82. Lee H-J. Microbe-host communication by small RNAs in extracellular vesicles: vehicles for transkingdom RNA transportation. *Int. J. Mol. Sci.* 2019;20(6):1487.

83. Gill S, Catchpole R, Forterre P. Extracellular membrane vesicles in the three domains of life and beyond. *FEMS Microbiol. Rev.* 2018;43(3):273-303.
84. Van der Pol E, Böing AN, Harrison P, Sturk A, Nieuwland R. Classification, functions, and clinical relevance of extracellular vesicles. *Pharmacol. Rev.* 2012;64(3):676-705.
85. Longatti A, Schindler C, Collinson A, Jenkinson L, Matthews C, Fitzpatrick L, et al. High affinity single-chain variable fragments are specific and versatile targeting motifs for extracellular vesicles. *Nanoscale.* 2018;10(29):14230-44.
86. Burkova EE, Dmitrenok PS, Bulgakov DV, Vlassov VV, Ryabchikova EI, Nevinsky GA. Exosomes from human placenta purified by affinity chromatography on sepharose bearing immobilized antibodies against CD81 tetraspanin contain many peptides and small proteins. *IUBMB Life.* 2018;70(11):1144-55.
87. Cocucci E, Meldolesi J. Ectosomes and exosomes: shedding the confusion between extracellular vesicles. *Trends Cell Biol.* 2015;25(6):364-72.
88. Greening DW, Simpson RJ. Understanding extracellular vesicle diversity—current status. *Expert Rev. Proteomics.* 2018;15(11):887-910.
89. Su F-H, Tabañag IDF, Wu C-Y, Tsai S-L. Decorating outer membrane vesicles with organophosphorus hydrolase and cellulose binding domain for organophosphate pesticide degradation. *Chem. Eng. J.* 2017;308:1-7.
90. Alves NJ, Turner KB, Daniele MA, Oh E, Medintz IL, Walper SA. Bacterial nanobioreactors—directing enzyme packaging into bacterial outer membrane vesicles. *ACS Appl. Mater. Interfaces.* 2015;7(44):24963-72.

91. Ohno S-i, Takanashi M, Sudo K, Ueda S, Ishikawa A, Matsuyama N, et al. Systemically injected exosomes targeted to EGFR deliver antitumor microRNA to breast cancer cells. *Mol. Ther.* 2013;21(1):185-91.
92. Arrighetti N, Corbo C, Evangelopoulos M, Pastò A, Zuco V, Tasciotti E. Exosome-like nanovectors for drug delivery in cancer. *Curr. Med. Chem.* 2019;25:1-15.
93. Alves NJ, Turner KB, Medintz IL, Walper SA. Protecting enzymatic function through directed packaging into bacterial outer membrane vesicles. *Sci. Rep.* 2016;6:24866.
94. Alves NJ, Moore M, Johnson BJ, Dean SN, Turner KB, Medintz IL, et al. Environmental decontamination of a chemical warfare simulant utilizing a membrane vesicle-encapsulated phosphotriesterase. *ACS Appl. Mater. Interfaces.* 2018;10(18):15712-9.
95. Collins BS. Gram-negative outer membrane vesicles in vaccine development. *Discovery Med.* 2011;12(62):7-15.
96. Bruce TF, Slonecki TJ, Wang L, Huang S, Powell RR, Marcus RK. Exosome isolation and purification via hydrophobic interaction chromatography using a polyester, capillary-channeled polymer fiber phase. *Electrophoresis.* 2019;40(4):571-81.
97. Dieudonné A, Pignol D, Prévéral S. Magnetosomes: biogenic iron nanoparticles produced by environmental bacteria. *Appl. Microbiol. Biotechnol.* 2019;103(9):3637-49.
98. Uebe R, Schüler D. Magnetosome biogenesis in magnetotactic bacteria. *Nat. Rev. Microbiol.* 2016;14(10):621-37.

99. Lohße A, Borg S, Raschdorf O, Kolinko I, Tompa É, Pósfai M, et al. Genetic dissection of the mamAB and mms6 operons reveals a gene set essential for magnetosome biogenesis in *Magnetospirillum gryphiswaldense*. J. Bacteriol. 2014;196(14):2658-69.
100. Islam T, Peng C, Ali I. Morphological and cellular diversity of magnetotactic bacteria: A review. J. Basic Microbiol. 2018;58(5):378-89.
101. Arakaki A, Nakazawa H, Nemoto M, Mori T, Matsunaga T. Formation of magnetite by bacteria and its application. J. R. Soc. Interface. 2008;5(26):977-99.
102. Ren E, Lei Z, Wang J, Zhang Y, Liu G. Magnetosome modification: From bio-nano engineering toward nanomedicine. Adv. Ther. 2018;1(6):1800080.
103. Sugamata Y, Uchiyama R, Honda T, Tanaka T, Matsunaga T, Yoshino T. Functional expression of thyroid-stimulating hormone receptor on nano-sized bacterial magnetic particles in *Magnetospirillum magneticum* AMB-1. Int. J. Mol. Sci. 2013;14(7):14426-38.
104. Xiang Z, Yang X, Xu J, Lai W, Wang Z, Hu Z, et al. Tumor detection using magnetosome nanoparticles functionalized with a newly screened EGFR/HER2 targeting peptide. Biomaterials. 2017;115:53-64.
105. Honda T, Yasuda T, Tanaka T, Hagiwara K, Arai T, Yoshino T. Functional expression of full-Length TrkA in the prokaryotic host *Magnetospirillum magneticum* AMB-1 by using a magnetosome display system. Appl. Environ. Microbiol. 2015;81(4):1472-6.
106. Ginet N, Pardoux R, Adryanczyk G, Garcia D, Brutesco C, Pignol D. Single-step production of a recyclable nanobiocatalyst for organophosphate pesticides biodegradation using functionalized bacterial magnetosomes. PloS One. 2011;6(6):e21442.

107. Mickoleit F, Schüler D. Generation of multifunctional magnetic nanoparticles with amplified catalytic activities by genetic expression of enzyme arrays on bacterial magnetosomes. *Adv. Biosyst.* 2018;2(1):1700109.
108. Honda T, Tanaka T, Yoshino T. Stoichiometrically controlled immobilization of multiple enzymes on magnetic nanoparticles by the magnetosome display system for efficient cellulose hydrolysis. *Biomacromolecules.* 2015;16(12):3863-8.
109. Bakhshi PK, Bain J, Gul MO, Stride E, Edirisinghe M, Staniland SS. Manufacturing man-Made magnetosomes: High-throughput *in situ* synthesis of biomimetic magnetite loaded nanovesicles. *Macromol. Biosci.* 2016;16(11):1555-61.
110. Rasiah IA, Rehm BH. One-step production of immobilized  $\alpha$ -amylase in recombinant *Escherichia coli*. *Appl. Environ. Microbiol.* 2009;75(7):2012-6.
111. Robins KJ, Hooks DO, Rehm BH, Ackerley DF. *Escherichia coli* NemaA is an efficient chromate reductase that can be biologically immobilized to provide a cell free system for remediation of hexavalent chromium. *PloS One.* 2013;8(3):e59200.
112. Hooks DO, Blatchford PA, Rehm BHA. Bioengineering of bacterial polymer inclusions catalyzing the synthesis of *N*-acetylneuraminic acid. *Appl. Environ. Microbiol.* 2013;79(9):3116-21.
113. Yang TH, Kwon M-A, Lee JY, Choi J-E, Oh JY, Song JK. *In situ* immobilized lipase on the surface of intracellular polyhydroxybutyrate granules: preparation, characterization, and its promising use for the synthesis of fatty acid alkyl esters. *Appl. Biochem. Biotechnol.* 2015;177(7):1553-64.
114. Ran G, Tan D, Dai W, Zhu X, Zhao J, Ma Q, et al. Immobilization of alkaline polygalacturonate lyase from *Bacillus subtilis* on the surface of bacterial

- polyhydroxyalkanoate nano-granules. Appl. Microbiol. Biotechnol. 2017;101(8):3247-58.
115. Tan D, Zhao J-P, Ran G-Q, Zhu X-L, Ding Y, Lu X-Y. Highly efficient biocatalytic synthesis of l-DOPA using *in situ* immobilized *Verrucomicrobium spinosum* tyrosinase on polyhydroxyalkanoate nano-granules. Appl. Microbiol. Biotechnol. 2019;103(14):5663-78.
  116. Ran G, Tan D, Zhao J, Fan F, Zhang Q, Wu X, et al. Functionalized polyhydroxyalkanoate nano-beads as a stable biocatalyst for cost-effective production of the rare sugar D-allulose. Bioresour. Technol. 2019;289:121673.
  117. Moldes C, García P, García JL, Prieto MA. *In vivo* immobilization of fusion proteins on bioplastics by the novel tag BioF. Appl. Environ. Microbiol. 2004;70(6):3205-12.
  118. Moldes C, Farinós GP, de Eugenio LI, García P, García JL, Ortego F, et al. New tool for spreading proteins to the environment: Cry1Ab toxin immobilized to bioplastics. Appl. Microbiol. Biotechnol. 2006;72(1):88-93.
  119. Chen S-Y, Chien Y-W, Chao Y-P. *In vivo* immobilization of D-hydantoinase in *Escherichia coli*. J. Biosci. Bioeng. 2014;118(1):78-81.
  120. Seo HM, Kim JH, Jeon JM, Song HS, Bhatia SK, Sathiyarayanan G, et al. *In situ* immobilization of lysine decarboxylase on a biopolymer by fusion with phasin: Immobilization of CadA on intracellular PHA. Process Biochem. 2016;51(10):1413-9.
  121. Li R, Yang J, Xiao Y, Long L. *In vivo* immobilization of an organophosphorus hydrolyzing enzyme on bacterial polyhydroxyalkanoate nano-granules. Microb. Cell Fact. 2019;18(1):166.

122. Giessen TW, Silver PA. A catalytic nanoreactor based on *in vivo* encapsulation of multiple enzymes in an engineered protein nanocompartment. *ChemBioChem*. 2016;17(20):1931-5.
123. Patterson D, Edwards E, Douglas T. Hybrid nanoreactors: coupling enzymes and small-molecule catalysts within virus-like particles. *Isr. J. Chem*. 2015;55(1):96-101.
124. Jordan PC, Patterson DP, Saboda KN, Edwards EJ, Miettinen HM, Basu G, et al. Self-assembling biomolecular catalysts for hydrogen production. *Nat. Chem*. 2016;8(2):179.
125. Bustos-Jaimes I, Soto-Román RA, Gutiérrez-Landa IA, Valadez-García J, Segovia-Trinidad CL. Construction of protein-functionalized virus-like particles of parvovirus B19. *J. Biotechnol*. 2017;263:55-63.
126. Cayetano-Cruz M, Coffeen CF, Valadez-García J, Montiel C, Bustos-Jaimes I. Decoration of virus-like particles with an enzymatic activity of biomedical interest. *Virus Res*. 2018;255:1-9.
127. Schoonen L, Maassen S, Nolte RJ, van Hest JC. Stabilization of a virus-like particle and its application as a nanoreactor at physiological conditions. *Biomacromolecules*. 2017;18(11):3492-7.
128. Chen Q, Sun Q, Molino NM, Wang S-W, Boder ET, Chen W. Sortase A-mediated multi-functionalization of protein nanoparticles. *Chem. Commun*. 2015;51(60):12107-10.
129. Lee MJ, Brown IR, Juodeikis R, Frank S, Warren MJ. Employing bacterial microcompartment technology to engineer a shell-free enzyme-aggregate for

- enhanced 1, 2-propanediol production in *Escherichia coli*. *Metab. Eng.* 2016;36:48-56.
130. Jakobson CM, Chen Y, Slininger MF, Valdivia E, Kim EY, Tullman-Ercek D. Tuning the catalytic activity of subcellular nanoreactors. *J. Mol. Biol.* 2016;428(15):2989-96.
131. Wagner HJ, Capitain CC, Richter K, Nessling M, Mampel J. Engineering bacterial microcompartments with heterologous enzyme cargos. *Eng. Life Sci.* 2017;17(1):36-46.
132. Bulutoglu B, Macazo FC, Bale J, King N, Baker D, Minteer SD, et al. Multimerization of an alcohol dehydrogenase by fusion to a designed self-assembling protein results in enhanced bioelectrocatalytic operational stability. *ACS Appl. Mater. Interfaces.* 2019;11(22):20022-8.
133. Choi H, Choi B, Kim GJ, Kim Hu, Kim H, Jung HS, et al. Fabrication of nanoreaction clusters with dual-functionalized protein cage nanobuilding blocks. *Small.* 2018;14(35):1801488.
134. Li H, Zheng G, Zhu S. Construction of an organelle-like nanodevice via supramolecular self-assembly for robust biocatalysts. *Microb. Cell Fact.* 2018;17(1):26.
135. Tetter S, Hilvert D. Enzyme encapsulation by a ferritin cage. *Angew. Chem., Int. Ed.* 2017;56(47):14933-6.
136. Lau YH, Giessen TW, Altenburg WJ, Silver PA. Prokaryotic nanocompartments form synthetic organelles in a eukaryote. *Nat. Commun.* 2018;9(1):1311.
137. Park M, Sun Q, Liu F, DeLisa MP, Chen W. Positional assembly of enzymes on bacterial outer membrane vesicles for cascade reactions. *PloS One.* 2014;9(5):e97103.

- 138.Chen S, Parlane NA, Lee J, Wedlock DN, Buddle BM, Rehm BH. New skin test for detection of bovine tuberculosis on the basis of antigen-displaying polyester inclusions produced by recombinant *Escherichia coli*. Appl. Environ. Microbiol. 2014;80(8):2526-35.
- 139.Parlane NA, Chen S, Jones GJ, Vordermeier HM, Wedlock DN, Rehm BHA, et al. Display of antigens on polyester inclusions lowers the antigen concentration required for a bovine tuberculosis skin test. Clin. Vaccine Immunol. 2016;23(1):19-26.
- 140.Hwang ET, Lee S. Multienzymatic cascade reactions via enzyme complex by immobilization. ACS Catal. 2019;9(5):4402-25.
- 141.Du J, Rehm BH. Purification of target proteins from intracellular inclusions mediated by intein cleavable polyhydroxyalkanoate synthase fusions. Microb. Cell Fact. 2017;16(1):184.
- 142.Du J, Rehm BH. Purification of therapeutic proteins mediated by *in vivo* polyester immobilized sortase. Biotechnol. Lett. 2018;40(2):369-73.
- 143.Hay ID, Hooks DO, Rehm BH. Use of bacterial polyhydroxyalkanoates in protein display technologies. Hydrocarbon and Lipid Microbiology Protocols: Springer; 2014. p. 71-86.
- 144.Rubio-Reyes P, Parlane NA, Wedlock DN, Rehm BH. Immunogenicity of antigens from *Mycobacterium tuberculosis* self-assembled as particulate vaccines. Int. J. Med. Microbiol. 2016;306(8):624-32.
- 145.Gonzalez-Miro M, Rodríguez-Noda LM, Fariñas-Medina M, Cedré-Marrero B, Madariaga-Zarza S, Zayas-Vignier C, et al. Bioengineered polyester beads co-

- displaying protein and carbohydrate-based antigens induce protective immunity against bacterial infection. *Sci. Rep.* 2018;8(1):1888.
146. Gonzalez-Miro M, Radecker A-M, Rodríguez-Noda LM, Fariñas-Medina M, Zayas-Vignier C, Hernández-Cedeño M, et al. Design and biological assembly of polyester beads displaying pneumococcal antigens as particulate vaccine. *ACS Biomater. Sci. Eng.* 2018;4(9):3413-24.
  147. Wong JX, Rehm BH. Design of modular polyhydroxyalkanoate scaffolds for protein immobilization by directed ligation. *Biomacromolecules.* 2018;19(10):4098-112.
  148. Zakeri B, Fierer JO, Celik E, Chittock EC, Schwarz-Linek U, Moy VT, et al. Peptide tag forming a rapid covalent bond to a protein, through engineering a bacterial adhesin. *Proc. Natl. Acad. Sci. U.S.A.* 2012;109(12):E690-E7.
  149. Wong JX, Gonzalez-Miro M, Sutherland-Smith AJ, Rehm BHA. Covalent Functionalization of Bioengineered Polyhydroxyalkanoate Spheres Directed by Specific Protein-Protein Interactions. *Front. Bioeng. Biotechnol.* 2020;8(44).
  150. Zhao H, Wei H, Liu X, Yao Z, Xu M, Wei D, et al. Structural insights on PHA binding protein PhaP from *Aeromonas hydrophila*. *Sci. Rep.* 2016;6:39424.
  151. Zhao H, Yao Z, Chen X, Wang X, Chen GQ. Modelling of microbial polyhydroxyalkanoate surface binding protein PhaP for rational mutagenesis. *Microb. Biotechnol.* 2017;10(6):1400-11.
  152. Kim J, Kim YJ, Choi SY, Lee SY, Kim KJ. Crystal structure of *Ralstonia eutropha* polyhydroxyalkanoate synthase C-terminal domain and reaction mechanisms. *Biotechnol. J.* 2017;12(1):1600648.

153. Kim YJ, Choi SY, Kim J, Jin KS, Lee SY, Kim KJ. Structure and function of the N-terminal domain of *Ralstonia eutropha* polyhydroxyalkanoate synthase, and the proposed structure and mechanisms of the whole enzyme. *Biotechnol. J.* 2017;12(1):1600649.
154. Wittenborn EC, Jost M, Wei Y, Stubbe J, Drennan CL. Structure of the catalytic domain of the class I polyhydroxybutyrate synthase from *Cupriavidus necator*. *J. Biol. Chem.* 2016;291(48):25264-77.
155. Contente ML, Dall'Oglio F, Tamborini L, Molinari F, Paradisi F. Highly efficient oxidation of amines to aldehydes with flow-based biocatalysis. *ChemCatChem.* 2017;9(20):3843-8.
156. Lee SL, O' Connor TF, Yang X, Cruz CN, Chatterjee S, Madurawe RD, et al. Modernizing pharmaceutical manufacturing: from batch to continuous production. *J Pharm. Innov.* 2015;10(3):191-9.
157. Peschke T, Skoupi M, Burgahn T, Gallus S, Ahmed I, Rabe KS, et al. Self-immobilizing fusion enzymes for compartmentalized biocatalysis. *ACS Catal.* 2017;7(11):7866-72.
158. Döbber J, Gerlach T, Offermann H, Rother D, Pohl M. Closing the gap for efficient immobilization of biocatalysts in continuous processes: HaloTag™ fusion enzymes for a continuous enzymatic cascade towards a vicinal chiral diol. *Green Chem.* 2018;20(2):544-52.
159. van den Biggelaar L, Soumillion P, Debecker DP. Biocatalytic transamination in a monolithic flow reactor: improving enzyme grafting for enhanced performance. *RSC Adv.* 2019;9(32):18538-46.

160. Tamborini L, Fernandes P, Paradisi F, Molinari F. Flow bioreactors as complementary tools for biocatalytic process intensification. *Trends Biotechnol.* 2018;36(1):73-88.
161. Thompson MP, Peñafiel I, Cosgrove SC, Turner NJ. Biocatalysis using immobilized enzymes in continuous flow for the synthesis of fine chemicals. *Org. Process Res. Dev.* 2018;23(1):9-18.
162. Truppo MD. Biocatalysis in the pharmaceutical industry: the need for speed. *ACS Med. Chem. Lett.* 2017;8(5):476-80.
163. Zhang W. Nanoparticle aggregation: principles and modeling. *Nanomaterial: Springer;* 2014. p. 19-43.
164. Thoniyot P, Tan MJ, Karim AA, Young DJ, Loh XJ. Nanoparticle–hydrogel composites: Concept, design, and applications of these promising, multi-functional materials. *Adv. Sci.* 2015;2(1-2):1400010.
165. Ogura K, Rehm BHA. Alginate Encapsulation of Bioengineered Protein-Coated Polyhydroxybutyrate Particles: A New Platform for Multifunctional Composite Materials. *Adv. Funct. Mater.* 2019;29(37):1901893.
166. DiCosimo R, McAuliffe J, Poulouse AJ, Bohlmann G. Industrial use of immobilized enzymes. *Chem. Soc. Rev.* 2013;42(15):6437-74.
167. Jegannathan KR, Nielsen PH. Environmental assessment of enzyme use in industrial production – a literature review. *J. Cleaner Prod.* 2013;42:228-40.
168. Abdelraheem EMM, Busch H, Hanefeld U, Tonin F. Biocatalysis explained: from pharmaceutical to bulk chemical production. *React. Chem. Eng.* 2019;4(11):1878-94.
169. Basso A, Serban S. Industrial applications of immobilized enzymes—A review. *Mol. Catal.* 2019;479:110607.

170. Goldsmith M, Tawfik DS. Directed enzyme evolution: beyond the low-hanging fruit. *Curr. Opin. Struct. Biol.* 2012;22(4):406-12.
171. Palomo JM, Guisan JM. Different strategies for hyperactivation of lipase biocatalysts. In: Sandoval G, editor. *Lipases and Phospholipases: Methods and Protocols*. Totowa, NJ: Humana Press; 2012. p. 329-41.
172. Ong SY, Chee JY, Sudesh K. Degradation of polyhydroxyalkanoate (PHA): a review. *J. Sib. Fed. Univ. Biol.* 2017;10(2):211-25.
173. Koller M. Biodegradable and biocompatible polyhydroxy-alkanoates (PHA): Auspicious microbial macromolecules for pharmaceutical and therapeutic applications. *Molecules*. 2018;23(2):362.
174. Nguyen T, Pellegrin B, Bernard C, Gu X, Gorham JM, Stutzman P, et al. Fate of nanoparticles during life cycle of polymer nanocomposites. *J. Phys.: Conf. Ser.* 2011;304:012060.
175. Bundschuh M, Filser J, Lüderwald S, McKee MS, Metreveli G, Schaumann GE, et al. Nanoparticles in the environment: where do we come from, where do we go to? *Environ. Sci. Eur.* 2018;30(1):6.

### Preface to Chapter 3

The recent advances exploiting the design space of *in vivo* self-assembled polyhydroxyalkanoate (PHA) particles as protein immobilization scaffolds have been presented in chapter 2. The one-step *in vivo* self-assembly of biologically active protein-coated PHA particle manufacturing process avoids the costly and laborious chemical crosslinking of proteins to the surface-reactive scaffolding materials. The oriented immobilization of proteins densely coated on PHA particles could strongly enhance the protein function. However, the biological complexity of the recombinant functionalization of PHA particles *in vivo* makes control of physicochemical properties and immobilized protein density on the PHA scaffolds difficult. Therefore, in chapter 3, a modular functionalization approach was introduced to the recombinant PHA particle technology utilizing the most established Tag/Catcher protein ligation system, SpyTag/SpyCatcher chemistry pair.

## Chapter 3

# Design of Modular Polyhydroxyalkanoate Scaffolds for Protein Immobilization by Directed Ligation

Jin Xiang Wong<sup>1,2</sup> and Bernd H. A. Rehm<sup>3\*</sup>

<sup>1</sup> School of Fundamental Sciences, Massey University, Private Bag, 11222 Palmerston North, New Zealand.

<sup>2</sup> MacDiarmid Institute of Advanced Materials and Nanotechnology, Victoria University of Wellington, Wellington 6140, New Zealand.

<sup>3</sup> Centre for Cell Factories and Biopolymers, Griffith Institute for Drug Discovery, Griffith University, Don Young Road, Nathan, 4111 Queensland, Australia.

**Publication status:** published in *Biomacromolecules* (Wong, J. X. and Rehm, B. H. A. (2018). Design of Modular Polyhydroxyalkanoate Scaffolds for Protein Immobilization by Directed Ligation. *Biomacromolecules*, 19 (10), 4098-4112.)

### 3.1 Abstract

*In vivo*-assembled polyhydroxyalkanoate (PHA) particles have been successfully bioengineered to display foreign protein functions toward high-value applications in medicine and industry. To further expand the design space of PHA particles toward immobilization of various functional proteins, we developed a tunable modular protein immobilization method implementing the SpyCatcher/SpyTag chemistry. We successfully displayed the SpyCatcher protein using translational fusion with the *Cupriavidus necator* PHA synthase (PhaC). The SpyCatcher domain displayed on the surface of PHA particles was accessible for cross-linker-free ligation with SpyTag-bearing proteins. We demonstrated tunable protein immobilization of various SpyTagged proteins on SpyCatcher-PHA particles, which ultimately enabled assembly of multiple proteins coating the surface of PHA particles. Overall, the functionality, stability, and recycling of proteins immobilized to SpyCatcher-PHA particles were either retained or enhanced in comparison to the soluble forms. This modular platform can be implemented as a generic tool for protein immobilization in an array of applications.

### 3.2 Introduction

Protein immobilization techniques have long been recognized as useful tools for real-world uses in biomedical and industrial sectors. Immobilization of proteins to the surface of support materials allows the design of favorable microenvironments to achieve optimum performance. Improvement in both the stability and functionality of immobilized proteins has

been reported to be due to nonspecific interactions between proteins and supporting materials, enhancing their functional conformation and orientation (1-5). However, adverse effects were also observed when interactions with surfaces unfavorably impacted the orientation and conformation of immobilized proteins (6-8). The close proximity between proteins upon immobilization can improve their functional performance and stability, as a result of the macromolecular crowding (9-11). Several studies reported an improvement in the  $V_{\max}$  of enzymes in crowded microenvironments due to an increase in effective concentration of enzymes (10, 12). Furthermore, an increase in the stability of proteins can be achieved by macromolecular crowding, because the protein folding/unfolding equilibrium is shifted towards the formation of thermodynamically rigid proteins (9, 13). Minton, who developed a statistical thermodynamic model based on the excluded volume effect to estimate the stability of globular proteins under temperature stress and in the presence of chaotropic agents, predicted that crowding of stable globular proteins sufficiently improved both the thermal and chaotropic stability (14). In contrast, other authors noted reduced protein functionality due to excessive crowding of proteins on solid supports (15, 16). Macromolecular crowding has also been linked to the formation of protein aggregation, which leads to strong inhibition of protein functionality (17, 18). Moreover, clustering different immobilized proteins on scaffolds also allows colocalization of proteins mimicking their organization in natural multiprotein complexes. Many attempts have been devoted to artificially reconstituting such systems (19-21). Protein immobilization is also crucial for industrial applications, especially in the case of enzymes, where it stabilizes enzymes and allows their use in continuous processing providing economic advantages related to recovery and reuse of enzymes (22).

Polyhydroxyalkanoates (PHAs) have been recently considered as support materials for *in vivo* protein immobilization. PHAs are deposited inside the bacterial cell as spherical polyester inclusions and are naturally produced under unbalanced nutrient conditions. Bacterial production strains can be developed that self-assemble PHAs to form shell–core structures, where the surface can be functionalized by protein engineering of PHA-binding proteins and chemical means (23). Recently, we showed that formation of such PHA particles inside bacterial cells can be tailored for the surface display of a range of protein functions by using recombinant DNA technology leading to the development of the PHA particle technology as a versatile platform for protein immobilization and display (24-30). This new technology is based on the translational fusion of functional proteins of interest to the N- and/or C-terminus of a PHA synthase (PhaC), which results in the *in vivo* self-assembly of PHA particles displaying these functional proteins (31, 32). PhaC itself catalyzes PHA synthesis and remains covalently attached to the surface of the PHA particles (33, 34). Although the use of PhaC as anchoring domain represents an efficient way of immobilizing proteins to PHA particles, the biological complexity of the bacterial production strain inherently limits control of PHA particle formation (24, 30). Misfolding, low-density surface display and a potential failure to achieve multifunctionality are some of the limitations of the use of the PHA particle technology. In addition, controlling the ratio of certain functionalities is challenging using the PHA particle technology where assembly of functional PHA particles occurs inside the bacterial cell. Furthermore, in some cases high-value functional proteins (*e.g.* eukaryotic therapeutic proteins) might require host manipulation of protein folding pathways including the ability to carry out post-translational modifications for proper folding and functionality. Such hosts are, however,

suboptimal for cost-effective production of the PHA carrier material (28, 29). Hence, in some cases, it might be advantageous to separately produce PHA particles and proteins of interest under their respective optimum conditions followed by *in vitro* chemical conjugation of the protein of interest to the PHA particle surface. However, these chemical modifications are often laborious, potentially disrupt the native functionality of proteins as well as lead to random protein orientation (35). To address these issues, the site-specific protein ligation system, SpyCatcher/SpyTag chemistry (36), derived from CnaB2 domain from the fibronectin-binding protein (FbaB) found in *Streptococcus pyogenes*, might offer an efficient alternative for oriented functional immobilization of proteins to PHA particles.

The SpyCatcher/SpyTag chemistry offers a very promising protein ligation tool as it can be carried out under a wide range of temperatures (4–37°C), pH values (5–8), and selection of buffers (anion or cation) and it does not require the use of chemical cross-linkers or enzymes. The SpyCatcher is a small protein comprising 116 amino acid residues. It is able to spontaneously form an isopeptide bond with a 13 amino acid residue short peptide (SpyTag) by simply mixing these two components together, without the need of additional enzymes or chemicals (37). In recent years, there has been growing interest in utilizing the SpyCatcher/SpyTag chemistry for the design of different modular scaffolding systems for protein immobilization, and surface functionalization, such as virus-like particles, various protein scaffolds/cages, gold nanoparticles, and silica supports for potential applications in vaccination, bioimaging, and synthetic biology (38-47).

The aim of this study was to design a generic modular immobilization system for proteins by merging the PHA surface display technology with the versatile SpyCatcher/SpyTag chemistry. Our aim was to display the SpyCatcher protein at high density on the surface of *in vivo* self-assembled PHA particles *via* translational fusion of SpyCatcher to the N- or C-terminus of PhaC. The SpyCatcher will serve as a covalent ligation site for SpyTagged functional proteins. To demonstrate the broad applicability of this new approach, we will design and produce several SpyTagged proteins, representing diverse functional categories, for site-specific ligation to SpyCatcher-coated PHA particles. This study will also investigate the tunability of the modular system to achieve multiple protein functions. Functionality, stability, and recycling of resulting functional PHA particles will be analyzed.

### **3.3 Experimental Section**

#### **3.3.1 Bacterial Strains, Genetic Manipulation, and Growth Conditions**

All the bacterial strains, plasmids, and primers used in the current study are listed in **Tables S1–S3** respectively. The SpyCatcher encoding DNA was synthesized by Genscript (Piscataway, USA), and primers were ordered from Integrated DNA Technologies (San Diego, USA). General DNA isolation, manipulation, and cloning procedures were performed as described elsewhere (48). For plasmid propagation and cloning, *E. coli* XL1-Blue (Stratagene, La Jolla, USA) was grown overnight (16 h) in Luria–Bertani, Lennox (LB-Lennox) medium (pH 7.5) at 37°C and shaking at 200 rpm. When needed, ampicillin (100 µg/mL) and chloramphenicol (50 µg/mL) were added. All the antibiotics used this

study were filtered through a 0.22  $\mu\text{m}$  cellulose acetate membrane filter (ReliaPrep, Ahlstrom-Munksjö, Helsinki, Finland). DNA sequences of the newly constructed plasmids were sequenced by Massey Genome Service (Palmerston North, New Zealand).

Newly constructed plasmids used for this study were transformed into competent *E. coli* BL21(DE3) cells (Invitrogen, Carlsbad, USA) and competent *E. coli* BL21(DE3) cells harboring plasmid pMCS69 for production of soluble free proteins and PHA particles, respectively. Plasmid pMCS69 present in the latter strain enables the production of the precursor *R*-3-hydroxybutyryl-coenzyme A (CoA), which is required for PHA synthesis. Detailed plasmid construction strategies can be found in the Supporting Information.

### **3.3.2 Polyhydroxyalkanoate (PHA) Particle Production and Isolation**

Overnight culture of the *E. coli* BL21 (DE3) strains were diluted 1:100 into fresh Luria–Bertani, Lennox (LB–Lennox) medium containing ampicillin and chloramphenicol supplemented with 1% (w/v) glucose. The culture medium was cultivated at 37°C and 200 rpm until an OD<sub>600</sub> value of 0.6–0.8 was achieved. PHA particle production was induced by the addition of filtered isopropyl  $\beta$ -D-1-thiogalactopyranoside (IPTG) into the culture to a final concentration of 1 mM. Cultures were grown for 48 h at 25°C. After harvesting by centrifugation (8,000 g at 4°C for 20 min) the cell pellets were washed with 10 mM Tris-HCl (pH 7.5) once using a homogenizer (MICCRA D-9 45132, Müllheim, Germany) prior to cell disruption. Cells were lysed as previously described, and PHA particles were

recovered by centrifugation (9,000 g at 4°C for 20 min) (49). Recovered PHA particles were then washed three times and resuspended in PHA particle storage buffer (50 mM Tris-HCl, 20% v/v ethanol, pH 7.5) and stored at 4°C for further use and analysis.

### **3.3.3 Production and Purification of Soluble Protein**

Overnight culture of the respective *E. coli* BL21 (DE3) strains were diluted 1:100 into fresh LB-Lennox medium containing ampicillin and cultivated at 37°C and 200 rpm until an OD<sub>600</sub> value of 0.6–0.8 was achieved. Protein production was induced by the addition of filtered IPTG to the culture to a final concentration of 1 mM. Cultures were harvested after 24 h incubation with shaking at 30°C. The cells were harvested by centrifugation (8,000 g at 4°C for 20 min) then washed with 10 mM Tris-HCl (pH 7.5) once using a homogenizer (MICCRA D-9 45132, Müllheim, Germany) prior to cell disruption. Washed cell pellets were resuspended in 1× protein lysis buffer (50 mM Tris-HCl, 300 mM NaCl, 10 mM imidazole, pH 7.5) to produce a 10 % cell slurry, and lysed by passing through a microfluidizer (M-110P, Microfluidics, Westwood, USA) at 1500 bar. After cell lysis, the lysate was centrifuged (9,500 g at 4°C for 1h) to remove the cellular debris. The supernatant was filtered through a 0.22 µm cellulose acetate membrane filter (ReliaPrep, Ahlstrom-Munksjö, Helsinki, Finland), and the clarified lysate loaded on to a 5 mL Protino Ni-NTA column (Macherey-Nagel, Düren, Germany) at 5 mL/min. The Ni-NTA column was washed with at least 5 column volumes of protein wash buffer (50 mM Tris-HCl, 300 mM NaCl, 50 mM imidazole, pH 7.5) to remove nonspecifically bound proteins. Those retained on the column were eluted with 5 column volumes of 50 mM Tris-HCl, 300 mM NaCl, 500 mM imidazole, pH 7.5. Eluted protein samples were concentrated and desalted using

a centrifugal concentrator (Vivaspin 20, GE Healthcare, Buckinghamshire, U.K.). Concentrated samples were stored at 4°C for further use and analysis.

### **3.3.4 Protein Analysis**

All fusion proteins were analyzed by sodium dodecyl sulfate–polyacrylamide gel electrophoresis (SDS–PAGE) as described elsewhere (50). Briefly, soluble protein and PHA particle samples were denatured with Laemmli buffer by heating at 95°C for 10 min and 15 min, respectively. The denatured protein samples were then separated on 10% (v/v) polyacrylamide separating gels with 4% (v/v) polyacrylamide stacking gels. The molecular mass of the samples was estimated using a GangNam-STAIN prestained protein standard marker (iNtRON Biotechnology, Seongnam, South Korea). SDS–PAGE gels were stained with 0.05% (w/v) Coomassie brilliant blue R-250 dye, 50% (v/v) ethanol and 10% (v/v) acetic acid for 30 min and then destained in 50% (v/v) ethanol and 10% (v/v) acetic acid for 2 h. Images of polyacrylamide gels were taken using Gel Doc XR+ system (Bio-Rad Laboratories, Hercules, USA).

### **3.3.5 Protein Quantification**

Protein concentrations were determined by measuring the band intensity from SDS–PAGE gels for densitometric analysis using Image Lab 5.2.1 software (Bio-Rad Laboratories, Hercules, USA) and comparing the value to a standard curve prepared from known concentrations of bovine serum albumin (BSA) standard as described elsewhere (51). The

determination of production yields of protein displayed on PHA particles (**Equations S1–S4**), molarity (**Equation S5**), percentage surface coverage and percentage ligation efficiency of SpyTagged protein covalently ligated to SpyCatcher protein on PHA particles (**Equations S6 and S7**) are shown in Supporting Information.

### **3.3.6 Proteomic analysis**

Purified protein bands from the SDS–PAGE gel were excised and subjected to tryptic in-gel digestion as described elsewhere (52). The resulting tryptic peptide samples were then analyzed by liquid chromatography-tandem mass spectrometry (LC–MS/MS) in School of Fundamental Sciences Mass Spectrometry Laboratory, Massey University (Palmerston North, New Zealand).

### **3.3.7 Immobilization of SpyTagged Proteins onto SpyCatcher-PHA Particles**

The feasibility of immobilizing SpyTagged *Aequorea victoria* green fluorescent protein bearing a His<sub>6</sub> tag (SpGFP-H6), SpyTagged *Agrobacterium radiobacter* organophosphohydrolase bearing a His<sub>6</sub> tag (SpOpdA-H6), and SpyTagged *Bacillus licheniformis*  $\alpha$ -amylase bearing a His<sub>6</sub> tag (SpBLA-H6) onto SpyCatcher-PHA particles was tested by incubating different SpyTagged proteins with SpyCatcher-PHA particles in 50 mM Tris-HCl, pH 7.5 overnight at 4°C with gentle rotary shaking (20 rpm) at a SpyCatcher:SpyTag reactant ratio of 3:1 or 4:1. After this time the samples were washed three times with 50 mM

Tris-HCl, pH 7.5 before being analyzed by SDS-PAGE. The reproducibility of this method was validated ( $n = 9$ ).

### **3.3.8 Optimization of SpyTag/SpyCatcher Chemistry**

For the reactant ratio to be optimized, SpyCatcher-PHA particles were mixed with different SpyTagged proteins at SpyCatcher:SpyTag reactant ratios of 3:1, 2:1, 1:1, 1:2, and 1:3 in 50 mM Tris-HCl, pH 7.5. The mixtures were incubated overnight at 4°C with gentle rotary shaking (20 rpm). Then, the samples were washed three times with 50 mM Tris-HCl, pH 7.5 before SDS-PAGE analysis. Meanwhile, the reaction time course of the ligation chemistry was determined by incubating different SpyTagged proteins with SpyCatcher-PHA particles at a SpyCatcher:SpyTag reactant ratio of 2:1 with a total reaction time of 24 h. Samples were collected at 1, 3, 6, 12, and 24 h, washed three times with 50 mM Tris-HCl, pH 7.5 then analyzed by SDS-PAGE.

### **3.3.9 Assembly of the Immobilized Multiprotein Complex using SpyCatcher-PHA**

#### **Particles**

For a proof-of-concept immobilized multiprotein complex system to be constructed using the SpyCatcher-PHA particle platform, SpBLA-H6 was first incubated with SpyCatcher-PHA particles at a SpyCatcher:SpyTag reactant ratio of 3:1 in 50 mM Tris-HCl, pH 7.5 overnight at 4°C with gentle rotary shaking (20 rpm). Next, the samples were centrifuged

at 15,000 g for 10 min, and the unbound proteins in each sample supernatant were discarded. The pellets were washed three times with 50 mM Tris-HCl, pH 7.5, and 10  $\mu$ L of each sample were taken for verification of protein ligation by SDS-PAGE analysis. The same procedures were repeated with SpGFP-H6 and SpOpdA-H6 at SpyCatcher:SpyTag reactant ratios of 3:1 and 4:1, respectively. The reproducibility of this method was validated ( $n = 9$ ).

### **3.3.10 Compositional Analysis of PHA Particles**

Approximately 75 mg of lyophilized PHA particles was subjected to methanolysis as described elsewhere (51, 53). The organic layer of all samples was recovered, filtered, and further analyzed by gas chromatography-mass spectroscopy (GC-MS) in Plant and Food Research (Palmerston North, New Zealand), using poly (*R*)-3-hydroxybutyric acid (PHB) as standard (51).

### **3.3.11 Zeta Potential Measurement**

The zeta potential of the PHA particles was determined by electrophoretic light scattering (ELS) coupled with phase analysis light scattering (PALS) using Zetasizer Nano ZS (Malvern Instruments, Malvern, U.K.). All PHA particle samples were measured at a concentration of 0.1% (w/v) of wet particles in 50 mM Tris-HCl, pH 7.5, and the soluble protein samples were measured in 50 mM Tris-HCl, pH 7.5. All measurements were made in triplicates.

### 3.3.12 PHA Particle Size Distribution Measurement

The particle size distribution of the PHA particles was determined by dynamic light scattering (DLS) analysis using a Mastersizer 3000 laser diffraction particle size analyzer (Malvern Instruments, Malvern, U.K.). The PHA particle samples were prepared at a concentration of 0.1% (w/v) of wet particles in 50 mM Tris-HCl, 20% (v/v) ethanol, pH 7.5. All measurements were made in triplicates. The determination of total SpyCatcher protein mass per wet particle (**Equations S8 and S9**) and number of SpyCatcher protein per surface area of wet PHA particle (**Equations S10–S13**) are shown in Supporting Information.

### 3.3.13 Fluorescence Screening, Microscopy Analysis, and Fluorescence Intensity Measurement

Fluorescence intensities of soluble free and immobilized SpGFP-H6 in 50 mM Tris-HCl, pH 7.5 were evaluated. The samples were first screened visually using the Safe Imager 2.0 Blue-Light Transilluminator (Invitrogen, Carlsbad, USA) and imaging of fluorescing samples excited with blue light at 470 nm. Fluorescence microscope images of the samples were taken using an Olympus BX51 fluorescent light microscope (Olympus Optical, Tokyo, Japan) at 100 $\times$  magnification using MicroPublisher 5.0 color CCD camera, QCapture Pro 6.0 application software. (QImaging, Surrey, Canada). The intensity of the fluorescence emitted by the samples was measured using FLUOstar Galaxy fluorimeter and Reader Control Software (BMG Labtech, Ortenberg, Germany) at excitation and emission

wavelengths of 380 and 520 nm, respectively. All fluorescence intensity measurements were made in triplicates.

#### **3.3.14 Starch Degradation Screen and Colorimetric Assay for $\alpha$ -Amylase**

The enzyme activity of immobilized and soluble free SpBLA-H6 with appropriate controls was first qualitatively verified using starch agar plates (54). Briefly, 1% starch agar was prepared by dissolving 1% (w/v) soluble starch and 1.5% (w/v) agar with 50 mM Tris-HCl, 300 mM NaCl buffer (pH 7.5) prior to autoclaving. All samples were incubated at 37°C for up to 24 h on the surface of the starch agar plates. After rapid screening, the enzyme activity of immobilized and free SpBLA-H6, together with the negative controls was measured in a modified reaction buffer (50 mM Tris-HCl, pH 7.5) (54) using an amylase assay kit (Abcam, Cambridge, U.K.). In this methods, nitrophenol liberated by SpBLA-H6 hydrolysis of ethylidene-pNP-G7 is monitored by the ELx808 Absorbance Microplate Reader with Gen5 reader control 1.02.8 application software (BioTeK Instruments, Winooski, USA) at OD405 nm at room temperature (25°C) for up to 3 h at 2 min intervals. All quantitative measurements were made in triplicates.

#### **3.3.15 Organophosphohydrolase Functionality Assay**

The enzyme activity of both the immobilized and soluble SpOpdA-H6 (50 mM Tris-HCl, pH 7.5) together with negative controls were assessed using an assay mixture of 250  $\mu$ M coumaphos dissolved in a modified reaction buffer (50 mM Tris-HCl, 20% (v/v) methanol,

pH 7.5) at 25 °C (55). Quantification of liberated chlorferon from coumaphos was determined using a FluoroMax-4 Spectrofluorometer and Jobin Yvon MicroMax 384 microwell plate reader at excitation and emission wavelengths of 355 and 450 nm, respectively, controlled by FluoEssence version 3.5 (HORIBA Scientific, Kyoto, Japan). Samples were added into the assay mixture and performed at room temperature (25°C) for emission was measured at 10 min intervals for up to 2 h. All quantitative measurements were made in triplicates.

#### **3.3.16 Thermal Stability**

Both immobilized and soluble enzymes were preincubated from 5 to 95°C at a temperature interval of 10°C using AccuBlock Mini Compact Dry Bath (Labnet International, Edison, USA) for 30 min. The resulting samples were then subjected to their respective functional assays for 1 h. All quantitative measurements were made in triplicates.

#### **3.3.17 pH Stability**

Immobilized and soluble free proteins at varying pH values were preincubated in the following solutions for 30 min at room temperature (25°C): pH 3 and 5 (50 mM sodium acetate), pH 7 and 9 (50 mM Tris-HCl) and pH 11 (50 mM disodium hydrogen orthophosphate). A Vivaspin 20 centrifugal concentrator (GE Healthcare, Buckinghamshire, U.K.) was used to perform the buffer exchange for soluble free proteins. After that, the samples

were resuspended in their reaction buffers, respectively, after pH treatment and assessed for their functionality for 1 h. All quantitative measurements were made in triplicates.

### **3.3.18 Recycling**

Both immobilized and soluble forms of functional proteins of interest were measured for recycling with their respective functional assays in five consecutive cycles at room temperature (2 h each cycle for SpOpdA-H6 and SpGFP-H6; 3 h each cycle for SpBLA-H6). Immobilized protein samples were centrifuged at 15,000 g for 10 min in a microcentrifuge at the end of the assessment cycle. The supernatant was discarded, and the samples were resuspended in fresh reaction buffers. A Vivaspin 20 centrifugal concentrator (GE Healthcare, Buckinghamshire, U.K.) was used to perform the buffer exchange for soluble free proteins at the end of the assay, and the protein samples were diluted with fresh reaction buffers. This procedure was repeated for five cycles. All quantitative measurements were made in triplicates.

## **3.4 Results and Discussion**

### **3.4.1 Design and Production of SpyCatcher-Displaying PHA Particles**

To enable efficient ligation of proteins without the need of chemical cross-linkers or enzymes, we designed and produced PHA particles displaying the SpyCatcher domain for ligation with SpyTagged proteins of interest, where a covalent isopeptide bond forms

between a lysine residue (Lys) on the SpyCatcher domain and an aspartic acid residue (Asp) on the SpyTag peptide (**Figures 1A and 1B**). Successful polymerase chain reaction (PCR) amplifications and ligations for each of the constructs were shown in plasmid construction strategies (Supporting Information). We successfully displayed SpyCatcher on the surface of PHA particles *via* surface-exposed PHA synthase (PhaC) (56) using translational fusion of SpyCatcher to both N- and C- terminus of PhaC as confirmed by sodium dodecyl sulfate–polyacrylamide gel electrophoresis (SDS–PAGE) (**Figure 1C**) and by proteomic analysis using liquid chromatography–tandem mass spectrometry (LC–MS/MS) (**Table S4**). The molecular mass of SpyCatcher-PhaC (SP) and PhaC-SpyCatcher (PS) fusion proteins are 68.4 kDa and 69.1 kDa, respectively, while wild-type PhaC (WT) has a molecular mass of 55.5 kDa. Placing the SpyCatcher protein at the N-terminus of PhaC significantly enhanced the production yields of SP fusion protein per PHA particle mass. We successfully overproduced the SP fusion proteins displayed on PHA particles (SP-P) resulting in yields of 194 nmoles SpyCatcher per g wet PHA particles, which was much higher than that found for the PS fusion protein displayed on PHA particles (PS-P) (**Figure 1D**). As it has been shown that the N-terminus fusion point of PhaC is located at a highly variable surface-exposed region of the protein that has been proven not to be essential to the PhaC activity (33, 57). In contrast, the C-terminus of PhaC is conserved and essential for PhaC activity. It is predicted to be attached to the inner hydrophobic core of the PHA particles, thus potentially affecting the surface exposure of any C-terminally fused domains (32). Therefore, and because of the high-density display of exposed SpyCatcher domains, the SP-P was selected to demonstrate the proof-of-concept for modular protein immobilization based on the SpyTag/SpyCatcher chemistry.

### 3.4.2 Immobilization of SpyTagged Proteins to SpyCatcher-PHA Particles: Confirmation and Optimization of Ligation Reactions towards Single and Multiprotein Display

To assess the accessibility of the SpyCatcher domain displayed on PHA particles for ligation, *i.e.* immobilization of soluble free SpyTagged proteins *via* spontaneous formation of a covalent isopeptide linkage, we designed and produced several SpyTagged proteins representing diverse functionalities (**Figure 1B**). The selected proteins were the *Aequorea victoria* green fluorescent protein (GFP), a biomarker commonly used in drug screening and diagnostic assays, the *Agrobacterium radiobacter* organophosphohydrolase (OpdA), an organophosphate pesticide-degrading enzyme considered for bioremediation, and the *Bacillus licheniformis*  $\alpha$ -amylase (BLA), a thermophilic industrially used starch-degrading enzyme. BLA and GFP are monomeric, whereas OpdA needs to form a dimer to become active. Successful PCR amplifications and ligations for each of the constructs were shown in plasmid Construction strategies (Supporting Information). By attaching a hexa-histidine tag to the N-terminus of the protein of interest, SpyTagged proteins could be purified using immobilized metal affinity chromatography (IMAC) (58-60). Recombinant proteins successfully produced were SpyTagged GFP bearing His<sub>6</sub> tag (SpGFP-H6), SpyTagged OpdA bearing His<sub>6</sub> tag (SpOpdA-H6), and SpyTagged BLA bearing His<sub>6</sub> tag (SpBLA-H6). Peptide tags were placed at the N-termini of each protein to avoid steric interference between the SpyTag peptide and hexa-histidine tag as well as to retain the accessibility of both peptide tags to their corresponding docking domains. The yield, purity, apparent molecular

weight, and identity of each SpyTagged proteins was confirmed by SDS–PAGE (**Figure 1E**) and LC–MS/MS (**Table S4**).

Prior to protein ligation optimization, the SP fusion protein on PHA particles and all soluble SpyTagged proteins were quantified by densitometry using a bovine serum albumin (BSA) standard curve (**Figures S1–S4**). A linear curve could describe the BSA standard curves generated for each densitometry analysis with  $r^2$  values of at least 0.98. Varying dilution factors were used for each sample to ensure the readings were within the standard curve linear range.

The various SpyTagged proteins were mixed with the SP-P as described in the Sections 3.3.7–3.3.9. SDS–PAGE analysis showed that after ligation an additional single protein band appeared in lanes 2–4 with an apparent molecular weight greater than the SP fusion protein alone (68.4 kDa). Bands at approximately 120.9, 104.0, and 94.2 kDa were the expected masses for SpBLA-SP-ligated protein (SpBLA-SP-L), SpOpdA-SP-ligated protein (SpOpdA-SP-L), and SpGFP-SP-ligated protein (SpGFP-SP-L) respectively (**Figure 1F**). This step also resulted in the production of single-protein immobilized SP-Ps: SpGFP-immobilized SP-P (SpGFP-SP-P), SpOpdA-immobilized SP-P (SpOpdA-SP-P), and SpBLA-immobilized SP-P (SpBLA-SP-P), respectively. All ligation products were confirmed by proteomic analysis using LC–MS/MS (**Table S4**). These results suggested successful immobilization of SpyTagged proteins through ligation with SP-P. Hence, the SP-P provides a useful generic tool to immobilize different SpyTagged proteins. To explore

the possibility of tunability of the SP-P, we further optimized the ligation reaction by varying the SpyCatcher-to-SpyTag ratio and the reaction time as shown in **Figures S5–S10**. Our optimization results showed that the ligation efficiency of SpyTag-to-SpyCatcher, *i.e.* the percentage of total SpyTag-bearing proteins successfully ligated to the SpyCatcher domains on PHA particles in the reaction mixture, of up to 83.2% could be achieved. The surface coverage of SpyTagged proteins on SP-P varied from 19.0 to 59.0%.

To demonstrate the proof-of-concept that different SpyTagged proteins can be immobilized to the same SP-P, we implemented a step-by-step immobilization strategy as shown in **Figure S11**. Each ligation step was monitored by SDS–PAGE analysis of PHA particle-associated proteins (**Figure 1G**). The gradual decrease in band intensity of SP fusion protein (68.4 kDa) correlated with the increasing formation of extra protein bands at higher molecular weights (120.9, 104.0, and 94.2 kDa) representing the various ligation products. The final ligation step sample as shown in lane 4 of **Figure 1G**, where the SP fusion proteins were ligated with three different SpyTagged proteins on the same PHA particle will be referred to as multifunctional SP-P (MF-SP-P). We also attempted another strategy to prepare the MF-SP-P, where we incubated SP-P with equimolar quantities of a mixture of different SpyTagged proteins. This proved to be less efficient than the stepwise method, presumably due to undesirable steric competition between the SpyTagged proteins at neighboring anchoring sites on SP-P. The protein surface coverage of SpOpdA-H6 immobilized on MF-SP-P was greater than for SpGFP-H6 and SpBLA-H6 (**Figure 1H**). Because OpdA is a dimer, the first ligated SpOpdA-H6 could sequester the second monomer *via*

protein–protein interaction and thereby facilitate ligation of SpOpdA-H6 onto MF-SP-P compared to other monomeric proteins.

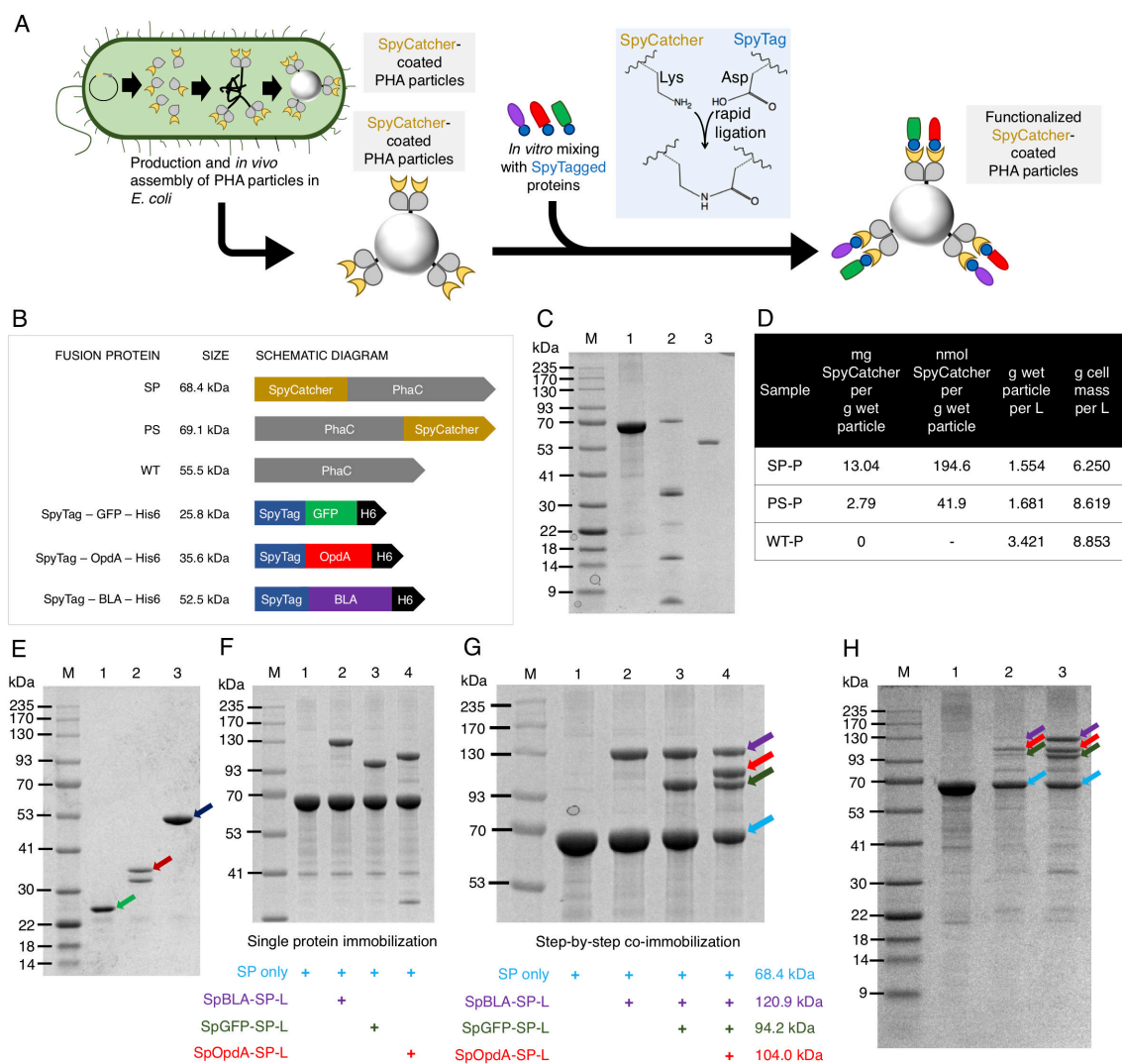


**Figure 1.** Design, production, and modular functionalization of SpyCatcher-PhaC PHA particles. **(A)** Schematic overview of production and modular functionalization of a generic modular PHA platform for protein immobilization using SpyCatcher/SpyTag chemistry. **(B)** Hybrid genes designed and used for this study. **(C)** SDS–PAGE analysis of SpyCatcher

fusion protein displayed on PHA particles. Lane M, Gangnam prestained protein marker; lane 1, SP fusion protein (68.4 kDa); lane 2, PS fusion protein (69.1 kDa); lane 3, WT protein (55.5 kDa). **(D)** Production yields of SpyCatcher protein displayed on PHA particles. **(E)** SDS–PAGE analysis of purified SpyTagged proteins. Lane M, Gangnam prestained protein marker; lane 1, SpGFP-H6 (25.8 kDa); lane 2, SpOpdA-H6 (35.6 kDa); lane 3, SpBLA-H6 (52.5 kDa). **(F)** SDS–PAGE analysis of various SpyTagged proteins immobilized on SP-P. Lane M, Gangnam prestained protein marker; lane 1, SP fusion protein only; lane 2, SpBLA-SP-L (120.9 kDa) and SP fusion protein (68.4 kDa); lane 3, SpGFP-SP-L (94.2 kDa) and SP fusion protein (68.4 kDa); lane 4, SpOpdA-SP-L (104.0 kDa) and SP fusion protein (68.4 kDa). **(G)** Visualization of step-by-step construction of MF-SP-P by SDS–PAGE analysis. Lane M, Gangnam prestained protein marker; lane 1, SP fusion protein only; lane 2, SpBLA-SP-L (120.9 kDa) and SP fusion protein (68.4 kDa); lane 3, SpBLA-SP-L (120.9), SpGFP-SP-L (104.0 kDa) and SP fusion protein (68.4 kDa); lane 4, SpBLA-SP-L (120.9 kDa, 20.1%), SpOpdA-SP-L (104.0 kDa, 24.3%), SpGFP-SP-L (94.2 kDa, 20.7%) and SP fusion protein (68.4 kDa, 35.5%). **(H)** Comparison of different preparation strategies of MF-SP-P. Lane M, Gangnam prestained protein marker; lane 1, SP only; lane 2, ligated proteins on MF-SP-P prepared using equimolar quantities of SpyTagged proteins self-assembling strategy; lane 3, ligated proteins on MF-SP-P prepared using stepwise reactant ratio modulated self-assembling strategy; purple arrow, SpBLA-SP-L; red arrow, SpOpdA-SP-L; green arrow, SpGFP-SP-L.

Furthermore, we analyzed the composition of the isolated SP-P against a pure poly (*R*)-3-hydroxybutyric acid (PHB) standard using gas chromatography–mass spectrometry

(GC–MS) as shown in **Figure 2A**. This confirmed that PHB was produced. It also showed that the content of PHB in SP-P was reduced by 28% when compared to that of the wild-type PHA particles (WT-P), implying an increased concentration displayed proteins over PHA mass upon fusion of the SpyCatcher protein to the N-terminus of PhaC. **Figure 1C** shows that the intensity of the protein band representing the SP fusion protein is increased compared to that of the WT band.

The zeta potential of the SP-P, WT-P, and functionalized SP-Ps was measured using electrophoretic light scattering (ELS) coupled with phase analysis light scattering (PALS) (**Figure 2B**). There was a reduction of the zeta potential of the PHA particles at pH 7.5 from  $-16.9 \pm 0.6$  to  $-29.3 \pm 0.2$  mV (mean  $\pm$  1 standard deviation (SD),  $n = 3$ ) upon genetic fusion of the SpyCatcher domain to the N-terminus of PhaC when compared to the WT-P. Meanwhile, as was expected, both SpGFP-H6 ( $-6.5 \pm 1.7$  mV) and SpBLA-H6 ( $-4.2 \pm 0.8$  mV) have net negative zeta potential values, while SpOpdA-H6 has a positive zeta potential value ( $4.9 \pm 1.1$  mV) at pH 7.5 (mean  $\pm$  1 SD,  $n = 3$ ), where these proteins have estimated isoelectric points of 6.26, 6.25, and 8.54, respectively (61). This result could further explain the faster ligation of SpOpdA-H6 onto SP-P compared to the others. Interestingly, we also noticed that the immobilization of SpyTagged proteins onto the surface of SP-P *via* SpyCatcher/SpyTag chemistry has no significant impact on the surface charge of SP-P. The zeta potentials of SpGFP-SP-P, SpOpdA-SP-P, SpBLA-SP-P, and MF-SP-P were  $-29.9 \pm 1.2$ ,  $-31.5 \pm 0.2$ ,  $-30.8 \pm 0.3$ , and  $-30.2 \pm 0.7$  mV (mean  $\pm$  1 SD,  $n = 3$ ), respectively (**Figure 2B**).

We performed dynamic light scattering (DLS) analysis to determine the particle size and size distribution of SP-P, WT-P, and various functionalized SP-Ps (**Figures 2C and 2D**). Additionally, particle distribution statistics are provided in **Table S4**. Statistically, SP-P has a larger Sauter mean diameter ( $D_{[3,2]}$ ) of 233 nm, and a lower specific surface area of 24480 m<sup>2</sup>/kg compared to those of WT-P. This discrepancy was mostly due to the high polydispersity of the SP-P as shown in the particle size distribution (**Figure 2C**), where SP-P tends to aggregate into two major aggregate clusters (approximately 1  $\mu$ m and 10–20  $\mu$ m), which statistically increases the size of the SP-P. The undesirable formation of these aggregates was presumably due to unspecific intermolecular and hydrophobic interactions and likely independent of surface charges (zeta potential), which were consistent across various functionalized SP-Ps. It is also noteworthy to mention that the particle size distribution (**Figure 2C**) suggested the individual SP-Ps have a smaller particle diameter (155 nm, blue arrow) when compared to WT-P (259 nm, black arrow). On the basis of the DLS analysis, the amount of the SpyCatcher domain displayed on SP-P was found to be ~0.091 fg per wet PHA particle. Furthermore, the SpyCatcher protein density at the surface of SP-P can be as close as  $\sim 8.4 \times 10^{14}$  SpyCatcher domains per  $\mu$ m<sup>2</sup>.

Surprisingly, we found out that the SpyTagged protein-functionalized PHA particles (SpGFP-SP-P, SpOpdA-SP-P, SpBLA-SP-P, and MF-SP-P) are consistently more dispersed than those prior to ligation, *i.e.* plain SP-P (**Figure 2D**). The  $D_{[3,2]}$  of all functionalized SP-Ps ranged from approximately 100 nm to 130 nm with the specific surface area ranging between approximately 41830 and 54550 m<sup>2</sup>/kg, which was a statistically significant increase compared to SP-P and WT-P (**Table S5**). The large aggregate clusters of

~10–20  $\mu\text{m}$  found in the SP-P were strongly diminished for all functionalized SP-Ps and only low levels of aggregation remained as shown in the particle size distribution, which suggested the surface functionalization of SP-Ps reduced nonspecific interactions between SP-Ps. As expected, we also noticed that functionalization of SP-P with different SpyTagged proteins consistently increased the diameter of individual SP-Ps from 155 nm (sky blue arrow) (**Figure 2C**) to ~ 180–200 nm (brown arrow) (**Figure 2D**) suggesting successful coating of SpyTagged proteins onto the SP-Ps *via* the SpyTag/SpyCatcher chemistry without affecting the assembled structure of the SP-Ps.

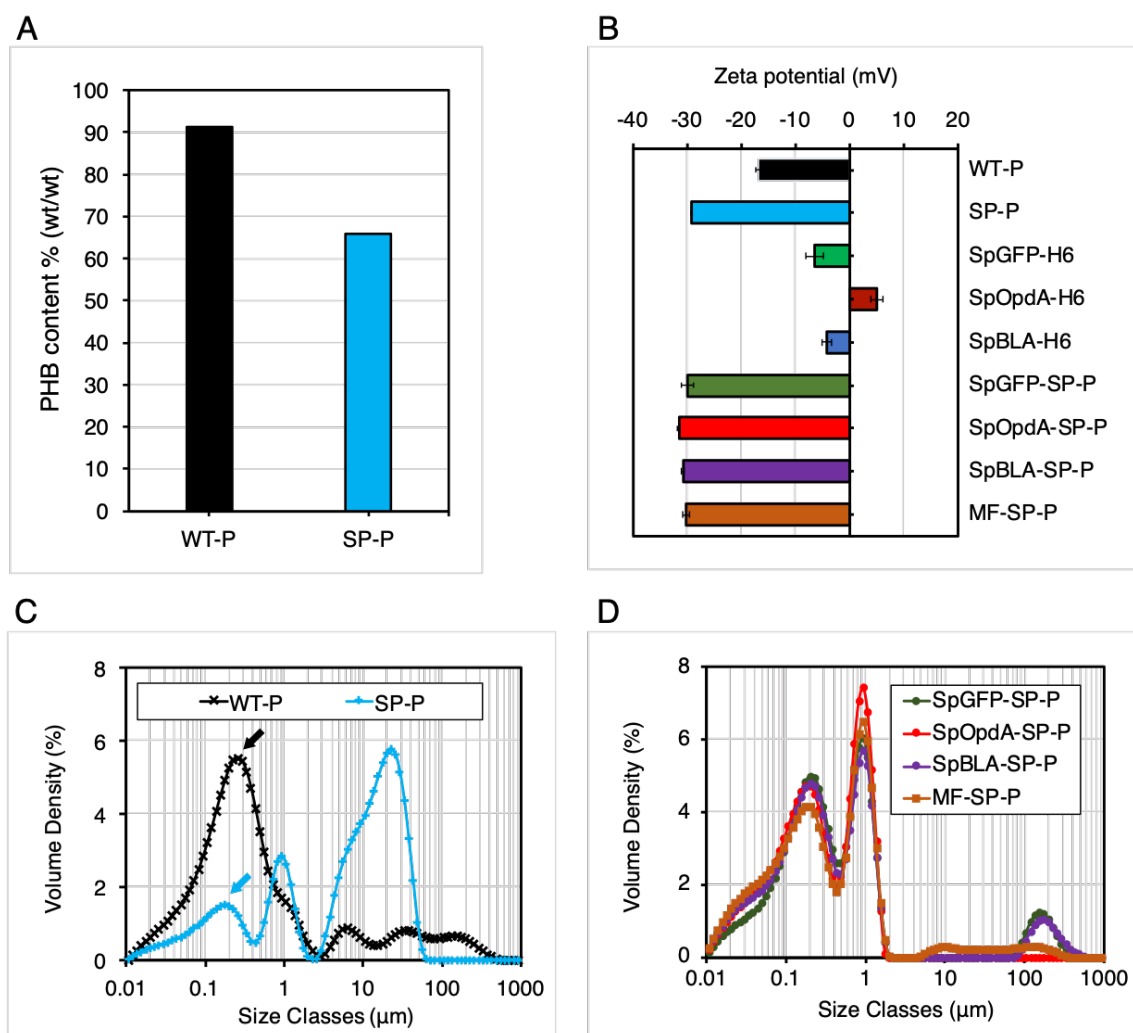


**Figure 2.** Physicochemical characterization of SpyCatcher-PhaC PHA particles. **(A)** Compositional analysis of PHA particles by GC–MS. **(B)** Zeta potential of PHA particles and soluble SpyTagged proteins by ELS/PALS (mean  $\pm$  1 SD,  $n = 3$ ). **(C)** Particle size distribution of SP-P and WT-P (mean  $\pm$  1 SD,  $n = 3$ ). **(D)** Particle size distribution of various functionalized SP-Ps by DLS analysis (mean  $\pm$  1 SD,  $n = 3$ ).

Tunable protein immobilization using the SP-P platform was achieved by varying the SpyCatcher:SpyTag ratios, which enabled control of the amount of SpyTagged proteins ligated

to SP-P. However, ligation reactions using increasing amounts of SpyTagged protein over SpyCatcher indicated that a significant fraction of SP fusion proteins remained unligated. Thus, the current conditions did not result in complete saturation of SP-P with the SpyTagged proteins of interest (**Figures S5–S10**). Possibly PHA particle aggregation might have restricted accessibility of SpyTagged proteins to the SpyCatcher domain displayed on PHA particles. Moreover, the protein surface properties such as zeta potential and hydrophobicity as well as the accessibility of the SpyTag itself could have interfered with the ligation reaction. Notably, the electrostatic attraction between the positively charged SpOpdA-H6 and the negatively charged SP-P facilitated ligation between the SpyCatcher domain and SpyTag when compared to both negatively charged SpGFP-H6 and SpBLA-H6, which were also used in this study.

In fact, previous studies described these ligation efficiency issues when immobilizing SpyTagged proteins onto other SpyCatcher-supporting scaffolds. Thrane *et al.* noted that coupling efficiency of several antigens onto the Spy-VLPs (SpyCatcher embedded virus-like particles) ranged from 33 to 88% and suggested that small proteins are less likely to be affected by steric hindrance during the ligation process (44). Meanwhile, Jia *et al.* also found a similar problem, where higher amounts of SpyCatcher proteins are needed to enhance the conjugation efficiency (47). Apart from raising the issue that large proteins are more susceptible to steric hindrance, they also argued that it might be due to the SpyCatcher proteins being trapped within the hyperbranched structure of the SpyCatcher polymer, which in turn, limited the accessibility of SpyTagged proteins to interact with the SpyCatcher protein (47).

For initial validation of successful modular functionalization of SP-P, *i.e.* to assess whether the functionality of the SpyTagged proteins was retained after immobilization on PHA particles, we first screened for fluorescence of immobilized SpGFP-H6 on the SP-P using soluble free SpGFP-H6 as positive control (**Figure 3**). SpyTagged GFP was produced, purified, and immobilized at SpyCatcher:SpyTag ratios of 3:1 to achieve an ~20% surface coverage on SP-P, to form SpGFP-SP-P and MF-SP-P. We also showed the reproducibility of this functionalization method ( $n = 9$ ) (**Figure S12**). For determining the amount of SpGFP-H6 immobilized on the PHA particles, both SpGFP-SP-P and MF-SP-P were subjected to SDS-PAGE analysis followed by densitometry analysis (**Figures S13 and S14**). Both SpGFP-SP-P and MF-SP-P in suspension emitted bright green fluorescence comparable to the soluble SpGFP-H6 prior to sedimentation by centrifugation (**Figure 3B (top)**). On the contrary, we noticed that the negative controls (WT-P and SP-P) did not emit the same intensity of fluorescence. Brighter fluorescence can be seen visually upon localization of particles by physical means, *i.e.*, centrifugation (**Figure 3B (bottom)**). Additional fluorescence screening images can be found in **Figures S17 and S18**. We measured the fluorescence intensity of the samples as described in the Experimental Section. From the bar graph in **Figure 3C**, the fluorescence intensity of both SpGFP-SP-P and MF-SP-P did show an equivalent signal compared to that of free SpGFP-H6. At the microscopic level, as shown in **Figure 3D**, both SpGFP-coated PHA particles also exhibited high local fluorescence on the PHA particles. These results indicate successful modular functionalization of SP-P using SpGFP-H6.

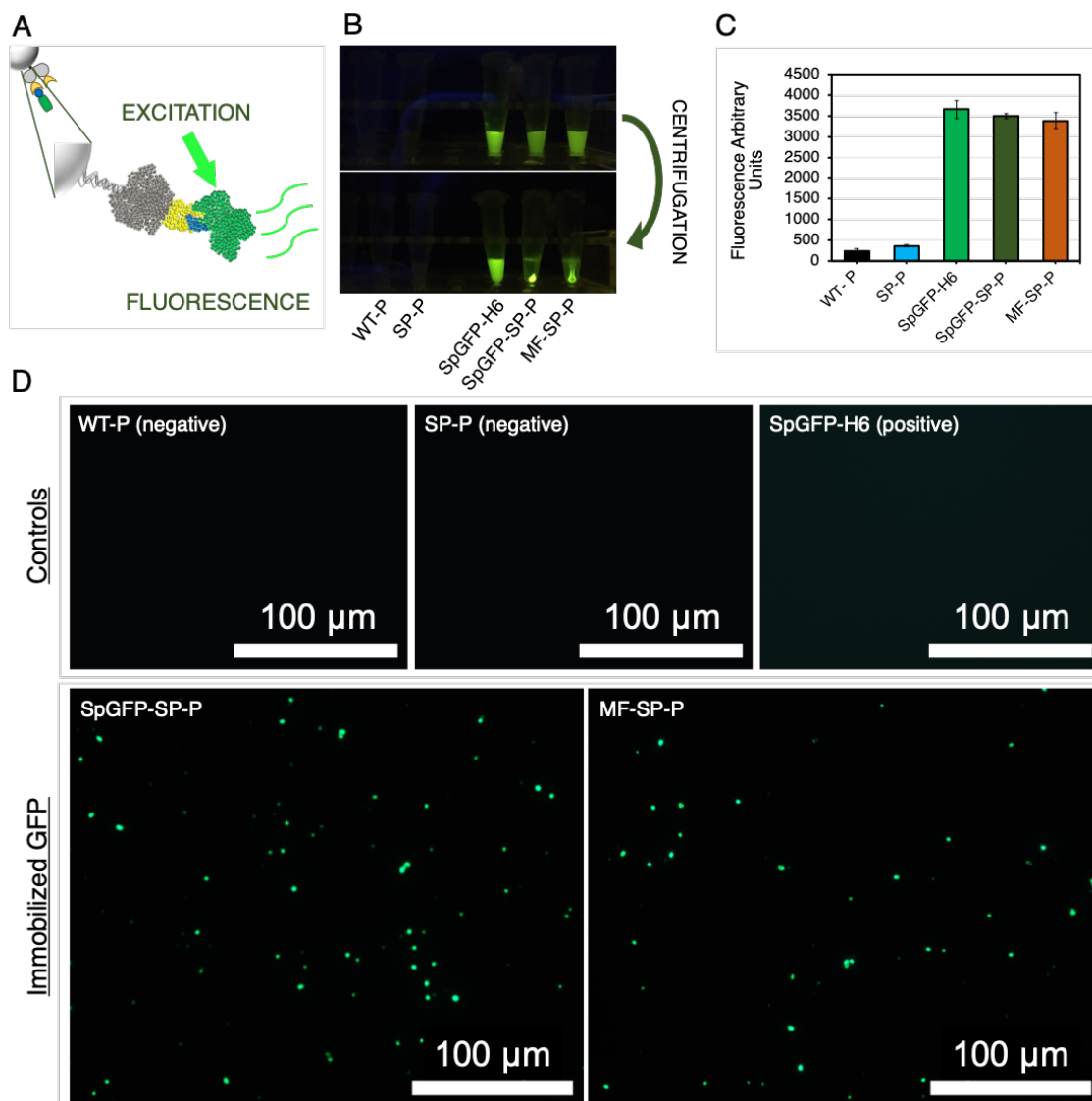


**Figure 3.** Fluorescence of SpGFP-H6 immobilized to SpyCatcher-PhaC PHA particles. **(A)** Schematic of immobilized SpGFP-H6 on the SP-P upon exposure to excitation light. **(B)** Fluorescence can be detected on immobilized SpGFP-H6 anchored on SP-P. **(C)** Arbitrary fluorescence intensity of the SpGFP-SP-P and MF-SP-P with controls (mean  $\pm$  1 SD,  $n = 3$ ). **(D)** Fluorescence microscopy analysis of the SpGFP-SP-P and MF-SP-P with controls.

### 3.4.3 Enzyme Immobilization Using SpyCatcher-PHA Particles

We tested the utility of SP-P as a scaffold for the immobilization of OpdA and BLA because of their vast potential in industry and agriculture. SpyTagged enzymes were produced, purified, and immobilized at SpyCatcher:SpyTag ratios of 4:1 and 3:1 for SpOpdA-H6 and SpBLA-H6, respectively, to achieve an ~20% surface coverage on SP-P, to form SpOpdA-SP-P, SpBLA-SP-P, and MF-SP-P. The SDS-PAGE analysis confirmed the successful immobilization of these enzymes on SP-P, and the reproducibility of this functionalization method was confirmed ( $n = 9$ ) (**Figure S12**). Densitometry was used to quantify enzymes immobilized to PHA particles (**Figures S14–S16**). The functionality of immobilized and free SpBLA-H6 was first qualitatively assessed using 1% (w/v) starch agar (**Figure S19**). All SpBLA-H6-containing samples created a clear transparent zone, which indicated starch hydrolysis. Then, we tested the enzyme activities of both immobilized and soluble free forms in their respective reaction mixture. We compared the substrate conversion rates of immobilized enzymes to those of purified soluble enzymes (**Figure 4**). Our findings suggested that both immobilized SpOpdA-H6 and SpBLA-H6 outperformed their soluble counterparts. The catalytic activity of immobilized SpOpdA-H6 on SpOpdA-SP-P ( $5.09 \pm 0.08$  U/mg) was around 9% higher when compared to free SpOpdA-H6 ( $4.66 \pm 0.26$  U/mg). Interestingly, we found that the immobilized SpOpdA-H6 on MF-SP-P ( $6.33 \pm 0.16$  U/mg) exhibited a much faster coumaphos degradation when compared to both SpOpdA-SP-P and soluble SpOpdA-H6 (mean  $\pm 1$  SD,  $n = 3$ ). Meanwhile, the specific activities of immobilized SpBLA-H6 on SpBLA-SP-P and MF-SP-P were  $3.72 \pm 0.03$  and  $3.67 \pm 0.04$  U/mg, respectively, which were ~30% higher than the soluble SpBLA-H6 activity of  $2.63 \pm 0.07$  U/mg (mean  $\pm 1$  SD,  $n = 3$ ).

These results suggested that the spatial organization and oriented display of enzymes on SP-P can increase the rate of the catalytic reaction. Furthermore, the close proximity between immobilized enzymes on the SP-P might have created macromolecular crowding effects leading to an enhanced substrate conversion rate of the enzymes studied. Kao *et al.* made a similar observation and showed that clustering of immobilized lysozyme on mesoporous silica nanoparticles is more active than its soluble counterpart due to artificially the created crowded microenvironment (62). Yang *et al.* also reported that the catalytic efficiency of both 7 $\alpha$ -hydroxysteroid dehydrogenase and 7 $\beta$ -hydroxysteroid dehydrogenase could be increased by controlling the density of immobilized enzymes of interest on chitosan-epoxy resin carriers (9). However, it may vary from case to case, as different proteins have different characteristics and surface clustering of some proteins on supporting scaffolds might have an adverse effect due to topological frustration and steric hindrance (63-65).

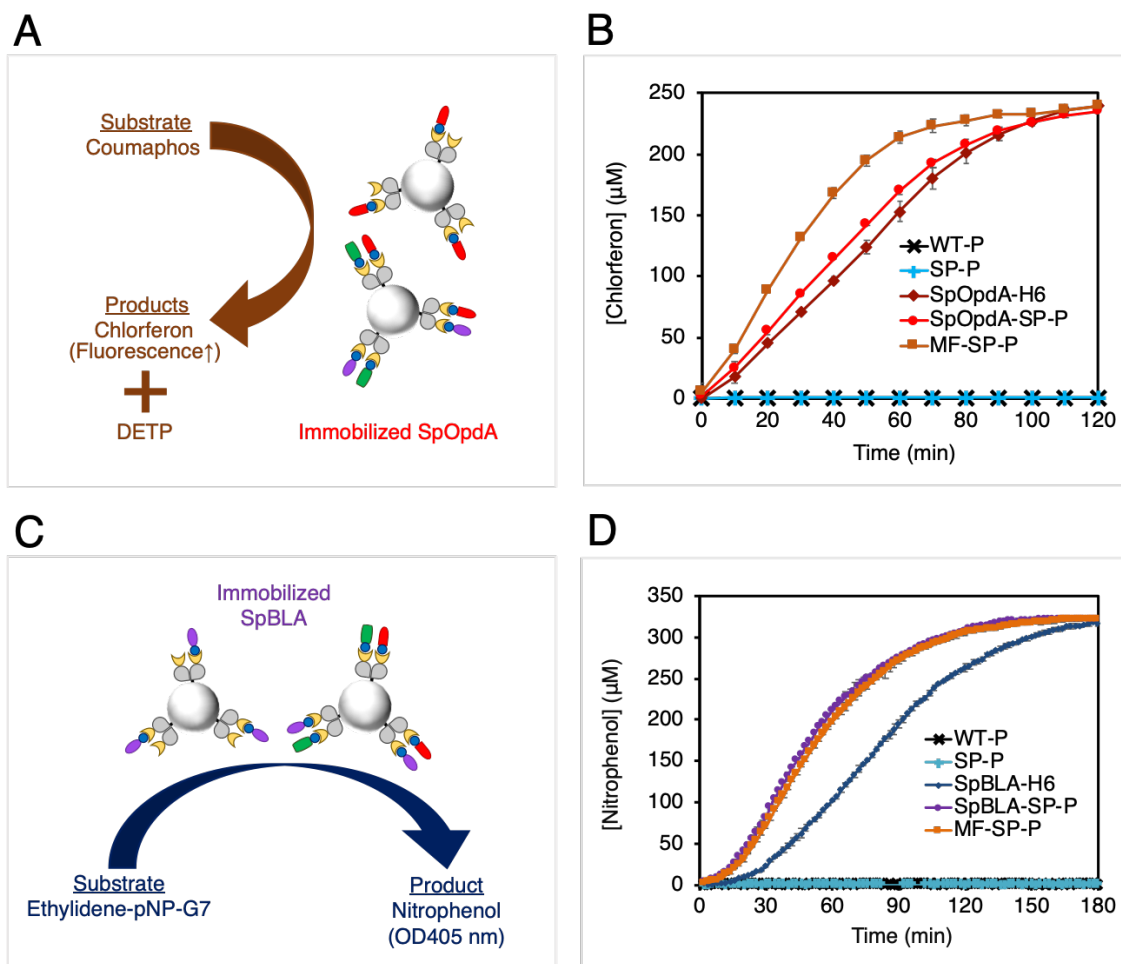


**Figure 4.** OpdA and BLA enzymatic functionality assays. **(A)** Schematic illustration of OpdA activity assay using coumaphos as substrate. Coumaphos is degraded into chlorferon and dietlythiophosphate (DETP) by immobilized SpOpdA-H6. **(B)** Reaction time course of coumaphos degradation hydrolyzed by SpOpdA-SP-P and MF-SP-P with appropriate controls (mean  $\pm$  1 SD,  $n = 3$ ). **(C)** Schematic illustration of BLA activity determined by 3,5-dinitrosalicylic acid colorimetric assay. Nitrophenol is released from ethylidene-pNP-G7 by enzyme activity of immobilized SpBLA-H6. **(D)** Reaction time course of ethylidene-pNP-G7 degradation hydrolyzed by SpBLA-SP-P and MF-SP-P with appropriate controls (mean  $\pm$  1 SD,  $n = 3$ ).

Alteration of material surface microenvironments upon covalent docking of enzymes could significantly affect the performance of immobilized enzymes, which might explain the enhanced activity of MF-SP-P compared to soluble SpOpdA-H6. A combination of surface charge, hydrophobicity/hydrophilicity, surface topology and orientation of active sites among enzymes and/or the material–protein interface allow the construction of favorable microenvironments, which could contribute to the enhanced performance and stability of an enzyme (5). The decoration of different functional proteins on MF-SP-P might have created a favorable microenvironment for SpOpdA-H6 to degrade coumaphos by channeling the substrate onto the active sites of the immobilized enzyme. This phenomenon might explain the improved coumaphos conversion rate by MF-SP-P compared to that by SpOpdA-SP-P, in contrast to immobilized SpBLA-H6 where there was no significant difference in substrate degradation rate for SpBLA-SP-P and MF-SP-P.

The activity of SpOpdA-H6 ligated to SP-P was greater than that of OpdA immobilized on PHA particles *via* direct translational fusion with PhaC. Blatchford *et al.* also reported up to 23% reduction in the conversion rate of coumaphos by PhaC-OpdA beads when compared to that by free OpdA (66). In contrast, BLA immobilized *via* translational fusion with PhaC on BLA-PhaC beads still retained the original substrate conversion rate of soluble BLA (54). However, when both immobilized enzymes were ligated to SP-P, they showed enhanced performance compared with their soluble counterparts at varying rates (**Figure 4**). As mentioned, implementation of this modular approach for immobilization of enzymes could eliminate potential protein misfolding and orientation issues that often happen with surface-displayed proteins on various support materials (28, 29, 67, 68). Furthermore, the

observed increase in catalytic performance of immobilized enzymes using the modular system as described in this study versus the PhaC-fusion based approach could be due to the changes in the physiochemical properties of the PHA particle itself, such as reduced particle size, which in turn leads to a larger surface area over volume ratio of the particles. Fusion of the SpyCatcher protein to the N-terminus of PhaC reduced the particle size of the individual PHA particles (155 nm) compared to that of the wild-type PHA particles (259 nm) as mentioned above. Rubio-Reyes *et al.* noticed a variation in particle size, ranging from 500 to 750 nm when different antigens were displayed on PHA beads (24). González-Miro *et al.* also reported that the particle size of PHA inclusions decreased from 500 nm to 100 nm upon fusion of PsaA to PhaC (30). These observations indicate that fusing different proteins to PhaC impacts the size and size distribution of PHA particles. However, functionalization of SP-P with various SpyTagged proteins *via* SpyTag/SpyCatcher chemistry appears to have minimal impact on the particle size plus a remarkable consistency in the particle dispersity as shown earlier. Therefore, this genetic fusion partner-dependent variability can be reduced by exploiting the modular SpyCatcher-PHA particle approach toward the development of a generic protein-immobilizing platform.

#### **3.4.4 Thermal Stability**

We evaluated the thermal stability of the immobilized and free SpyTagged proteins for their functional performance at varying preincubation temperatures (**Figures 5A–5C**), as described in the Section 3.3.16. The modular immobilization of SpyTagged proteins retained the inherent thermal stability of the soluble form. We observed the same loss of

fluorescence intensity in both immobilized and soluble free SpGFP-H6 as shown in **Figure 5A**. Rapid loss of fluorescence in all samples started at 75°C and was abolished at 85°C, which is in good agreement with the reported values of the GFP melting temperature (76–78°C) (69, 70). This observation shows that the immobilized SpGFP-H6 retained the thermal stability of free SpGFP-H6.

Moreover, immobilized SpOpdA-H6 retained the thermal stability of free SpOpdA-H6, as illustrated in **Figure 5B**. In general, the substrate conversion rate of immobilized and free SpOpdA-H6 remained stable until 65°C, consistent with the reported apparent melting point of free SpOpdA-H6 and PhaC-OpdA PHA beads (66). Interestingly, we detected an early decline in SpOpdA-H6 performance on the MF-SP-P, where we observed ~22% loss in enzyme activity as a result of 10°C rise in temperature from 45 to 55°C. This observation can be explained by the thermal dissociation of unique surface microenvironment created on MF-SP-P as discussed above. Presumably, loss of these surface properties that facilitate better coumaphos degradation resulted in a reduced catalytic performance of MF-SP-P at a lower temperature, although only, back to the rate similar to those of SpOpdA-SP-P.

We noted an increased substrate conversion rate of free SpBLA-H6 at temperatures ranging from 55 to 85°C as shown in **Figure 5C**, in line with several reported studies (71-73). Overall, immobilized SpBLA-H6 on both SpBLA-SP-P and MF-SP-P showed the same thermal stability as that of soluble SpBLA-H6. However, immobilized SpBLA-H6 on MF-SP-P appeared to be slightly more susceptible to thermal degradation in the high-

temperature range when compared to SpBLA-SP-P and soluble SpBLA-H6. This phenomenon could be due to the structural destabilization and shielding of active sites caused by the other immobilized proteins unfolding at elevated temperatures. Although SpBLA-SP-P and soluble SpBLA-H6 were still relatively stable at 85°C, we noticed a ~14% reduction in the activity of SpBLA-H6 on MF-SP-P. We also found that a further increase in temperature between 85 and 95°C resulted in an approximate 27, 16, and 35% loss of activity for soluble SpBLA-H6, SpBLA-SP-P, and MF-SP-P, respectively. Interestingly, immobilized SpBLA-H6 in both SpBLA-SP-P and MF-SP-P maintained high levels of activity in the low-temperature range, whereas higher temperatures were required for BLA immobilized by direct translational fusion to PhaC on PHA beads. The amylase activity of BLA-PhaC beads produced by Rasiah and Rehm had a similar temperature dependency to that of the soluble free BLA (54) suggesting that a broader optimum working temperature range can be achieved using the SpyCatcher-PHA particle approach for thermostable enzymes.

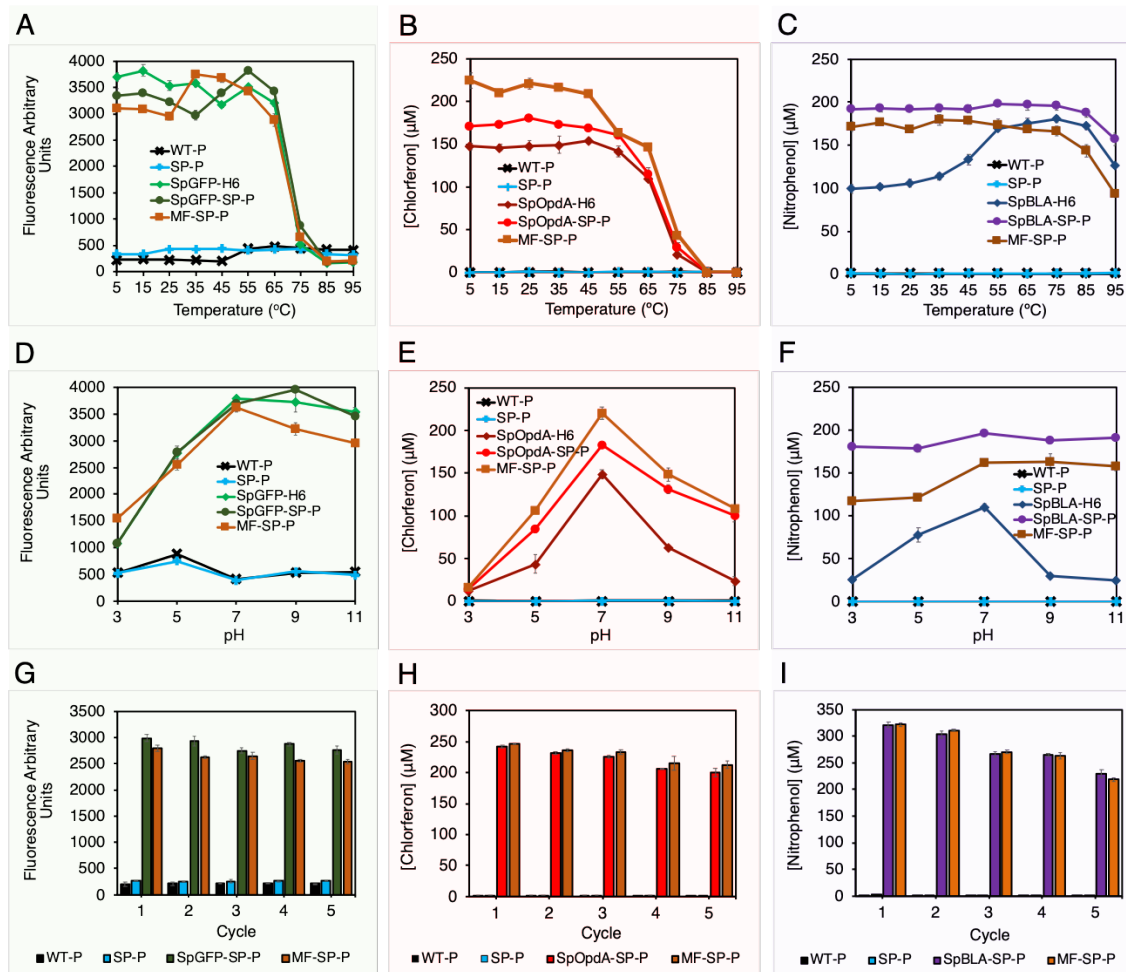


**Figure 5.** Stability and recycling of SpyTagged proteins immobilized to SpyCatcher-PhaC PHA particles. **(A)** Arbitrary fluorescence intensity of immobilized SpGFP-H6 on SpGFP-SP-P and MF-SP-P with controls at varying temperatures (mean  $\pm$  1 SD,  $n = 3$ ). **(B)** Amount of chlorferon released from coumaphos hydrolyzed by immobilized SpOpdA-H6 on SpOpdA-SP-P and MF-SP-P with controls at varying temperatures (mean  $\pm$  1 SD,  $n = 3$ ). **(C)** Amount of nitrophenol liberated from ethylidene-pNP-G7 by immobilized SpBLA-H6 on SpBLA-SP-P and MF-SP-P with controls at varying temperatures (mean  $\pm$  1 SD,  $n = 3$ ). **(D)** Arbitrary fluorescence intensity of immobilized SpGFP-H6 on SpGFP-SP-P and MF-SP-P with controls at varying pH values (mean  $\pm$  1 SD,  $n = 3$ ). **(E)** Amount of

chlorferon released from coumaphos hydrolyzed by immobilized SpOpdA-H6 on SpOpdA-SP-P and MF-SP-P with controls at varying pH values (mean  $\pm$  1 SD,  $n = 3$ ). **(F)** Amount of nitrophenol liberated from ethylidene-pNP-G7 by immobilized SpBLA-H6 on SpBLA-SP-P and MF-SP-P with controls at varying pH values (mean  $\pm$  1 SD,  $n = 3$ ). **(G)** Arbitrary fluorescence intensity of immobilized SpGFP-H6 on SpGFP-SP-P and MF-SP-P with controls over five cycles (mean  $\pm$  1 SD,  $n = 3$ ). **(H)** Amount of chlorferon released from coumaphos hydrolyzed by immobilized SpOpdA-H6 on SpOpdA-SP-P and MF-SP-P with controls over five cycles (mean  $\pm$  1 SD,  $n = 3$ ). **(I)** Amount of nitrophenol liberated from ethylidene-pNP-G7 by immobilized SpBLA-H6 on SpBLA-SP-P and MF-SP-P with controls over five cycles (mean  $\pm$  1 SD,  $n = 3$ ).

### 3.4.5 pH Stability

The stability of enzymes in acidic and alkaline environments is of interest as it affects possible applications in various bioprocesses. To determine the pH stability of both immobilized and soluble proteins, we exposed the various proteins to different pH values ranging from pH 3.0 to 11.0 and then assessed their functionality (**Figures 5D–5F**). GFP is known to be relatively stable in weak alkaline solutions but degrades under acidic conditions, consistent with the pH stability profile of free SpGFP-H6 as shown in **Figure 5D** (74). We observed a similar trend for immobilized SpGFP-H6 on both SpGFP-SP-P and MF-SP-P over the pH range studied. However, we noted an  $\sim$ 17% reduction in the signal of immobilized SpGFP-H6 on MF-SP-P under alkaline conditions which was compensated by a higher fluorescence at pH 3. Although the causes for these are not understood, it is possibly

a result of steric effects caused by the other immobilized proteins, leading to a minimal shift in resistance to pH-triggered destabilization. Jin *et al.* reported a similar observation for the co-immobilization of chloroperoxidase (CPO) and horseradish peroxidase (HRP) on zinc oxide-silicon dioxide composite scaffolds, where reduced enzyme activity was observed for the co-immobilized peroxidases at their respective optimum pH values of 3 and 6 (75). However, this was compensated with higher performance at pH 5 and better tolerance against pH fluctuations (75).

As shown in **Figure 5E**, the SP-P stabilized the immobilized SpOpdA-H6 on both SpOpdA-SP-P and MF-SP-P under alkaline conditions as there was only an approximately 27 and 32% loss in substrate conversion rate at pH 9 when compared to the activity under optimum conditions at neutral pH. In contrast soluble SpOpdA-H6 showed ~55% reduction in substrate conversion rate at pH 9. We observed a notable further deterioration in the SpOpdA-H6 catalytic functionality at pH 11 for all of the samples. Though half of the maximum SpOpdA-H6 activity was retained for SpOpdA-SP-P and MF-SP-P at pH 11, only ~20% of the optimum activity was retained for free SpOpdA-H6. Poor resistance of free SpOpdA-H6 to low pH in this study is consistent with previous findings (76). However, we found improved stability at low pH for SpOpdA-SP-P and MF-SP-P at pH 5, where approximately half of their activity was retained, in contrast to ~32% being retained for soluble free SpOpdA-H6. These data suggested that ligation of SpOpdA-H6 to SP-P strongly increased the pH stability of the enzymes. Venning-Slatter *et al.* also observed the strong loss of OpdA relative catalytic activity at pH 3, when it was immobilized on PHA or GFP particles using translational fusions for *in situ* immobilization. However, their

claim that OpdA immobilized on either PHA or GFP particles was able to withstand a broader pH range was not found for OpdA immobilized to PHA particle *via* ligation (77). Shorter preincubation times (10 min) for their samples in buffers of varying pH could explain this difference. We pretreated our samples in different buffers for a longer time (30 min) before subjecting them to the functional assay. Our results are in good agreement with those obtained by Milani *et al.* and Tang *et al.*, where they preincubated their immobilized OpdA samples for 5 and 1 h, respectively (78, 79).

It is also noteworthy to find that SpBLA-H6 immobilized on SP-P is less susceptible to pH inactivation, especially SpBLA-SP-P as shown in **Figure 5F**. Only ~30% of the optimum substrate conversion rate was retained for soluble free SpBLA-H6 at both low and high pH levels, in agreement with previously published results (71, 73). The stability of SpBLA-H6 ligated to SP-P resembled what had been achieved by using *in situ* immobilization of SpBLA-H6 to PHA particles (54, 77). Whereas SpBLA-SP-P and MF-SP-P retained most of the optimal catalytic performance of SpBLA-H6 at pH 7 (approximately 92 and 72%, respectively) at pH 3. BLA-PHA particles performed poorly at the same pH value (54).

Overall, the pH stability profile of the proteins immobilized to SP-P *via* ligation was improved, particularly at higher pH values. This stabilizing effect is likely to be due to non-specific interactions between proteins and the scaffolding material encouraged by macromolecular crowding (80, 81). Using on-surface circular dichroism spectroscopy, White *et al.* demonstrated analytically that macromolecular crowding of a synthetic peptide BASE-

C, (AQLKKKLQANKKKLAQLKWKLQALKKKLAQGGS) using covalent attachment onto thiol-reactive surfaces drastically shifted the threshold pH for a conformational change from random coil to  $\alpha$ -helical structure (pH 9 in soluble free state to higher than pH 4 in immobilized state). They suggested that the dense packing of BASE-C on the supporting scaffold created an excluded volume effect, driving the change in protein folding *via* hydrophobic interactions (82). In the case of immobilized SpGFP-H6 and SpOpdA-H6, nonspecific stabilizing effects such as electrostatic and hydrophobic interactions could have been disrupted under acidic conditions allowing the ionization of crucial amino acid residues constituting catalytic sites or other structurally important electrostatic interactions. In contrast, the stabilizing interactions for immobilized SpBLA-H6 were able to withstand low pH, so that at least 80% of the SpBLA-H6 activity was retained.

### 3.4.6 Recycling

Although proteins are widely used for a variety of medical and industrial applications, it can be challenging to use them in continuous processing because of their lack of stability as well as the difficulties in separating them from the bulk environment for reuse. Protein immobilization techniques can adapt enzymes to current continuous processing technologies by facilitating their recovery and reuse (83, 84). To show that proteins ligated to SP-P are reusable, we repeated the functional assay of the respective samples in five cycles. Panels G–I in **Figure 5** show the comparison of the repeated use of the immobilized proteins. Respective soluble proteins were recovered by ultrafiltration, and their recycling is shown in **Figure S20**. Overall, the immobilized proteins showed a similar retention of

activity when compared to the respective soluble proteins over five cycles. As shown in **Figure 5G**, immobilized SpGFP-H6 on SpGFP-SP-P and MF-SP-P retained approximately 92 and 91% of the initial fluorescence signal over the cycles, whereas the soluble counterpart retained ~91% (**Figure S20**).

We observed a slightly improved recycling for SpOpdA-H6. **Figure 5H** indicates a notable reuse of the immobilized form of this enzyme, where approximately 83 and 86% of SpOpdA-H6 catalytic activity was retained for SpOpdA-SP-P and MF-SP-P, respectively, compared to 80% of that for free SpOpdA-H6 (**Figure S20**). Venning-Slater *et al.* reported that the OpdA-displaying GFP particles retained ~81% of the substrate conversion rate after seven cycles, which is comparable to our findings (77). Our results suggested that SpOpdA-H6 ligated to SP-P retained a greater proportion of its activity over more cycles of use when compared to OpdA immobilized on polyamide nanofibrous scaffolds or cross-linked to chitosan beads using glutaraldehyde. In these cases, only ~60% of OpdA functionality was retained after five repeated uses (78, 85).

A slight loss of BLA catalytic activity occurred for both SpBLA-SP-P (27%) and MF-SP-P (31%), (**Figure 5I**), whereas soluble SpBLA-H6 only lost 24% of its activity (**Figure S20**). Our results are consistent with previous studies conducted by Gangadharan *et al.* and Radovanović *et al.*, where a ~30% loss in functionality of immobilized amylase over five cycles was reported (86, 87). Additionally, immobilized SpBLA-H6 stable over a greater

number of cycles than BLA displayed on self-assembled protein particles, where less than 10% of the optimum performance was retained at the fourth cycle (77).

### 3.5 Conclusions

In this study, we developed a versatile modular platform for protein immobilization by merging the *in vivo* PHA particle display technology with the *in vitro* SpyTag/SpyCatcher chemistry. SpyTagged proteins can be anchored onto the SpyCatcher-displaying PHA particles *via* rapid formation of a covalent isopeptide bond by simply mixing the two components at room temperature. Our results also revealed that this modular platform shows versatility and tunability through control of molar ratio of SpyTagged proteins to SpyCatcher-PHA particles. This technology allows the convenient co-immobilization of multiple protein functions, leading to the reconstitution of multiprotein complexes at the surface of PHA particles and multifunctionality. Both macromolecular crowding and the creation of favorable microenvironments on the surface of the scaffolding material as well as an oriented display could explain the overall retained or enhanced functionality and stability. In contrast to the *in vivo* PHA particle immobilization, the SpyCatcher-PHA particle approach reduces the risk of protein misfolding because the target protein is produced in a recombinant system that has already been optimized for maximum solubility and/or activity and is separate from particle production. The SpyCatcher-PHA particle approach offers a generic protein immobilization platform where SpyTagged target proteins can be efficiently ligated to a polymeric support material without the need of costly chemical cross-linkers or enzymes.

## **Author Contributions**

**Wong, J. X.** and Rehm, B. H. A. conceived the main conceptual ideas of this study. **Wong, J. X.** designed the study and performed all the experiments. **Wong, J. X.** prepared the manuscript in consultation with Rehm, B. H. A. All authors provided critical feedback and approved to the final version of the manuscript.

## **Funding**

This work was supported by the MacDiarmid Institute of Advanced Materials and Nanotechnology (New Zealand) and School of Fundamental Sciences, Massey University (New Zealand) and Griffith Institute for Drug Discovery, Griffith University (Australia).

## **Conflict of Interest Statement**

B. H. A. Rehm is co-founder and shareholder of PolyBatics Ltd that commercializes veterinary TB diagnostic products related to the PHA particle technology.

## **Acknowledgements**

We thank Manawatu Microscopy and Imaging Centre (Palmerston North, New Zealand) for their assistance with microscopy, and Trevor Loo for his assistance with LC–MS/MS analysis.

### 3.6 References

1. Hoarau M, Badieyan S, Marsh ENG. Immobilized enzymes: understanding enzyme–surface interactions at the molecular level. *Org. Biomol. Chem.* 2017;15(45):9539-51.
2. Rodrigues RC, Ortiz C, Berenguer-Murcia Á, Torres R, Fernández-Lafuente R. Modifying enzyme activity and selectivity by immobilization. *Chem. Soc. Rev.* 2013;42(15):6290-307.
3. Zhao Z, Fu J, Dhakal S, Johnson-Buck A, Liu M, Zhang T, et al. Nanocaged enzymes with enhanced catalytic activity and increased stability against protease digestion. *Nat. Commun.* 2016;7:10619.
4. Fu J, Liu M, Liu Y, Woodbury NW, Yan H. Interenzyme substrate diffusion for an enzyme cascade organized on spatially addressable DNA nanostructures. *J. Am. Chem. Soc.* 2012;134(12):5516-9.
5. Talbert JN, Goddard JM. Enzymes on material surfaces. *Colloids Surf., B.* 2012;93:8-19.
6. Zhang D-H, Yuwen L-X, Peng L-J. Parameters affecting the performance of immobilized enzyme. *J. Chem.* 2013;2013.

7. Guzik U, Hupert-Kocurek K, Wojcieszńska D. Immobilization as a strategy for improving enzyme properties-application to oxidoreductases. *Molecules*. 2014;19(7):8995-9018.
8. Schroeder MM, Wang Q, Badieyan S, Chen Z, Marsh ENG. Effect of surface crowding and surface hydrophilicity on the activity, stability and molecular orientation of a covalently tethered enzyme. *Langmuir*. 2017;33(28):7152-9.
9. Yang Q, Wang B, Zhang Z, Lou D, Tan J, Zhu L. The effects of macromolecular crowding and surface charge on the properties of an immobilized enzyme: activity, thermal stability, catalytic efficiency and reusability. *RSC Adv*. 2017;7(60):38028-36.
10. Balcells C, Pastor I, Vilaseca E, Madurga S, Cascante M, Mas F. Macromolecular crowding effect upon *in vitro* enzyme kinetics: mixed activation–diffusion control of the oxidation of NADH by pyruvate catalyzed by lactate dehydrogenase. *J. Phys. Chem. B*. 2014;118(15):4062-8.
11. Zaak H, Siar E-H, Kornecki JF, Fernandez-Lopez L, Pedrero SG, Virgen-Ortíz JJ, et al. Effect of immobilization rate and enzyme crowding on enzyme stability under different conditions. The case of lipase from *Thermomyces lanuginosus* immobilized on octyl agarose beads. *Process Biochem*. 2017;56:117-23.
12. Morán-Zorzano MT, Viale AM, Muñoz FJ, Alonso-Casajús N, Eydallín GG, Zugasti B, et al. *Escherichia coli* AspP activity is enhanced by macromolecular crowding and

- by both glucose - 1, 6 - biphosphate and nucleotide - sugars. FEBS Lett. 2007;581(5):1035-40.
13. Jia J, Peng X, Qi W, Su R, He Z. Effects of macromolecular crowding on alkaline phosphatase unfolding, conformation and stability. *Int. J. Biol. Macromol.* 2017;101:373-82.
  14. Minton AP. Effect of a concentrated “inert” macromolecular cosolute on the stability of a globular protein with respect to denaturation by heat and by chaotropes: a statistical-thermodynamic model. *Biophys. J.* 2000;78(1):101-9.
  15. Cao X, Li Y, Zhang Z, Yu J, Qian J, Liu S. Catalytic activity and stability of glucose oxidase/horseradish peroxidase co-confined in macroporous silica foam. *Analyst.* 2012;137(24):5785-91.
  16. Fernandez-Lopez L, Pedrero SG, Lopez-Carroble N, Gorines BC, Virgen-Ortíz JJ, Fernandez-Lafuente R. Effect of protein load on stability of immobilized enzymes. *Enzyme Microb. Technol.* 2017;98:18-25.
  17. Niwa T, Sugimoto R, Watanabe L, Nakamura S, Ueda T, Taguchi H. Large-scale analysis of macromolecular crowding effects on protein aggregation using a reconstituted cell-free translation system. *Front. Microbiol.* 2015;6:1113.

18. Siddiqui GA, Naeem A. Aggregation of globular protein as a consequences of macromolecular crowding: A time and concentration dependent study. *Int. J. Biol. Macromol.* 2018;108:360-6.
19. You C, Zhang Y-HP. Self-assembly of synthetic metabolons through synthetic protein scaffolds: one-step purification, co-immobilization, and substrate channeling. *ACS Synth. Biol.* 2012;2(2):102-10.
20. Fontes CM, Gilbert HJ. Cellulosomes: highly efficient nanomachines designed to deconstruct plant cell wall complex carbohydrates. *Annu. Rev. Biochem.* 2010;79:655-81.
21. Xia L, Van Nguyen K, Holade Y, Han H, Dooley K, Atanassov P, et al. Improving the Performance of Methanol Biofuel Cells Utilizing an Enzyme Cascade Bioanode with DNA-Bridged Substrate Channeling. *ACS Energy Lett.* 2017;2(6):1435-8.
22. DiCosimo R, McAuliffe J, Poulouse AJ, Bohlmann G. Industrial use of immobilized enzymes. *Chem. Soc. Rev.* 2013;42(15):6437-74.
23. Parlane NA, Gupta SK, Rubio-Reyes P, Chen S, Gonzalez-Miro M, Wedlock DN, et al. Self-assembled protein-coated polyhydroxyalkanoate beads: properties and biomedical applications. *ACS Biomater. Sci. Eng.* 2016;3(12):3043-57.

24. Rubio-Reyes P, Parlane NA, Wedlock DN, Rehm BH. Immunogenicity of antigens from *Mycobacterium tuberculosis* self-assembled as particulate vaccines. *Int. J. Med. Microbiol.* 2016;306(8):624-32.
25. Lee JW, Parlane NA, Rehm BH, Buddle BM, Heiser A. Engineering mycobacteria for the production of self-assembling biopolyesters displaying mycobacterial antigens for use as a tuberculosis vaccine. *Appl. Environ. Microbiol.* 2017;83(5):e02289-16.
26. Hay ID, Du J, Reyes PR, Rehm BH. *In vivo* polyester immobilized sortase for tagless protein purification. *Microb. Cell Fact.* 2015;14(1):190.
27. Hooks DO, Rehm BH. Surface display of highly-stable *Desulfovibrio vulgaris* carbonic anhydrase on polyester beads for CO<sub>2</sub> capture. *Biotechnol. Lett.* 2015;37(7):1415-20.
28. Du J, Rehm BH. Purification of target proteins from intracellular inclusions mediated by intein cleavable polyhydroxyalkanoate synthase fusions. *Microb. Cell Fact.* 2017;16(1):184.
29. Du J, Rehm BH. Purification of therapeutic proteins mediated by *in vivo* polyester immobilized sortase. *Biotechnol. Lett.* 2018;40(2):369-73.

30. González-Miro M, Rodríguez-Noda L, Fariñas-Medina M, García-Rivera D, Vérez-Bencomo V, Rehm BH. Self-assembled particulate PsaA as vaccine against *Streptococcus pneumoniae* infection. *Heliyon*. 2017;3(4):e00291.
31. Peters V, Rehm BH. *In vivo* monitoring of PHA granule formation using GFP-labeled PHA synthases. *FEMS Microbiol. Lett.* 2005;248(1):93-100.
32. Jahns AC, Rehm BH. Tolerance of the *Ralstonia eutropha* class I polyhydroxyalkanoate synthase for translational fusions to its C terminus reveals a new mode of functional display. *Appl. Environ. Microbiol.* 2009;75(17):5461-6.
33. Rehm BH. Polyester synthases: natural catalysts for plastics. *Biochem. J.* 2003;376(1):15-33.
34. Grage K, Jahns AC, Parlane N, Palanisamy R, Rasiah IA, Atwood JA, et al. Bacterial Polyhydroxyalkanoate Granules: Biogenesis, Structure, and Potential Use as Nano-/Micro-Beads in Biotechnological and Biomedical Applications. *Biomacromolecules*. 2009;10(4):660-9.
35. Sletten EM, Bertozzi CR. Bioorthogonal chemistry: Fishing for Selectivity in a Sea of Functionality. *Angew. Chem., Int. Ed.* 2009;48(38):6974-98.

36. Zakeri B, Fierer JO, Celik E, Chittock EC, Schwarz-Linek U, Moy VT, et al. Peptide tag forming a rapid covalent bond to a protein, through engineering a bacterial adhesin. *Proc. Natl. Acad. Sci. U.S.A.* 2012;109(12):E690-E7.
37. Reddington SC, Howarth M. Secrets of a covalent interaction for biomaterials and biotechnology: SpyTag and SpyCatcher. *Curr. Opin. Chem. Biol.* 2015;29:94-9.
38. Brune KD, Leneghan DB, Brian IJ, Ishizuka AS, Bachmann MF, Draper SJ, et al. Plug-and-Display: decoration of virus-like particles via isopeptide bonds for modular immunization. *Sci. Rep.* 2016;6:19234.
39. Zhang G, Quin M, Schmidt-Dannert C. A self-assembling protein scaffold system for easy in vitro co-immobilization of biocatalytic cascade enzymes. *ACS Catal.* 2018.
40. Ma W, Saccardo A, Roccatano D, Aboagye-Mensah D, Alkaseem M, Jewkes M, et al. Modular assembly of proteins on nanoparticles. *Nat. Commun.* 2018;9(1):1489.
41. Bae Y, Kim GJ, Kim H, Park SG, Jung HS, Kang S. Engineering tunable dual functional protein cage nanoparticles using bacterial superglue. *Biomacromolecules.* 2018.
42. Zhang X-J, Wang X-W, Sun J, Su C, Yang S, Zhang W-B. Synergistic enhancement of enzyme performance and resilience via orthogonal peptide-protein chemistry enabled multilayer construction. *Biomacromolecules.* 2018.

43. Zhang X-J, Wang X-W, Da X-D, Shi Y, Liu C, Sun F, et al. A versatile and robust approach to stimuli-responsive protein multilayers with biologically enabled unique functions. *Biomacromolecules*. 2018;19(3):1065-73.
44. Thrane S, Janitzek CM, Matondo S, Resende M, Gustavsson T, Jongh WA, et al. Bacterial superglue enables easy development of efficient virus-like particle based vaccines. *J. Nanobiotechnol*. 2016;14(1):30.
45. Brune KD, Buldun CM, Li Y, Taylor IJ, Brod F, Biswas S, et al. Dual plug-and-display synthetic assembly using orthogonal reactive proteins for twin antigen immunization. *Bioconjugate Chem*. 2017;28(5):1544-51.
46. Bruun TUJ, Andersson A-MC, Draper SJ, Howarth M. Engineering a rugged nanoscaffold to enhance plug-and-display vaccination. *ACS Nano*. 2018.
47. Jia L, Minamihata K, Ichinose H, Tsumoto K, Kamiya N. Polymeric SpyCatcher Scaffold Enables Bioconjugation in a Ratio - Controllable Manner. *Biotechnol. J*. 2017;12(12).
48. Sambrook J, Fritsch EF, Maniatis T. *Molecular cloning: a laboratory manual*: Cold Spring Harbor Laboratory Press; 1989.
49. Gonzalez-Miro M, Rodríguez-Noda LM, Fariñas-Medina M, Cedré-Marrero B, Madariaga-Zarza S, Zayas-Vignier C, et al. Bioengineered polyester beads co-

- displaying protein and carbohydrate-based antigens induce protective immunity against bacterial infection. *Sci. Rep.* 2018;8(1):1888.
50. Laemmli UK. Cleavage of structural proteins during the assembly of the head of bacteriophage T4. *Nature.* 1970;227(5259):680.
51. Hay ID, Hooks DO, Rehm BH. Use of bacterial polyhydroxyalkanoates in protein display technologies. *Hydrocarbon and Lipid Microbiology Protocols: Springer*; 2014. p. 71-86.
52. Shevchenko A, Tomas H, Havli J, Olsen JV, Mann M. In-gel digestion for mass spectrometric characterization of proteins and proteomes. *Nat. Protoc.* 2006;1(6):2856.
53. Braunegg G, Sonnleitner B, Lafferty R. A rapid gas chromatographic method for the determination of poly- $\beta$ -hydroxybutyric acid in microbial biomass. *Appl. Microbiol. Biotechnol.* 1978;6(1):29-37.
54. Rasiah IA, Rehm BH. One-step production of immobilized  $\alpha$ -amylase in recombinant *Escherichia coli*. *Appl. Environ. Microbiol.* 2009;75(7):2012-6.
55. Harcourt R, Horne I, Sutherland T, Hammock B, Russell R, Oakeshott J. Development of a simple and sensitive fluorimetric method for isolation of coumaphos-hydrolysing bacteria. *Lett. Appl. Microbiol.* 2002;34(4):263-8.

56. Mayer F, Hoppert M. Determination of the thickness of the boundary layer surrounding bacterial PHA inclusion bodies, and implications for models describing the molecular architecture of this layer. *J. Basic Microbiol.* 1997;37(1):45-52.
57. Schubert P, Krüger N, Steinbüchel A. Molecular analysis of the *Alcaligenes eutrophus* poly (3-hydroxybutyrate) biosynthetic operon: identification of the N terminus of poly (3-hydroxybutyrate) synthase and identification of the promoter. *J. Bacteriol.* 1991;173(1):168-75.
58. Karimi M, Depicker A, Hilson P. Recombinational cloning with plant gateway vectors. *Plant Physiol.* 2007;145(4):1144-54.
59. Liu Y, Hu B, Xu Y, Bo J, Fan S, Wang J, et al. Improvement of the acid stability of *Bacillus licheniformis* alpha-amylase by error - prone PCR. *J. Appl. Microbiol.* 2012;113(3):541-9.
60. Thakur S, Reddy MV, Siddavattam D, Paul A. A fluorescence based assay with pyranine labeled hexa-histidine tagged organophosphorus hydrolase (OPH) for determination of organophosphates. *Sens. Actuators, B.* 2012;163(1):153-8.
61. Gasteiger E, Hoogland C, Gattiker A, Wilkins MR, Appel RD, Bairoch A. Protein identification and analysis tools on the ExPASy server. *The Proteomics Protocols Handbook*: Springer; 2005. p. 571-607.

62. Kao K-C, Lin T-S, Mou C-Y. Enhanced activity and stability of lysozyme by immobilization in the matching nanochannels of mesoporous silica nanoparticles. *J. Phys. Chem. C*. 2014;118(13):6734-43.
  
63. Yamada K, Iizawa Y, Yamada Ji, Hirata M. Retention of activity of urease immobilized on grafted polymer films. *J. Appl. Polym. Sci.* 2006;102(5):4886-96.
  
64. Chae HJ, In M-J, Kim EY. Optimization of protease immobilization by covalent binding using glutaraldehyde. *Appl. Biochem. Biotechnol.* 1998;73(2-3):195-204.
  
65. Ganapathi S, Butterfield DA, Bhattacharyya D. Flat-sheet and hollow fiber membrane bioreactors: A study of the kinetics and active site conformational changes of immobilized papain including sorption studies of reaction constituents. *J. Chem. Technol. Biotechnol.* 1995;64(2):157-64.
  
66. Blatchford PA, Scott C, French N, Rehm BH. Immobilization of organophosphohydrolase OpdA from *Agrobacterium radiobacter* by overproduction at the surface of polyester inclusions inside engineered *Escherichia coli*. *Biotechnol. Bioeng.* 2012;109(5):1101-8.
  
67. Rehm FB, Grage K, Rehm BH. Applications of microbial biopolymers in display technology. *Consequences of Microbial Interactions with Hydrocarbons, Oils, and Lipids: Production of Fuels and Chemicals*. 2016:1-17.

68. Rehm FB, Chen S, Rehm BH. Bioengineering toward direct production of immobilized enzymes: a paradigm shift in biocatalyst design. *Bioengineered*. 2018;9(1):6-11.
69. Nicholls SB, Hardy JA. Structural basis of fluorescence quenching in caspase activatable-GFP. *Protein Sci*. 2013;22(3):247-57.
70. Tsien RY. The green fluorescent protein. *Annu. Rev. Biochem*. **1998**;67:509-44.
71. Abdel-Fattah YR, Soliman NA, El-Toukhy NM, El-Gendi H, Ahmed RS. Production, purification, and characterization of thermostable  $\alpha$ -amylase produced by *Bacillus licheniformis* isolate AI20. *J. Chem*. 2012;2013.
72. Declerck N, Machius M, Joyet P, Wiegand G, Huber R, Gaillardin C. Hyperthermostabilization of *Bacillus licheniformis*  $\alpha$ -amylase and modulation of its stability over a 50°C temperature range. *Protein Eng*. 2003;16(4):287-93.
73. Ivanova VN, Dobрева EP, Emanuilova EI. Purification and characterization of a thermostable  $\alpha$ -amylase from *Bacillus licheniformis*. *J. Biotechnol*. 1993;28(2-3):277-89.
74. Ward WW. Properties of the coelenterate green-fluorescent proteins. *Bioluminescence and Chemiluminescence: Basic Chemistry and Analytical Applications*. 1981:225-34.

75. Jin X, Li S, Long N, Zhang R. A robust and stable nano - biocatalyst by co - immobilization of chloroperoxidase and horseradish peroxidase for the decolorization of azo dyes. *J. Chem. Technol. Biotechnol.* 2018;93(2):489-97.
76. Cheng YD, Karns JS, Torrents A. Characterization of a phosphotriesterase from genetically-engineered *Escherichia coli*. *Journal of Environmental Science & Health Part B.* 1998;33(4):347-67.
77. Venning-Slater M, Hooks DO, Rehm BH. *In vivo* self-assembly of stable green fluorescent protein fusion particles and their uses in enzyme immobilization. *Appl. Environ. Microbiol.* 2014;80(10):3062-71.
78. Milani MM, Lotfi AS, Mohsenifar A, Mikaili P, Kamelipour N, Dehghan J. Enhancing organophosphorus hydrolase stability by immobilization on chitosan beads containing glutaraldehyde. *Res. J. Environ. Toxicol.* 2015;9(1):34-44.
79. Tang X, Liang B, Yi T, Manco G, Liu A. Cell surface display of organophosphorus hydrolase for sensitive spectrophotometric detection of p-nitrophenol substituted organophosphates. *Enzyme Microb. Technol.* 2014;55:107-12.
80. Minton AP. Excluded volume as a determinant of macromolecular structure and reactivity. *Biopolymers.* 1981;20(10):2093-120.

81. Sarkar M, Li C, Pielak GJ. Soft interactions and crowding. *Biophys. Rev.* 2013;5(2):187-94.
82. White SJ, Johnson SD, Sellick MA, Bronowska A, Stockley PG, Wälti C. The Influence of Two-Dimensional Organization on Peptide Conformation. *Angew. Chem.* 2015;127(3):988-92.
83. Hanefeld U, Gardossi L, Magner E. Understanding enzyme immobilisation. *Chem. Soc. Rev.* 2009;38(2):453-68.
84. Sheldon RA. Enzyme immobilization: the quest for optimum performance. *Adv. Synth. Catal.* 2007;349(8-9):1289-307.
85. Yan X-Y, Jiang Y-J, Zhang S-P, Gao J, Zhang Y-F. Dual-functional OPH-immobilized polyamide nanofibrous membrane for effective organophosphorus toxic agents protection. *Biochem. Eng. J.* 2015;98:47-55.
86. Gangadharan D, Nampoothiri KM, Sivaramakrishnan S, Pandey A. Immobilized bacterial  $\alpha$ -amylase for effective hydrolysis of raw and soluble starch. *Food Res. Int.* 2009;42(4):436-42.
87. Radovanović M, Jugović B, Gvozdenović M, Jokić B, Grgur B, Bugarski B, et al. Immobilization of  $\alpha$ -amylase via adsorption on magnetic particles coated with polyaniline. *Starch-Stärke.* 2016;68(5-6):427-35.

### 3.7 Supporting Information

#### Strains, plasmids and primers used in this study

**Table S1.** Bacterial strains used in the current study.

Bacterial strains	Characteristics	References
<i>Escherichia coli</i> XL1-Blue	<i>recA1 endA1 gyrA96 thi-1 hsdR17 supE44 RelA1 lac</i> [F' <i>proAB lacI<sup>q</sup>ZΔM15</i> Tn10 ( <i>Tet<sup>r</sup></i> )]	Stratagene
<i>Escherichia coli</i> BL21(DE3)	F' <i>dcm ompT hsdS</i> (r <sub>B</sub> -m <sub>B</sub> -) gal λ(DE3)	Invitrogen

**Table S2.** Plasmids constructed and used in the current study.

Plasmids	Characteristics	References
pET14b	Ap <sup>r</sup> ; T7 promoter	Novagen
pMSC69	Cm <sup>r</sup> ; pBBR1MCS derivative containing genes <i>phaA</i> and <i>phaB</i> from <i>C. necator</i> co-linear to <i>lac</i> promoter.	(Amara & Rehm, 2003)
pUC57_SpyCatcher-Hsa-SpyCatcher	pET14b derivative consisting two <i>SpyCatcher</i> genes flanking at both 5'	Genscript cooperation

	and 3' end of <i>Hsa PolIII</i> intein.	
pET14b-ZZ-linker-ZZ- phaC- L	pET14b derivative consisting <i>zz-linker- zz</i> fused to the 5' end of <i>phaC</i> via a linker sequence and <i>L-domain</i> fused to the 3' end of <i>phaC</i> .	(Rajendran & Rehm, 2012)
pET14b_PhaC_linker_GFP	pET14b derivative consisting <i>gfp</i> fused to the 3' end of <i>phaC</i> via a linker sequence.	(Jahns & Rehm, 2009)
pET14b_phaC_linker_OpdA	pET14b derivative consisting <i>opda</i> fused to the 3' end of <i>phaC</i> via a linker sequence.	(Blatchford et al., 2012)
pET14b-BLAlphaC	pET14b derivative consisting <i>BLA(+ss)</i> fused to the 5' end of <i>phaC</i> .	(Rasiah & Rehm, 2009)
pET14b_PhaC_linker_ SpyCatcher	pET14b derivative consisting <i>SpyCatcher</i> fused to the 3' end of <i>phaC</i> via a linker sequence.	This study
pET14b_ZZ_ _ZZ_PhaC_ linker_SpyCatcher	pET14b_ZZ_ _ZZ_PhaC_ linker_L derivative consisting	This study

	<i>SpyCatcher</i> at 3' end of <i>phaC</i>	
pET14b_SpyCatcher_PhaC_ linker_SpyCatcher	pET14b_ZZ_ _ZZ_PhaC_ linker_SpyCatcher derivative consisting <i>SpyCatcher</i> at both 5' end and 3' end of <i>phaC</i> .	This study
pET14b_SpyCatcher_PhaC	pET14b_SpyCatcher_PhaC_ linker_SpyCatcher derivative consisting <i>SpyCatcher</i> at 5' end of <i>phaC</i> .	This study
pET14b_SpyTag-GFP-His <sub>6</sub>	pET14b_PhaC_linker_GFP derivative consisting <i>SpyTag</i> at 5' end of <i>gfp</i> and hexahistidine tag at 3' end of <i>gfp</i> .	This study
pET14b_SpyTag-OpdA- His <sub>6</sub> .	pET14b_PhaC_linker_OpdA derivative consisting <i>SpyTag</i> at 5' end of <i>opda</i> and hexahistidine tag at 3' end of <i>opda</i> .	This study
pET14b_SpyTag-BLA-His <sub>6</sub> .	pET14b_ BLAphaC derivative consisting <i>SpyTag</i> at 5' end of <i>bla</i> and hexahistidine tag at 3' end of <i>bla</i> .	This study

**Table S3.** Primers constructed and used in the current study.

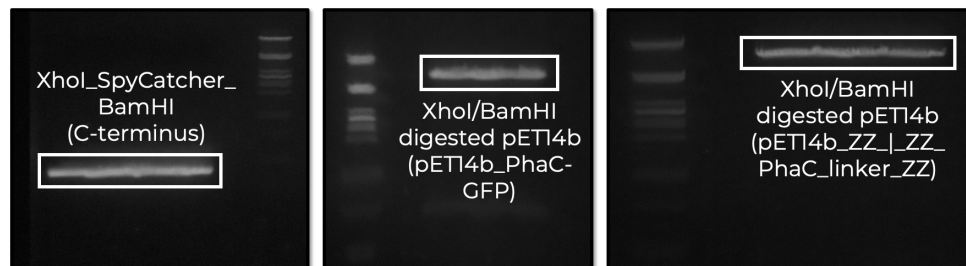
Primers	Restriction sites	Sequence	References
N_SpyC_FWD	XbaI & SpeI	5'TATATCTAGAAATAAGGAGAT ACTAGTATGGGTGCGATGGTTG ATACCCTG	This study
N_SpyC_RVR_1	AvrII	5'TTTATACCTAGGAATGTGCGC ATCGCCTTTGGT	This study
N_SpyC_RVR_2	BamHI	5'TTTATAGGATCCTTACCATATG TGCCTTGGCTTTGACGTATC	This study
C_SpyC_FWD	XhoI	5'TATATACTCGAGGGTGCGATG GTTGATACCCTGAGC	This study
C_SpyC_RVR	BamHI	5'TTTATAGGATCCTTAAATGTGC GCATCGCCTTTGGT	This study
SpyTag-GFP-His <sub>6</sub> _FWD	SpeI	5'ATATTTACTAGTATGGCTCATA TTGTGATGGTGGATGCGTATAA ACCGACCAAAGGAGGTGGAAGT	This study

		AAAGGAGAAGAACTTTTCACTG GA	
SpyTag-GFP- His <sub>6</sub> _RVR	BamHI	5'ATATTTGGATCCTCAGTGATG ATGGTGATGATGTTTGTATAGTT CATCCATGCCATGTGT	This study
SpyTag-OpdA- His <sub>6</sub> _FWD	SpeI	5'ATATTTACTAGTATGGCTCATA TTGTGATGGTGGATGCGTATAA ACCGACCAAAGGAGGTGGAAGC ATGGCCCGACCAATCGGTACAG GC	This study
SpyTag-OpdA- His <sub>6</sub> _RVR	BamHI	5'ATATTTGGATCCTCAGTGATG ATGGTGATGATGCGACGCCCGC ACGGTCGGTGA	This study
SpyTag-BLA- His <sub>6</sub> _FWD	SpeI	5'ATATTTACTAGTATGGCTCATA TTGTGATGGTGGATGCGTATAA ACCGACCAAAGGAGGTGGAGCT AACCTGAACGGTACCCTGATG	This study
SpyTag-BLA- His <sub>6</sub> _RVR	BamHI	5'ATATTTGGATCCTCAGTGATG ATGGTGATGATGGCGCTGGACG TAGATGGAAACAGA	This study

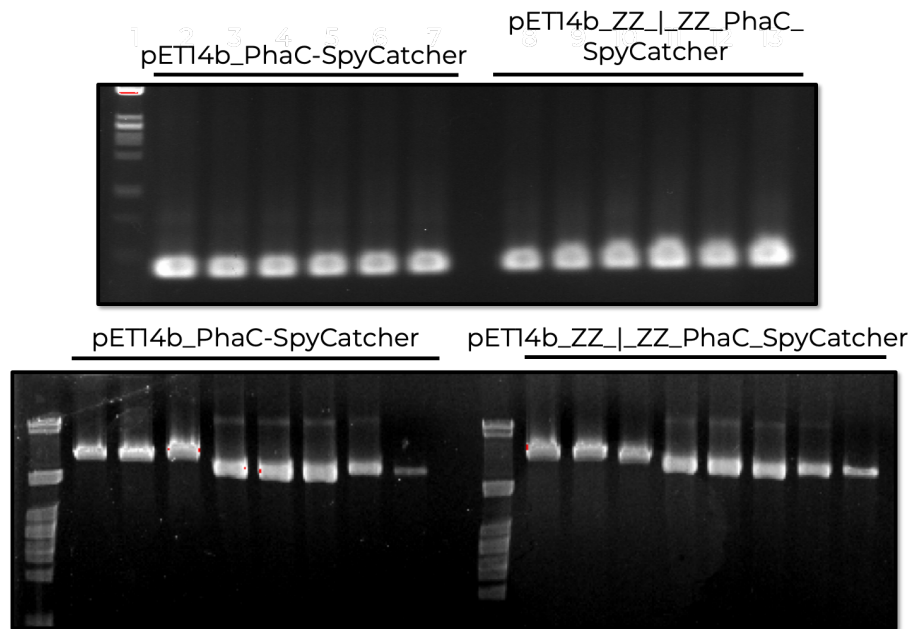
## Plasmid construction strategies.

SpyCatcher DNA fragments flanked by different restriction sites were amplified using pUC57\_SpyCatcher-Hsa-SpyCatcher, synthesized by Genscript Corporation (Piscataway, NJ).

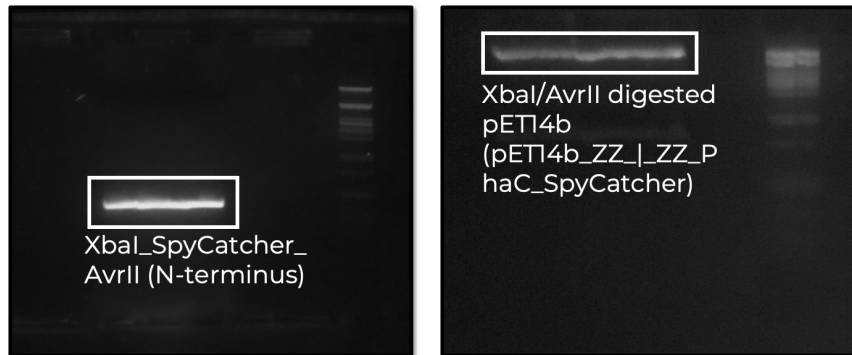
In this study, for plasmid pET14b\_PhaC\_linker\_SpyCatcher, the SpyCatcher DNA fragment flanked by XhoI and BamHI was amplified using primers C\_SpyC\_FWD and C\_SpyC\_RVR. The resulting PCR product, plasmid pET14b\_PhaC\_linker\_GFP and plasmid pET14b\_ZZ\_|\_ZZ\_PhaC\_L were digested with both restriction enzymes XhoI and BamHI.



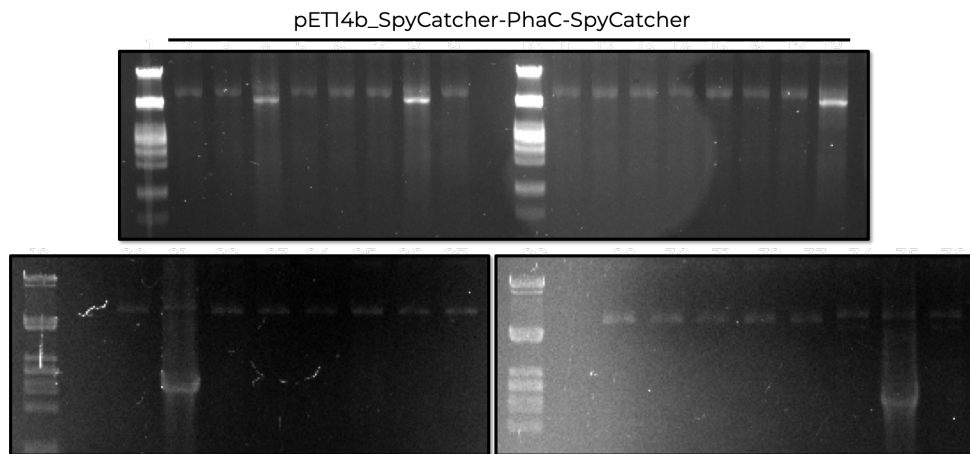
The digested PCR fragment was ligated into the respective digested vectors, to replace the gene corresponding to GFP and C-terminal ZZ domain respectively with SpyCatcher gene, resulting in plasmid pET14b\_PhaC\_linker\_SpyCatcher and pET14b\_ZZ\_|\_ZZ\_PhaC\_linker\_SpyCatcher.



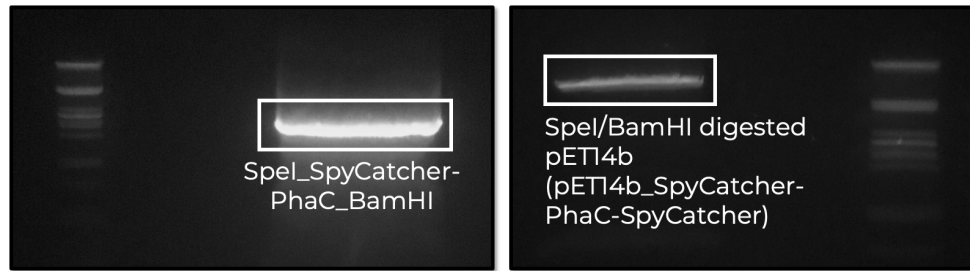
SpyCatcher DNA fragment flanked by XbaI and AvrII was amplified using primers N\_SpyC\_FWD and N\_SpyC\_RVR\_1. The resulting PCR product and plasmid pET14b\_ZZ\_|\_ZZ\_PhaC\_linker\_SpyCatcher were digested with restriction enzymes XbaI and AvrII.



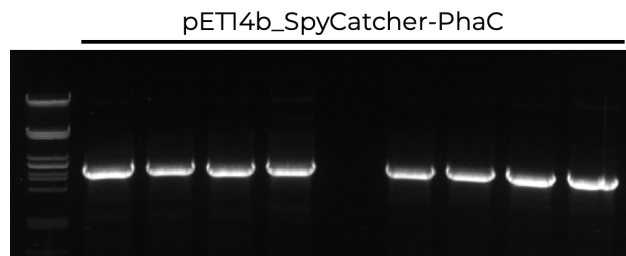
The digested PCR fragment and vector were ligated, resulting in plasmid pET14b\_SpyCatcher\_PhaC\_linker\_SpyCatcher.



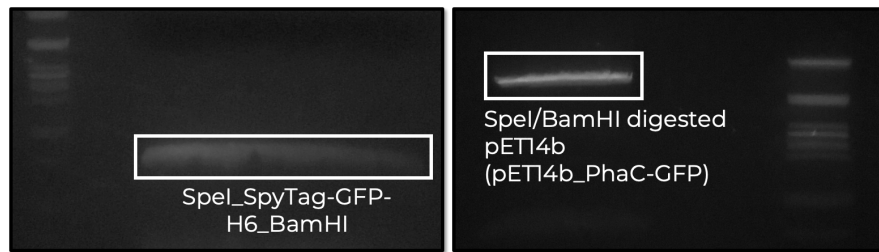
Using pET14b\_SpyCatcher\_PhaC\_linker\_SpyCatcher as template, primers N\_SpyC\_FWD and N\_SpyC\_RVR\_2 were used to amplify the region corresponding from N-terminal SpyCatcher to C-terminal end of PhaC. The resulting PCR product and plasmid pET14b\_PhaC\_linker\_GFP were digested with restriction enzymes SpeI and BamHI.



The digested PCR fragment and vector were ligated, resulting in plasmid pET14b\_SpyCatcher\_PhaC.

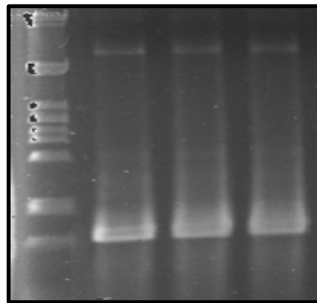


Spy- and His-tagged green fluorescent protein (GFP), SpyTag-GFP-His<sub>6</sub> was constructed using pET14b\_phaC\_linker\_GFP as template. The gene corresponding to GFP was amplified to add SpyTag (AHIVMVDAKYK PTK) at the N-terminal region and hexahistidine tag (HHHHHH) at the C-terminal region. The resulting PCR product and plasmid pET14b\_PhaC\_linker\_GFP were digested with restriction enzymes SpeI and BamHI.



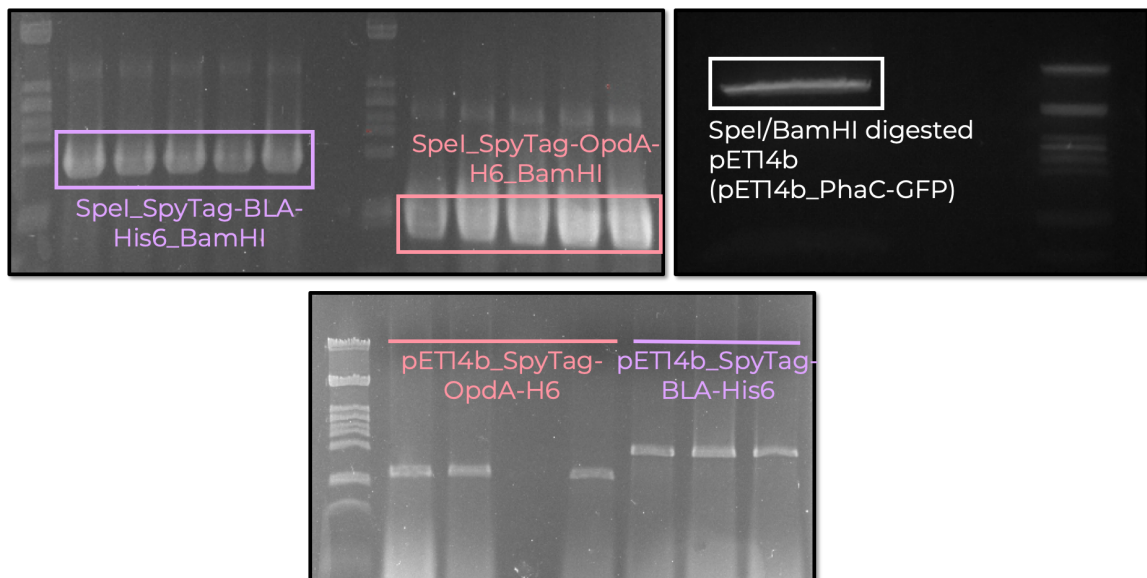
The digested PCR fragment and vector were ligated, resulting in plasmid pET14b\_SpyTag-GFP-His<sub>6</sub>.

pET14b\_SpyTag-GFP-H6



Spy- and His-tagged organophosphohydrolase (OpdA), SpyTag-OpdA-His<sub>6</sub> was constructed using pET14b\_phaC\_OpdA as template. The gene corresponding to OpdA was amplified to add SpyTag (AHIVMVDAKYK PTK) at the N-terminal region and hexahistidine tag (HHHHHH) at the C-terminal region. The resulting PCR product and plasmid pET14b\_PhaC\_linker\_GFP were digested with restriction enzymes SpeI and BamHI. The digested PCR fragment and vector were ligated, resulting in plasmid pET14b\_SpyTag-OpdA-His<sub>6</sub>.

Spy- and His-tagged *Bacillus licheniformis*  $\alpha$ -amylase (BLA), SpyTag-BLA-His<sub>6</sub> was constructed using pET14b\_phaC\_linker\_BLA as template. The gene corresponding to BLA was amplified to add SpyTag (AHIVMVDAKYK PTK) at the N-terminal region and hexahistidine tag (HHHHHH) at the C-terminal region. The resulting PCR product and plasmid pET14b\_PhaC\_linker\_GFP were digested with restriction enzymes SpeI and BamHI. The digested PCR fragment and vector were ligated, resulting in plasmid pET14b\_SpyTag-BLA-His<sub>6</sub>.



## Equations used in this study

**Equations S1–S4:** Determination of production yields of protein displayed on PHA particles

$$\frac{\text{mass of total protein}}{\text{mass of PHA particle}}$$

= Total mass of protein per mass of PHA particle (**Equation S1**)

$$\frac{\text{mass of total protein}}{\text{mass of PHA particle}} \times \frac{M_w \text{ of target protein}}{M_w \text{ of total protein}}$$

= Target mass of protein per mass of PHA particle (**Equation S2**)

$$\frac{\text{mass of total protein} / \text{mass of PHA particle}}{\text{molecular weight of of total protein}}$$

= Number of moles of total protein per mass PHA particle (**Equation S3**)

$$\frac{\text{mass of total protein} / \text{mass of PHA particle}}{\text{molecular weight of of total protein}} \times \frac{M_w \text{ of target protein}}{M_w \text{ of total protein}}$$

= Number of moles of target protein per mass PHA particle (**Equation S4**)

**Equation S5:** Determination of molarity

$$\frac{\text{mass of target protein}}{\text{molecular weight of target protein} \times \text{volume of PHA particle slurry}} = \text{Molarity (**Equation S5**)}$$

**Equations S6 and S7:** Determination of percentage surface coverage and percentage ligation efficiency of SpyTagged protein covalently ligated to SpyCatcher protein on PHA particles

$$\frac{\text{band intensity of immobilized SpyTagged protein}}{\text{band intensity of immobilized SpyTagged protein} + \text{band intensity of unligated SpyCatcher protein}} \times 100\%$$

= Percentage surface coverage (**Equation S6**)

$$\frac{\text{band intensity of immobilized SpyTagged protein}}{\text{band intensity of immobilized SpyTagged protein} + \text{band intensity of unligated soluble SpyTagged protein in supernatant}} \times 100\%$$

= Percentage ligation efficiency (**Equation S7**)

**Equations S8 and S9:** Determination of total SpyCatcher protein mass per wet particle

$$\frac{1}{(\text{Density of PHA particle slurry}) \left( \frac{4}{3} \pi (\text{Sauter mean diameter})^3 \right)}$$

= Number of PHA particles per mass of wet PHA particle (**Equation S8**)

$$\frac{\text{Mass of SpyCatcher per mass of wet PHA particle}}{\text{Number of PHA particles per mass of wet PHA particle}}$$

= Mass of protein domain per wet PHA particle (**Equation S9**)

**Equations S10–S13:** Determination of number of SpyCatcher protein per surface area of wet PHA particle

$$= \frac{\text{Number of moles of SpyCatcher protein per mass of wet PHA particle}}{\text{Avogadro's constant}} = \text{Total number of SpyCatcher protein per mass of wet PHA particle (Equation S10)}$$

$$= \frac{\text{Total number of SpyCatcher protein per mass of wet PHA particle}}{\text{Number of PHA particles per mass of wet PHA particle}} = \text{Total number of SpyCatcher protein per wet PHA particle (Equation S11)}$$

$$= \frac{\text{Specific surface area}}{\text{Number of PHA particles per mass of wet PHA particle}} = \text{Surface area per wet PHA particle (Equation S12)}$$

$$= \frac{\text{Total number of SpyCatcher domain displayed per wet PHA particle}}{\text{Surface area per wet PHA particle}} = \text{Total number of SpyCatcher domain protein per surface area of wet PHA particle (Equation S13)}$$

**Identification of fusion proteins by liquid chromatography-tandem mass spectrometry (LC–MS/MS)**

**Table S4.** LC–MS/MS analysis of fusion proteins.

Fusion protein	Amino acid coverage (%)	Peptide fragments identified by LC–MS/MS.*
<b>SpyCatcher-PhaC (SP)</b>	85.8%	<b>G1-K31, R35-R60, T66-K108, G112-I116,</b> P117-R118, S135-R193, D197-R219, F221-R227, F234-R260. F265-R299, N304-K353, Y369-R418, D425-K617, F620-K637, S641-K681, L715-N733.
<b>SpyTagged</b> <i>Aequorea victoria</i> green fluorescent protein bearing His <sub>6</sub> tag ( <b>SpGFP-H6</b> )	93.1%	<b>A1-K14,</b> G15-R89, R95-R138, G143-K254
<b>SpyTagged</b> <i>Agrobacterium radiobacter</i> Organophosphohydrolase	78.5%	<b>A1-K14,</b> G34-R59, A84-R90, L104-R130, S134-R156, V160-R267, A273-R282, I288-R323, E330-R355.

bearing His <sub>6</sub> tag ( <b>Sp</b> OpdA-H6)		
<b>SpyTagged</b> <i>Bacillus licheniformis</i> $\alpha$ -amylase bearing His <sub>6</sub> tag ( <b>Sp</b> BLA-H6)	88.5%	<b>A1-K14</b> , G15-R91, Y94-R144, A154-K187, A198-R246, D260-R266, T269-K332, A337-R392, H399-R454, Q460-R500
<b>Sp</b> GFP-H6 ligated with <b>SP</b> ( <b>Sp</b> GFP- <b>SP</b> -L)	78.4%	<b>A1-K14</b> , G19-K57, L69-R89, S102-K123, A126-R138, G143-K172, H185-K225, R231-K254, <b>R295-R310</b> , <b>T316-K368</b> , S395-R453, D457-R479, F494-R520, I523-R559, N564-R571, I574-K613, Y629-R678, D685-K677, F680-K897, S900-K941, K982-N993
<b>Sp</b> OpdA-H6 ligated with <b>SP</b> ( <b>Sp</b> OpdA- <b>SP</b> -L)	79.1%	<b>A1-K14</b> , <b>G34-R59</b> , <b>A84-R100</b> , <b>L104-R130</b> , <b>S134-R156</b> , <b>V162-R267</b> , <b>A273-R282</b> , <b>I288-R323</b> , <b>E330-R355</b> , <b>R398-R413</b> , <b>D431-K471</b> , <b>G475-I479</b> , P480-R481, S498-R556, D560-R590, F597-R623, I626-R662, N667-K716, Y732-R780, D788-K980, F983-K1000, S1004-K1044, K1085-N1096

SpBLA-H6 ligated with SP (SpBLA-SP-L)	78.2%	<b>A1-K14</b> , G15-K87, Y94-K105, D111- R142, A154-R163, W172-R186, A198- R246, D260-R266, E272-K332, A337- K387, H399-K406, Q410-K453, Q460- <b>R500</b> , <b>R542-R557</b> , <b>T563-K615</b> , S642- R700, D704-K716, F727-R734, F741- R767, F772-R806, N811-R818, I821- K860, Y866-R925, D932-K1137, S1148- K1188, K1229-N1240.
--	-------	--

\***Gold bold, SpyCatcher**; **Blue bold, SpyTag**; Black, PhaC; Green, GFP; **Red, OpdA**;  
Purple, BLA.

**Densitometric protein quantification of SP fusion protein on PHA particles and SpyTagged proteins for SpyTag/SpyCatcher chemistry ligation optimization.**

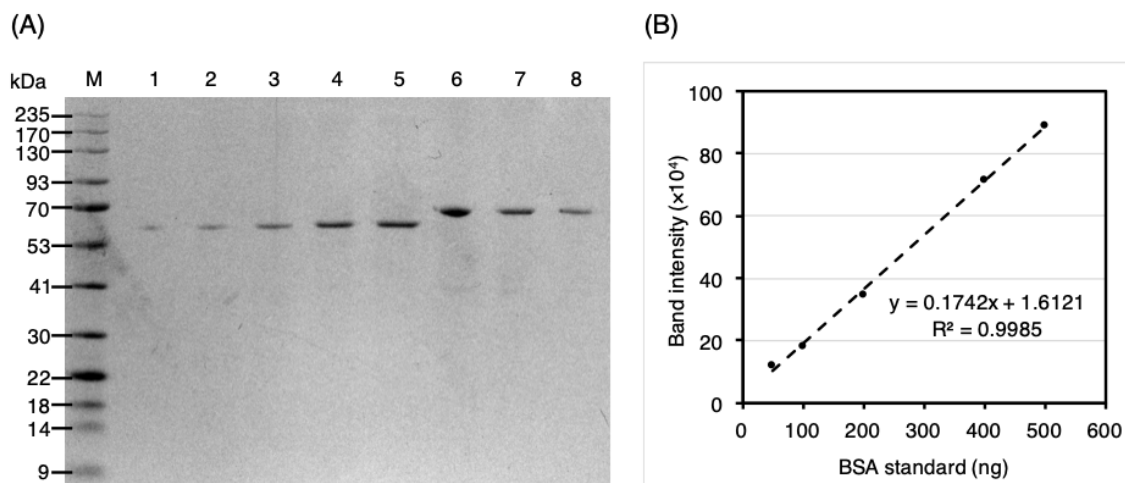


**Figure S1.** Densitometric protein quantification of SP fusion protein on PHA particles using BSA standard. **(A)** SDS–PAGE analysis of SP fusion protein at varying dilution factors. Lane M, Gangnam pre-stained protein marker; lane 1, BSA (5 ng); lane 2, BSA (100 ng); lane 3, BSA (200 ng); lane 4, BSA (400 ng); lane 5, BSA (500 ng); lane 6, SP (dilution factor of 47); lane 7, SP (dilution factor of 94); lane 8, SP (dilution factor of 187). **(B)** BSA standard curve obtained from the SDS–PAGE analysis for densitometric analysis.

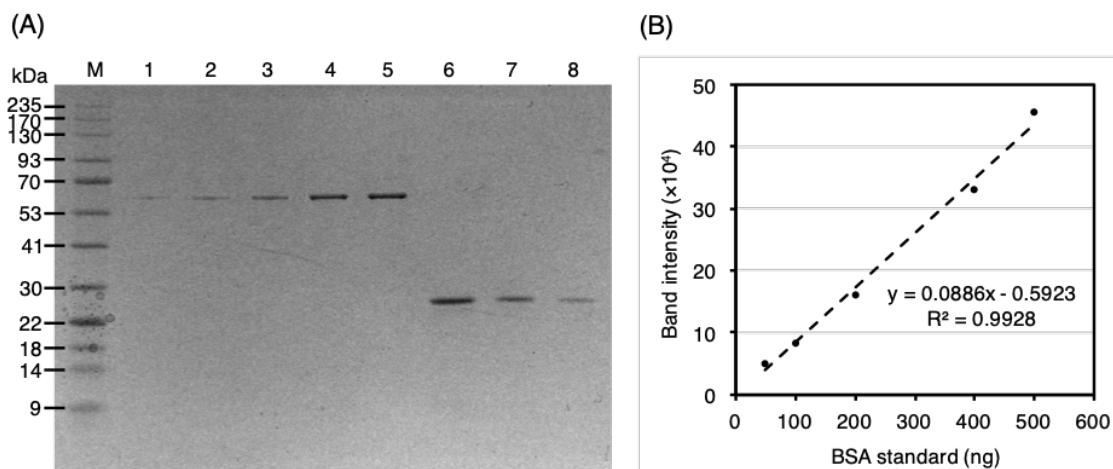


**Figure S2.** Densitometric protein quantification of SpGFP-H6 using BSA standard. **(A)** SDS-PAGE analysis of SpGFP-H6 at varying dilution factors. Lane M, Gangnam pre-stained protein marker; lane 1, BSA (5 ng); lane 2, BSA (100 ng); lane 3, BSA (200 ng); lane 4, BSA (400 ng); lane 5, BSA (500 ng); lane 6, SpGFP-H6 (dilution factor of 6); lane 7, SpGFP-H6 (dilution factor of 12); lane 8, SpGFP-H6 (dilution factor of 24). **(B)** BSA standard curve obtained from the SDS-PAGE analysis for densitometric analysis.

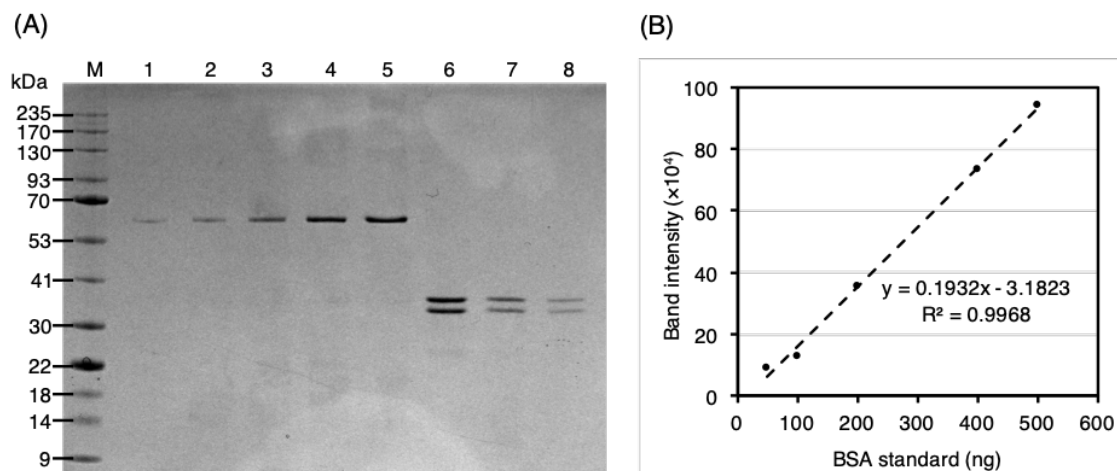


**Figure S3.** Densitometric protein quantification of SpOpdA-H6 using BSA standard. **(A)** SDS-PAGE analysis of SpOpdA-H6 at varying dilution factors. Lane M, Gangnam pre-stained protein marker; lane 1, BSA (5 ng); lane 2, BSA (100 ng); lane 3, BSA (200 ng); lane 4, BSA (400 ng); lane 5, BSA (500 ng); lane 6, SpOpdA-H6 (dilution factor of 6); lane 7, SpOpdA-H6 (dilution factor of 12); lane 8, SpOpdA-H6 (dilution factor of 24). **(B)** BSA standard curve obtained from the SDS-PAGE analysis for densitometric analysis.

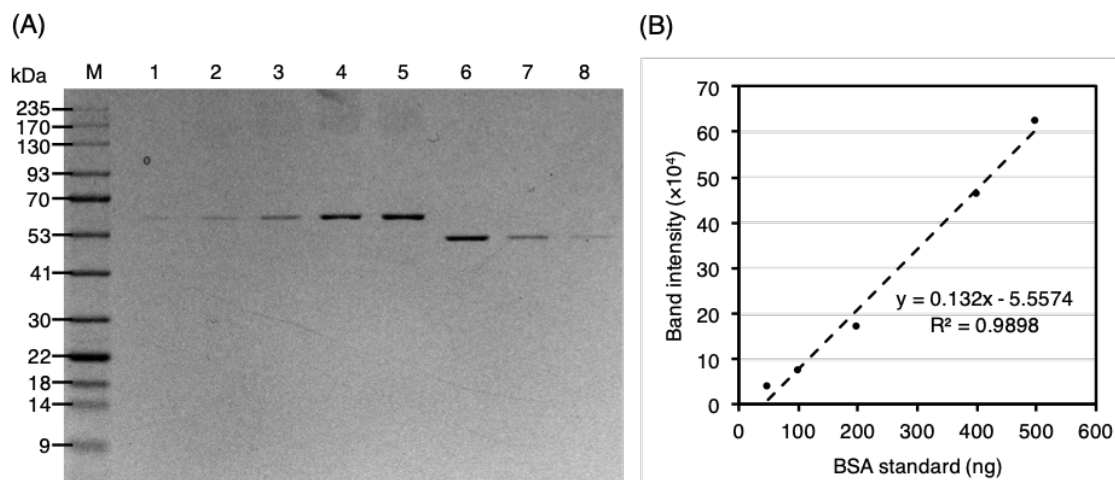


**Figure S4.** Densitometric protein quantification of SpBLA-H6 using BSA standard. **(A)** SDS-PAGE analysis of SpBLA-H6 at varying dilution factors. Lane M, Gangnam pre-stained protein marker; lane 1, BSA (5 ng); lane 2, BSA (100 ng); lane 3, BSA (200 ng); lane 4, BSA (400 ng); lane 5, BSA (500 ng); lane 6, SpBLA-H6 (dilution factor of 30); lane 7, SpBLA-H6 (dilution factor of 59); lane 8, SpBLA-H6 (dilution factor of 117). **(B)** BSA standard curve obtained from the SDS-PAGE analysis for densitometric analysis.

## Ligation optimization of SpyTagged proteins onto SpyCatcher-PhaC PHA particles

(SP-P).

### 1) Varying reactant ratio of SpyCatcher:SpyTag

	SP fusion protein and SpGFP-H6				
Ratio (SpyCatcher:SpyTag)	3:1	2:1	1:1	1:2	1:3
Total reactants ( $\mu\text{M}$ )	10	10	10	10	10
SP fusion protein ( $\mu\text{M}$ )	7.5	6.6	5.0	3.4	2.5
SpGFP-H6 ( $\mu\text{M}$ )	2.5	3.4	5.0	6.6	7.5
% Surface coverage	20.8	33.0	43.3	48.6	53.3
% Ligation efficiency	62.4	66.0	43.3	24.3	17.8

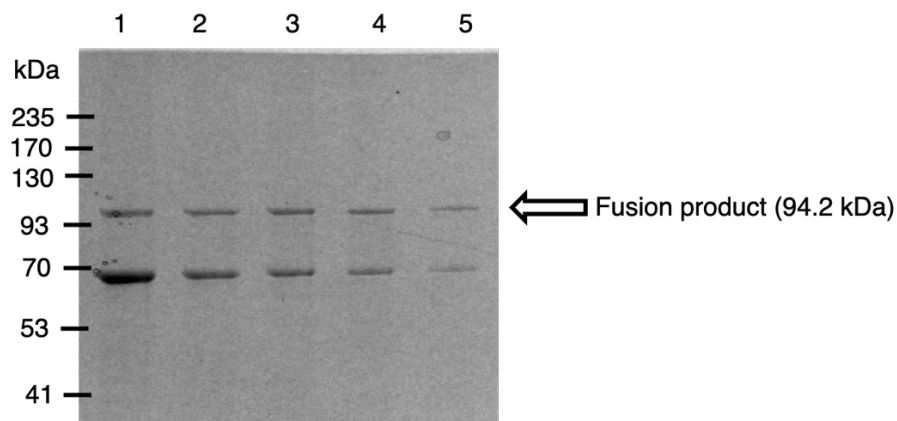


**Figure S5.** Optimization of ligation reactant ratio of SP-P over soluble SpGFP-H6 at total reactant concentration of 10  $\mu\text{M}$  at 4°C in 50 mM Tris-HCl for 24 hours. Lane 1, 3:1; lane 2, 2:1; lane 3, 1:1; lane 4, 1:2; lane 5, 1:3.

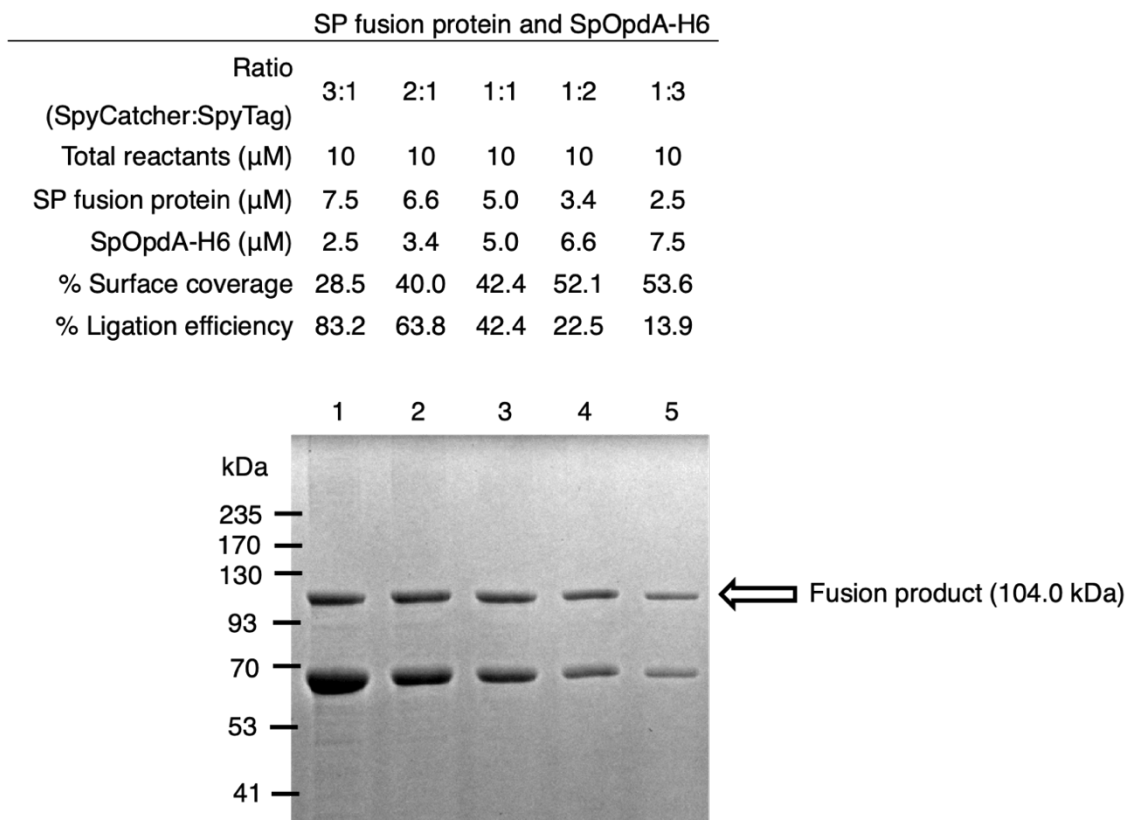


**Figure S6.** Optimization of ligation reactant ratio of SP-P over soluble SpOpdA-H6 at total reactant concentration of 10  $\mu\text{M}$  at 4°C in 50 mM Tris-HCl for 24 hours. Lane 1, 3:1; lane 2, 2:1; lane 3, 1:1; lane 4, 1:2; lane 5, 1:3.

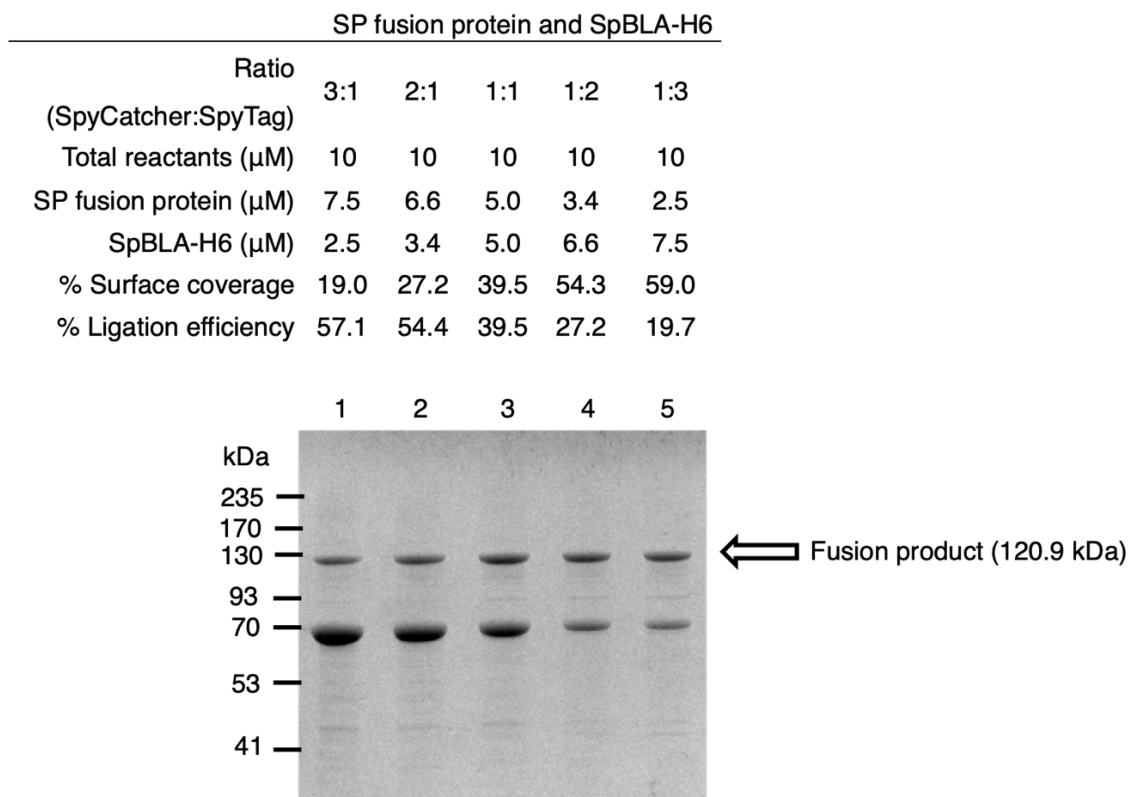


**Figure S7.** Optimization of ligation reactant ratio of SP-P over soluble SpBLA-H6 at total reactant concentration of 10  $\mu\text{M}$  at 4°C in 50 mM Tris-HCl for 24 hours. Lane 1, 3:1; Lane 2, 2:1; lane 3, 1:1; lane 4, 1:2; lane 5, 1:3.

## 2) Reaction time

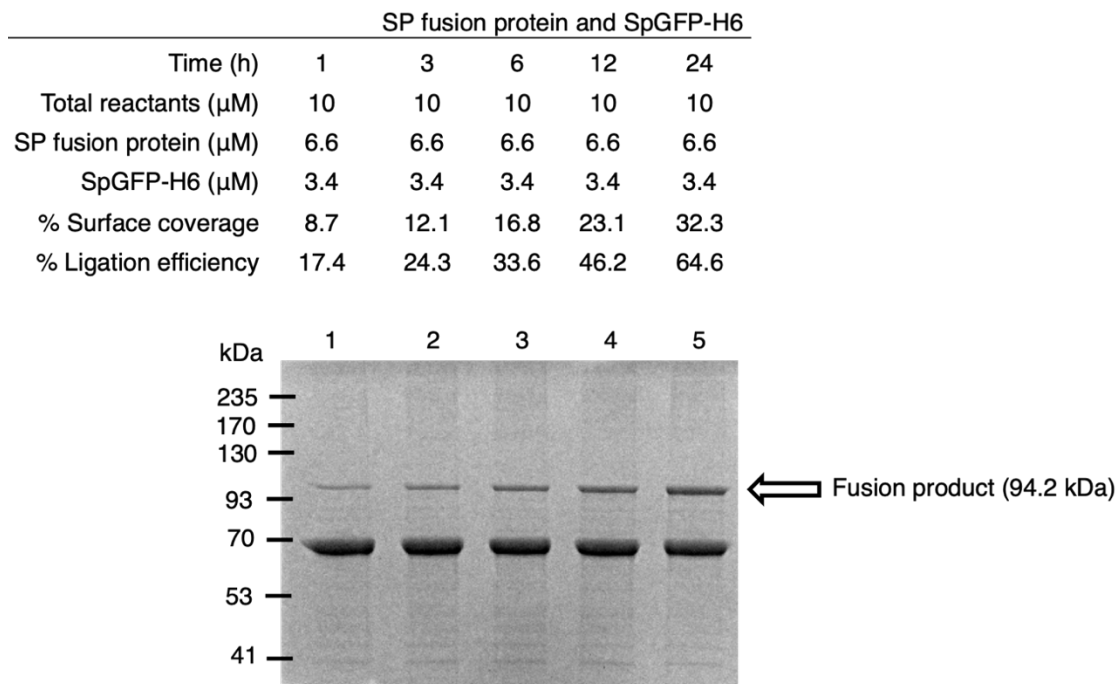


**Figure S8.** Optimization of ligation time of SP-P with SpGFP-H6 at reactant ratio of 2:1 (SpyCatcher:SpyTag) at 4°C in 50 mM Tris-HCl. Lane 1, 1 hour; lane 2, 3 hours; lane 3, 6 hours; lane 4, 12 hours; lane 5, 24 hours.

SP fusion protein and SpOpdA-H6					
Time (h)	1	3	6	12	24
Total reactants ( $\mu$ M)	10	10	10	10	10
SP fusion protein ( $\mu$ M)	6.6	6.6	6.6	6.6	6.6
SpOpdA-H6 ( $\mu$ M)	3.4	3.4	3.4	3.4	3.4
% Surface coverage	32.3	35.9	37.4	41.0	44.0
% Ligation efficiency	64.6	71.8	74.8	82.0	88.0

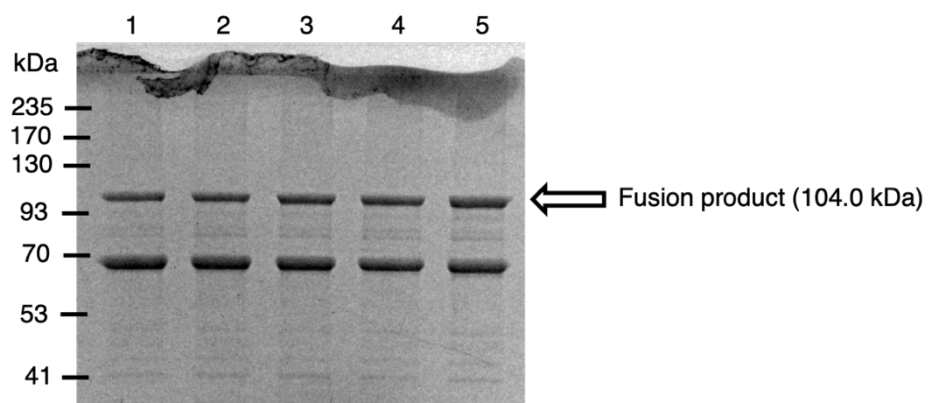


**Figure S9.** Optimization of ligation time of SP-P with SpOpdA-H6 at reactant ratio of 2:1 (SpyCatcher:SpyTag) at 4°C in 50 mM Tris-HCl. Lane 1, 1 hour; lane 2, 3 hours; lane 3, 6 hours; lane 4, 12 hours; lane 5, 24 hours.

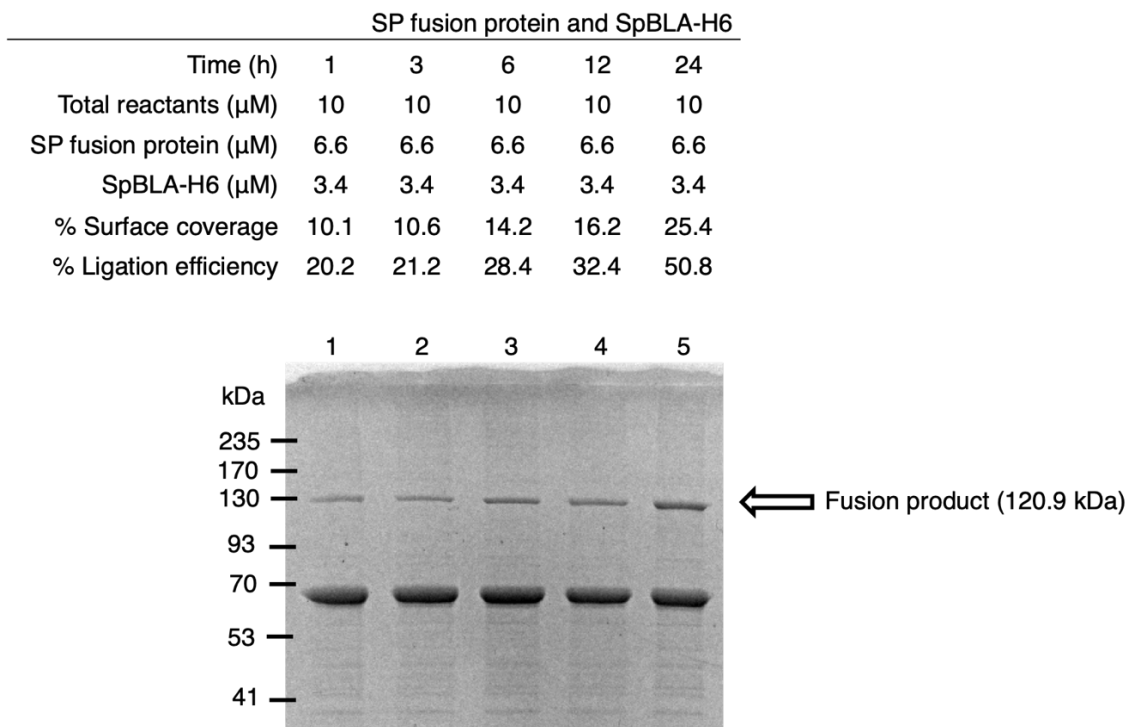


**Figure S10.** Optimization of ligation time of SP-P with SpBLA-H6 at reactant ratio of 2:1 (SpyCatcher:SpyTag) at 4°C in 50 mM Tris-HCl. Lane 1, 1 hour; lane 2, 3 hours; lane 3, 6 hours; lane 4, 12 hours; lane 5, 24 hours.

## Step-wise multi-functionalization of SpyCatcher-PhaC PHA particles

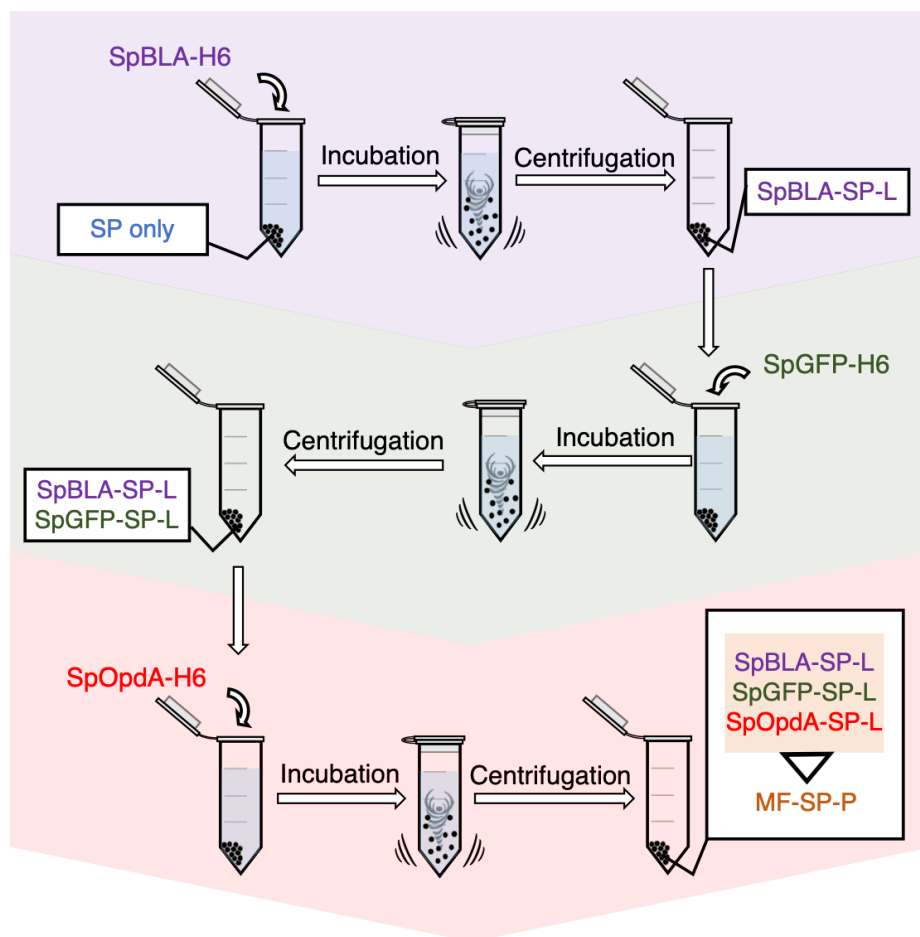


**Figure S11.** Step-wise fabrication of multifunctional SpyCatcher-PhaC PHA particles (MF-SP-P). Schematic overview of fabrication strategy of MF-SP-P by immobilizing several SpyTagged proteins onto the SP-P. A step-by-step reactant ratio modulated approach was used by mixing each SpyTagged functional proteins with the SP-P at limiting concentration.

**Table S5.** Particle size distribution statistics of various PHA particles used in this study. D [3,2] represents the Sauter mean diameter, D [4,3] represents the volume moment mean diameter and Dx represents the particle size corresponding to X% cumulative size distribution. All the samples were measured three times with standard deviation of 5% of the mean value.

Parameters	WT-P	SP-P	SpGFP-SP-P
<b>Specific surface area</b>	38060 m <sup>2</sup> /kg	24480 m <sup>2</sup> /kg	41830 m <sup>2</sup> /kg
<b>D [3,2]</b>	0.15 µm	0.23 µm	0.14 µm
<b>D [4,3]</b>	20.4 µm	10.8 µm	13.1 µm
<b>Dx (10)</b>	0.19 µm	0.32 µm	0.06 µm
<b>Dx (50)</b>	0.52 µm	53.8 µm	0.29 µm
<b>Dx (90)</b>	7.33 µm	183 µm	1.35 µm
Parameters	SpOpdA-SP-P	SpBLA-SP-P	MF-SP-P
<b>Specific surface area</b>	51430 m <sup>2</sup> /kg	50760 m <sup>2</sup> /kg	54550 m <sup>2</sup> /kg
<b>D [3,2]</b>	0.11 µm	0.11 µm	0.10 µm
<b>D [4,3]</b>	0.44 µm	13.9 µm	4.44 µm

<b>D<sub>x</sub> (10)</b>	0.04 μm	0.04 μm	0.04 μm
<b>D<sub>x</sub> (50)</b>	0.25 μm	0.26 μm	0.26 μm
<b>D<sub>x</sub> (90)</b>	1.08 μm	1.32 μm	1.28 μm

## Validation of the reproducibility of PHA modular functionalization

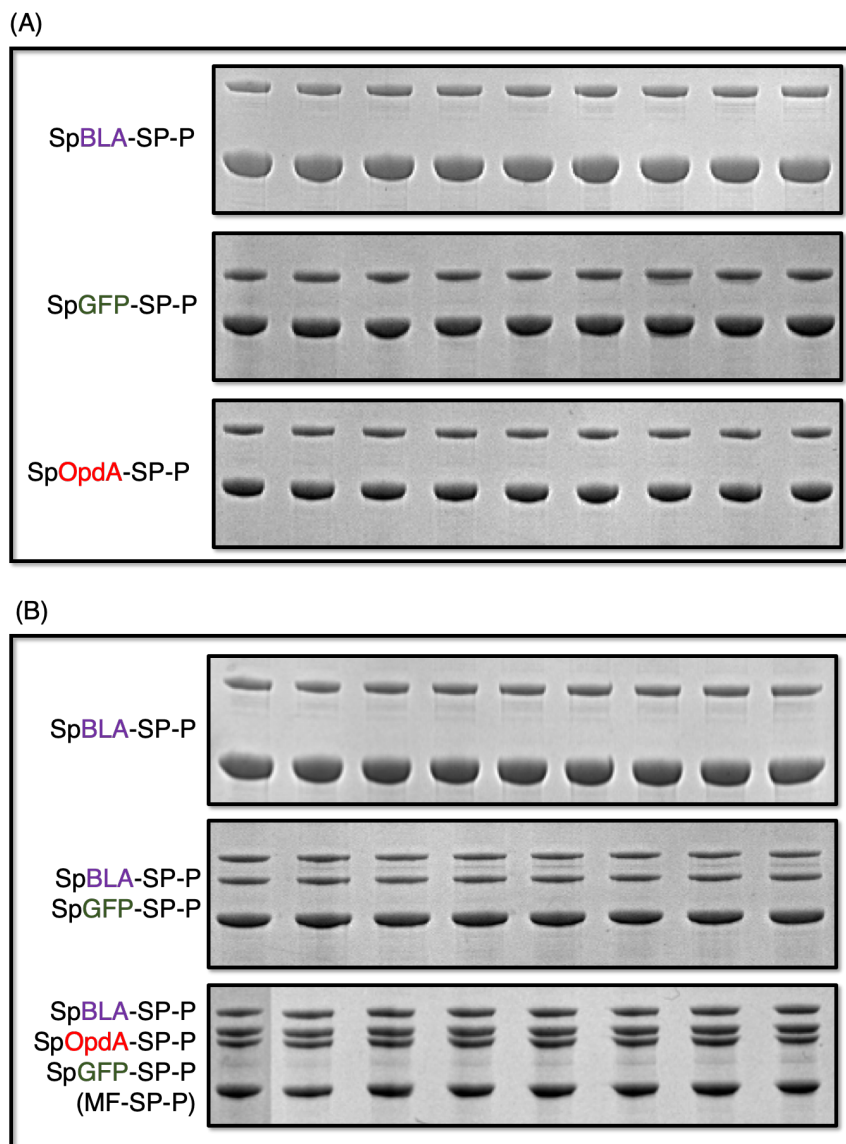


**Figure S12.** Validation of the reproducibility of modular functionalization of SpyCatcher-PhaC PHA particles ( $n=9$ ). **(A)** Single protein immobilization. **(B)** Step-by-step fabrication of multifunctional SpyCatcher-PhaC PHA particles (MF-SP-P).

**Densitometric protein quantification of immobilized SpyTagged proteins on various functionalized SpyCatcher-PhaC PHA particles.**

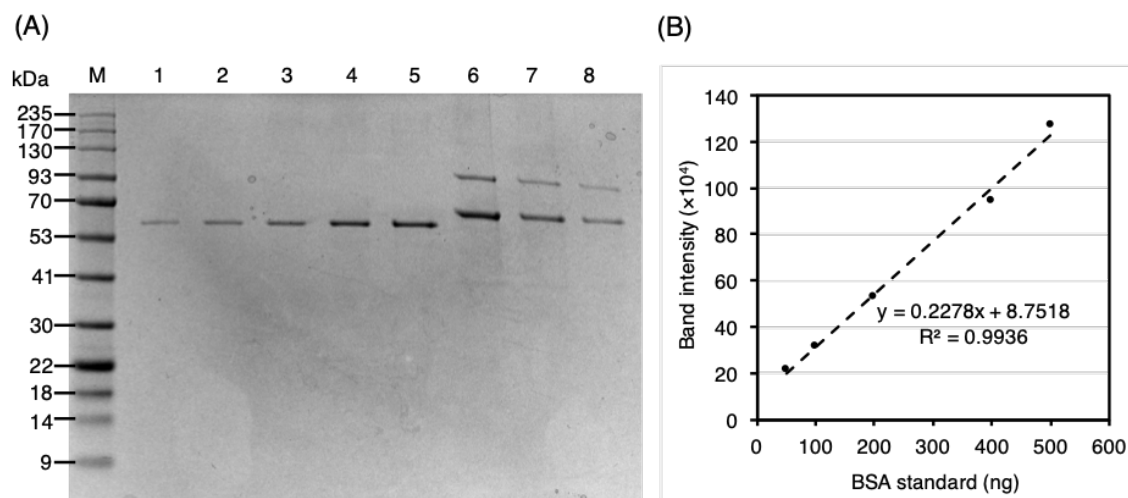


**Figure S13.** Densitometric protein quantification of SpGFP-SP-L on PHA particles using BSA standard. **(A)** SDS–PAGE analysis of SpGFP-SP-L at varying dilution factors. Lane M, Gangnam pre-stained protein marker; lane 1, BSA (5 ng); lane 2, BSA (100 ng); lane 3, BSA (200 ng); lane 4, BSA (400 ng); lane 5, BSA (500 ng); lane 6, SpGFP-SP-L (dilution factor of 6); lane 7, SpGFP-SP-L (dilution factor of 12); lane 8, SpGFP-SP-L (dilution factor of 24). **(B)** BSA standard curve obtained from the SDS–PAGE analysis for densitometric analysis; SpGFP-SP-L, SpGFP-H6 ligated with SP.

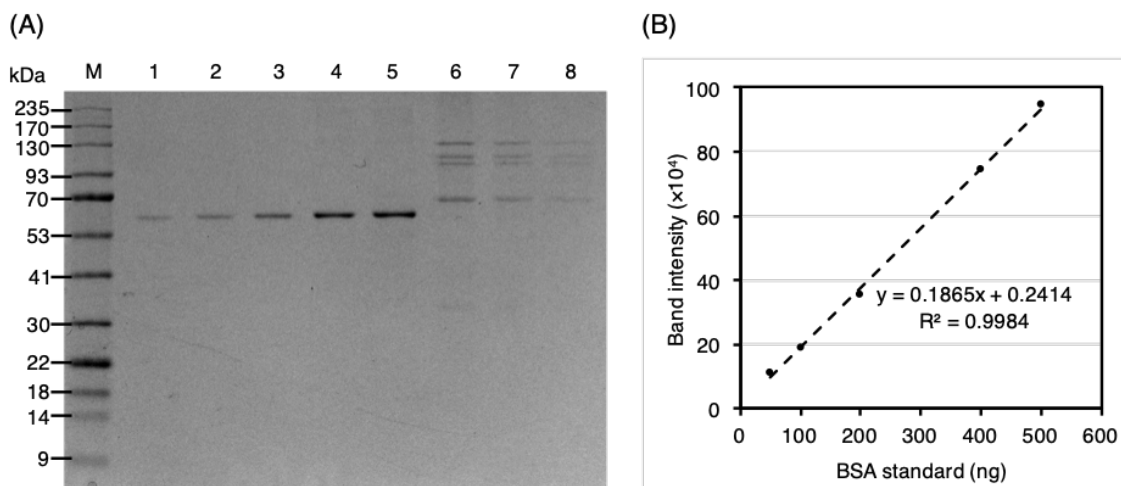


**Figure S14.** Densitometric protein quantification of immobilized multi-proteins (MF-SP-L) on PHA particles using BSA standard. **(A)** SDS-PAGE analysis of MF-SP-L at varying dilution factors. Lane M, Gangnam pre-stained protein marker; lane 1, BSA (5 ng); lane 2, BSA (100 ng); lane 3, BSA (200 ng); lane 4, BSA (400 ng); lane 5, BSA (500 ng); lane 6, MF-SP-L (dilution factor of 12); lane 7, MF-SP-L (dilution factor of 24); lane 8, MF-SP-L (dilution factor of 48). **(B)** BSA standard curve obtained from the SDS-PAGE analysis for densitometric analysis.

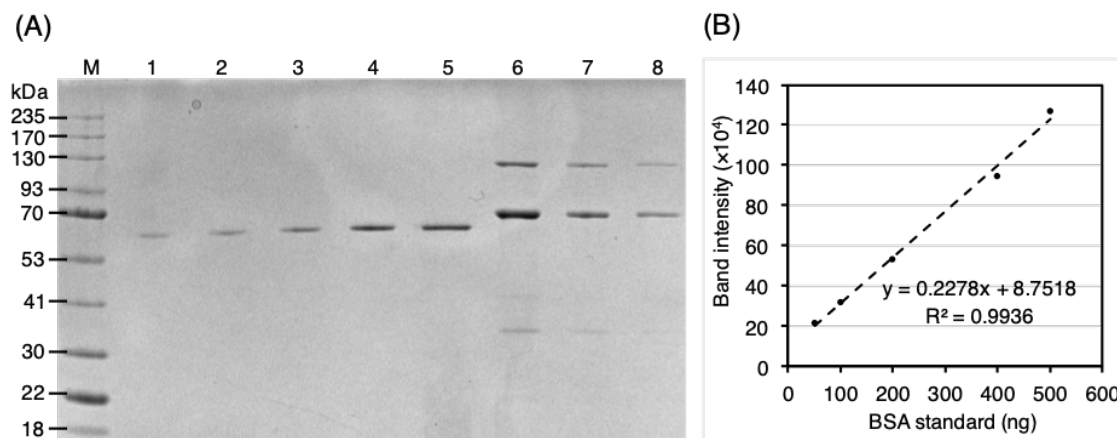


**Figure S15.** Densitometric protein quantification of SpOpdA-SP-L on PHA particles using BSA standard. **(A)** SDS–PAGE analysis of SpOpdA-SP-L at varying dilution factors. Lane M, Gangnam pre-stained protein marker; lane 1, BSA (5 ng); lane 2, BSA (100 ng); lane 3, BSA (200 ng); lane 4, BSA (400 ng); lane 5, BSA (500 ng); lane 6, SpOpdA-SP-L (dilution factor of 6); lane 7, SpOpdA-SP-L (dilution factor of 12); lane 8, SpOpdA-SP-L (dilution factor of 24). **(B)** BSA standard curve obtained from the SDS–PAGE analysis for densitometric analysis; SpOpdA-SP-L, SpOpdA-H6 ligated with SP.

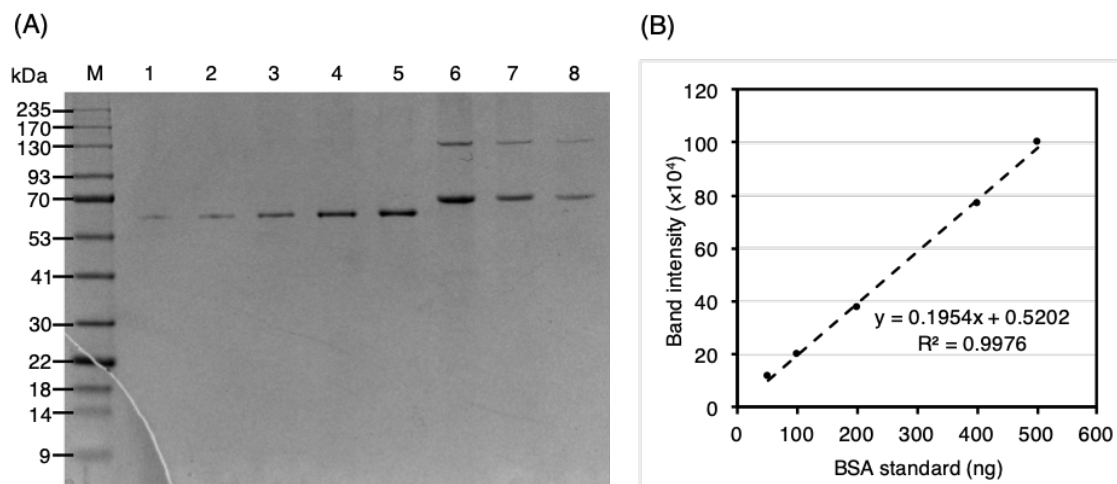


**Figure S16.** Densitometric protein quantification of SpBLA-SP-L on PHA particles using BSA standard. **(A)** SDS-PAGE analysis of SpBLA-SP-L at varying dilution factors. Lane M, Gangnam pre-stained protein marker; lane 1, BSA (5 ng); lane 2, BSA (100 ng); lane 3, BSA (200 ng); lane 4, BSA (400 ng); lane 5, BSA (500 ng); lane 6, SpBLA-SP-L (dilution factor of 6); lane 7, SpBLA-SP-L (dilution factor of 12); lane 8, SpBLA-SP-L (dilution factor of 24). **(B)** BSA standard curve obtained from the SDS-PAGE analysis for densitometric analysis; SpBLA-SP-L, SpBLA-H6 ligated with SP.

**Additional images of fluorescence screening of SpGFP-H6 immobilized to Spy-Catcher-PhaC PHA particles.**

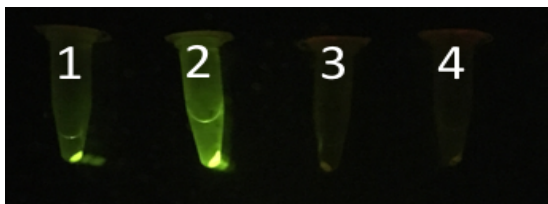


**Figure S17.** Fluorescence can be detected on SpGFP-SP-P. Pelleted particles in the Eppendorf tubes were placed on a blue light transilluminator and imaged. Tube 1 & 2, SpGFP-SP-P prepared at reactant ratio of 1:3 and 1:10 (SpyCatcher:SpyTag) respectively; tube 3, SP-P only ; Tube 4, WT-P. WT-P, wild-type PhaC PHA particles; SP-P, SpyCatcher-PhaC PHA particles; SpGFP-SP-P, SpGFP immobilized SP-P.

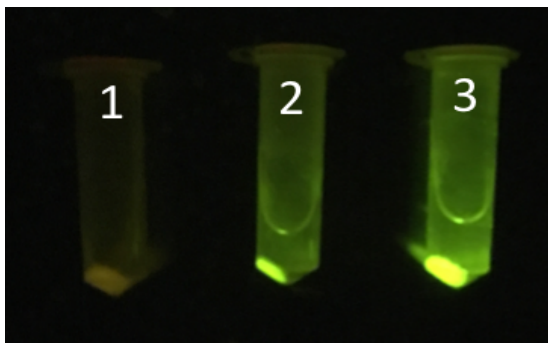


**Figure S18.** Fluorescence intensity of the SpGFP-SP-P at varying ligation time. Tube 1, 0 h; tube 2, 3 h; tube 3, 24 h; SpGFP-SP-P, SpGFP immobilized SP-P.

## Starch degradation screen of the immobilized SpBLA-H6 on SpyCatcher-PhaC

### PHA particles

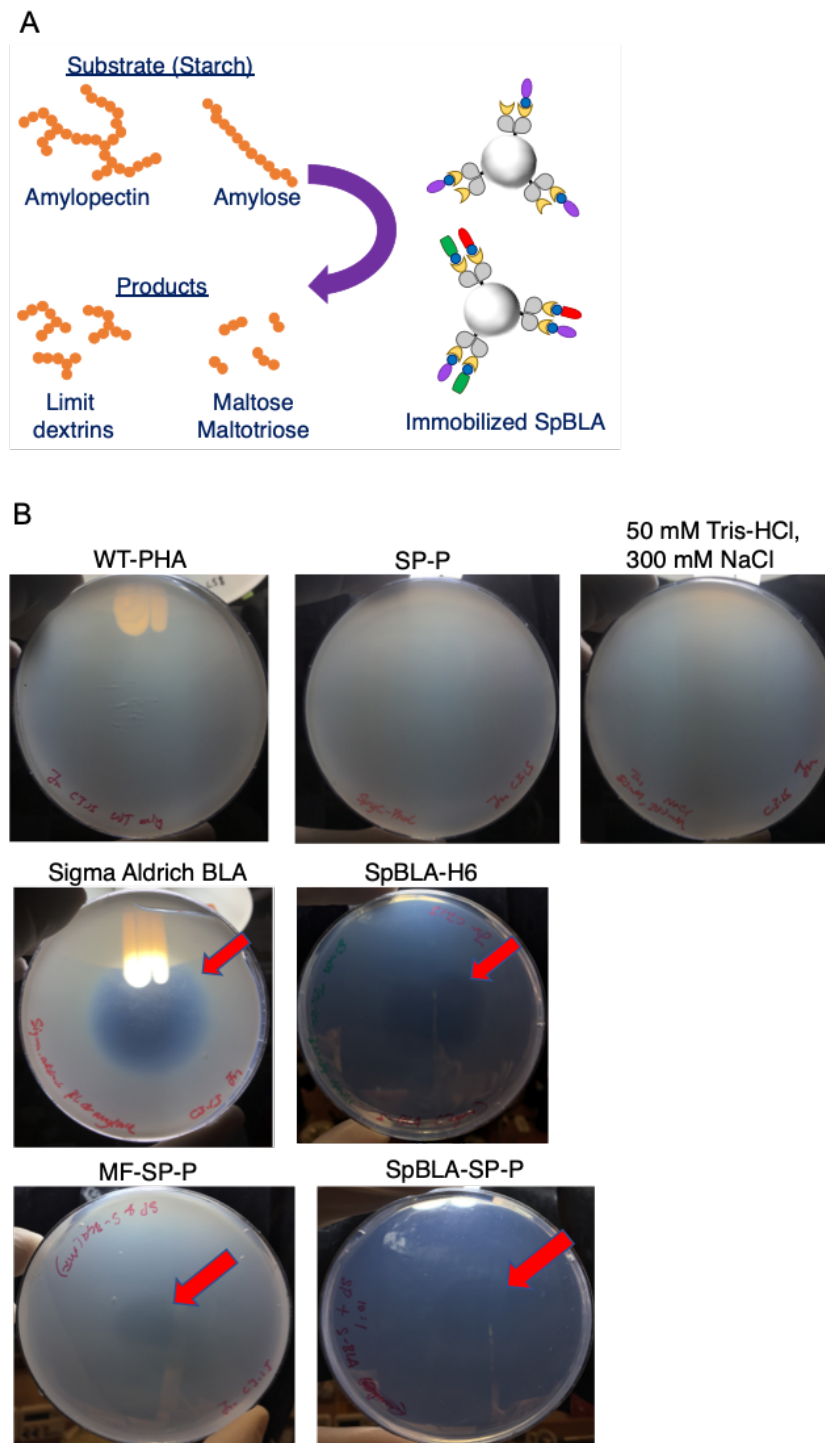


**Figure S19.** Starch degradation screen. **(A)** Schematic illustration of starch degradation by SpBLA-H6. **(B)** Clear transparent hydrolysis zone, degraded by SpBLA-H6 on the 1% starch agar plate can be observed on the SpBLA-H6-loaded samples, either in immobilized or free soluble form. Immobilized SpBLA-H6 samples were being localized at the middle of the starch agar plate by SpyCatcher-PHA particles. The PHA particles were removed before being imaged. WT-P, wild-type PhaC PHA particles; SP-P, SpyCatcher-PhaC PHA particles; SpBLA-SP-P, SpBLA-H6 immobilized SP-P; MF-SP-P, multifunctional SP-P.

## Recyclability of soluble free SpyTagged proteins

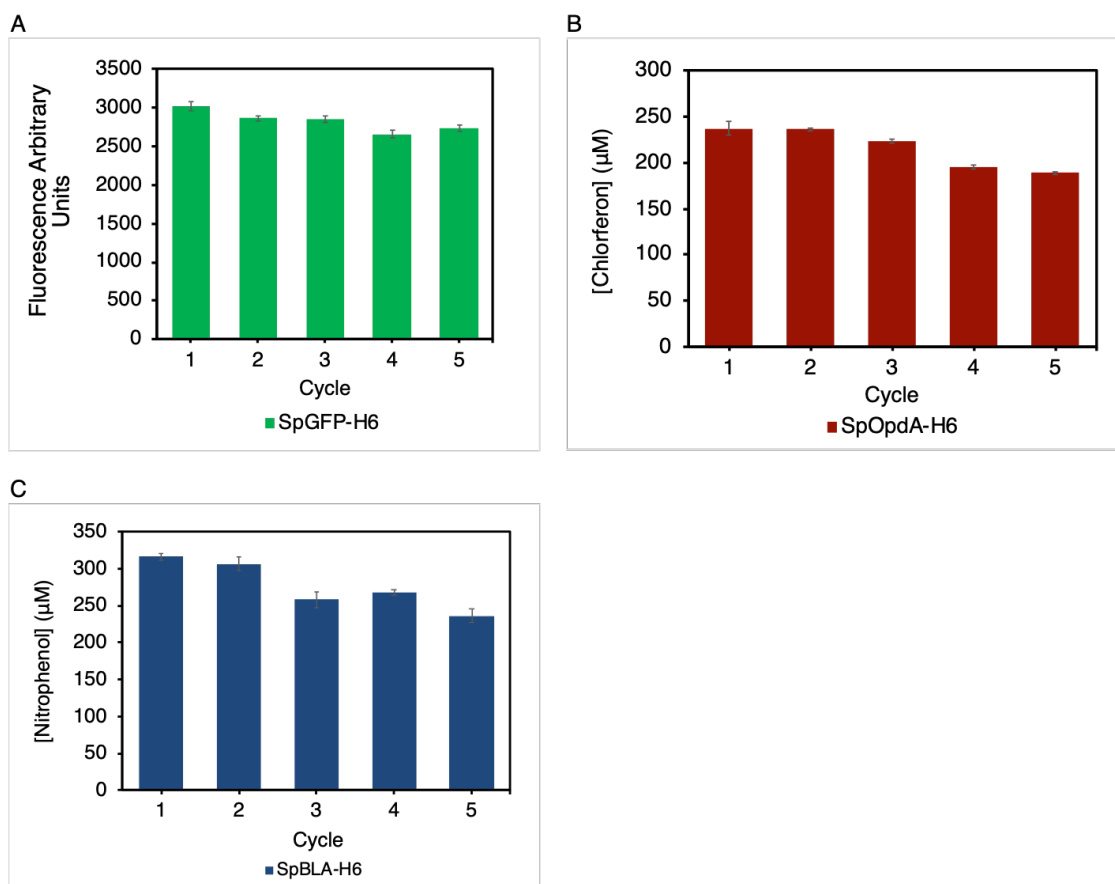


**Figure S20.** Recyclability of soluble free SpyTagged proteins as positive control. Soluble free proteins were recycled using ultrafiltration as described in the Experimental Section. **(A)** Arbitrary fluorescence intensity of SpGFP-H6 over five cycles (mean  $\pm$  1 SD,  $n = 3$ ). **(B)** Amount of chlorferon released from coumaphos hydrolyzed by SpOpdA-H6 over five cycles (mean  $\pm$  1 SD,  $n = 3$ ). **(C)** Amount of nitrophenol liberated from ethylidene-pNP-G7 by SpBLA-H6 over five cycles (mean  $\pm$  1 SD,  $n = 3$ ).

## Preface to Chapter 4

The previous chapter described the *in vitro* modular functionalization of recombinant PHA particles simply by mixing at defined Tag/Catcher reactant ratio. Tunable spatial immobilization of various SpyTagged proteins on the SpyCatcher-coated PHA particles was demonstrated, which ultimately lead to successful multi-functionalization of the particles using an *in vitro* sequential immobilization strategy. Overall, the immobilized functional proteins showed retained or improved activity and stability when compared to their soluble counterparts. However, the multiple-step preparation procedures and the use of purified components imply higher production costs and longer times, leading to process inefficiency. In order to expand the design space of this approach, therefore, in chapter 4, we developed several streamlined strategies to enable simpler modular decoration of the PHA particles. We also designed several bimodular PHA scaffolds by installing various combinations of Tag/Catcher systems on PHA particles.

## Chapter 4

# Covalent Functionalization of Bioengineered Polyhydroxyalkanoate Particles Directed by Specific Protein-Protein Interactions

Jin Xiang Wong<sup>1,2</sup>, Majela Gonzalez-Miro<sup>1</sup>, Andrew J. Sutherland-Smith<sup>1</sup>, Bernd H. A. Rehm<sup>3\*</sup>

<sup>1</sup> School of Fundamental Sciences, Massey University, Private Bag, 11222 Palmerston North, New Zealand

<sup>2</sup> MacDiarmid Institute of Advanced Materials and Nanotechnology, Victoria University of Wellington, Wellington 6140, New Zealand

<sup>3</sup> Centre for Cell Factories and Biopolymers, Griffith Institute for Drug Discovery, Griffith University, Don Young Road, Nathan, 4111 Queensland, Australia

**Publication status:** published in *Frontiers in Bioengineering and Biotechnology* (Wong, J. X., Gonzalez-Miro, M., Sutherland-Smith, A. J., and Rehm, B. H. A. (2020). Covalent Functionalization of Bioengineered Polyhydroxyalkanoate Particles Directed by Specific Protein-Protein Interactions. *Frontiers in Bioengineering and Biotechnology*, 8:44.)

## 4.1 Abstract

Bioengineered polyhydroxyalkanoate (PHA) particles assembled in engineered bacteria are showing promising potential in protein immobilization for high-value applications. Here, we have designed innovative streamlined approaches to add functional proteins from complex mixtures (*e.g.* without prior purification) to bioengineered PHA particles directly harnessing the specificity of the SpyTag/SpyCatcher mediated protein ligation. *Escherichia coli* was engineered to assemble PHA particles displaying the SpyCatcher domain while simultaneously producing a SpyTagged target protein, which was then *in vivo* specifically ligated to the PHA particles. To further demonstrate the specificity of this ligation reaction, we incubated isolated SpyCatcher-coated PHA particles with cell lysates containing SpyTagged target protein, which also resulted in specific ligation mediating surface functionalization. An even cruder approach was used by lysing a mixture of cells, either producing PHA particles or target protein, which resulted in specific surface functionalization suggesting that ligation between the SpyCatcher-coated PHA particles and the SpyTagged target proteins is highly specific. To expand the design space of this general modular approach towards programmable multi-functionalization, *e.g.* one-pot construction of immobilized multienzyme cascade systems on PHA particles, we designed various recombinant bimodular PHA particles utilizing alternative Tag/Catcher pairs (*e.g.* SnoopTag/SnoopCatcher and SdyTag/SdyCatcher systems). One of our bimodular PHA particles resulted in the simultaneous multi-functionalization of plain PHA particles in one-step with two differently tagged proteins in both *in vitro* and *ex vivo* reaction conditions while remaining functional. Our bimodular PHA particles also showed high orthogonality with the non-target peptide tag and exhibited decent robustness against repeated

freeze–thaw treatment. We have shown the utility of these approaches by using a fluorescent protein, a monomeric amylase, and a dimeric organophosphate hydrolase as target proteins and thus established a versatile toolbox for dynamic functionalization of PHA particles for biomedical and industrial applications.

## 4.2 Introduction

Metabolic pathways often require biochemical processes that are dependent on multiprotein complexes assembled on a variety of biological scaffolds found in compartments in numerous prokaryotic and eukaryotic organisms (1-3). Artificial organization of immobilized multiprotein complexes, where multiple individual proteins working in consortia to carry out specific tasks have been reported to be crucial in driving the development of next-generation biocatalysis (4). The exciting approach of creating such biomimetic scaffold structures to place the active sites of proteins in proximity thus increasing the local concentrations of these active units, can result in further improving both the function and robustness of the relevant proteins (5, 6). Precise control of immobilized multiprotein complexes on defined scaffolds also enables efficient substrate directionality (*e.g.* physical channeling) and shielding of unstable intermediates from the bulk phase (7, 8). Therefore, there is a growing interest in biomaterials research that aims to develop customizable generic biological scaffolds. With the advances in the field of synthetic biology, it is feasible to employ a bottom-up approach in constructing artificial multifunctional scaffolds, focusing on three components: task-specific functional domains of interest, bioorthogonal immobilization sites, and generic scaffolding platforms.

Bioengineered polyhydroxyalkanoates (PHAs) have been proven as promising scaffolds for one-step *in vivo* protein immobilization. PHAs are polyesters produced in nature by microorganisms and stored in their cytosol under excess carbon and nutrient-deprived conditions. Several bacterial strains can be engineered to allow production and *in vivo* directed self-organization of shell-core like particles with surface functionalization achieved by genetic manipulation of PHA-associated proteins and/or chemical modification after isolation (9). Notably, this can be achieved by genetic fusion of protein domains of interest to surface-exposed PHA-associated proteins such as the PHA synthase (PhaC). PhaC is an essential enzyme in the microbial synthesis of PHA particles as it catalyzes polymerization of (*R*)-3-hydroxybutyryl-coenzyme A (CoA) to PHA and remains covalently attached to the PHA polymer chain *via* the active site cysteine residue as a dimeric protein (10). We harnessed the surface-exposed arrangement of *Cupriavidus necator* (formerly *Ralstonia eutropha*) PhaC on bacterial PHA particles by genetically combining PhaC with a variety of protein domains for uses in therapeutic protein production and purification (11, 12), vaccine production (13, 14), diagnostic tools (15), and biocatalysis (16, 17). However, the utilization of PhaC as the docking domain for the surface display of different functional proteins does not provide control over properties, such as surface coverage and orientation of the attached proteins, potential failure in protein folding (*e.g.* eukaryotic proteins) (11, 12), inability to enable post-translational modifications and a lack of control over the concentration of immobilized functional proteins. In addition, the direct genetic fusion of functional proteins to PhaC impacted particle assembly, which influenced production yields and particle sizes (13, 14). Although the PHA particle display technology has led to

multiple successful prototypes, its complex biological assembly enables less control over surface functionalization.

To overcome these limitations, we propose to merge the PHA particle display technology with the recently developed SpyTag/SpyCatcher chemistry derived from *Streptococcus pyogenes* (**Figure 1A**) (18). A spontaneous covalent isopeptide bond forms between a lysine residue of the SpyCatcher domain (13 kDa) and an aspartic acid of its pairing peptide SpyTag (13 amino acid residues) in a site-specific manner, without the need of additional reagents nor enzymes at broad ligation conditions (19). The advantageous properties of the SpyTag/SpyCatcher chemistry makes it an excellent protein ligation tool for surface functionalization of various organic and inorganic materials, such as virus-like particles (20-22), protein-based scaffolds (23-26), gold nanoparticles (27), silica (28, 29), quantum dots (30, 31), and crystalline graphene (32). We recently developed a modular PHA platform using SpyTag/SpyCatcher chemistry, where we successfully showed that purified SpyTagged proteins could ligate to SpyCatcher-coated PHA particles *in vitro* with decent tunability (33). Relatively consistent physicochemical properties of PHA particles were achieved, regardless of the functional moieties decorating the particulate PHA scaffold, while retaining or enhancing functionality of the immobilized target proteins. This approach allows robust and covalent functionalization of PHA particles without being constrained by the direct genetic fusion method.

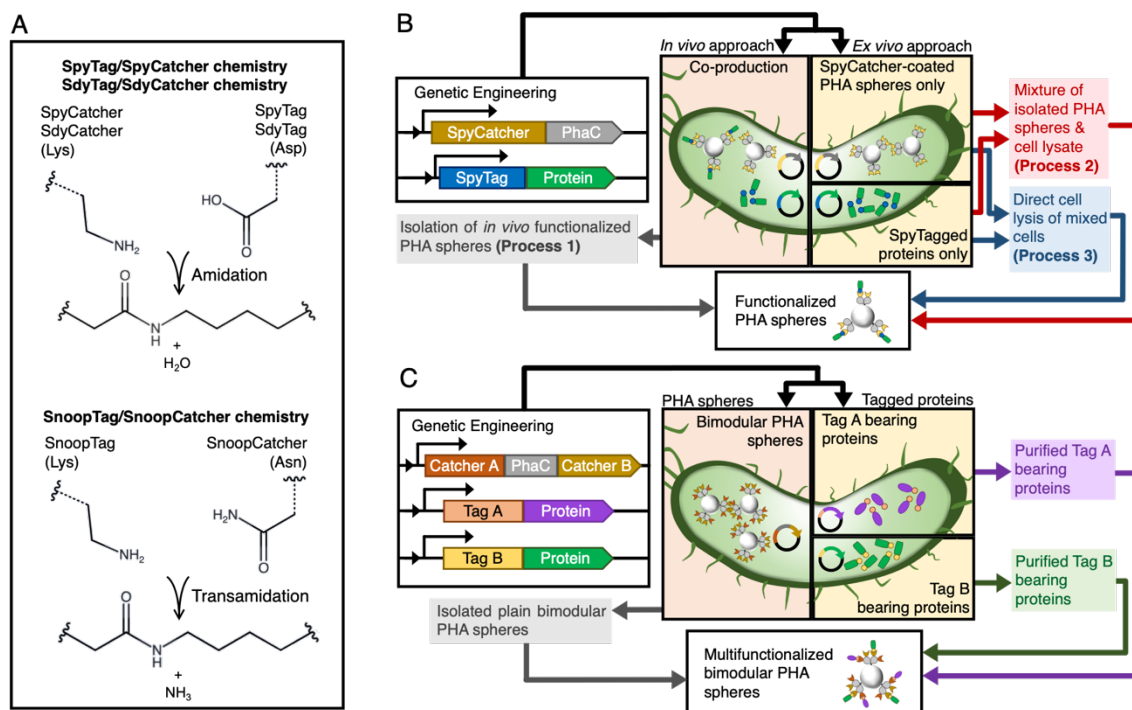


**Figure 1.** Schematic of modular functionalization of PHA particles. **(A)** Three Tag/Catcher systems. **(B)** Various one-pot modular functionalization processes established in this study. **(C)** Simultaneous dual functionalization of PHA particles using combinations of Catcher domains displayed on PHA particles.

In this study, we first aimed to streamline this modular functionalization approach using different process steps, testing whether SpyTagged proteins could be ligated to SpyCatcher-coated PHA particles without the need to purify soluble tagged proteins by using one *in vivo* and two *ex vivo* functionalization processes, namely processes 1-3 (**Figure 1B and S1–S3**). By doing this, we are not only avoiding purification of individual components but also using a single lysis step, which further improves the time taken for production and reduces cost. Functionalization occurs during the cell lysis step, and we propose that the

immediate release of target components from the bacterial cells leads to specific covalent ligation between PHA particle and target protein *ex vivo* during the cell disruption process. Nevertheless, although our previous study presented that SpyCatcher-coated PHA particles able to co-localize different SpyTagged proteins, the sequential and reactant ratio-dependent strategies proposed could impose manufacturing burdens (33). Therefore, to expand the concept of modularity beyond our initial studies based on SpyTag/SpyCatcher chemistry, we attempted to incorporate two non-cross reacting directed peptide-protein pairs with PHA particle technology to construct an efficient bimodular polymeric scaffolding platform (**Figure 1C**). In addition to the PHA particle technology compatible SpyTag/SpyCatcher chemistry pair, we further considered alternative orthogonal Tag/Catcher pairs, namely SdyTag/SdyCatcher derived from *Streptococcus dysgalactiae* (34) and SnoopTag/SnoopCatcher derived from *Streptococcus pneumoniae* (35), for the construction of our bimodular polymeric scaffolding platform (**Figure 1A**). We also genetically fused different covalent peptide tags to the N-terminus of *Aequorea victoria* green fluorescent protein (GFP) and *Bacillus licheniformis*  $\alpha$ -amylase (BLA) to allow site-specific protein ligation to the Catcher domain-displaying PHA particles.

## 4.3 Materials and Methods

### 4.3.1 Bacterial Strains, Genetic Manipulation, and Culture Conditions

All the bacterial strains, plasmids, and primers used in the current study are listed in **Tables S1–S3**, respectively. The primers used for genetic manipulation were obtained from Integrated DNA Technologies (San Diego, USA). DNA extraction and genetic engineering

procedures were performed as described (36). For plasmid harboring and cloning, *E. coli* XL1-Blue (Stratagene, La Jolla, USA) was grown overnight (16 h) in Luria–Bertani, Lennox medium (LB-Lennox) at pH 7.5 at 37°C and shaken at 200 rpm. If required, ampicillin (100 µg/mL), chloramphenicol (50 µg/mL) and kanamycin (50 µg/mL) were introduced. All the antibiotics used this study were filtered through a 0.22 µm cellulose acetate membrane filter (ReliaPrep, Ahlstrom-Munksjö, Helsinki, Finland). Detailed plasmid construction strategies are described in the Supplementary Material. Positive clones were transformed into the appropriate competent *E. coli* BL21(DE3) cells (Invitrogen, Carlsbad, USA), or competent *E. coli* BL21(DE3) cells harboring plasmid pMCS69 for the production of soluble proteins and PHA particles, respectively. Plasmid pMCS69 allows the synthesis of the precursor *R*-3-hydroxybutyryl-CoA, which is essential to biosynthesis of PHA particles.

#### **4.3.2 Polyhydroxyalkanoate (PHA) Particle and Soluble Protein Production**

An overnight culture of the production strains was inoculated at a 100-fold dilution into fresh LB-Lennox medium containing the appropriate antibiotics supplemented with 1% (w/v) glucose. The medium was cultured at 37°C and shaken at 200 rpm until an OD<sub>600</sub> of ~0.6 was achieved. After this, filtered isopropyl β-D-1-thiogalactopyranoside (IPTG) was added to a final concentration of 1 mM to the culture to induce protein production. Cells were harvested after 24 h incubation at 30°C for soluble protein production, and 48 h at 25°C for PHA particle production.

### 4.3.3 Protein Analysis

All fusion proteins were analyzed by sodium dodecyl sulfate–polyacrylamide gel electrophoresis (SDS-PAGE) as described elsewhere (37). Briefly, soluble protein and PHA particle samples were denatured with Laemmli buffer by heating at 95°C for 10 min and 15 min, respectively. Then, the denatured protein samples were separated on 10% (v/v) polyacrylamide separating gels with 4% (v/v) polyacrylamide stacking gels. The molecular mass of the samples was estimated using GangNam-STAIN prestained standard marker (iNtRON Biotechnology, Seongnam, South Korea). SDS-PAGE gels were stained with 0.05% (w/v) Coomassie brilliant blue R-250 dye, 50% (v/v) ethanol and 10% (v/v) acetic acid for 30 min and then destained in 50% (v/v) ethanol and 10% (v/v) acetic acid for 2 h. Images of polyacrylamide gels were taken using Gel Doc XR+ system (Bio-Rad Laboratories, Hercules, USA).

### 4.3.4 Protein Quantification

Protein concentrations were determined by measuring the band intensity from SDS-PAGE gels by densitometric analysis using Image Lab 5.2.1 software (Bio-Rad Laboratories, Hercules, USA) and comparing the value to a standard curve prepared from known concentrations of bovine serum albumin (BSA) standard as described elsewhere (38). The determination of production yields of protein displayed on PHA particles (**Equations S1–S4**), molarity (**Equation S5**), percentage surface coverage and percentage ligation efficiency of SpyTagged protein covalently ligated to SpyCatcher protein on PHA particles (**Equations S6 and S7**) are shown in Supporting Information.

#### **4.3.5 Proteomic analysis**

Purified protein bands from the SDS-PAGE gel were excised and subjected to tryptic hydrolysis as described (38, 39). The resulting extracted tryptic peptide samples were then analyzed by liquid chromatography–tandem mass spectrometry (LC–MS/MS) in School of Fundamental Sciences Mass Spectrometry Laboratory, Massey University (Palmerston North, New Zealand) (38).

#### **4.3.6 Isolation of Plain Catcher Domain-coated PHA Particles and *In Vivo* Functionalized Catcher Domain-coated PHA Particles (Process 1)**

The cell pellets harvested by centrifugation (8,000 g at 4°C for 20 min) were resuspended and washed with 10 mM Tris-HCl (pH 7.5) prior to cell lysis. Washed cells were mechanically disrupted by passing through a M-110P microfluidizer (Microfluidics, Westwood, USA) at least three times (1500 bar). After cell lysis, PHA particles were recovered by centrifugation (9,500 g at 4°C for 30 min). Recovered PHA particles were then washed at least three times and resuspended in PHA storage buffer (50 mM Tris-HCl, 20% v/v ethanol, pH 7.5) and stored at 4°C for further analysis.

#### **4.3.7 Isolation and *Ex Vivo* Functionalization of Catcher Domain-coated PHA Particles (Process 2)**

Plain Catcher domain-coated PHA particles were isolated as described in Process 1 above. Meanwhile, the cell pellets containing tagged soluble proteins were washed in 10 mM Tris-HCl (pH 7.5) once before cell lysis. Washed cell pellets were resuspended in 50 mM Tris-HCl (pH 7.5) to make a 10% cell slurry and mechanically disrupted as described above. After cell lysis, the whole-cell lysate was centrifuged (9,500 g at 4°C for 1 h) to remove the insoluble cellular debris. The supernatant was filtered through a 0.22 µm cellulose acetate membrane filter (ReliaPrep, Ahlstrom-Munksjö, Helsinki, Finland). The resulting *E. coli* cleared lysate containing tagged soluble proteins was then mixed with the plain Catcher domain-coated PHA particles for 24 h at 25°C with gentle rotary shaking (20 rpm). After this time, the functionalized PHA particles were recovered by centrifugation (9,500 g at 4°C for 30 min) and washed at least three times with 50 mM Tris-HCl (pH 7.5) then resuspended in PHA storage buffer (50 mM Tris-HCl, 20% v/v ethanol, pH 7.5) and stored at 4°C for further analysis.

#### **4.3.8 Isolation and *Ex Vivo* Functionalization of Catcher Domain-coated PHA Particles (Process 3)**

Growth media were harvested after 24 h incubation at 30°C. The cultures were centrifuged (8,000 g at 4°C for 20 min) and washed in 10 mM Tris-HCl (pH 7.5) once before cell lysis. Washed cell pellets containing tagged soluble proteins and Catcher domain-coated PHA

particles were mixed at a mass ratio of 1:1 and resuspended to form a 10% cell slurry which was sonicated using 10 s pulses for 5 min at an output setting of 2.5 (Virsonic 600, SP Scientific, Gardiner, NY). After cell lysis, functionalized PHA particles were recovered by centrifugation (9,500 g at 4°C for 30 min) and washed at least three times with 50 mM Tris-HCl (pH 7.5). The washed PHA particle pellets were then resuspended in PHA storage buffer (50 mM Tris-HCl, 20% v/v ethanol, pH 7.5) and stored at 4°C for further analysis.

#### **4.3.9 Isolation and Purification of Tagged Soluble Protein**

The cell pellets recovered by centrifugation (8,000 g at 4 °C for 20 min) were washed with 20 mM Tris-HCl (pH 7.5) at least once prior to cell lysis. Washed cell pellets were resuspended in 1× protein lysis buffer (50 mM Tris-HCl, 300 mM NaCl, 40 mM imidazole, pH 7.5) to 10% cell slurry and mechanically disrupted by passing through a M-110P microfluidizer (Microfluidics, Westwood, USA) at least three times (1500 bar). The whole-cell lysate was subjected to centrifugation (9,500 g at 4 °C for 1 h) to remove the cellular debris. The resulting clarified lysate was filtered through a 0.22 µm polyethersulfonate membrane filter before loading on to a 5 mL nickel-nitrilotriacetic acid (Ni-NTA) chromatography column (HisTrap HP, GE Healthcare, Buckinghamshire, U.K.) at 5 mL/min using a peristaltic pump (LongerPump, Longer Precision Pump, Hebei, China). At least 5 column volumes (5 mL/min) of protein wash buffer (50 mM Tris-HCl, 300 mM NaCl, 50 mM imidazole, pH 7.5) were used to remove any nonspecifically bound proteins. Immobilized proteins were eluted from the resins by the addition of at least 5 column volumes of protein elution buffer (50 mM Tris-HCl, 300 mM NaCl, 500 mM imidazole,

pH 7.5). The eluate was concentrated and desalted using a centrifugal concentrator (Vivaspin 20, GE Healthcare, Buckinghamshire, U.K.) then stored at 4 °C for further analysis.

#### **4.3.10 *In Vitro* Functionalization of Various Catcher Domain-coated PHA Particles**

To functionalize Catcher domain-coated PHA particles they were mixed and incubated with tagged *Aequorea victoria* green fluorescent protein (GFP), *Agrobacterium radiobacter* organophosphohydrolase (OpdA) or *Bacillus licheniformis*  $\alpha$ -amylase (BLA) at a Catcher:Tag reactant ratio of 1:5 (50 mM Tris-HCl, pH 7.5) at 4 °C under constant rotary shaking overnight at 20 rpm. The PHA particles were washed at least three times (50 mM Tris-HCl, pH 7.5) to remove the unbound soluble proteins and stored at 4 °C for further use and analysis.

#### **4.3.11 Compositional Analysis of PHA Particles**

Approximately 75 mg of lyophilized PHA particles was subjected to methanolysis as described elsewhere (38, 40). The organic layer of all samples was recovered, filtered, and further analyzed by gas chromatography–mass spectroscopy (GC–MS) in Plant and Food Research (Palmerston North, New Zealand), using poly-(*R*)-3-hydroxybutyrate (PHB) as a standard (38).

#### **4.3.12 Scanning Electron Microscopy (SEM) and Transmission Electron Microscopy (TEM) Analysis**

PHA particles were processed for SEM and TEM by the Manawatu Microscopy and Imaging Centre (MMIC, Massey University, Palmerston North, New Zealand). SEM micrographs of the processed samples were imaged using a FEI Quanta 200 Environmental Scanning Electron Microscope, and TEM micrographs of the processed samples were imaged using an FEI Tecnai G2 BioTwin Transmission Electron Microscope.

#### **4.3.13 Particle Size Distribution (PSD) Measurement**

The particle size distribution of the PHA particles was determined by dynamic light scattering (DLS) analysis using a Mastersizer 3000 laser diffraction particle size analyzer (Malvern Instruments, Malvern, U.K.) at room temperature (25°C) with a helium–neon (He–Ne,  $\lambda = 632.8$  nm) laser. The PHA particle samples were prepared at a concentration of 0.1% (w/v) of wet PHA particles in 50 mM Tris-HCl, 20% (v/v) ethanol, pH 7.5. All measurements were made in triplicates.

#### **4.3.14 Fluorescence Microscopy Analysis**

Soluble or immobilized GFP in 50 mM Tris-HCl, pH 7.5 was evaluated for fluorescence emission using fluorescence microscopy imaging using an Olympus BX51 Fluorescent Light Microscope (Olympus Optical, Tokyo, Japan) at 100 $\times$  magnification with a

MicroPublisher 5.0 color CCD camera and QCapture Pro 6.0 application software (QImaging, Surrey, Canada).

#### **4.3.15 Qualitative Starch Degradation Screen**

Enzymatic activity of soluble, or immobilized, BLA was qualitatively verified using starch agar plates (16). Briefly, 1% starch agar was prepared by dissolving 1% (w/v) starch and 1.5% (w/v) agar with 50 mM Tris-HCl, 300 mM NaCl buffer (pH 7.5) prior to autoclaving. All samples were incubated at 37°C up to 24 h on the surface of the starch agar plates. After that, the starch agar plates were washed with deionized water once before subjected to Lugol's iodine staining for 5 min at room temperature (25°C), before draining and washing with deionized water again prior to imaging.

#### **4.3.16 Organophosphohydrolase Functionality Assay**

Enzymatic activity of soluble, or immobilized OpdA (50 mM Tris-HCl, pH 7.5) with negative controls was measured using an assay mixture of 250  $\mu$ M coumaphos dissolved in a modified reaction buffer (50 mM Tris-HCl, 20% (v/v) methanol, pH 7.5) at a fixed concentration of soluble, or immobilized OpdA (0.5  $\mu$ M) (41). Quantification of liberated chlorferon from coumaphos was determined by fluorescence using a FluoroMax®-4 Spectrofluorometer and a Jobin Yvon MicroMax 384 microwell-plate reader controlled by Fluorescence version 3.5 (HORIBA Scientific, Kyoto, Japan) at excitation and emission wavelengths of 355 and 450 nm, respectively. Samples were added into the assay mixture and

the fluorescence measured at 10 min intervals for up to 2 h at room temperature (25°C). All measurements were made in triplicates.

#### **4.3.17 Heat–Cooling Cycle Stability**

A suspension of plain SnoopCatcher-PhaC-SpyCatcher fusion protein-displaying PHA particles (NPP-P) in 50 mM Tris-HCl (pH 7.5) was subjected to up to five cycles of incubation at 95°C for 15 min and cooled down with an ice bath at 4°C for 15 min. All the samples were washed with 50 mM Tris-HCl (pH 7.5) three times before mixed with tagged proteins at a Catcher-Tag reactant ratio of 1:5 (50 mM Tris-HCl, pH 7.5) at 4 °C under constant rotary shaking overnight at 20 rpm. The functionalized Catcher domain-coated PHA particles were washed at least three times (50 mM Tris-HCl, pH 7.5) to remove the unbound soluble tagged proteins and stored at 4 °C before subjected to SDS-PAGE analysis and blue light exposure.

#### **4.3.18 Freeze–Thaw Cycle Stability**

A suspension of plain NPP-P in 50 mM Tris-HCl (pH 7.5) was subjected to up to five freeze–thaw cycles, where the samples were frozen at –20°C for overnight and thawed at 4°C for 8 h (50 mM Tris-HCl, pH 7.5). Then, the thawed samples were washed at least three times (50 mM Tris-HCl, pH 7.5). The washed Catcher domain-coated PHA particles were incubated with tagged proteins at 4 °C overnight under constant rotary incubation at 20 rpm using a Catcher-Tag reactant ratio of 1:5. All the functionalized Catcher domain-

coated PHA particles were washed at least three times (50 mM Tris-HCl, pH 7.5) to remove the unbound soluble tagged proteins and stored at 4 °C before subjected to SDS-PAGE analysis and blue light exposure.

## 4.4 Results

This study presents several innovative approaches to further expand the design space of PHA particles as an advanced platform technology to manufacture functional materials for biomedical and industrial uses. We will first report the results showing the efficiency of the streamlined processes to functionalize our modular SpyCatcher-coated PHA particles. Then, we detail the utility of multiple orthogonal protein ligation systems, which ultimately enable simultaneous dual functionalization of our bimodular PHA particles.

### 4.4.1 Production and Characterization of SpyCatcher-coated PHA Particles.

We used genetically engineered *Escherichia coli* (*E. coli*) to produce the SpyCatcher-coated PHA particles, where we utilized IPTG inducible plasmid systems with different antibiotic selection markers for single and/or co-production of SpyCatcher-coated PHA particles and SpyTagged proteins. All bacterial strains, plasmids, and primers used in this study are listed in **Tables S1–S3**. Detailed plasmid construction strategies are given in the Supporting Information (**Appendix S1**). We showed that gene fusion of SpyCatcher to the N- and C-termini of surface-exposed PhaC, namely SpyCatcher-PhaC-SpyCatcher fusion protein (SPS) (**Table S4**) resulted in overproduction of SpyCatcher domains on the surface

of PHA particles, using our previously developed SpyCatcher-PhaC (SP) fusion protein as reference (33). The PhaC-SpyCatcher fusion protein (PS) was not used as it had been shown not to be optimal (33). **Figure 2A** shows the overproduction of two fusion proteins that LC–MS/MS (**Table S5**) showed were the SPS and SP fusion proteins. The apparent molecular weight of SPS and SP fusion proteins corresponds to the theoretical masses of 81.8 kDa and 68.4 kDa, respectively, compared to wild-type PhaC (WT) at 55.5 kDa. Unlike the SP fusion protein-displaying PHA particles (SP-P), mixing the SPS fusion protein-displaying PHA particles (SPS-P) with any SpyTagged proteins will give rise to three different ligated protein products (**Figure S4**).

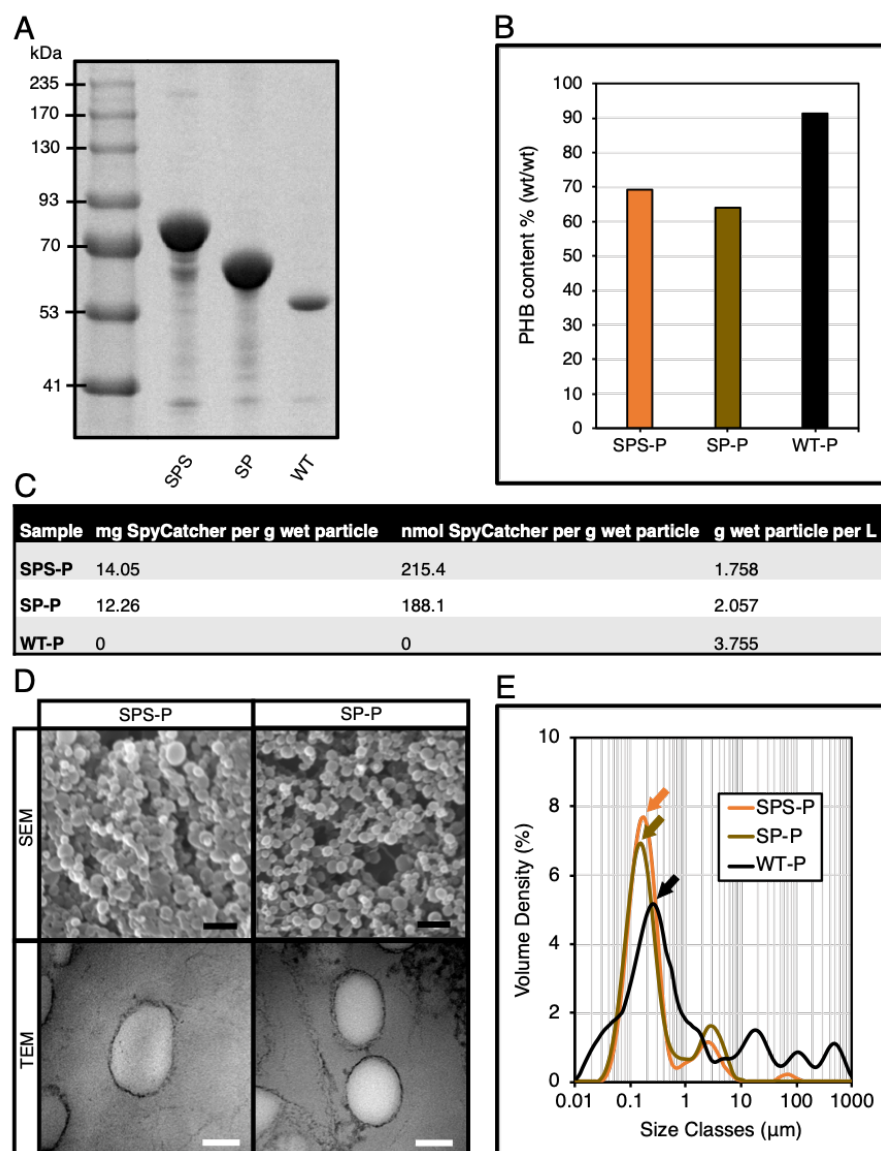


**Figure 2.** Production and characterization of SpyCatcher-coated PHA particles. **(A)** SDS-PAGE analysis of various isolated SpyCatcher-coated PHA particles. **(B)** Compositional analysis of SpyCatcher-coated PHA particles by GC–MS analysis. **(C)** Production yields of SpyCatcher domains displayed on PHA particles. **(D)** SEM and TEM micrographs of SpyCatcher-coated PHA particles. Black scale bar, 1  $\mu\text{m}$ ; white scale bar, 100 nm. **(E)** Particle size distribution of SpyCatcher-coated PHA particles by DLS analysis (mean,  $n = 3$ ).

GC–MS analysis of the different recombinant SpyCatcher-coated PHA particles allowed a comparison of the PHA composition of SPS-P with our previously developed SP-P (33), using pure poly-(*R*)-3-hydroxybutyrate (PHB) as a standard (**Figure S5**). We confirmed the production of different recombinant PHA particles, where PHB contributed to ~65–70% of the particle dry weight, which was significantly lower than WT displaying PHA particles (WT-P) (**Figure 2B**). Lower PHB content correlated with increased fusion protein content (**Figure 2B**). Hence variation in protein production might contribute to variation in PHB content. Additionally, we quantified the production yields of the PHA particles (**Figure 2C**). Scanning electron microscopy (SEM) and transmission electron microscopy (TEM) analyses indicated the successful self-assembly of genetically-engineered PHA particles into the expected spherical shape (**Figure 2D**). Dynamic light scattering (DLS) analysis was used to determine the particle size and size distribution of the recombinant particles (**Figure 2E**) and showed both SPS-P and SP-P were monodisperse, with a major peak at ~176 nm (orange arrow) and ~155 nm (gold arrow), respectively, which were smaller than WT-P at ~259 nm (black arrow).

#### **4.4.2 Surface Functionalization of SpyCatcher-coated PHA Particles using Processes**

##### **1–3.**

We proposed three streamlined processes (processes 1–3) to functionalize the plain SpyCatcher-coated PHA particles as illustrated in **Figure 1B** and the detailed flowcharts in **Figure S1–S3**. To visualize the accessibility of the SpyCatcher domains immobilized to PHA particles available for covalent ligation with the SpyTagged proteins, we first

constructed an N-terminally SpyTagged *Aequorea victoria* green fluorescent protein, namely SpGFP, using the gene fusion approach to enable directed protein ligation to SpyCatcher-coated PHA particles (**Table S4**). Process 1 described the *in vivo* modular functionalization of SpyCatcher-coated PHA particles, where the production of both SpyCatcher-coated PHA particles and SpyTagged proteins take place within the same cell, resulting in *in vivo* functionalization prior isolation of PHA particles. In process 2, isolated SpyCatcher-coated PHA particles were mixed with the cleared cell lysate containing soluble SpyTagged proteins to produce *ex vivo* functionalized PHA particles. In process 3, a cruder version of process 2, was implemented where cells containing SpyCatcher-coated PHA particles and cells containing SpyTagged proteins were mixed before being subjected to cell lysis.

We successfully functionalized SP-P and SPS-P inside bioengineered *E. coli* with SpGFP using process 1 (**Figures 3A and S6**). Additional protein bands appeared at 94.2 kDa, corresponding to SpGFP-SP ligated protein (SpGFP-SP-L), and 116.5 kDa and 140.1 kDa for SpGFP-SPS ligated proteins (SpGFP-SPS-Ls). These protein bands appeared above the molecular weight corresponding to SP (68.4 kDa) and SPS (81.8 kDa) only fusion proteins. At ~34% and ~27% surface coverage of SpGFP-SP-L formed on SP-P (SpGFP-SP-P) and SpGFP-SPS-Ls on SPS-P (SpGFP-SPS-P), respectively, we observed bright fluorescence using fluorescence microscopy (**Figure 3A**). We found that direct mixing of isolated SpyCatcher-coated PHA particles with the SpGFP-containing cleared cell lysate using process 2 resulted in protein band migration of a larger fraction of SP and SPS fusion proteins to SpGFP-SP-L and SpGFP-SPS-Ls, respectively, as revealed by SDS-PAGE analysis

(**Figure 3A**). Interestingly, we noted that the amount of SpGFP immobilized to both SP-P and SPS-P were ~3–4 fold higher than those observed in process 1. Consequently, SpGFP-SP-P and SpGFP-SPS-P prepared using process 2 showed a higher fluorescence intensity than those prepared using process 1.

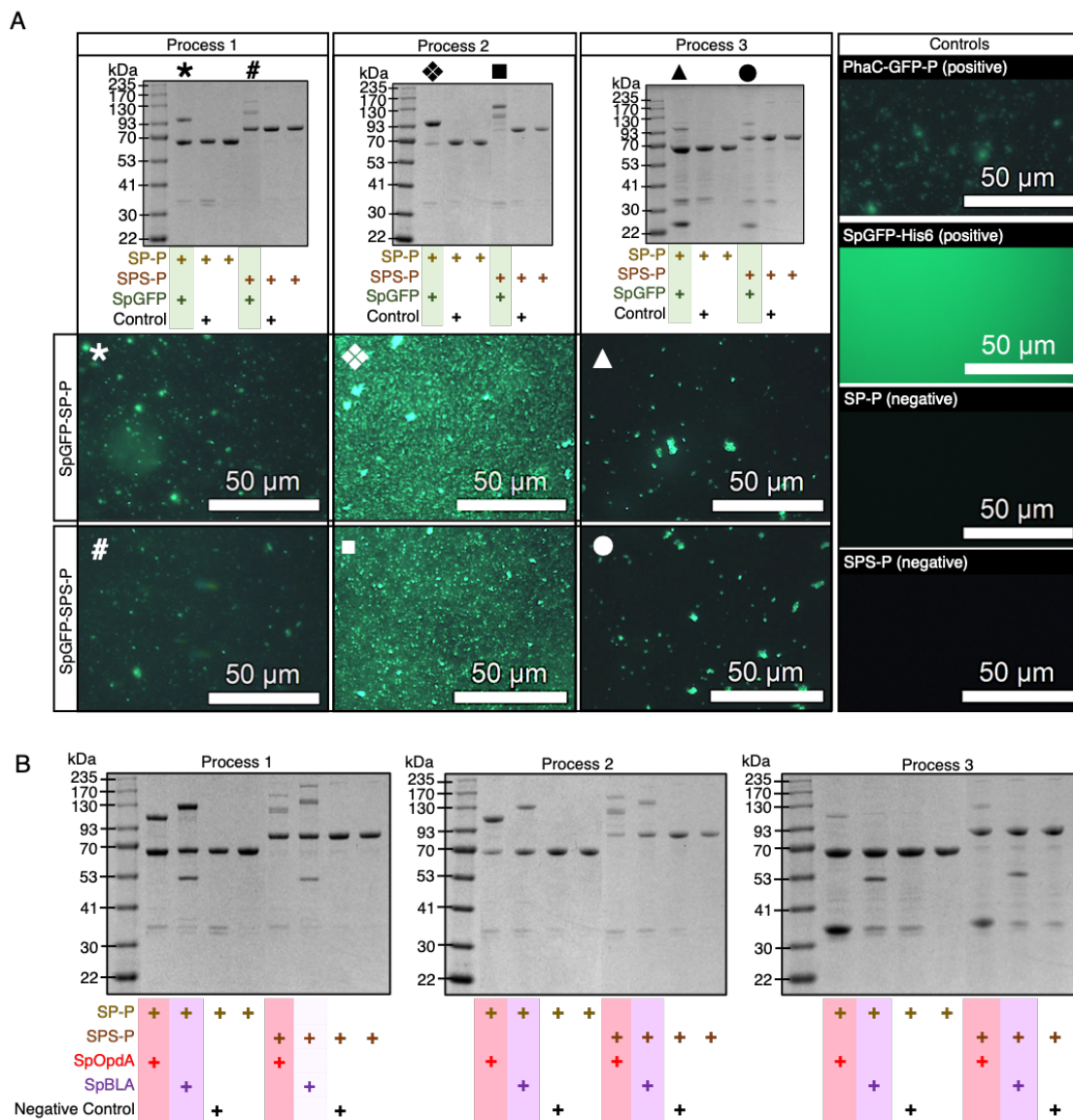


**Figure 3.** Modular functionalization of SpyCatcher-coated PHA particles with various SpyTagged proteins implementing processes 1–3 using different plain SpyCatcher-coated PHA particles as negative controls. **(A)** SDS-PAGE and fluorescence microscopy analyses of SpGFP immobilized on SP-Ps and SPS-Ps. **(B)** SDS-PAGE analysis of SpyTagged OpdA (SpOpdA) and SpyTagged BLA (SpBLA) immobilized on SP-Ps and SPS-Ps.

Meanwhile, we noted that SpGFP-SP-P and SpGFP-SPS-P prepared using process 3 was the least efficient approach as reflected by the faint protein bands of SpGFP-SP-L and SpGFP-SPS-Ls, at a total surface SpGFP coverage of only ~11% and ~17%, respectively, on SpGFP-SP-P and SpGFP-SPS-P (**Figure 3A**). We also noted an extra protein band at 25.5 kDa, that corresponded to SpGFP as confirmed by LC-MS/MS (**Table S5**), as part of the protein profile of SpGFP-SP-P and SpGFP-SPS-P produced using process 3. We deduced that this could be due to specific non-covalent binding between SpyTag and SpyCatcher, where ligation was not completed. SpGFP was able to diffuse into the interface layer between the bulk phase (cell lysate) and the solid surface of PHA particles prior to protein ligation. However, the covalent ligation between the SpyTag and SpyCatcher was possibly still incomplete after the cell lysis step, due to the much shorter time for SpGFP to ligate onto the SpyCatcher domains on PHA particles using process 3, compared to the other processes. Also, a large amount of cellular debris and background proteins might have contributed to the lower protein ligation efficiency. We initially postulated that the presence of this extra band was caused by the incomplete disruption of *E. coli* containing the SpGFP. However, this explanation is unlikely as we observed an overall low level of background proteins in plain SPS-P and SP-P preparations using process 3 (**Figure 3A**). Nevertheless, all the SpGFP-SP-Ps and SpGFP-SPS-Ps, including those prepared using process 3 could emit green fluorescence similar to those of positive controls, soluble SpGFP bearing His<sub>6</sub> tag (SpGFP-H6) (33) and PhaC-GFP fusion protein displaying PHA particles (PhaC-GFP-P) (42) prepared using the direct gene fusion method, and in contrast to the negative controls (**Figure 3A**).

After successful functionalization of SP-P and SPS-P using SpGFP and to demonstrate the versatility of our proposed processes, we designed further SpyTagged proteins representing diverse functions such as two different enzymes. The chosen enzyme candidates were the dimeric organophosphohydrolase (OpdA), an enzyme from *Agrobacterium radiobacter* that can hydrolyze organophosphate pesticides, and the monomeric  $\alpha$ -amylase from *Bacillus licheniformis* (BLA), a thermophilic  $\alpha$ -linked polysaccharide-degrading enzyme that can hydrolyze starch. We fused the SpyTag peptide to the N-terminus of both enzymes, to create SpOpdA and SpBLA (**Table S4**). The SDS-PAGE profiles of all *in vivo* and *ex vivo* enzyme-functionalized SP-P and SPS-P using processes 1–3 are presented in **Figure 3B**. Briefly, for process 1, the surface coverage of SpyTagged enzymes on SP-P and SPS-P varied from ~30–51% (**Figures 3B and S6**). Interestingly, we noticed a distinct protein band (52.3 kDa) corresponding to SpBLA, confirmed by LC–MS/MS (**Table S5**), as part of the protein profile of both SP and SPS particles displaying SpBLA (**Figures 3B and S6**).

We speculate that although specific binding occurred ligation was incomplete. Since this phenomenon is unique to SpBLA only using process 1, we suggest that this could be due to its higher molecular weight compared to other SpyTagged proteins since larger proteins are more prone to steric hindrance for protein ligation as noted previously (43). Hence, possibly a longer reaction time is necessary to allow complete ligation of SpBLA with the SpyCatcher domains on PHA particles. Meanwhile, functionalization of SP-P and SPS-P using process 2 achieved up to ~76% particle surface coverage using both the SpyTagged enzymes of interest, with distinctive clear protein bands corresponding to the ligated products only (**Figure 3B**). However, the overall particle surface coverage of SP-P and SPS-P

by both SpyTagged enzymes using process 3 was less than satisfactory, ranging from  $\sim <1$ –16% for both SP-P and SPS-P (**Figure 3B**) due to incomplete ligation as noted in the case of SpGFP immobilization.

Next, all the functionalized SP-Ps and SPS-Ps were subjected to DLS analysis. Particle size distribution analysis revealed that immobilizing SpyTagged proteins onto SP-P and SPS-P using processes 1–2 slightly increased the diameter of individual SP-P and SPS-P (**Figures 4A and 4B**). This outcome implies successful ligation of various SpyTagged proteins to the SpyCatcher-coated PHA particles, without affecting the assembled architecture and monodispersity of SP-P and SPS-P in general. The high polydispersity of SpBLA-SP-P obtained using process 1 indicates the slight inconsistency of functionalized PHA particles using the *in vivo* approach (**Figure 4A**). We also observed a high degree of particle polydispersity and likely altered architecture of PHA particles in the case of samples prepared using process 3, possibly due to the excessive mechanical strain on the PHA particles during the functionalization process (**Figure 4C**).

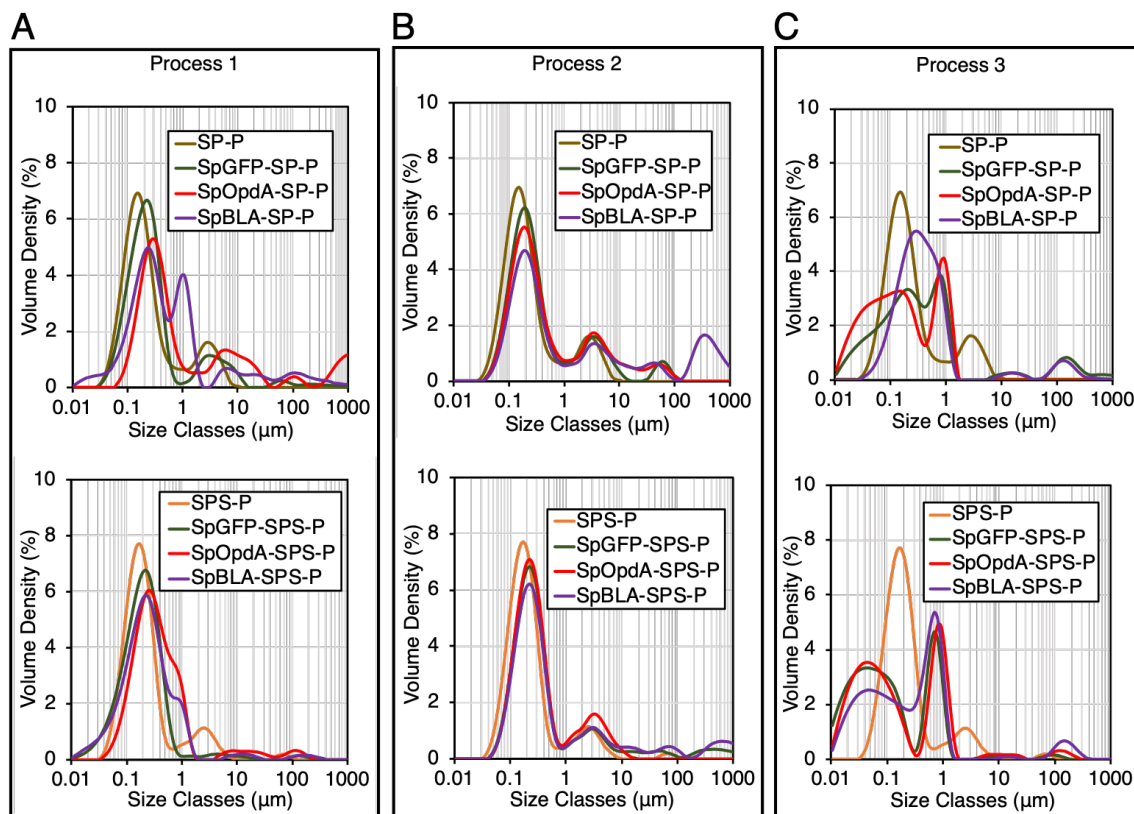


**Figure 4.** Particle size distribution of various functionalized SpyCatcher-coated PHA particles produced using processes 1–3 by DLS analysis (mean,  $n = 3$ ). The particle size distribution of plain SP-P and SPS-P determined in Figure 2 are shown as negative controls. Particle size distribution of various functionalized SP-Ps and SPS-Ps produced using (A) process 1, (B) process 2 or (C) process 3.

#### 4.4.3 Enzymatic Performance of Functionalized SpyCatcher-coated PHA Particles using the Proposed Processes.

After demonstrating successful immobilization of SpyTagged enzymes onto both SP-P and SPS-P, we first qualitatively tested the enzymatic performance of immobilized BLA on 1%

(w/v) starch agar (**Figure 5A**). We used soluble SpBLA bearing His<sub>6</sub> tag (SpBLA-H6) (33) and BLA-PhaC fusion protein displayed on PHA particles (BLA-PhaC-P) (16) generated using direct gene fusion method as positive controls. All BLA-containing samples created a clear transparent zone on a starch agar plate stained by Lugol's solution, indicating starch degradation (**Figure 5B**).

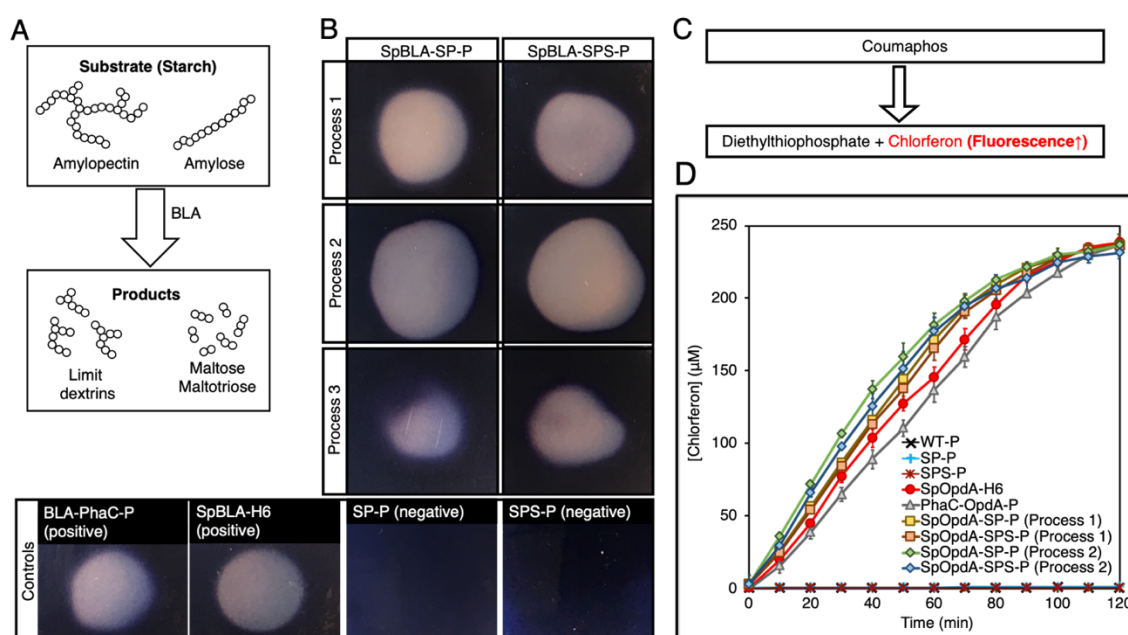


**Figure 5.** Enzymatic assay of SpBLA and SpOpdA functionalized SpyCatcher-coated PHA particles. **(A)** Schematic illustration of starch hydrolysis by BLA. **(B)** Formation of clear hydrolytic zone on Lugol's iodine stained 1% starch agar plate hydrolyzed by SpBLA-SP-P and SpBLA-SPS-P prepared using processes 1–3. **(C)** Schematic of OpdA activity assay using coumaphos as substrate. **(D)** Reaction time course of SpOpdA-SP-P and SpOpdA-SPS-P coumaphos hydrolysis to chlorferon by functionalized particles produced using processes 1–2, with appropriate controls (mean  $\pm$  1 SD,  $n = 3$ ).

Then, we quantitatively determined the enzymatic performance of both soluble and immobilized forms of OpdA using coumaphos as substrate (**Figure 5C**), and by assessing the liberated chlorferon from coumaphos degradation relative to a standard curve (**Figure S7**). We determined the approximate protein concentration of both soluble and covalently immobilized OpdA (with the relevant controls), using densitometric analysis by SDS-PAGE and bovine serum albumin (BSA) to produce a standard curve (**Figures S8–S16**). All standard curves were linear with  $R^2$  values of at least  $\sim 0.98$ . For the quantitative OpdA assay, we excluded samples prepared by process 3 due to the extremely low amount of OpdA covalently immobilized to PHA particles. We also used our previously developed constructs, soluble SpOpdA bearing His<sub>6</sub> tag (SpOpdA-H6) (33) and PhaC-OpdA fusion protein displayed on PHA particles (PhaC-OpdA-P) (17) prepared using the direct gene fusion method as positive controls. We observed subtle improvements in the catalytic activity of immobilized OpdA compared to the positive controls (**Figure 5D**). The catalytic activities of SpOpdA-SP-P and SpOpdA-SPS-P produced by process 2 ( $5.43 \pm 0.3$  U/mg and  $5.29 \pm 0.4$  U/mg) and those produced by process 1 ( $5.14 \pm 0.2$  U/mg and  $4.95 \pm 0.4$  U/mg), were higher than SpOpdA-H6 ( $4.42 \pm 0.4$  U/mg) and PhaC-OpdA-P ( $4.17 \pm 0.2$  U/mg). This observation is consistent with macromolecular crowding increasing enzyme activity as discussed previously (33), as the surface densities of SpOpdA immobilized on individual SP-P and SPS-P using process 2 are higher than that of those produced using process 1. A higher density of OpdA clustering on individual PHA particles created an excluded volume effect, which in turn drives the coumaphos conversion rate forward.

#### 4.4.4 Design and Production of Bimodular PHA Particles.

To construct bimodular PHA particles based on the covalent site-specific protein ligation technology, we designed several fusion proteins consisting of combinations of orthogonal Catcher pairs (SpyCatcher, SnoopCatcher, and SdyCatcher<sup>DANG Short</sup>) genetically fused to the N-terminus and C-terminus of PhaC for the purpose of this study. They are SdyCatcher-PhaC-SnoopCatcher fusion protein (DPN), SnoopCatcher-PhaC-SdyCatcher fusion protein (NPD), SpyCatcher-PhaC-SnoopCatcher fusion protein (PPN), and SnoopCatcher-PhaC-SpyCatcher fusion protein (NPP) (**Table S4**), as detailed in the Supporting Information (**Appendix S1**). Then we inserted the constructed genes into IPTG-inducible plasmid vectors and transformed into *E. coli* for the biosynthesis of various combinations of Catcher domain-displaying PHA particles. **Tables S1–S3** list all the bacterial strains, plasmids, and primers used for this study. Although theoretically-possible, the SpyCatcher—SdyCatcher pair was not considered in this study due to the reported low level of cross-reactivity between these two Tag/Catcher pairs in the literature (34). **Figure 6A** illustrates the overproduction of the various fusion proteins displayed on the surface of PHA particles, providing a high density of Catcher domains spatially distributed on the surface of PHA particles. The apparent molecular weights of DPN, NPD, PPN, and NPP fusion proteins correspond to the theoretical masses of 79.8 kDa, 86.0 kDa, 81.5 kDa, and 86.3 kDa, respectively. The production yields of DPN fusion protein displaying PHA particles (DPN-P), NPD fusion protein displaying PHA particles (NPD-P), PPN fusion protein displaying PHA particles (PPN-P), and NPP-P are tabulated (**Figure 6B**).

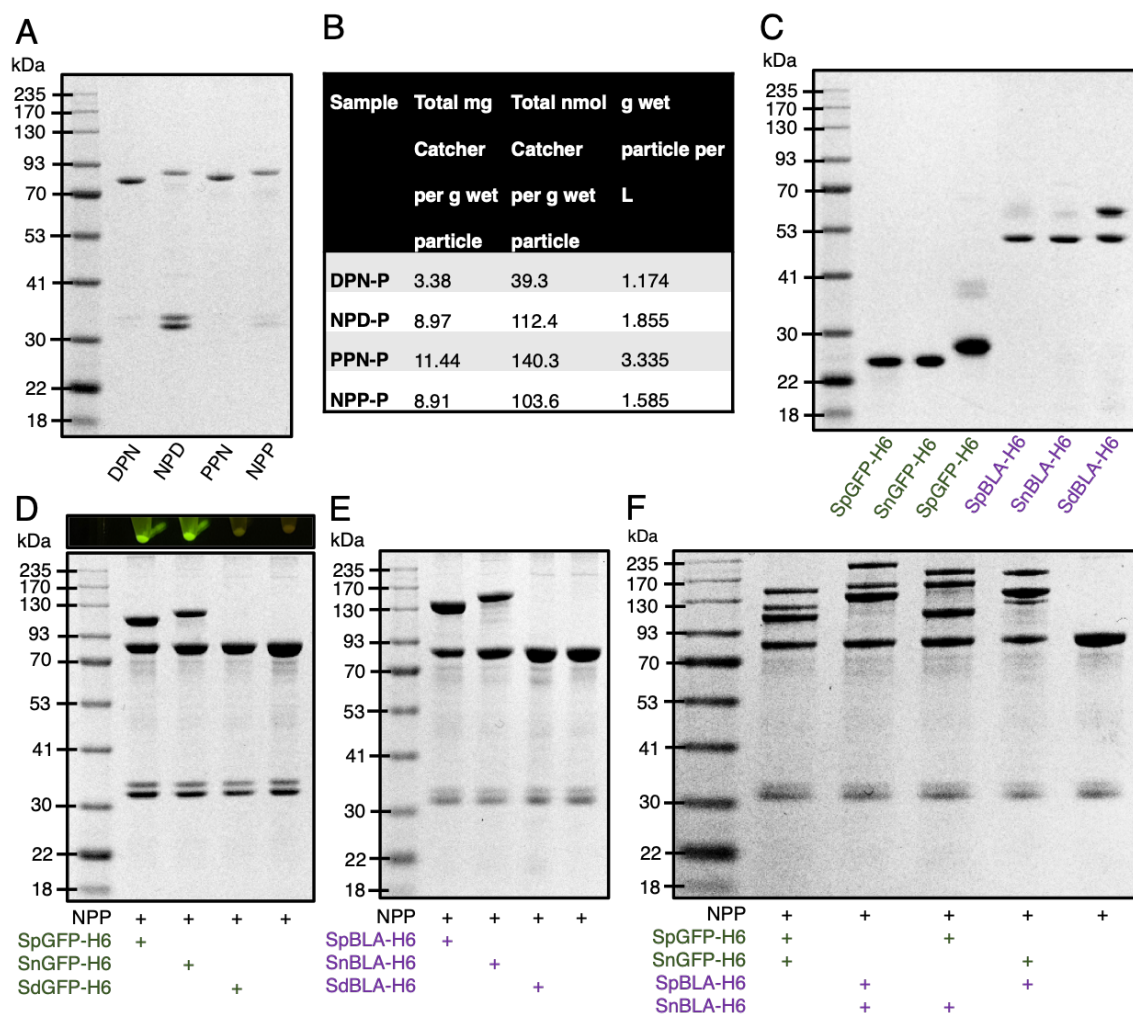


**Figure 6.** Production and functionalization of various Catcher domain-coated PHA particles *in vitro*. **(A)** SDS-PAGE analysis of various Catcher domains displayed on PHA particles. **(B)** Production yields of various Catcher domain-coated PHA particles. **(C)** SDS-PAGE analysis of various tagged GFPs and BLAs. **(D)** SDS-PAGE analysis of various tagged GFPs immobilized on NPP-Ps and visualized by blue light exposure. **(E)** SDS-PAGE analysis of various tagged BLAs immobilized on NPP-Ps. **(F)** SDS-PAGE analysis of simultaneous dual-functionalization of NPP-Ps using various tagged GFPs and BLAs.

Next, to allow simultaneous covalent ligation of multiple proteins onto the various Catcher domain-coated PHA particles *in vitro* in one-step, we incorporated different peptide tags (*e.g.* SnoopTag and SdyTag) to the N-terminus of both GFP and BLA. These peptide tags are covalently specific to their respective Catcher domains (*e.g.* SnoopCatcher and SdyCatcher). In addition, to enable simple purification of these fusion proteins using Ni-NTA metal affinity chromatography for *in vitro* protein ligation, we fused a hexahistidine (His<sub>6</sub>) tag to the C-terminus of these fusion proteins (**Table S4**). This configuration could potentially avoid steric hindrance between the covalent tag and His<sub>6</sub> tag (33). The genetic fusion of these peptide tags to the selected proteins resulted in the generation of SnoopTagged GFP bearing His<sub>6</sub> tag (SnGFP-H6), SnoopTagged BLA bearing His<sub>6</sub> tag (SnBLA-H6), SdyTagged GFP bearing His<sub>6</sub> tag (SdGFP-H6) and SdyTagged BLA bearing His<sub>6</sub> tag (SdBLA-H6) (**Table S4**). Then, we recombinantly biosynthesized these soluble fusion proteins in *E. coli* BL21(DE3) strain. As anticipated, the fusion of these peptide tags did not hinder the recombinant production and Ni-NTA affinity purification of these tagged GFPs and BLAs, using our previously developed SpGFP-H6 and SpBLA-H6 fusion proteins as reference (**Figure 6C**) (33).

We performed the densitometry analysis for all the Catcher domain-displaying on PHA particles and purified tagged proteins using a BSA standard curve (**Figures S17–S19**). The concentration of each sample was diluted to fit into the linear range of the standard, where the value of  $R^2$  of the linear curve obtained for each densitometric analysis was at least  $\sim 0.99$ .

#### 4.4.5 Screening of Bimodular PHA Particles Suitable for Efficient Simultaneous Dual-Functionalization.

For validation of the accessibility of tagged proteins for covalent protein ligation with various Catcher domain-displaying PHA particles, we first incubated DPN-P, NPD-P, PPN-P, and NPP-P with excess SpGFP-H6, SnGFP-H6, and SdGFP-H6 *in vitro*. We observed varying levels of protein ligation after incubation of tagged GFPs with various combinations of Catcher domain-displaying PHA particles (**Figures S20–22 and 6D**). It is suggested that only a small fraction DPN fusion protein displayed on the PHA particle can ligate with SpGFP-H6 and SnGFP-H6 as visualized by SDS-PAGE analysis (**Figure S20**). These samples are also able to fluoresce under blue light when compared to the control PHA particles. Note that although SdGFP-DPN ligated proteins (SdGFP-DPN-L) could not be visualized clearly by SDS-PAGE, pelleted SdGFP-DPN-L-displaying PHA particles (SdGFP-DPN-P) were able to emit very weak green fluorescence under blue light (**Figure S20**).

Similarly, the covalent tag of both SpGFP-H6 and SdGFP-H6 showed limited accessibility to the Catcher domains displayed on NPD-P individually, where most of the NPD fusion proteins did not undergo isopeptide covalent ligation after incubation (**Figure S21**). Interestingly, we noticed that ~42% of the NPD fusion proteins displayed on PHA particles were able to ligate with SnGFP-H6, forming SnGFP-NPD ligated protein (SnGFP-NPD-L) of size 111.1 kDa (**Figure S21**). This is supported by the strong fluorescence emitted by SnGFP-NPD-L-displaying PHA particles (SnGFP-NPD-P) under blue light (**Figure**

**S21**). Meanwhile, ~45% of PPN-fusion protein displayed on PHA particles (PPN-P) was able to immobilize purified SpGFP-H6 *in vitro*, as shown on SDS-PAGE by the appearance of a large fraction of PPN fusion proteins to forming SpGFP-PPN ligated protein (SpGFP-PPN-L) of size 114.1 kDa, much larger when compared to immobilized SdGFP-H6 and SnGFP-H6 on PPN-P (**Figure S22**). This is further evidenced by the higher fluorescence level of SpGFP-PPN-L displaying PHA particles (SpGFP-PPN-P) when compared to SdGFP-PPN ligated protein displaying PHA particles (SdGFP-PPN-P), and PPN-SnGFP ligated protein displaying PHA particles (PPN-SnGFP-P) (**Figure S22**).

Interestingly, NPP-P ligated both SpGFP-H6 and SnGFP-H6 without showing notable cross-reactivity (**Figure 6D**). Formation of intense SDS-PAGE bands corresponding to NPP-SpGFP ligated protein (NPP-SpGFP-L) and SnGFP-NPP ligated protein (SnGFP-NPP-L) at a molecular weight of 108.5 kDa and 118.8 kDa respectively (**Figure 6D**), indicated successful protein ligation. We further found that ~49% and ~35% of NPP fusion protein could ligate with SpGFP-H6 and SnGFP-H6, and both of the ligated proteins displaying PHA particles fluoresced strongly under blue light (**Figure 6D**). Besides, we noted that NPP-P showed good reaction orthogonality against SdGFP-H6 (**Figure 6D**). We observed a similar trend with the use of differently tagged BLAs to functionalize plain NPP-P, which resulted in the formation of NPP-SpBLA ligated protein (NPP-SpBLA-L) (137.4 kDa) and SnBLA-NPP ligated protein (SnBLA-NPP-L) (148.7 kDa) (**Figure 6E**). Therefore, and due to the non-optimal accessibility of other Catcher domains displayed on DPN-P, NPD-P, and PPN-P by various tagged GFPs, we selected only the NPP-P construct as our prototype for proof-of-concept simultaneous dual functionalization of bimodular PHA

particles. As expected, NPP-P could immobilize various purified SpyTagged and SnoopTagged proteins simultaneously *in vitro*, as unveiled by the generation of numerous ligated proteins that formed larger than the NPP fusion protein (86.3 kDa) (**Figure 6F**). In addition, we implemented process 2 mentioned above to demonstrate that NPP-P can be readily functionalized without using purified tagged proteins. NPP-P could react with SpGFP-H6 and SnGFP-H6 in cleared *E. coli* lysate, individually and simultaneously, as revealed by the formation of various ligated proteins that appeared above the molecular weight corresponding to NPP fusion protein (86.3 kDa) (**Figure S23**).

The inconsistent ligation results observed in using DPN-P, NPD-P, and PPN-P to form a protein immobilization platforms, where we fused various Catcher domains at the different insertion sites of the PHA-binding PhaC, could be due to the misfolding of the fusion proteins displayed on PHA particles. The individual components of the designed fusion proteins, especially in the case of SnoopCatcher fused to the C-terminus of PhaC in the current study, possibly could not fully replicate the native protein conformation, *i.e.* non-optimal protein folding as noted previously due to steric hindrance (44). Failure in fully replicating the native structure of the individual protein domains in the context of fusion proteins could result in impaired protein ligation owing to restricted accessibility of the tagged proteins to the reactive site of the Catcher domains. In addition, wild-type PhaC displaying PHA particles and their recombinant variants often exhibited a negative surface charge at pH 7.5. The isoelectric point (pI) of PHA particles in suspension typically varies between approximately 5–6 (13, 45, 46). However, the predicted pI of the SdyTag peptide itself is pH 3.9, much lower than those compared to both SpyTag and SnoopTag at pH 8.6 and pH 8.5,

respectively (47). Therefore, at a ligation reaction pH value of 7.5, both SdyTag peptide and PHA particles are predominantly negatively charged. Consequently, electrostatic repulsion between these two components is likely responsible for the low ligation yield observed between the SdyTagged proteins onto the PHA particles.

#### **4.4.6 Structural Characterization of Selected Bimodular PHA Particles.**

To characterize the structure of NPP-P, we analyzed the plain NPP-P using both SEM and TEM. Both electron microscopy techniques confirmed the spherical structure of the NPP-P as indicated by the micrographs (**Figure 7A**), suggesting successful *in vivo* self-assembly of our bimodular PHA particles as expected. We also further determined the particle size distribution of various NPP-P using DLS analysis (**Figures 7B–7E**). We found that plain NPP-P is homogeneous and has a narrow particle size distribution with a maximum of ~214 nm, similar to that of WT-P (**Figure 7B**). We then measured the particle size distribution of various functionalized NPP-Ps, using NPP-P determined in **Figure 7B**, PhaC-GFP-P (42), and BLA-PhaC-P (16) as controls. The diameter of both single and multiple proteins immobilized individual NPP-Ps increased slightly from ~214 nm to ~243 nm, suggesting successful immobilization of various tagged proteins on NPP-P (**Figures 7C–7E**). The particle size distribution of PhaC-GFP-P and BLA-PhaC-P peaked at ~597 nm and ~314 nm, respectively, further validating the impact of using direct protein fusion approach on the PHA particle uniformity as mentioned earlier. However, we also observed consistent aggregation behavior of various functionalized NPP-Ps in the ~4–5  $\mu\text{m}$  diameter range

(Figures 7C–7E), contrary to those observed in functionalized SPS-Ps and SP-Ps (Figures 4A–4C).

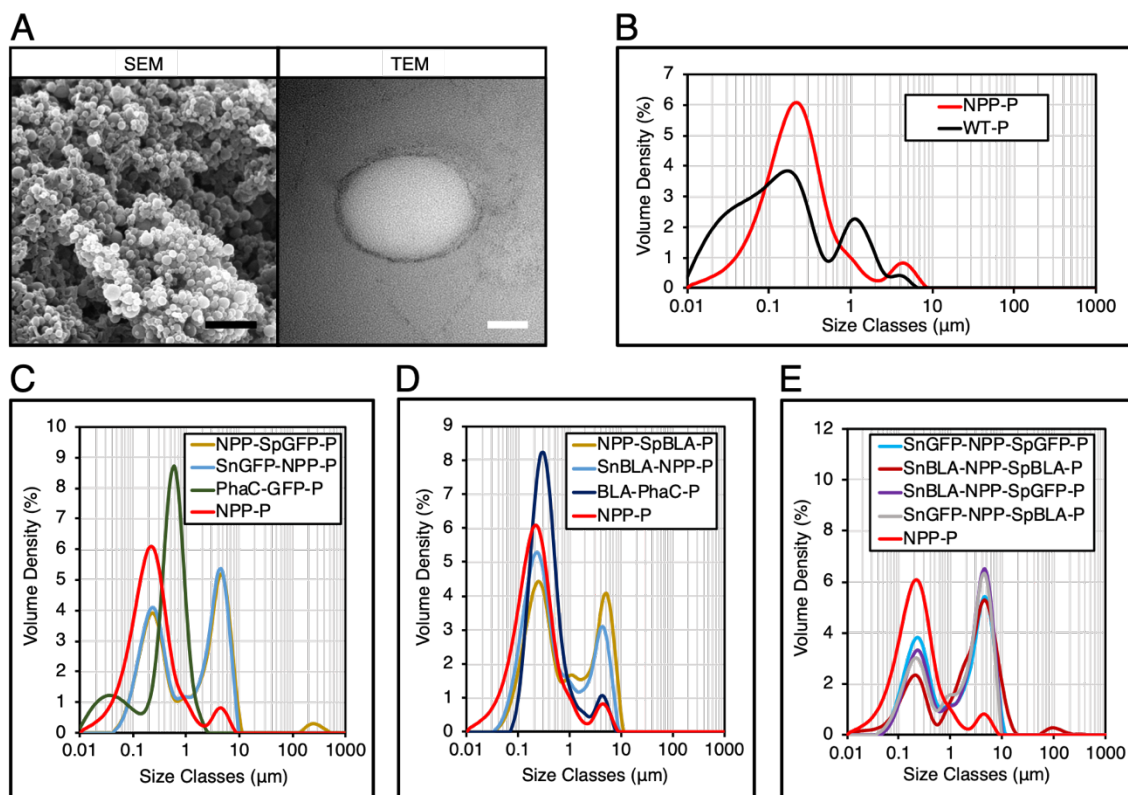


**Figure 7.** Structural characterization of various NPP-Ps. **(A)** SEM and TEM micrographs of plain NPP-P. Black scale bar, 1  $\mu\text{m}$ ; white scale bar, 100 nm. **(B)** Particle size distribution of plain NPP-P by DLS analysis (mean,  $n = 3$ ). **(C)** Particle size distribution of SpGFP-H6 and SnGFP-H6 immobilized NPP-Ps by DLS analysis (mean,  $n = 3$ ) using particle size distribution of plain NPP-P determined in Figure 7B as negative control and PhaC-GFP-P as positive control. **(D)** Particle size distribution of SpBLA-H6 and SnBLA-H6 immobilized NPP-Ps by DLS analysis (mean,  $n = 3$ ) using particle size distribution of plain NPP-P determined in Figure 7B as negative control and BLA-PhaC-P as positive control. **(E)**

Particle size distribution of various dual-functionalized NPP-Ps by DLS analysis (mean,  $n = 3$ ) using particle size distribution of plain NPP-P determined in Figure 7B as negative control.

#### 4.4.7 Robustness of Functionalized Bimodular PHA Particles.

It was crucial to ensure the robustness of the scaffolding platform against harsh working and storage environments to satisfy different task-specific applications. We subjected the NPP-P to five rounds of heat-cooling treatment before subsequent *in vitro* functionalization with SnGFP-H6 and SpBLA-H6. We observed that the NPP-P tended to aggregate from the fourth cycle of heat-cooling, making homogenization of the PHA particle suspension challenging (data not shown). After five cycles of heat treatment, less than ~4% of the NPP fusion protein was able to immobilize SnGFP-H6 to form SnGFP-NPP-L (**Figure 8A**). Meanwhile, ~21% of NPP fusion protein on PHA particles could immobilize SpBLA-H6 to generate NPP-SpBLA-L, and less than ~2% of NPP fusion protein on PHA particles could immobilize both SnGFP-H6 and SpBLA-H6 to form SnGFP-NPP-SpBLA ligated proteins (SnGFP-NPP-SpBLA-L) (**Figure 8A**). This observation infers that the Snoop-Catcher fused to the N-terminus of PhaC is prone to heat denaturation after repeated heat-cooling treatment, and therefore, could not interact with SnGFP-H6 to generate either SnGFP-NPP-L or SnGFP-NPP-SpBLA-L on PHA particles. After that, the robustness of the NPP-P to multiple freeze-thaw cycles was tested. Plain NPP-Ps were suspended in 50 mM Tris-HCl (pH 7.5) and subjected to up to five cycles of freeze-thaw treatment before incubation under controlled conditions with purified SnGFP-H6 and SpBLA-H6 *in vitro*.

We did not include any cryoprotectants in this study to assume the worst-case scenario, *e.g.* in the event where freezing or thawing of stored samples occurred during storage or transportation. We first confirmed that the resuspension of plain NPP-P using the same buffer still could be performed easily before proceeding to the next step (data not shown). Remarkably, we observed no significant loss of both immobilized proteins on our bimodal PHA particles after the fifth cycle of freeze–thaw treatment (**Figure 8B**).

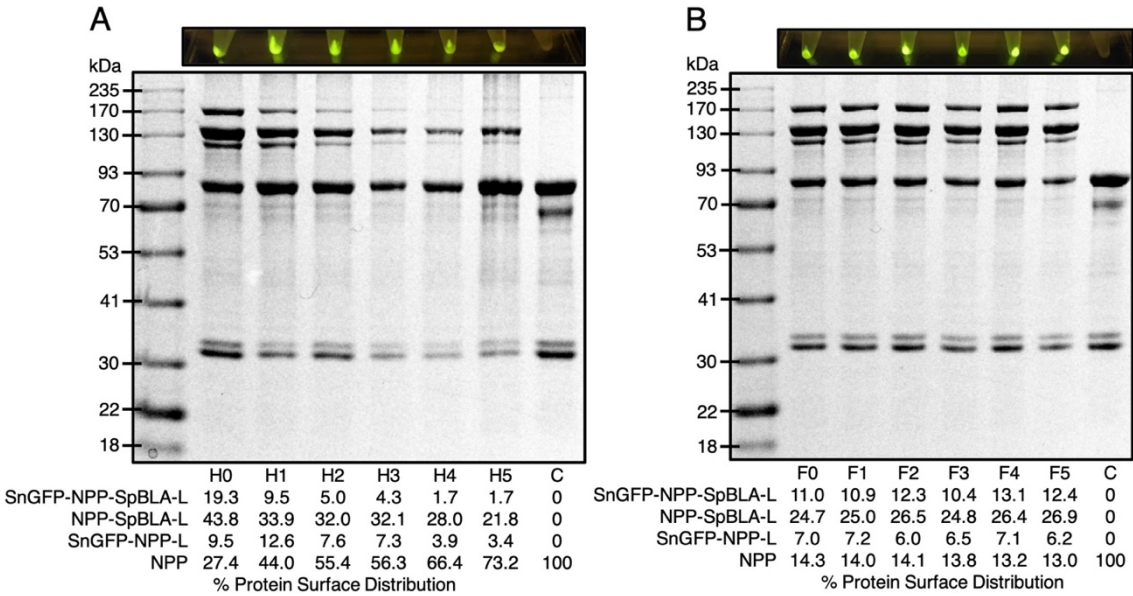


**Figure 8.** Exposure of plain NPP-P to extreme conditions prior functionalization as visualized by SDS-PAGE analysis and screening of samples under blue light. **(A)** NPP-P could immobilize tagged proteins after five consecutive heat–cooling treatment. (Hx, x=round of heat–cooling treatment). **(B)** NPP-P could immobilize tagged proteins after five consecutive freeze–thaw treatment. (Fx, x=round of freeze–thaw treatment).

#### 4.4.8 Functional Performance of Functionalized Bimodular PHA Particles.

To ascertain the functionality of the immobilized proteins on NPP-P, we first carried out fluorescence microscopy analysis on all the functionalized NPP-Ps. We used soluble GFP and PhaC-GFP-P (33, 42) as positive controls and plain NPP-P and WT-P as negative controls. As expected, all the SpGFP-H6 and SnGFP-H6 immobilized on NPP-Ps in suspension were able to fluoresce, similar to the positive controls (**Figure 9**). Meanwhile, non-GFP immobilizing PHA particles and the negative controls could not emit green fluorescence (**Figure 9**). We also further tested the functionality of immobilized BLA on NPP-P by loading all the functionalized NPP-Ps on 1% (w/v) starch agar (33). We used soluble BLAs and BLA-PhaC-P (16, 33) as positive controls and plain NPP-P and WT-P as negative controls. All BLA-immobilized PHA particles could create a transparent hydrolyzed zone on a Lugol's iodine stained starch agar plate, comparable to those of positive controls, further suggesting successful starch hydrolysis by the functionalized PHA particles (**Figure 10**).

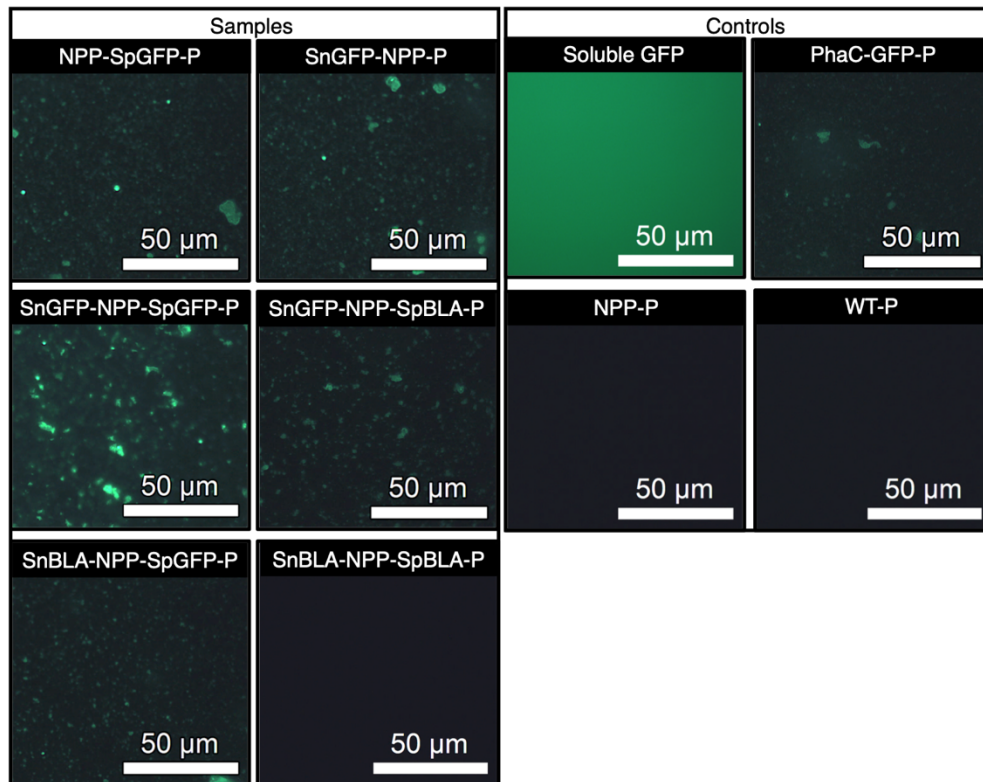


**Figure 9.** Fluorescence microscopy analysis of SpGFP-H6 and SnGFP-H6 functionalized NPP-Ps with appropriate positive and negative controls.

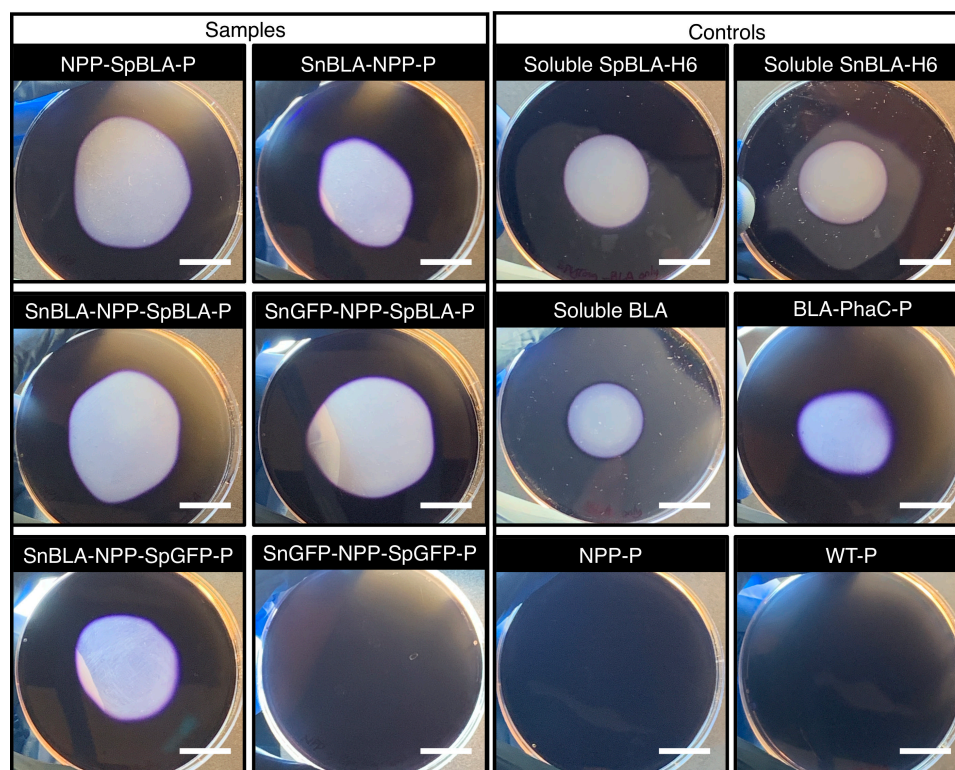


**Figure 10.** Qualitative starch degradation assay hydrolyzed by SpBLA-H6 and SnBLA-H6 functionalized NPP-Ps with appropriate positive and negative controls. White scale bar, 2 cm.

#### 4.5 Discussion

Increasing evidence indicates that fusing different target foreign proteins to PHA-associated proteins such as PhaC to facilitate surface functionalization of PHA particles, in some circumstances could adversely affect the density and functionality of target protein on PHA particles (44, 48), as well as the physicochemical uniformity of the recombinant PHA particles (13, 14, 46). We had previously proposed a modular design concept to functionalize PHA particles *in vitro* using the SpyTag/SpyCatcher chemistry (33). This modular design

prevents the risk of several inconsistencies that are commonly encountered in direct gene fusion recombinant PHA particle technology (as mentioned) that has hindered its further progress beyond proof-of-concept. The use of purified components and subsequent *in vitro* protein ligation could result in higher production costs and time consumption in large-scale manufacturing, and thereby raising costs. Also, the sole reliance of this approach on SpyTag/SpyCatcher chemistry makes multi-functionalization of the modular PHA particles less attractive in terms of processability, despite our previous demonstration that different SpyTagged proteins could be equally as well spatially distributed on SpyCatcher-coated PHA particles *in vitro* (33). Therefore, a simplified functionalization process needed to be developed in order to overcome the drawbacks of this approach. In this study, we sought to implement several cost-effective, innovative strategies to develop a simpler modular functionalization of our PHA particles.

We first explored processes designed to functionalize SpyCatcher-coated PHA particles thus avoiding the necessity of using purified soluble SpyTagged proteins to functionalize SpyCatcher-coated PHA particles. Previous studies have reported that similar streamlined processes using SpyTag/SpyCatcher chemistry to functionalize other protein-based nanoparticles (21, 26, 49). However, it was important to examine these processes in polymeric materials such as PHAs. Overall, processes 1 and 2, but not process 3 could be used to satisfactorily immobilize an adequate concentration of SpyTagged proteins to SP-P and SPS-P with varying ligation efficiencies. N-terminally SpyTagged proteins with different quaternary structures and molecular sizes can be immobilized covalently using these processes. Process 1 might be more suitable in the case where efficient processability is

paramount for large-scale manufacturing, allowing functionalized PHA particles to be isolated directly after bacterial cultivation for immediate use. We did note, however that in some instances, process 1, sometimes resulted in nonspecific adsorption of one of the SpyTagged proteins onto the surface of PHA particles (**Figure 3B**). The cytoplasmic environment within the cell possibly triggered the creation of favorable conditions that facilitated the nonspecific adsorption of SpBLA onto the SpyCatcher-coated PHA particles. Therefore, there is some uncertainty in using this process as a general approach to decorate PHA particles

While process 2 requires an extra step when compared to process 1 it could offer a similar level of particle uniformity to that reported previously using an *in vitro* functionalization approach (33). This process is still able to avoid the necessity of setting up downstream processes to recover highly purified proteins, which typically account for more than 70% of the total recombinant protein production costs for enzymes, up to 90% for therapeutic proteins (50). These observations indicate that process 2 may be the preferred approach for a standardized process to functionalize PHA particles in a scenario where stringent control of the particle uniformity and reproducibility are essential. This is especially vital in the case of using PHA particles in high-value applications, *e.g.* pharmaceutical and biomedical applications. Inconsistency in the inherent characteristics of particulate scaffolds (*e.g.* particle size and surface charge) could severely affect the performance and reproducibility of these functionalized scaffolds in some cases (51).

The second part of this study involved investigating the suitability of the PHA particle display technology for the incorporation of two orthogonal reactive Tag/Catcher pairs to achieve multi-functionalization. Successful multi-functionalization of particulate scaffolds, including our previously developed SpyCatcher-coated PHA particles, had been previously reported using SpyTag/SpyCatcher chemistry only (23, 24, 33, 52). However, these proof-of-concept demonstrations were shown to require careful optimization of the reactant ratios as well as multiple steps to yield precise outcomes. Hence they are not practical for industrial-scale production. Several recent reports have described the use of different Tag/Catcher systems to functionalize protein-based scaffolds (22, 53). Therefore, we attempted to design a polymeric PHA scaffold able to simultaneously immobilize different functional proteins using various combinations of Tag/Catcher pairs, moving away from sole dependence on the SpyTag/SpyCatcher chemistry.

Initial validation of different Tag/Catcher pairs showed, however, that the performance of constructs other than NPP-P, were less than satisfactory. NPP-P was able to specifically immobilize both purified SnoopTagged and SpyTagged proteins in a simultaneous manner in *in vitro* environments. We also demonstrated the use of process 2 to functionalize NPP-P simultaneously in one-step under *ex vivo* reaction conditions, and thereby suggesting that the processability of this bimodular design is potentially comparable to our previously developed SpyCatcher-coated PHA particles. However, we noted that the various functionalized NPP-Ps tend to form a high amount of aggregates at ~4–5  $\mu\text{m}$  observed from the particle size distribution (**Figures 7C–7E**). The undesirable formation of these polymeric

clusters could be due to nonspecific interactions independent of the electrostatic interactions, as observed previously (33).

Even though direct genetic fusion remains a common approach to functionalize recombinant PHA particles (9, 54), one of its main limitations is that the poor control of immobilized protein density (33). We previously introduced the concept of modularity by merging the SpyTag/SpyCatcher system with the PHA particle technology (33). This modular scaffolding platform could easily be tuned by controlling the ratio of Tag-to-Catcher (33). Although not shown in this study, we expect that our bimodular PHA particles to be as easily tuned *in vitro* due to the highly specific nature of the Tag/Catcher systems. Ultimately, we hope to expand this unprecedented level of controllability to both *in vivo* and *ex vivo* reaction conditions using processes 1–2. By precisely optimizing the production levels of both tagged proteins and Catcher domain-coated PHA particles it should be feasible to achieve a Tag/Catcher reactant ratio that will circumvent laborious purification steps often necessary for *in vivo* and *ex vivo* ligation reactions. A subsequent study looking at tuning several aspects of the process, such as gene optimization (*e.g.* codon and vector optimization), transfection conditions (*e.g.* type and choice of expression systems), and cultivation conditions (*e.g.* inducer concentration, temperature, and post-induction period) should be carefully designed to achieve the target outcomes (55-57).

The findings in this study have extended the information required to develop our modular PHA particle display technology as an emerging platform for surface display of proteins

without compromising its advantages. We envision that these strategies may open new avenues for functionalizing PHA particles for the cost-effective production of various high-value-added PHA particle processes. These processes could make the modular functionalization approach more appealing from a cost-effective standpoint (*e.g.* one-step manufacturing) while able to offer improved particle uniformity compared to the PhaC-based direct gene fusion approach. Any inconsistencies of the particle uniformity can cause significant differences in their functional properties, and therefore severely affect the product quality. These positive outcomes further indicate that a versatile toolbox for the robust production of designer PHA particles could be established.

### **Author Contributions**

Contributions: **Wong, J. X.** and Rehm, B. H. A. conceived the main conceptual ideas of this study. **Wong, J. X.** and Rehm, B. H. A. designed the study and **Wong, J. X.** performed all the experiments except part of the DNA cloning work. Gonzalez-Miro, M. performed part of the cloning work. Rehm, B. H. A. and Sutherland-Smith, A. J. provided technical feedback. **Wong, J. X.** took the lead in writing the paper in consultation with Rehm, B. H. A., Sutherland-Smith, A. J., and Gonzalez-Miro, M. All authors have given approval to the final version of the manuscript.

## **Funding**

This work was supported by the MacDiarmid Institute of Advanced Materials and Nanotechnology (New Zealand) and School of Fundamental Sciences, Massey University (New Zealand) and Griffith Institute for Drug Discovery, Griffith University (Australia).

## **Conflict of Interest Statement**

B. H. A. Rehm is co-founder and shareholder of PolyBatics Ltd that commercializes veterinary TB diagnostic products related to the PHA particle technology.

## **Acknowledgments**

We thank Manawatu Microscopy and Imaging Centre (Palmerston North, New Zealand) for their assistance with microscopy, and Trevor Loo for his assistance with LC-MS/MS analysis.

## 4.6 References

1. Cornejo E, Abreu N, Komeili A. Compartmentalization and organelle formation in bacteria. *Curr. Opin. Cell Biol.* 2014;26:132-8.
2. Diekmann Y, Pereira-Leal JB. Evolution of intracellular compartmentalization. *Biochem. J.* 2013;449(2):319-31.
3. Amara AA, Rehm BH. Replacement of the catalytic nucleophile cysteine-296 by serine in class II polyhydroxyalkanoate synthase from *Pseudomonas aeruginosa*-mediated synthesis of a new polyester: identification of catalytic residues. *Biochem. J.* 2003;374(2):413-21.
4. Ren S, Li C, Jiao X, Jia S, Jiang Y, Bilal M, et al. Recent progress in multienzymes co-immobilization and multienzyme system applications. *Chem. Eng. J.* 2019;373:1254-78.
5. Bae J, Kuroda K, Ueda M. Proximity effect among cellulose-degrading enzymes displayed on the *Saccharomyces cerevisiae* cell surface. *Appl. Environ. Microbiol.* 2015;81(1):59-66.
6. Hwang ET, Lee S. Multienzymatic cascade reactions via enzyme complex by immobilization. *ACS Catal.* 2019;9(5):4402-25.

7. Qu J, Cao S, Wei Q, Zhang H, Wang R, Kang W, et al. Synthetic multienzyme complexes, catalytic nanomachineries for cascade biosynthesis *in vivo*. ACS Nano. 2019.
8. Siu K-H, Chen RP, Sun Q, Chen L, Tsai S-L, Chen W. Synthetic scaffolds for pathway enhancement. Curr. Opin. Biotechnol. 2015;36:98-106.
9. Parlane NA, Gupta SK, Rubio-Reyes P, Chen S, Gonzalez-Miro M, Wedlock DN, et al. Self-assembled protein-coated polyhydroxyalkanoate beads: properties and biomedical applications. ACS Biomater. Sci. Eng. 2016;3(12):3043-57.
10. Tian J, Sinskey AJ, Stubbe J. Class III polyhydroxybutyrate synthase: Involvement in chain termination and reinitiation. Biochemistry. 2005;44(23):8369-77.
11. Du J, Rehm BH. Purification of target proteins from intracellular inclusions mediated by intein cleavable polyhydroxyalkanoate synthase fusions. Microb. Cell Fact. 2017;16(1):184.
12. Du J, Rehm BH. Purification of therapeutic proteins mediated by *in vivo* polyester immobilized sortase. Biotechnol. Lett. 2018;40(2):369-73.
13. Gonzalez-Miro M, Rodríguez-Noda LM, Fariñas-Medina M, Cedré-Marrero B, Madariaga-Zarza S, Zayas-Vignier C, et al. Bioengineered polyester beads co-

- displaying protein and carbohydrate-based antigens induce protective immunity against bacterial infection. *Sci. Rep.* 2018;8(1):1888.
14. Rubio-Reyes P, Parlane NA, Wedlock DN, Rehm BH. Immunogenicity of antigens from *Mycobacterium tuberculosis* self-assembled as particulate vaccines. *Int. J. Med. Microbiol.* 2016;306(8):624-32.
  15. Parlane NA, Chen S, Jones GJ, Vordermeier HM, Wedlock DN, Rehm BHA, et al. Display of antigens on polyester inclusions lowers the antigen concentration required for a bovine tuberculosis skin test. *Clin. Vaccine Immunol.* 2016;23(1):19-26.
  16. Rasiah IA, Rehm BH. One-step production of immobilized  $\alpha$ -amylase in recombinant *Escherichia coli*. *Appl. Environ. Microbiol.* 2009;75(7):2012-6.
  17. Blatchford PA, Scott C, French N, Rehm BH. Immobilization of organophosphohydrolase OpdA from *Agrobacterium radiobacter* by overproduction at the surface of polyester inclusions inside engineered *Escherichia coli*. *Biotechnol. Bioeng.* 2012;109(5):1101-8.
  18. Zakeri B, Fierer JO, Celik E, Chittock EC, Schwarz-Linek U, Moy VT, et al. Peptide tag forming a rapid covalent bond to a protein, through engineering a bacterial adhesin. *Proc. Natl. Acad. Sci. U.S.A.* 2012;109(12):E690-E7.

19. Reddington SC, Howarth M. Secrets of a covalent interaction for biomaterials and biotechnology: SpyTag and SpyCatcher. *Curr. Opin. Chem. Biol.* 2015;29:94-9.
20. Brune KD, Leneghan DB, Brian IJ, Ishizuka AS, Bachmann MF, Draper SJ, et al. Plug-and-Display: decoration of virus-like particles via isopeptide bonds for modular immunization. *Sci. Rep.* 2016;6:19234.
21. Bruun TUJ, Andersson A-MC, Draper SJ, Howarth M. Engineering a rugged nanoscaffold to enhance plug-and-display vaccination. *ACS Nano.* 2018.
22. Brune KD, Buldun CM, Li Y, Taylor IJ, Brod F, Biswas S, et al. Dual plug-and-display synthetic assembly using orthogonal reactive proteins for twin antigen immunization. *Bioconjugate Chem.* 2017;28(5):1544-51.
23. Choi H, Choi B, Kim GJ, Kim Hu, Kim H, Jung HS, et al. Fabrication of nanoreaction clusters with dual - functionalized protein cage nanobuilding blocks. *Small.* 2018;14(35):1801488.
24. Bae Y, Kim GJ, Kim H, Park SG, Jung HS, Kang S. Engineering tunable dual functional protein cage nanoparticles using bacterial superglue. *Biomacromolecules.* 2018.

25. Swartz AR, Chen W. SpyTag/SpyCatcher functionalization of E2 nanocages with stimuli-responsive Z-ELP affinity domains for tunable monoclonal antibody binding and precipitation properties. *Bioconjugate Chem.* 2018;29(9):3113-20.
26. Zhang G, Quin M, Schmidt-Dannert C. A self-assembling protein scaffold system for easy in vitro co-immobilization of biocatalytic cascade enzymes. *ACS Catal.* 2018.
27. Ma W, Saccardo A, Roccatano D, Aboagye-Mensah D, Alkaseem M, Jewkes M, et al. Modular assembly of proteins on nanoparticles. *Nat. Commun.* 2018;9(1):1489.
28. Zhang X-J, Wang X-W, Sun J, Su C, Yang S, Zhang W-B. Synergistic enhancement of enzyme performance and resilience via orthogonal peptide-protein chemistry enabled multilayer construction. *Biomacromolecules.* 2018.
29. Zhang X-J, Wang X-W, Da X-D, Shi Y, Liu C, Sun F, et al. A versatile and robust approach to stimuli-responsive protein multilayers with biologically enabled unique functions. *Biomacromolecules.* 2018;19(3):1065-73.
30. Brizendine RK, Anuganti M, Cremo CR. Using the SpyTag SpyCatcher system to label smooth muscle myosin II filaments with a quantum dot on the regulatory light chain. *Cytoskeleton.* 2019;76(2):192-9.

31. Ke X, Zhang Y, Zheng F, Liu Y, Zheng Z, Xu Y, et al. SpyCatcher–SpyTag mediated in situ labelling of progeny baculovirus with quantum dots for tracking viral infection in living cells. *Chem. Commun.* 2018;54(10):1189-92.
32. Tyagi A, Liu X, Abidi IH, Gao Z, Park BM, Zeng X, et al. Modular functionalization of crystalline graphene by recombinant proteins: a nanoplatfrom for probing biomolecules. *Nanoscale.* 2018;10(47):22572-82.
33. Wong JX, Rehm BH. Design of modular polyhydroxyalkanoate scaffolds for protein immobilization by directed ligation. *Biomacromolecules.* 2018;19(10):4098-112.
34. Tan LL, Hoon SS, Wong FT. Kinetic controlled Tag-Catcher interactions for directed covalent protein assembly. *PloS One.* 2016;11(10):e0165074.
35. Veggiani G, Nakamura T, Brenner MD, Gayet RV, Yan J, Robinson CV, et al. Programmable polyproteins built using twin peptide superglues. *Proc. Natl. Acad. Sci. U.S.A.* 2016;113(5):1202-7.
36. Sambrook J, Fritsch EF, Maniatis T. *Molecular cloning: a laboratory manual*: Cold Spring Harbor Laboratory Press; 1989.
37. Laemmli UK. Cleavage of structural proteins during the assembly of the head of bacteriophage T4. *Nature.* 1970;227(5259):680.

38. Hay ID, Hooks DO, Rehm BH. Use of bacterial polyhydroxyalkanoates in protein display technologies. *Hydrocarbon and Lipid Microbiology Protocols*: Springer; 2014. p. 71-86.
39. Shevchenko A, Tomas H, Havli J, Olsen JV, Mann M. In-gel digestion for mass spectrometric characterization of proteins and proteomes. *Nat. Protoc.* 2006;1(6):2856.
40. Brauneegg G, Sonnleitner B, Lafferty R. A rapid gas chromatographic method for the determination of poly- $\beta$ -hydroxybutyric acid in microbial biomass. *Appl. Microbiol. Biotechnol.* 1978;6(1):29-37.
41. Harcourt R, Horne I, Sutherland T, Hammock B, Russell R, Oakeshott J. Development of a simple and sensitive fluorimetric method for isolation of coumaphos-hydrolysing bacteria. *Lett. Appl. Microbiol.* 2002;34(4):263-8.
42. Jahns AC, Rehm BH. Tolerance of the *Ralstonia eutropha* class I polyhydroxyalkanoate synthase for translational fusions to its C terminus reveals a new mode of functional display. *Appl. Environ. Microbiol.* 2009;75(17):5461-6.
43. Thrane S, Janitzek CM, Matondo S, Resende M, Gustavsson T, Jongh WA, et al. Bacterial superglue enables easy development of efficient virus-like particle based vaccines. *J. Nanobiotechnol.* 2016;14(1):30.

44. Hooks DO, Blatchford PA, Rehm BHA. Bioengineering of bacterial polymer inclusions catalyzing the synthesis of *N*-acetylneuraminic acid. *Appl. Environ. Microbiol.* 2013;79(9):3116-21.
45. González-Miro M, Rodríguez-Noda L, Fariñas-Medina M, García-Rivera D, Vérez-Bencomo V, Rehm BH. Self-assembled particulate PsaA as vaccine against *Streptococcus pneumoniae* infection. *Heliyon.* 2017;3(4):e00291.
46. Gonzalez-Miro M, Radecker A-M, Rodríguez-Noda LM, Fariñas-Medina M, Zayas-Vignier C, Hernández-Cedeño M, et al. Design and biological assembly of polyester beads displaying pneumococcal antigens as particulate vaccine. *ACS Biomater. Sci. Eng.* 2018;4(9):3413-24.
47. Gasteiger E, Hoogland C, Gattiker A, Wilkins MR, Appel RD, Bairoch A. Protein identification and analysis tools on the ExPASy server. *The Proteomics Protocols Handbook*: Springer; 2005. p. 571-607.
48. Hay ID, Du J, Burr N, Rehm BH. Bioengineering of bacteria to assemble custom-made polyester affinity resins. *Appl. Environ. Microbiol.* 2015;81(1):282-91.
49. Hagen A, Sutter M, Sloan N, Kerfeld CA. Programmed loading and rapid purification of engineered bacterial microcompartment shells. *Nat. Commun.* 2018;9(1):2881.

50. Doran PM. In: Doran PM, editor. *Bioprocess Engineering Principles* (Second Edition). London: Academic Press; 2013. p. vii-viii.
51. Desai N. Challenges in development of nanoparticle-based therapeutics. *AAPS J.* 2012;14(2):282-95.
52. Kim H, Choi H, Bae Y, Kang S. Development of target-tunable P22 VLP-based delivery nanoplatfoms using bacterial superglue. *Biotechnol. Bioeng.* 2019;116(11):2843-51.
53. Williams DM, Kaufman G, Izadi H, Gahm AE, Prophet SM, Vanderlick KT, et al. Facile protein immobilization using engineered surface-active biofilm proteins. *ACS Appl. Nano Mater.* 2018;1(6):2483-8.
54. Gonzalez-Miro M, Chen S, Gonzaga ZJ, Evert B, Wibowo D, Rehm BHA. Polyester as antigen carrier toward particulate vaccines. *Biomacromolecules.* 2019;20(9):3213-32.
55. Goverdhana S, Puntel M, Xiong W, Zirger JM, Barcia C, Curtin JF, et al. Regulatable gene expression systems for gene therapy applications: progress and future challenges. *Mol. Ther.* 2005;12(2):189-211.

56. Gutiérrez-González M, Farías C, Tello S, Pérez-Etcheverry D, Romero A, Zúñiga R, et al. Optimization of culture conditions for the expression of three different insoluble proteins in *Escherichia coli*. *Sci. Rep.* 2019;9(1):16850.
57. Trösemeier J-H, Rudolf S, Loessner H, Hofner B, Reuter A, Schulenburg T, et al. Optimizing the dynamics of protein expression. *Sci. Rep.* 2019;9(1):7511.

## 4.7 Supporting Information

**Table S1.** Bacterial strains used in the current study.

Bacterial strains	Characteristics	References
<i>Escherichia coli</i> XL1-Blue	<i>recA1 endA1 gyrA96 thi-1 hsdR17</i> <i>supE44 RelA1 lac</i> [F' <i>proAB</i> <i>lacI<sup>q</sup>ZΔM15 Tn10 (Tet<sup>r</sup>)</i> ]	Stratagene
<i>Escherichia coli</i> BL21(DE3)	F <sup>-</sup> <i>dcm ompT hsdS</i> (r <sub>B</sub> -m <sub>B</sub> -) gal λ(DE3)	Invitrogen

**Table S2.** Plasmids constructed and used in the current study.

Plasmids	Characteristics	References
pET14b	Ap <sup>r</sup> ; T7 promoter.	Novagen
pMSC69	Cm <sup>r</sup> ; pBBR1MCS derivative containing genes <i>phaA</i> and <i>phaB</i> from <i>C. necator</i> co-linear to <i>lac</i> promoter.	(3)
pET14b_SpyCatcher_PhaC	pET14b encoding <i>SpyCatcher</i> fused to the N-terminus of <i>phaC</i> via a linker sequence.	(33)
pET14b_SpyCatcher_PhaC_	pET14b encoding two <i>SpyCatcher</i>	(33)*

linker_SpyCatcher	flanking at both N- and C- termini of <i>phaC</i> .	
pCOLADuet-1	Km <sup>r</sup> ; T7 promoter; ColA replicon.	Novagen
pBluescript_II_SK(+)_SdyCatcher-SnoopCatcher	Ap <sup>r</sup> .	Biomatik
pET14b_SpyTag-GFP-His6	pET14b derivative encoding <i>SpyTag</i> at N-terminus of <i>gfp</i> and hexahistidine tag at 3' end of <i>gfp</i> .	(33)
pET14b_SpyTag-OpdA-His6.	pET14b derivative encoding <i>SpyTag</i> at N-terminus of <i>opda</i> and hexahistidine tag at 3' end of <i>opda</i> .	(33)
pET14b_SpyTag-BLA-His6.	pET14b encoding <i>SpyTag</i> at N-terminus of <i>bla</i> and hexahistidine tag at C-terminus of <i>bla</i> .	(33)
pCOLASolo-1_SpyTag-GFP	pCOLADuet-1 derivative encoding <i>SpyTag</i> fused at the N-terminus of <i>gfp</i> for single protein production.	This study
pCOLASolo-1_SpyTag-OpdA	pCOLADuet-1 derivative <i>SpyTag</i>	This study

	fused at the N-terminus of <i>opda</i> for single protein production.	
pCOLASolo-1_SpyTag-BLA	pCOLADuet-1 derivative <i>SpyTag</i> fused at the N-terminus of <i>bla</i> for single protein production.	This study
pET14b_C2	pET14b derivative consisting <i>C2 gene</i> .	Unpublished work
pET14b_SdyCatcher-PhaC-SnoopCatcher	pET14b derivative consisting <i>SdyCatcher</i> fused to the N-terminus of <i>phaC</i> and <i>SnoopCatcher</i> to the C-terminus of <i>phaC</i> via a linker sequence.	This study
pET14b_SnoopCatcher-PhaC-SdyCatcher	pET14b derivative consisting <i>SnoopCatcher</i> fused to the N-terminus of <i>phaC</i> and <i>SdyCatcher</i> to the C-terminus of <i>phaC</i> via a linker sequence.	This study
pET14b_SpyCatcher-PhaC-SnoopCatcher	pET14b derivative consisting <i>SpyCatcher</i> fused to the N-terminus of <i>phaC</i> and <i>SnoopCatcher</i> to the C-terminus of	This study

	<i>phaC</i> via a linker sequence.	
pET14b_SnoopCatcher-PhaC-SpyCatcher	pET14b derivative consisting <i>SnoopCatcher</i> fused to the N-terminus of <i>phaC</i> and <i>SpyCatcher</i> to the C-terminus of <i>phaC</i> via a linker sequence.	This study
pET14b_SnoopTag-L-GFP-His6	pET14b_PhaC_linker_GFP derivative consisting <i>SnoopTag</i> at N-terminus of <i>gfp</i> and hexahistidine tag at C-terminus of <i>gfp</i> .	This study
pET14b_SnoopTag-L-BLA-His6.	pET14b_BLAphaC derivative consisting <i>SnoopTag</i> at N-terminus of <i>bla</i> and hexahistidine tag at C-terminus of <i>bla</i> .	This study
pET14b_SdyTag-L-GFP-His6	pET14b_PhaC_linker_GFP derivative consisting <i>SdyTag</i> at N-terminus of <i>gfp</i> and hexahistidine tag at C-terminus of <i>gfp</i> .	This study
pET14b_SdyTag-L-BLA-His6.	pET14b_ BLAphaC derivative consisting <i>SdyTag</i> at N-terminus of	This study

	<i>bla</i> and hexahistidine tag at C-terminus of <i>bla</i> .	
--	--	--

\*constructed previously (33) as an intermediate plasmid for construction of pET14b\_Spy-Catcher\_PhaC.

**Table S3.** Primers constructed and used in the current study.

Primers	Restriction sites	Sequence	References
NcoI-XhoI-SpyTag	NcoI & XhoI	5'ATATTTCCATGGGACTCGAGG CTCATATTGTGATGGTGGATGCG	This study
AvrII-STOP-OpdA	AvrII	5'ATATTTCTAGGTTACGACGCC CGCACGG	This study
AvrII-STOP-BLA	AvrII	5'ATATTTCTAGGTTAGCGCTGG ACGTAGATGGAAACAG	This study
AvrII-STOP-GFP	AvrII	5'ATATTTCTAGGTTATTTGTAT AGTTCATCCATGCCATGTGTAAT CCCAG	This study
SpeI-(START)-SnoopCatcher	SpeI	5'ATATATACTAGTATGCATATG AAACCGCTGCGTGCC	This study

AvrII- SnoopCatcher	AvrII	5'ATATATCCTAGGTTTCGGCGG AATCGGTTTCATTGG	This study
XhoI- SnoopCatcher	XhoI	5'ATATATCTCGAGCATATGAAA CCGCTGCGTGGC	This study
BamHI- (STOP)- SnoopCatcher	BamHI	5'ATATATGGATCCTCATTTTCGGC GGAATCGGTTTCATTGG	This study
SpeI- (START)- SdyCatcher	SpeI	5'ATATATACTAGTATGGGTAGT AGTGGTCTGAGC	This study
AvrII- SdyCatcher	AvrII	5'ATATATCCTAGGGCTATCCAC CCAAATCTGGC	This study
XhoI- SdyCatcher	XhoI	5'ATATATCTCGAGGGTAGTAGT GGTCTGAGC	This study
BamHI- (STOP)- SdyCatcher	BamHI	5'ATATATGGATCCTCAGCTATCC ACCCAAATCTGGC	This study

SpeI-START-SnoopTag-L-GFP	SpeI	5'TATACTAGTATGGGGAAACTC GGCGATATTGAATTTATTAAAGT GAACAAAGGCAGTGGTTCGGGA TCAGGAAGTAAAGGAGAAGAAC TTTTCACTGGAG	This study
SpyTag-GFP-His6_RVR	BamHI	5'ATATTTGGATCCTCAGTGATG ATGGTGATGATGTTTGTATAGTT CATCCATGCCATGTGT	(33)
SpeI-START-SnoopTag-L-BLA	SpeI	5'TATACTAGTATGGGGAAACTG GGCGATATTGAATTTATTAAAGT GAACAAAGGCAGTGGTTCGGGA TCAGGAGCTAACCTGAACGGTA CCCTGATG	This study
SpyTag-BLA-His6_RVR	BamHI	5'ATATTTGGATCCTCAGTGATG ATGGTGATGATGGCGCTGGACG TAGATGGAAACAGA	(33)
SpeI-START-SdyTag-L-GFP	SpeI	5'AATACTAGTATGGATCCGATT GTGATGATTGATAACGATAAAC CGATTACCGGCAGTGGTTCGGG	This study

		ATCCGGAAGTAAAGGAGAAGAA CTTTTCACTGGAG	
XhoI-STOP- His6-GFP	XhoI	5'ATATTTCTCGAGTCAGTGATG ATGGTGATGATGTTTGTATAGTT CATCCATGCCATGTGT	This study
SpeI-START- SdyTag-L- BLA	SpeI	5'TATACTAGTATGGATCCGATT GTGATGATTGATAACGATAAAC CGATTACCGGCAGTGGTTCGGG ATCTGGAGCTAACCTGAACGGT ACCCTGATG	This study
XhoI-STOP- His6-BLA	XhoI	5'ATATTTCTCGAGTCAGTGATG ATGGTGATGATGGCGCTGGACG TAGATGGAAACAGA	This study

**Table S4.** Amino acid sequence of fusion proteins

Fusion protein	Amino acid sequence
Wild-type <i>Cupriavidus</i> <i>necator</i> PhaC (WT)	ATGKGAAASTQEGKSQPFKVTPGPFDPATWLE WSRQWQGTEGNHAAASGIPGLDALAGVKIA PAQLGDIQQRYSKDFSAWQAMAEGKAEATG PLHRRFAGDAWRTNLPYRFAAFYLLNARA LTELADAVEADAKTRQRIRFAISQWVDAMSPA NFLATNPEAQRLLES GGESLRAGVRNM MEDL TRGKISQTDESAFEVGRNVAVTEGAVVFENEY FQLLQYKPLTDKVHARPLLMVPPCINKYYILDL QPESLVRHVVEQGHTVFLVSWRNP DASMAGS TWDDYIEHAAIRAIEVARDISGQDKINVLGFCV GGTIVSTALAVLAARGEHPAASVTLLTLLDFA DTGILDVVFDEGHVQLREATLGGGAGAPCALL RGLELANTFSFLRPNDLVWNYVVDNYLKGNT VPFDLLFWNGDATNLP GPWYC WYLRHTYLQN ELKVPGKLTVC GVPVDLASIDVPTYIYGSREDH IVPWTAAAYASTALLANKLRFVLGASGHIAGVIN PPAKNKRSHWTNDALPESPQQWLAGAIEHHGS WWPDWTAWLAGQAGAKRAAPANYGNARYR AIEPAPGRYVKAKAHMVLAV AIDKR*

<p><b>SpyCatcher-PhaC-</b></p> <p><b>SpyCatcher (SPS)</b></p>	<p><b>MGAMVDTLSGLSSEQGQSGDMTIEEDSATHI</b></p> <p><b>KFSKRDEDGKELAGATMELRDSSGKTISTWI</b></p> <p><b>SDGQVKDFYLYPGKYTFVETAAPDGYEVAT</b></p> <p><b>AITFTVNEQQQVTVNGKATKGDAHIPRHMA</b></p> <p>TGKGAAASTQEGKSQPFKVTPGPFDPATWLEW</p> <p>SRQWQGTEGNHAAASGIPGLDALAGVKIAPA</p> <p>QLGDIQQRYMKDFSALWQAMAEGKAEATGPL</p> <p>HDRRFAGDAWRTNLPYRFAAFYLLNARALT</p> <p>ELADAVEADAKTRQRIRFAISQWVDAMSPANF</p> <p>LATNPEAQRLLES GGESLRAGVRNM MEDLTR</p> <p>GKISQTDESAFEVGRNVA VTEGAVVFENEYFQ</p> <p>LLQYKPLTDKVHARPLLMVPPCINKYYILDLP</p> <p>ESSLVRHVVEQGHTVFLVSWRNP DASMAGST</p> <p>WDDYIEHAAIRAIEVAR DISGQDKINVLGFCVG</p> <p>GTIVSTALAVLAARGEHPAASVTLLTTLLDFAD</p> <p>TGILDVVFVDEGHVQLREATLGGGAGAPCALLR</p> <p>GLELANTFSFLRPNDLVWNYVVDNYLKGNTP</p> <p>VPFDLLFWNGDATNLP GPWYCWYLRHTYLQN</p> <p>ELKVP GKLTVC GVPVDLASIDVPTYIYGSREDH</p> <p>IVPWTAAYASTALLANKLR FVLGASGHIAGVIN</p> <p>PPAKNKRSHWTNDALPESPQQWLAGAIEHHGS</p> <p>WWPDWTAWLAGQAGAKRAAPANYGNARYR</p> <p>AIEPAPGRYVKAKAHMVLAV AIDKRGGGGGL</p>
---	--

	<p>EGAMVDTLSGLSSEQGQSGDMTIEEDSATHI</p> <p>KFSKRDEDGKELAGATMELRDSSGKTISTWI</p> <p>SDGQVKDFYLYPGKYTFVETAAPDGYEVAT</p> <p>AITFTVNEQGQVTVNGKATKGDAHI*</p>
SpyCatcher-PhaC (SP)	<p>MGAMVDTLSGLSSEQGQSGDMTIEEDSATHI</p> <p>KFSKRDEDGKELAGATMELRDSSGKTISTWI</p> <p>SDGQVKDFYLYPGKYTFVETAAPDGYEVAT</p> <p>AITFTVNEQGQVTVNGKATKGDAHIPRHMA</p> <p>TGKGAAASTQEGKSQPFKVTPGPFDPATWLEW</p> <p>SRQWQGTEGNHAAASGIPGLDALAGVKIAPA</p> <p>QLGDIQQRYSKDFSAWQAMAEGKAEATGPL</p> <p>HDRRFAGDAWRTNLPYRFAAFYLLNARALT</p> <p>ELADAVEADAKTRQRIRFAISQWVDAMSPANF</p> <p>LATNPEAQRLLESSESRLRAGVRNMEDLTR</p> <p>GKISQTDESAFEVGRNVAVTEGAVVFENEYFQ</p> <p>LLQYKPLTDKVHARPLLMVPPCINKYYILDLP</p> <p>ESSLVRHVVEQGHTVFLVSWRNPDASMAGST</p> <p>WDDYIEHAAIRAIEVARDISGQDKINVLGFCVG</p> <p>GTIVSTALAVLAARGEHPAASVTLLTTLLDFAD</p> <p>TGILDVVFVDEGHVQLREATLGGGAGAPCALLR</p> <p>GLELANTFSFLRPNDLVWNYVVDNYLKGNTF</p> <p>VPFDLLFWNGDATNLPWPWCWYLRHTYLQN</p>

	<p>ELKVPGKLTVCVGPVDLASIDVPTYIYGSREDH</p> <p>IVPWTAAYASTALLANKLRFVLGASGHIAGVIN</p> <p>PPAKNKRSHWTNDALPESPQQWLAGAIEHHGS</p> <p>WWPDWTAWLAGQAGAKRAAPANYGNARYR</p> <p>AIEPAPGRYVKAKAHMVRIRLLTKPERKLSWL</p> <p>LPPLSNN*</p>
<p><b>SdyCatcher</b>-PhaC-</p> <p><b>SnoopCatcher</b></p> <p>(<b>DPN</b>)</p>	<p><b>MGSSGLSGETGQSGNTTIEEDSTTHVKFSKR</b></p> <p><b>DANGKELAGAMIELRNLSGQTIQSWISDGTV</b></p> <p><b>KVFYLMPGTYQFVETAAPEGYELAAPITFTI</b></p> <p><b>DEKGQIWVDS</b>PRHMATGKGAAASTQEGKSQP</p> <p>FKVTPGPFDPATWLEWSRQWQGTEGNHAAA</p> <p>SGIPGLDALAGVKIAPAQLGDIQQRYSKDFSAL</p> <p>WQAMAEGKAEATGPLHDDRFAAGDAWRTNLP</p> <p>YRFAAAFYLLNARALTELADEADAKTRQRI</p> <p>RFAISQWVDAMSPANFLATNPEAQRLLESNGGE</p> <p>SLRAGVRNMEDLTRGKISQTDESAFEVGRNV</p> <p>AVTEGAVVFENEYFQLLQYKPLTDKVHARPLL</p> <p>MVPPCINKYYILDLQPESSLVRHVVEQGHTVFL</p> <p>VSWRNPDASMAGSTWDDYIEHAAIRAIEVARD</p> <p>ISGQDKINVLGFCVGGTIVSTALAVLAARGEHP</p> <p>AASVTLLTTLLDFADTGILDVVFDEGHVQLREA</p> <p>TLGGGAGAPCALLRGLELANTFSFLRPNDLVW</p>

	<p>             NYVVDNYLKGNTVPFDLLFWNGDATNLPGP              WYCWYLRHTYLQNELKVP GKLTVC GVPVDLA              SIDVPTYIYGSREDHIVPWTAAAYASTALLANKL              RFVLGASGHIAGVINPPAKNKRSHWTNDALPE              SPQQWLAGAIEHHGSWWPDWTAWLAGQAGA              KRAAPANYGNARYRAIEPAPGRYVKAKAHMV              LAVAIDKRGGGGGLE<b>HMKPLRGAVFSLQKQ</b>  <b>HPDYPDIYG AIDQNGTYQNVRTGEDGKLTF</b>  <b>KNLS DGKYRLFENSEPAGYKPVQNKPIVAFQ</b>  <b>IVNGEVRDVT SIVPQDIPATYEFTNGKHYITN</b>  <b>EIPPK*</b> </p>
<p> <b>SnoopCatcher-PhaC-</b>  <b>SdyCatcher</b>  <b>(NPD)</b> </p>	<p> <b>MHMKPLRGAVFSLQKQHPDYPDIYG AIDQN</b>  <b>GT YQNVRTGEDGKLTFKNLS DGKYRLFENS</b>  <b>EPAGYKPVQNKPIVAFQIVNGEVRDVT SIVP</b>  <b>QDIPATYEFTNGKHYITNEIPPKPRH MATGK</b>              GAAASTQEGKSQPFKVTPGPFDPATWLEWSRQ              WQGTEGN GHAAASGIPGLDALAGVKIAPAQLG              DIQQRYMKDFSALWQAMAEGKAEATGPLHDR              RFAGDAWRTNLPYRFAAAFYLLNARALTELA              DAVEADAKTRQRIRFAISQWVDAMSPANFLAT              NPEAQRL LIESGGESLRAGVRNM MEDLTRGKIS              QTDESAFEVGRNVAVTEGAVVFENEYFQLLQY </p>

	KPLTDKVHARPLLMVPPCINKYYILDLQPESSL VRHVVEQGHTVFLVSWRNPDASMAGSTWDD YIEHAAIRAIEVARDISGQDKINVLGFCVGGTIV STALAVLAARGEHPAASVTLLTLLDFADTGIL DVFVDEGHVQLREATLGAGAPCALLRGLEL ANTFSFLRPNDLVWNYVVDNYLKGNTPVPFDL LFWNGDATNLPGPWYCWYLRHTYLQNELKVP GKLTVCVGPVDLASIDVPTYIYGSREDHIVPWT AAYASTALLANKLRFVLGASGHIAGVINPPAK NKRSHWTNDALPESPQQWLAGAIEHHGSWWP DWTAWLAGQAGAKRAAPANYGNARYRAIEP APGRYVKAKAHMVLAVAIKRGGGGGGLE <b>GSS</b> <b>GLSGETGQSGNTTIEEDSTTHVKFSKRDANG</b> <b>KELAGAMIELRNLSGQTIQSWISDGTVKVfy</b> <b>LMPGTYQFVETAAPEGYELAAPITFTIDEKG</b> <b>QIWVDS*</b>
<b>SpyCatcher-PhaC-</b> <b>SnoopCatcher (PPN)</b>	MGAMVDTL <b>SGLSSEQGQSGDMTIEEDSATHI</b> <b>KFSKRDEDGKELAGATMELRDSSGKTISTWI</b> <b>SDGQVKDFYLYPGKYTFVETAAPDGYEVAT</b> <b>AITFTVNEQQQVTVNGKATKGD</b> <b>AHIPRHMA</b> TGKGAAASTQEGKSQPFKVTPGFPDPATWLEW SRQWQGTEGNGHAAASGIPGLDALAGVKIAPA

	<p>             QLGDIQQRYMKDFSALWQAMAEGKAEATGPL              HDRRFAGDAWRTNLPYRFAAAFYLLNARALT              ELADAVEADAKTRQRIRFAISQWVDAMSPANF              LATNPEAQRLLES GGESLRAGVRNM MEDLTR              GKISQTDESAFEVGRNVAVTEGAVVFENEYFQ              LLQYKPLTDKVHARPLLMVPPCINKYYILDLP              ESSLVRHVVEQGHTVFLVSWRNP DASMAGST              WDDYIEHAAIRAIEVARDISGQDKINVLGFCVG              GTIVSTALAVLAARGEHPAASVTLLTTLLDFAD              TGILDVVFVDEGHVQLREATLGGGAGAPCALLR              GLELANTFSFLRPNDLVWNYVVDNYLKGNT              VPFDLLFWNGDATNLP GPWYC WYLRHTYLQN              ELKVP GKLTVC GVPVDLASIDVPTIYIGSREDH              IVPWTAAYASTALLANKLR FVLGASGHIAGVIN              PPAKNKRSHWTNDALPESPQQWLAGAIEHHGS              WWPDWTAWLAGQAGAKRAAPANYGNARYR              AIEPAPGRYVKAKAHMVLAV AIDKRGGGGGL              EHMKPLRGAVFSLQKQHPDYPDIYG AIDQN              GTYQNVRTGEDGKLTFKNLSDGKYRLFENS              EPAGYKPVQNKPIVAFQIVNGEVRDVT SIVP              QDIPATYEFTNGKH YITNEPIPPK* </p>
--	---

<b>SnoopCatcher-PhaC-</b> <b>SpyCatcher</b> <b>(NPP)</b>	<b>M</b> <b>H</b> <b>M</b> <b>K</b> <b>P</b> <b>L</b> <b>R</b> <b>G</b> <b>A</b> <b>V</b> <b>F</b> <b>S</b> <b>L</b> <b>Q</b> <b>K</b> <b>Q</b> <b>H</b> <b>P</b> <b>D</b> <b>Y</b> <b>P</b> <b>D</b> <b>I</b> <b>Y</b> <b>G</b> <b>A</b> <b>I</b> <b>D</b> <b>Q</b> <b>N</b> <b>G</b> <b>T</b> <b>Y</b> <b>Q</b> <b>N</b> <b>V</b> <b>R</b> <b>T</b> <b>G</b> <b>E</b> <b>D</b> <b>G</b> <b>K</b> <b>L</b> <b>T</b> <b>F</b> <b>K</b> <b>N</b> <b>L</b> <b>S</b> <b>D</b> <b>G</b> <b>K</b> <b>Y</b> <b>R</b> <b>L</b> <b>F</b> <b>E</b> <b>N</b> <b>S</b> <b>E</b> <b>P</b> <b>A</b> <b>G</b> <b>Y</b> <b>K</b> <b>P</b> <b>V</b> <b>Q</b> <b>N</b> <b>K</b> <b>P</b> <b>I</b> <b>V</b> <b>A</b> <b>F</b> <b>Q</b> <b>I</b> <b>V</b> <b>N</b> <b>G</b> <b>E</b> <b>V</b> <b>R</b> <b>D</b> <b>V</b> <b>T</b> <b>S</b> <b>I</b> <b>V</b> <b>P</b> <b>Q</b> <b>D</b> <b>I</b> <b>P</b> <b>A</b> <b>T</b> <b>Y</b> <b>E</b> <b>F</b> <b>T</b> <b>N</b> <b>G</b> <b>K</b> <b>H</b> <b>Y</b> <b>I</b> <b>T</b> <b>N</b> <b>E</b> <b>P</b> <b>I</b> <b>P</b> <b>P</b> <b>K</b> <b>P</b> <b>R</b> <b>H</b> <b>M</b> <b>A</b> <b>T</b> <b>G</b> <b>K</b> GAAASTQEGKSQPFKVTPGPFDPATWLEWSRQ WQGTEGNHAAASGIPGLDALAGVKIAPAQLG DIQQRYMKDFSALWQAMAEGKAEATGPLHDR RFAGDAWRTNLPYRFAAAFYLLNARALTELA DAVEADAKTRQRIRFAISQWVDAMSPANFLAT NPEAQRLLIESGGESLRAGVRNMMEDLTRGKIS QTDESAFEVGRNVAVTEGAVVFENEYFQLLQY KPLTDKVHARPLLMVPPCINKYYILDLQPSSL VRHVVEQGHTVFLVSWRNPDASMAGSTWDD YIEHAAIRAIEVARDISGQDKINVLGFCVGGTIV STALAVLAARGEHPAASVTLLTTLDFADTGIL DVFVDEGHVQLREATLGAGAPCALLRGLEL ANTFSFLRPNDLVWNYVVDNYLKGNTVPFIDL LFWNGDATNLPGPWYCWYLRHTYLQNELKVP GKLTVCVGPVDLASIDVPTYIYGSREDHIVPWT AAYASTALLANKLRFLVGASGHIAGVINPPAK NKRSHWTNDALPESPQQWLAGAIEHHGSWWP DWTAWLAGQAGAKRAAPANYGNARYRAIEP APGRYVKAKAHMVLAVAIIDKRGGGGGLE <b>G</b> <b>A</b>
--	---

	<p><b>MVDTLSGLSSEQGQSGDMTIEEDSATHIKFS</b></p> <p><b>KRDEDGKELAGATMELRDSSGKTISTWISDG</b></p> <p><b>QVKDFYLYPGKYTFVETAAPDGYEVATAITF</b></p> <p><b>TVNEQGQVTVNGKATKGDAHI*</b></p>
<p><b>SpyTagged</b>     <i>Aequorea</i></p> <p><i>victoria</i> green fluorescent protein (<b>Sp</b>GFP)</p>	<p><b>MAHIVMVDAYKPTK</b>GGGSKGEELFTGVVPIL</p> <p>VELDGDVNGHKFSVSGEGEGDATYGKLTLKFI</p> <p>CTTGKLPVPWPTLVTTLTYGVCFSRYPDHMK</p> <p>RHDFFKSAMPEGYVQERTIFFKDDGNYKTRAE</p> <p>VKFEGDTLVNRIELKGIDFKEDGNILGHKLEYN</p> <p>YNSHNVYIMADKQKNGIKVNFKIRHNIEDGSV</p> <p>QLADHYQQNTPIGDGPVLLPDNHYSTQSALS</p> <p>KDPNEKRDHMLLEFVTAAGITHGMDELYK*</p>
<p><b>SpyTagged</b>     <i>Aequorea</i></p> <p><i>victoria</i> green fluorescent protein bearing His<sub>6</sub> tag (<b>Sp</b>GFP-H6)</p>	<p><b>MAHIVMVDAYKPTK</b>GGGSKGEELFTGVVPIL</p> <p>VELDGDVNGHKFSVSGEGEGDATYGKLTLKFI</p> <p>CTTGKLPVPWPTLVTTLTYGVCFSRYPDHMK</p> <p>RHDFFKSAMPEGYVQERTIFFKDDGNYKTRAE</p> <p>VKFEGDTLVNRIELKGIDFKEDGNILGHKLEYN</p> <p>YNSHNVYIMADKQKNGIKVNFKIRHNIEDGSV</p> <p>QLADHYQQNTPIGDGPVLLPDNHYSTQSALS</p> <p>KDPNEKRDHMLLEFVTAAGITHGMDELYKH</p> <p>HHHHH*</p>

<b>SpyTagged</b> <i>Agrobacterium</i> <i>radiobacter</i> Organophosphohydrolase (SpOpdA)	MGLEAHIVMVDAYKPTKGGGSMARPIGTGDLI NTVRGPIPVSEAGFTLTHEHICGSSAGFLRAWPE FFGSRKALAEKAVRGLRHARAAGVQTIVDVST FDIGRDVRLLAEVSRADVHIVAATGLWFDPPPL SMRMRSVEELTQFFLREIQHGIEDTGIRAGIIKV ATTGKATPFQELVLKAAARASLATGVPVTTHTS ASQRDGEQQAAIFESEGLSPSRVCIGHSDDTDD LSYLTGLAARGYLVGLDRMPYSAIGLEGNASA LALFGTRSWQTRALLIKALIDRGYKDRILVSHD WLFGFSSYVTNIMDVMDRINPDGMAFVPLRVIP FLREKGVPPETLAGVTVANPARFLSPTVRAS*
<b>SpyTagged</b> <i>Agrobacterium</i> <i>radiobacter</i> Organophosphohydrolase bearing His <sub>6</sub> tag (SpOpdA-H6)	MGLEAHIVMVDAYKPTKGGGSMARPIGTGDLI NTVRGPIPVSEAGFTLTHEHICGSSAGFLRAWPE FFGSRKALAEKAVRGLRHARAAGVQTIVDVST FDIGRDVRLLAEVSRADVHIVAATGLWFDPPPL SMRMRSVEELTQFFLREIQHGIEDTGIRAGIIKV ATTGKATPFQELVLKAAARASLATGVPVTTHTS ASQRDGEQQAAIFESEGLSPSRVCIGHSDDTDD LSYLTGLAARGYLVGLDRMPYSAIGLEGNASA LALFGTRSWQTRALLIKALIDRGYKDRILVSHD

		<p>WLFGFSSYVTNIMDVMDRINPDGMAFVPLRVIP</p> <p>FLREKGVPPETLAGVTVANPARFLSPTVRASHH</p> <p>HHHH*</p>
<p><b>SpyTagged</b></p> <p><i>licheniformis</i></p> <p>(SpBLA)</p>	<p><i>Bacillus</i></p> <p><math>\alpha</math>-amylase</p>	<p>MAHIVMVDAYKPTKGGGANLNGTLMQYFEW</p> <p>YMPNDGQHWKRLQNDSAYLAEHGITAVWIPP</p> <p>AYKGTSQADVGYGAYDLYDLGEFHQKGTVRT</p> <p>KYGTKGELQSAIKSLHSRDINVYGDVVINHKG</p> <p>GADATEDVTAVEVDPADRNRVISGEVRIKAWT</p> <p>HFHFPGRGSTYSDFKWHWYHFDGTDWDESRK</p> <p>LNRIYKFQGKAWDWEVSNEFGNYDYLMYADI</p> <p>DYDHPDVVAEIKRWGTWYANELQLDGFRLDA</p> <p>VKHIKFSFLRDWVNVHREKTGKEMFTVAEYW</p> <p>SYDLGALENYLNKTNFNHVSFVDVPLHYQFHAA</p> <p>STQGGGYDMRKLNSTVVSKHPLKAVTFVDN</p> <p>HDTQPGQSLESTVQTFWKPLAYAFILTRESGYP</p> <p>QVFYGD MYGT KGDSQREIPALKHKIEPILKARK</p> <p>QYAYGAQH DYFDHHDIVGWTREGDSSVANSG</p> <p>LAALITDGP GGAKRMYVGRQNAGETWHDITG</p> <p>NRSEPVVINSEGWGEFHVNGGSVSIYVQR*</p>
<p><b>SpyTagged</b></p> <p><i>licheniformis</i></p>	<p><i>Bacillus</i></p> <p><math>\alpha</math>-amylase</p>	<p>MAHIVMVDAYKPTKGGGANLNGTLMQYFEW</p> <p>YMPNDGQHWKRLQNDSAYLAEHGITAVWIPP</p>

bearing His <sub>6</sub> tag ( <b>Sp</b> BLA-H6)	AYKGTSQADVGYGAYDLYDLGEFHQKGTVRT KYGTKGELQSAIKSLHSRDINVGDVVINHKG GADATEDVTAVEVDPADRNRVISGEVRIKAWT HFHFPGRGSTYSDFKWHWYHFDGTDWDESRK LNRIYKFQGKAWDWEVSNEFGNYDYLMYADI DYDHPDVVAEIKRWGTWYANELQLDGFRLDA VKHIKFSFLRDWVNHVREKTGKEMFTVAEYW SYDLGALENYLNKTNFNHVSFVPLHYQFHAA STQGGGYDMRKLLNSTVVSKHPLKAVTFVDN HDTQPGQSLESTVQTFWKPLAYAFILTRESGYP QVFYGD MYG TKGDSQREIPALKHKIEPILKARK QYAYGAQHDFDHHDIVGWTREGDSSVANSG LAALITDGP GGAKRMYVGRQNAGETWHDITG NRSEPVVINSEGWGEFHVNGGSVSIYVQRHHH HHH*
<b>SnoopTagged</b> <i>Aequorea victoria</i> green fluorescent protein bearing His <sub>6</sub> tag ( <b>Sn</b> GFP-H6)	<b>M</b> <b>G</b> <b>K</b> <b>L</b> <b>G</b> <b>D</b> <b>I</b> <b>E</b> <b>F</b> <b>I</b> <b>K</b> <b>V</b> <b>N</b> <b>K</b> GSGSGSGSGSGEELFTGVV PILVELDGDVNGHKFSVSGEGEGDATYGKLTL KFICTTGKLPVPWPTLVTTLTYGVQCFSRYPDH MKRHDFFKSAMPEGYVQERTIFFKDDGNYKTR AEVKFEGDTLVNRIELKGIDFKEDGNILGHKLE YNYNSHNVYIMADKQKNGIKVNFKIRHNIEDG SVQLADHYQQNTPIGDGPVLLPDNHYLSTQSA

	LSKDPNEKRDHMLLEFVTAAGITHGMDELYK HHHHHH*
<b>SnoopTagged</b> <i>Bacillus</i> <i>licheniformis</i> $\alpha$ -amylase bearing His <sub>6</sub> tag ( <b>Sn</b> BLA- H6)	<b>MGKLGDI</b> <b>EFIKVNK</b> GSGSGSGANLNGTLMQY FEWYMPNDGQHWKRLQNDSAYLAEHGITAV WIPPAYKGTSQADVGYGAYDLYDLGEFHQKG TVRTKYGTKGELQSAIKSLHSRDINVYGDVVIN HKGGADATEDVTAVEVDPADRNRVISGEVRIK AWTHFHFPGRGSTYSDFKWHWYHFDGTDWD ESRKLNRIFYKFQGKAWDWEVSNEFGNYDYLM YADIDYDHPDVVAEIKRWGTWYANELQLDGF RLDAVKHIKFSFLRDWVNHVREKTGKEMFTV AEYWSYDLGALENYLNKTNFNHVSFVPLHY QFHAASTQGGGYDMRKLLNSTVVSKHPLKAV TFVDNHDTQPGQSLESTVQTFWKPLAYAFILTR ESGYPQVFYGD MYGTKGDSQREIPALKHKIEPI LKARKQYAYGAQHDFDHHDIVGWTREGDSS VANGLAALITDGP GAKRMYVGRQNAGETW HDITGNRSEPVVINSEGWGEFHVNGGSVSIYVQ RHHHHHH*
<b>SdyTagged</b> <i>Aequorea</i> <i>victoria</i> green fluorescent	<b>MDPIVMIDNDKPITGSGSGSGSKGEELFTGVV</b> PILVELDGDVNGHKFSVSGEGEGDATYGKLT

protein bearing His <sub>6</sub> tag (SdGFP-H6)	KFICTTGKLPVPWPTLVTTLTYGVCFSRYPDH MKRHDFFKSAMPEGYVQERTIFFKDDGNYKTR AEVKFEGDTLVNRIELKGIDFKEDGNILGHKLE YNYNSHNVYIMADKQKNGIKVNFKIRHNIEDG SVQLADHYQQNTPIGDGPVLLPDNHYLSTQSA LSKDPNEKRDHMLLEFVTAAGITHGMDELYK HHHHHH*
SdyTagged <i>Bacillus</i> <i>licheniformis</i> $\alpha$ -amylase bearing His <sub>6</sub> tag (SdBLA- H6)	MDPIVMIDNDKPITGSGSGSGANLNGTLMQYF EWYMPNDGQHWKRLQNDSAYLAEHGITAVWI PPAYKGT SQADVG YGAYDLYDLGEFHQKGTV RTKYGTKGELQSAIKSLHSRDINVYGDVVINHK GGADATEDVTAVEVDPADRNRVISGEVRIKAW THFHFPGRGSTYSDFKWHWYHFDGTDWDESR KLNRIYKFQGKA WDWEVSNEFGNYDYLMYA DIDYDHPDVVAEIKRWGTWYANELQLDGFRL DAVKHIKFSFLRDWVNHVREKTGKEMFTVAE YWSYDLGALENYLNKTNFNHSVFDVPLHYQF HAASTQGGGYDMRKLLNSTVVSKHPLKAVTF VDNHDTQPGQSLESTVQTWFKPLAYAFILTRES GYPQVFYGD MYG TKGDSQREIPALKHKIEPILK ARKQYAYGAQH DYFDHHDIVGWTREGDSSVA NSGLAALITDGP GGAKRMYVGRQNAGETWHD

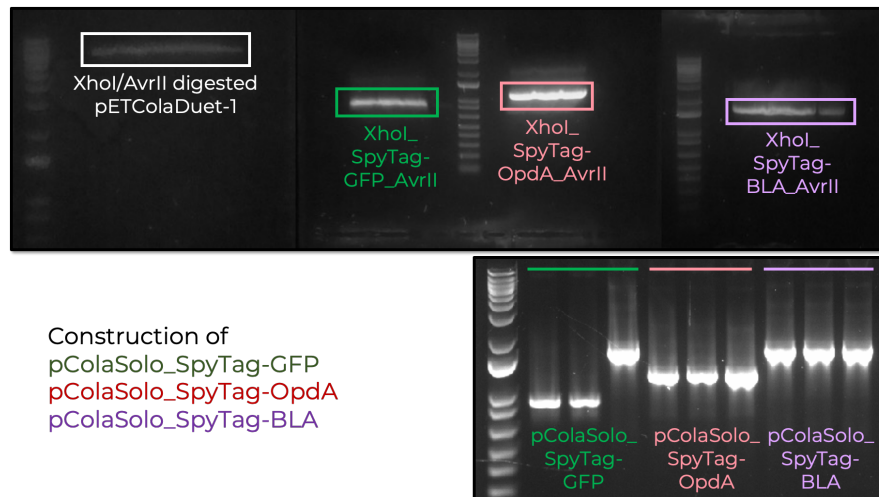
	ITG NRSEP VVINSEGWGEFHVNGGSVSIYVQRH HHHHH*
--	---

## Appendix S1. Experimental section

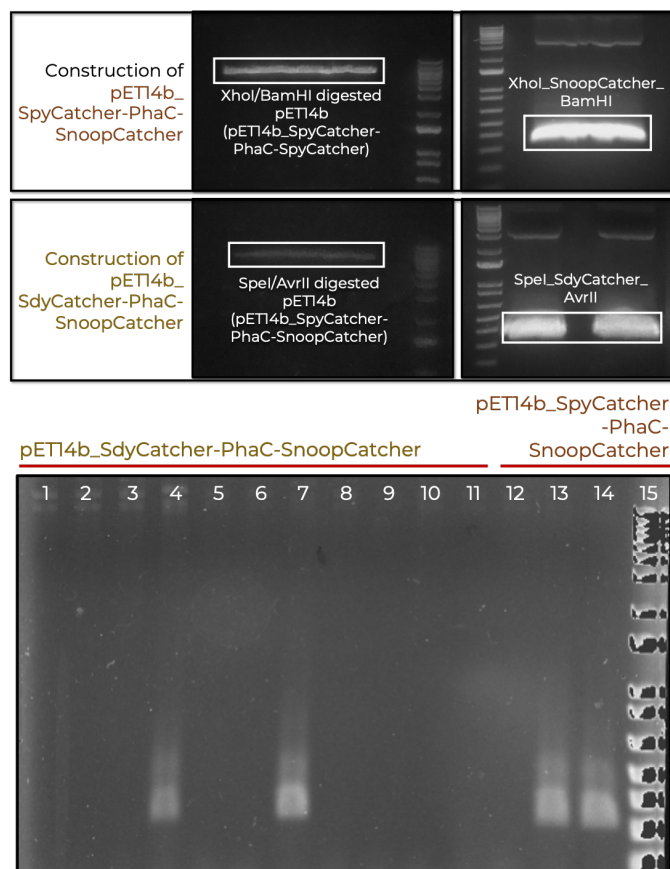
### Plasmid construction strategies

To construct pCOLASolo-1\_SpyTag-OpdA, the gene encoding SpyTag-OpdA from pET14b\_SpyTag-OpdA-His6 was PCR-amplified using primers NcoI-XhoI-SpyTag and AvrII-STOP-OpdA, which also introduce NcoI and XhoI restriction sites before the start codon, and AvrII after the stop codon. The resulting PCR product and vector pCOLADuet-1 were digested with NcoI and AvrII and ligated, which resulted in plasmid pCOLASolo-1\_SpyTag-OpdA. Likewise, to construct His6-tagless SpyTagged BLA, the SpyTag-BLA cDNA from plasmid pET14b\_SpyTag-BLA-His6 was amplified with primers NcoI-XhoI-SpyTag and AvrII-STOP-BLA and the resulting PCR product cloned into the NcoI/AvrII sites of vector pCOLADuet-1. The resulting plasmid was named pCOLASolo-1\_SpyTag-BLA. Plasmid pCOLASolo-1\_SpyTag-GFP was generated by amplifying the SpyTag-GFP cDNA from plasmid pET14b\_SpyTag-GFP-His6 using primers NcoI-XhoI-SpyTag and AvrII-STOP-GFP. The resulting PCR product and pCOLASolo-1\_SpyTag-OpdA were digested with XhoI and AvrII and ligated. The resulting plasmid was designated as

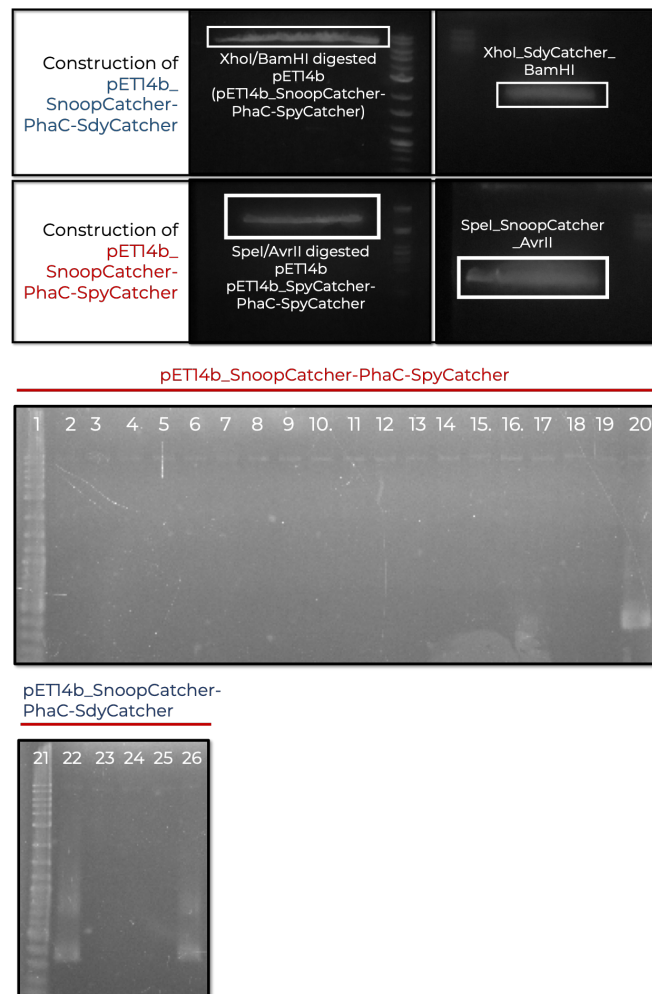
pCOLASolo-1\_SpyTag-GFP. All the inserts were confirmed by ABI DNA sequencing prior transformation into appropriate particle and protein production strains.



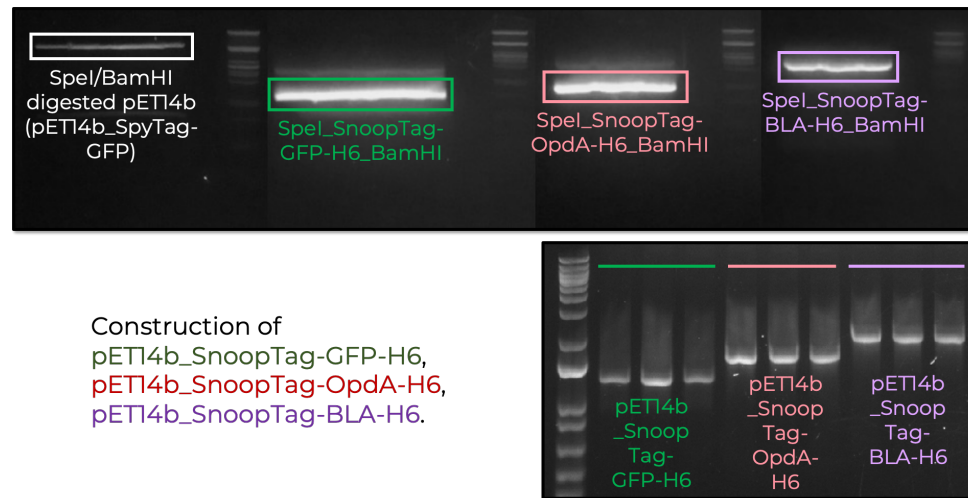
To generate pET14b\_SpyCatcher-PhaC-SnoopCatcher, gene encoding SnoopCatcher was first amplified from pBluescript\_II\_SK(+)\_SdyCatcher-SnoopCatcher using primers XhoI-SnoopCatcher and BamHI-STOP-SnoopCatcher into XhoI/BamHI sites of plasmid pET14b\_SpyCatcher-PhaC-linker\_SpyCatcher, which resulted in pET14b\_SpyCatcher-PhaC-SnoopCatcher. SdyCatcher cDNA amplified from pBluescript\_II\_SK(+)\_SdyCatcher-SnoopCatcher using primers SpeI-START-SdyCatcher and AvrII-SdyCatcher was then ligated into pET14b\_SpyCatcher-PhaC-SnoopCatcher at SpeI/AvrII restriction sites, and thereby constructing pET14b\_SdyCatcher-PhaC-SnoopCatcher.



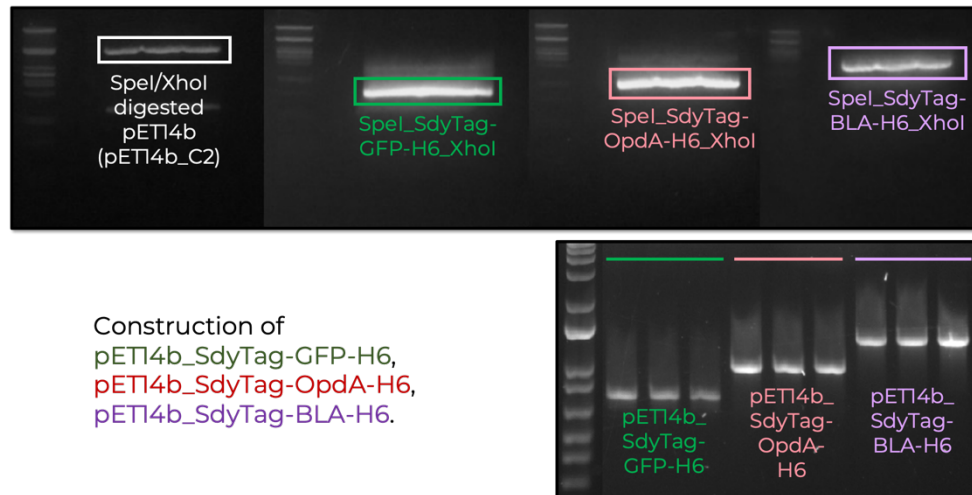
To create pET14b\_SpyCatcher-PhaC-SnoopCatcher, SnoopCatcher cDNA was first amplified from pBluescript\_II\_SK(+)\_SdyCatcher-SnoopCatcher using primers SpeI-START-SnoopCatcher and AvrII-SnoopCatcher into SpeI/AvrII sites of plasmid pET14b\_SpyCatcher-PhaC\_linker\_SpyCatcher, which resulted in pET14b\_SnoopCatcher-PhaC-SpyCatcher. Gene encoding SdyCatcher amplified from pBluescript\_II\_SK(+)\_SdyCatcher-SnoopCatcher using primers XhoI-SdyCatcher and BamHI-STOP-SdyCatcher was then ligated into pET14b\_SnoopCatcher-PhaC-SdyCatcher at XhoI/BamHI restriction sites, and thereby constructing pET14b\_SnoopCatcher-PhaC-SdyCatcher.



For construction of plasmid pET14b\_SnoopTag-linker-GFP-His6, we inserted the SnoopTag-GFP cDNA PCR-amplified from pET14b\_PhaC\_linker\_GFP using primers SpeI-START-SnoopTag-linker-GFP and SpyTag-GFP-His6\_RVR, into the SpeI and BamHI digested pET14b\_SpyTag-GFP-His6. The resulting plasmid was named as pET14b\_SnoopTag-L-GFP-His6. Likewise, to create pET14b\_SnoopTag-BLA-His6, the *bla* gene from plasmid pET14b-BLAphaC was amplified with primers SpeI-START-SnoopTag-linker-BLA and SpyTag-BLA-His6\_RVR and by cloning the resulting PCR product into SpeI/BamHI sites of vector pET14b\_SpyTag-GFP-His6. The resulting plasmid was named pET14b\_SnoopTag-L-BLA-His6.



Plasmid pET14b\_SdyTag-L-GFP-His6 was constructed by inserting the *SdyTag-gfp* gene PCR-amplified from pET14b\_PhaC\_linker\_GFP using primers SpeI-START-SdyTag-linker-GFP and XhoI-STOP-His6-GFP and ligated into the SpeI and XhoI digested pET14b\_C2. The resulting plasmid was named as pET14b\_SdyTag-L-GFP-His6. To produce pET14b\_SdyTag-L-BLA-His6, the *bla* gene from plasmid pET14b-BLAlphaC was amplified with primers SpeI-START-SdyTag-linker-BLA and XhoI-STOP-His6-BLA and by cloning the resulting PCR product into SpeI/XhoI sites of vector pET14b\_C2. The resulting plasmid was named pET14b\_SdyTag-L-BLA-His6.



## Equations used in this study

**Equations S1–S4:** Determination of production yields of protein displayed on PHA particles

$$\frac{\text{mass of total protein}}{\text{mass of PHA particle}}$$

= Total mass of protein per mass of PHA particle (**Equation S1**)

$$\frac{\text{mass of total protein}}{\text{mass of PHA particle}} \times \frac{M_w \text{ of target protein}}{M_w \text{ of total protein}}$$

= Target mass of protein per mass of PHA particle (**Equation S2**)

$$\frac{\text{mass of total protein} / \text{mass of PHA particle}}{\text{molecular weight of of total protein}}$$

= Number of moles of total protein per mass PHA particle (**Equation S3**)

$$\frac{\text{mass of total protein} / \text{mass of PHA particle}}{\text{molecular weight of of total protein}} \times \frac{M_w \text{ of target protein}}{M_w \text{ of total protein}}$$

= Number of moles of target protein per mass PHA particle (**Equation S4**)

**Equation S5:** Determination of molarity

$$\frac{\text{mass of target protein}}{\text{molecular weight of target protein} \times \text{volume of PHA particle slurry}} = \text{Molarity (**Equation S5**)}$$

**Equations S6 and S7:** Determination of percentage surface coverage and percentage ligation efficiency of SpyTagged protein covalently ligated to SpyCatcher protein on PHA particles

$$\frac{\text{band intensity of immobilized SpyTagged protein}}{\text{band intensity of immobilized SpyTagged protein} + \text{band intensity of unligated SpyCatcher protein}} \times 100\%$$

= Percentage surface coverage (**Equation S6**)

$$\frac{\text{band intensity of immobilized SpyTagged protein}}{\text{band intensity of immobilized SpyTagged protein} + \text{band intensity of unligated soluble SpyTagged protein in supernatant}} \times 100\%$$

= Percentage ligation efficiency (**Equation S7**)

**Table S5.** Protein identification by liquid chromatography-tandem mass spectrometry (LC-MS/MS).

Process	Fusion protein	Amino acid coverage (%)	Peptide fragments identified by LC-MS/MS.	Remark
N/A	<b>SpyCatcher</b> -PhaC- <b>SpyCatcher</b> (SPS only)	73.9%	<b>R36-R51, T57-K68, Y77-K109, S136-R194, D198-K210, F235-R261, F266-R289, N328-K354, Y370-I418, D426-Y560, V572-K682, A709-K758, R762-S780, T783-K794, Y803-K835.</b>	From purified SP-P
N/A	<b>SpyCatcher</b> -PhaC (SP only)	74.7%	<b>R36-K68, Y77-K109, V141-R194, D198-K210, F235-R300, I315-K354, Y370-R419, D427-R562, V572-K638, S642-A681, K723-N734.</b>	From purified SPS-P
N/A	<i>Ralstonia eutropha</i>	83.9%	S19-R103, T112-R144, I147-R183, N188-R195, K197-K237,	From purified WT-P

	PhaC (WT only)		Y253-R302, D309-K521, S525-G563.	
1	SP only	70.5%	<b>R36-K99</b> , S136-R194, D198-R220, F235-R300, I315-K354, Y370-R419, D426-R562, V572-K638, S642-K682, K723-N734.	Unbound SP on SP-P.
1	<b>SpGFP-SP</b> ligated protein ( <b>SpGFP-SP-L</b> )	62.5%	<b>G14-H40, L68-R88, L156-D170, I182-K224, R230-K253, T310-V320, Y330-G361</b> , V394-K435, D451-K463, F488-K512, F522-R542, I568-K607, Y623-R672, D679-R815, T830-K871, F874-K891, S895K935, K976-N987.	
1	<b>SpOpdA-SP</b> ligated protein ( <b>SpOpdA-SP-L</b> )	46.9%	<b>P38-F60, A87-R103, A114-R134, S137-R147, A185-A240, M250-R270, I291-R326</b> , V501-R516, D558-K570, F595-K619, F626-R649, N688-K714, Y730-R743, D761-I778, D786-R850, G867-R922, L936-K978, K1083-N1094.	

1	SpBLA-SP ligated protein (SpBLA-SP- L)	55.3%	R41-K87, G124-R142, W172- R186, A198-R246, E272-R322, A337-K387, Q410-K453, Q460- R500, V641-R656, D698-K710, F735-K759, F766-R789, N828- K854, Y870-R919, D926-R1062, L1076-K1118, F1121-K1138, K1223-N1234.	
1	SpBLA (SP)	72.4%	G15-Q86, D111-V145, W172- R186, A198-R246, T269-R320, A337-K387, K409-K453, Q460- R500.	Unbound SpBLA after mixing with SP
1	SPS only	55.2%	R36-R51, T57-K67, Y77-K109, V141-R156, D198-K210, F235- K259, F266-R289, N328-K354, Y370-R419, D426-R490, G507- K533, L576-K618, A709-K758, R762-R777, T783-K794, Y803- K838.	Unbound SPS on SPS-P.

1	<b>SpGFP-SPS</b> ligated protein ( <b>SpGFP-SPS</b> -Ls)	68.4%	<b>G15-K42, L69-R89, L157-A170, H185-S224, R231-K254, R290-R305, T311-Q320, Y331-K363, S390-R448, D452-R474, F489-A555, I569-K608, Y624-R673, D680-K892, S896-K936, A963-K1012, R1016-L1030, T1037-K1048, Y1056-K1089, G1112-K1139, L1166-R1186, L1254-K1269, H1282-K1322, D1329-K1351.</b>	Protein ligation with either N- or C- terminus SpyCatcher
1	<b>SpGFP-SPS</b> ligated protein ( <b>SpGFP-SPS</b> -L)	37.2%	<b>G15-K42, L69-R89, I183-K225, D232-K254, T311-Q320, D452-K464, F489-R499, F520-R543, N582-K608, Y624-R673, I687-A708, E745-K787, LTV830-A870, A963-R974, T1037-K1048, G1112-K1139, L1166-R1186, K1279-L1320, D1329-K1351.</b>	Protein ligation with both N- or C- terminus SpyCatcher
1	<b>SpOpdA-</b> <b>SPS</b> ligated	51.6%	<b>G37-F60, A87-G102, A114-R134, D203-A240, M250-R270,</b>	Protein ligation

	proteins  ( <b>SpOpdA</b> - <b>SPS</b> -Ls)		<b>I291-R314, E333-R351, R396-R411, Y437-K469, V501-R516, D558-K570, F595-DAK619, F626-R649, N688-K714, Y730-R775, D786-R850, G867-K893, L936-K978, A1069-K1118, R1122-R1137, Y1163-K1195, P1241-R1265, A1290-R1306, A1317-R1337, S1340-R1350, D1406-R1444, M1453-R1473, I1494-R1517, E1536-R1554.</b>	with either N- or C- terminus SpyCatcher
1	<b>SpOpdA</b> - <b>SPS</b> ligated protein ( <b>SpOpdA</b> - <b>SPS</b> -L)	38.2%	<b>A87-R103, A114-F145, A185-A240, M250-R270, I291-R314, V501-R516, F595-K619, F626-R649, N689-K714, Y730-I778, D786-R815, G867-K893, L936-K978, A1069-K1118, A1290-R1306, A1317-R1337, A1398-R1444, M1453-PR1473, I1494-R1517.</b>	Protein ligation with both N- or C- terminus SpyCatcher

1	SpBLA-SPS ligated proteins (SpBLA- SPS-Ls)	58.1%	R41-Q86, D111-A140, A154- R163, W172-R186, A198-R246, E272-R322, A337-K387, E431- K453, Q460-R500, R536-L550, V641-R656, D698-K710, F735- K759, F766-R789, I815-K854, Y870-R919, D926-K1033, T1064- K1118, F1121-K1138, A1209- K1258, R1262-E1275, R1384- K1430, D1454-R1485, A1497- R1506, W1515-R1529, A1541- R1589, E1615-R1665, A1680- K1730, E1774-K1796, Q1803- R1843.	Protein ligation with either N- or C- terminus SpyCatcher
1	SpBLA-SPS ligated protein (SpBLA- SPS-L)	28.6%	R41-K64, G124-A140, W232- R246, E272-K293, A337-T370, E431-K453, A746-K759, F766-R789, N828- K854, N899-R919, D927R955, G1007-K1033, L1076-K1118, A1209-K1258, R1384-Y1406, G1467-R1485, W1575-R1589,	Protein ligation with both N- or C- terminus SpyCatcher

			<b>E1615-K1636, V1681-R1714, E1774-D1790.</b>	
1	<b>SpBLA</b> (SPS)	72.6%	<b>G15-K86, D111-V145, W172-R186, A198-R246, T269-R320, A337-K387, Q410-K453, Q460-R500.</b>	Unbound SpBLA after mixing with SPS
2	SP only	66.9%	<b>R36-L50, T57-K68, Y77-K109,</b> V141-R156, I183-R194, F235-K259, F266-SLR300, I268-K354, Y370-R419, D426-R562, L576-K618, F621-K638, S666-A681, K723-N734.	Unbound SP on SP-P.
2	<b>SpGFP-SP</b> ligated protein ( <b>SpGFP-SP-L</b> )	53.4%	<b>G15-K42, L157-D171, I183-K225, R231-K254, D291-R305, T311-V321,</b> V395-R410, D452-FK464, F489-K513, F520-R554, I569-K608, Y624-R673, D680-R816, L830-K872, F875-K892, K977-N988.	

2	<b>SpOpdA-SP</b> ligated protein ( <b>SpOpdA-SP-L</b> )	51.2%	<b>G37-F60, A87-AR103, A114-R134, S137-R147, A185-A240, M250-R270, I291-R326, E333-R348,</b> V501-R516, D558-K570, F595-K619, A627-R649, N688-K714, Y730-R779, D786-R922, L936- K998.	
2	<b>SpBLA-SP</b> ligated protein ( <b>SpBLA-SP-L</b> )	64.6%	<b>G15-K87, G124-R142, A154-R163, W172-R186, A198-R246, E272-R322, A337-K387, Y411-AK453, Q460-R500, T557-K568,</b> V641-R656, I683-K635, F735-K759, F766-R800, N828-K854, Y870-R919, D926-K1118, F1121-K1138, S1142-K1182.	
2	<b>SPS</b> only (Process 1)	76.6%	<b>R36-R51, T57-K68, Y77-K109,</b> V141-K208, F235-R261, I264-R300, N305-R312, I315-K354, Y370-R419, D426-R562, V572-K638, S642-K682, A709- <b>K758,</b>	Unbound SPS on SPS-P after mixing.

			<b>R762-R777, T783-K794, Y803-K835.</b>	
2	<b>SpGFP-SPS</b> ligated protein ( <b>SpGFP-SPS-Ls</b> )	53.6%	<b>G15-K42, L69-Y90, I183-254, R290-R305, T311-K322, Y331-K363, V395-R410, I437-R448, D452-K464, F489-K513, F520-R554, N582-K605, Y624-R673, I687-K787, L830-K872, A963-K1012, R1016-K1048, Y1057-K1089, G1112-K1139, L1166-R1186, I1280-K1322, D1329-K1351.</b>	Protein ligation with either N- or C- terminus SpyCatcher
2	<b>SpGFP-SPS</b> ligated protein ( <b>SpGFP-SPS-L</b> )	36.1%	<b>G15-K42, T113-K123, I183-K225, D232-K254, I437-R448, F489-K513, F520-R554, N582-K608, Y624-R637, N653-R673, I687-R709, G761-K787, L830-K872, A963-K1012, G1112-K1139, T1210-K1220, I1280-K1322, D1329-K1351.</b>	Protein ligation with both N- or C- terminus SpyCatcher

2	<b>SpOpdA-</b> <b>SPS</b> ligated proteins ( <b>SpOpdA-</b> <b>SPS-Ls</b> )	41.5%	<b>A114-R134, S137-R147, A185-</b> <b>A240, M250-R270, I291-R314,</b> <b>D397-R411,</b> V501-R516, D558- K570, F595-K619, F626-R649, I675-K714, H744-R779, D786- R815, G867-R922, L936-K978, F981-K998, A1069- <b>K1118,</b> <b>D1123-R1137, A1317-R1337,</b> <b>S1340-R1350, A1388-R1444,</b> <b>M1453-R1473, I1494-R1517.</b>	Protein ligation with either N- or C- terminus SpyCatcher
2	<b>SpOpdA-</b> <b>SPS</b> ligated protein ( <b>SpOpdA-</b> <b>SPS-L</b> )	44.6%	<b>G37-R62, A87-R103, A114-</b> <b>R147, A185-A240, M250-R270,</b> <b>E333-R351, R396-R411,</b> V501- R554, F595-K619, F626-R649, N688-K714, Y730-R779, D786- R815, L936-K978, F981-K998, A1069- <b>K1118, R1122-R1137,</b> <b>G1240-R1260, A1290-R1306,</b> <b>A1317-R1350, A1388-R1441,</b> <b>M1453-R1473, E1536-R1554.</b>	Protein ligation with both N- or C- terminus SpyCatcher

2	SpBLA-SPS ligated proteins (SpBLA- SPS-Ls)	43.7%	G65-K87, G124-R142, A198- R246, E272-K293, A337-K387, E431-K453, S474-R500, T557- K568, V641-R656, F735-K759, F766-R800, I768-K854, H884- R919, D926-R990, G1007-K1033, L1076-K1118, F1121-K1137, A1209-K1258, T1283-K1294, G1408-K1430, G1467-R1485, A1541-R1589, E1615-K1636, A1680-K1730, E1774-K1796, S1817-R1843.	Protein ligation with either N- or C- terminus SpyCatcher
2	SpBLA-SPS ligated protein (SpBLA- SPS-L)	46.7%	R41-K87, G124-R142, A198- R246, E272-R322, A337-R371, E431-K453, S474-R500, V641- R656, D698-K710, F735-K759, F766-R800, I815-K854, Y870- R919, D926-R955, G1007-K1033, L1076-K1118, A1209-K1258, R1262-R1276, R1384-K1430, G1467-R1485, A1541-R1589,	Protein ligation with both N- or C- terminus SpyCatcher

			<b>E1615-R1665, A1680-R1714, E1774-K1796, S1817-R1843.</b>	
3	<b>SP only</b>	76.4%	<b>R36-L50, T57-K68, Y77-K109, S136-R194, D198-R220, F235-R261, I264-R300, I268-D353, Y370-R419, D426-K682, K723-N734.</b>	Unbound SP on SP-P.
3	<b>SpGFP-SP</b> ligated protein ( <b>SpGFP-SP-L</b> )	55.9%	<b>G14-K41, L68-R88, A125-R137, L156-K171, I182-K224, D231-K253, D290-R304, Y330-K362, V394-R409, D451-K463, F488-K512, F519-R542, I521-K607, Y623-R672, D679-R815, L829-K817, K976-N987.</b>	
3	<b>SpGFP (SP)</b>	61.0%	<b>G15-L58, F62-R89, A126-R138, L157-K172, I183-K225, R231-K254.</b>	Unbound SpGFP after mixing with SP
3	<b>SpOpdA-SP</b> ligated	46.2%	<b>G37-A73, A87-R103, A114-R134, S137-R147, A185-A240,</b>	

	protein  ( <b>SpOpdA-SP-L</b> )		<b>M250-R270, I291-R326,</b> V501-R516, D558-K570, F595-K619, F626-R649, N688-K714, Y730-R743, N316-R779, D786-R850, G867-R922, L936-TK978, K1083-N1094.	
3	<b>SpOpdA</b> (SP)	72.8%	<b>G18-R62, A87-R106, A114-R134, S137-R159, A171-A240, M250-R270, A276-R285, I291-R326, E333-R351.</b>	Unbound  SpOpdA  after mixing  with SP
3	<b>SpBLA-SP</b>  ligated  protein  ( <b>SpBLA-SP-L</b> )	53.9%	<b>R41-K87, A198-R246, E272-R322, A337-K387, E431-K453, S474-R500, R536-R550,</b> V641-R656, D698-K710, F735-K759, F766-R800, N828-K854, Y871-R919, D926-R1062, L1076-K1118, F1121-K1138, L1224-N1234.	
3	<b>SpBLA</b> (SP)	75.0%	<b>G15-K87, D111-R144, I152-R163, W172-K187, A198-K251,</b>	Unbound  SpBLA

			<b>E272-R322, A337-T386, Y411-R454, Q460-R500.</b>	after mixing with SP
3	<b>SPS</b> only (Process 1)	77.3%	<b>R36-K68, Y77-K109, V141-R194, D198-K210, F235-R261, I264-R300, I315-K354, Y371-R419, D426-K638, S642-K682, A709-K758, R762-R777, T783-K794, Y803-K835.</b>	Unbound SPS on SPS-P after mixing.
3	<b>SpGFP-SPS</b> ligated protein ( <b>SpGFP-SPS</b> -Ls)	51.2%	<b>G15-K42, L69-Y90, I183-K225, D232-K254, R290-K322, Y311-K363, V395-R410, D452-K464, F489-K513, F520-R543, N582-K608, Y624-R673, D680-R744, G761-K787, L830-K872, A963-K1012, R1016-R1031, T1037-K1048, Y1057-K1089, G1112-K1139, L1166-R1186, I1280-K1322, D1329-K1351.</b>	Protein ligation with either N- or C- terminus SpyCatcher
3	<b>SpGFP-SPS</b> ligated	50.3%	<b>G15-K42, L69-R89, T113-R138, H185-K225, D232-K254, R290-</b>	Protein ligation

	protein  ( <b>SpGFP-SPS-L</b> )		<b>R305, T311-K322</b> , V395-R410, D452-K464, F489-K513, F520-R554, N582-K608, Y624-R673, D680-R709, E745-K787, L830-872, F875-K892, A963- <b>K1012</b> , <b>R1016-R1031, T1037-K1048, G1112-K1139, L1166-R1186, T1210-R1235, H1282-K1320, D1329-K1351.</b>	with both N- or C-terminus  SpyCatcher
3	<b>SpGFP</b>  ( <b>SPS</b> )	67.7%	<b>G15-K57, F62-R89, A126-R138, L157-K172, I183-K254.</b>	Unbound  SpGFP after mixing with SPS
3	<b>SpOpdA-SPS</b> ligated proteins  ( <b>SpOpdA-SPS-Ls</b> )	60.3%	<b>G18-R62, A87-R103, A114-R134, S137-R147, A185-A240, M250-R270, I291-R326, E333-R351, R396-R411, T417-K428, Y437-K469, V501-R516, D558-FK570, F595-K619, F626-R660, N688-K714, Y730-R779, D786-K893, L936-K978, A1069-K1118, R1122-R1137, T1143-K1154,</b>	Protein ligation with either N- or C-terminus  SpyCatcher

			<b>Y1163-K1195, G1221-1265,</b> <b>A1290-R1306, A1317-R1337,</b> <b>S1340-R1350, A1390-A1443,</b> <b>M1453-R1473, I1494-R1529,</b> <b>E1536-R1554.</b>	
3	<b>SpOpdA-</b> <b>SPS</b> ligated protein <b>(SpOpdA-</b> <b>SPS-L)</b>	40.7%	<b>A87-R103, A114-R134, S137-</b> <b>R147, D203-A240, M250-R270,</b> <b>I291-R326, E333-R351, V501-</b> <b>R516, F595-R605, F626-R649,</b> <b>N688-K714, Y730-R743, N758-</b> <b>R779, D786-R815, E851-R922,</b> <b>L936-K978, A1069-K1118,</b> <b>R1122-R1137, A1290-R1306,</b> <b>A1317-R1337, S1340-R1350,</b> <b>D1406-R1444, M1453-R1473,</b> <b>I1494-R1529, E1536-R1554.</b>	Protein ligation with both N- or C- terminus SpyCatcher
3	<b>SpOpdA</b> <b>(SPS)</b>	75.6%	<b>G18-R62, A87-R106, A114-</b> <b>R134, S137-R159, K164-A240,</b> <b>G242-R270, I291-R324, E333-</b> <b>R351.</b>	Unbound SpOpdA after mixing with SPS

3	<b>SpBLA-SPS</b> ligated proteins ( <b>SpBLA-SPS</b> -Ls)	46.6%	<b>R41-K87, W172-R186, A198-R246, E272-R322, A337-T370, E431-K453, S474-R500, T557-K568,</b> V641-R656, F735-K759, F766-R789, N828-K854, Y870-R919, D926-R990, G1007-K1033, L1076-K1118, A1209- <b>K1258, T1283-K1294, R1384-K1430, W1515-R1529, A1541-R1589, E1615-R1665, A1680-T1713, E1774-K1796, S1817-R1843.</b>	Protein ligation with either N- or C- terminus SpyCatcher
3	<b>SpBLA</b> ( <b>SPS</b> )	73.8%	<b>G15-K87, D111-R142, A154-R163, W172-K187, A198-R246, E272-R322, A337-K387, K409-R454, Q460-R500.</b>	Unbound SpBLA after mixing with SPS

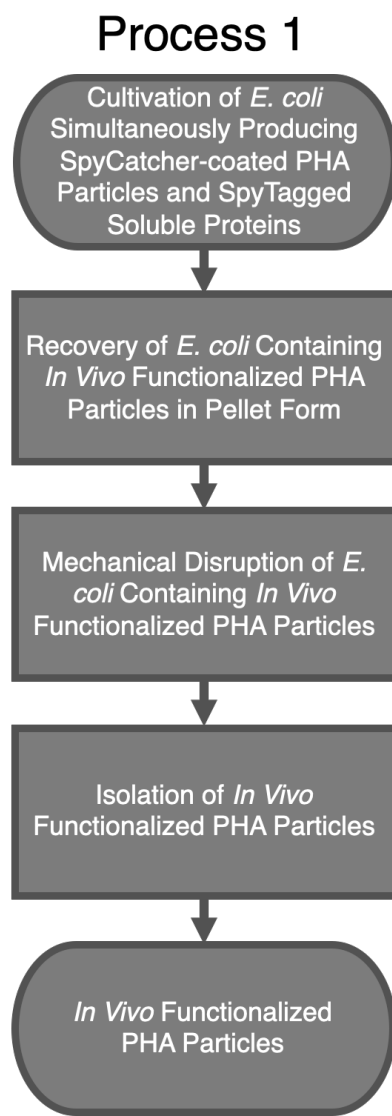


**Figure S1.** Flowchart of *in vivo* functionalization of SpyCatcher-coated PHA particles using process 1.

## Process 2

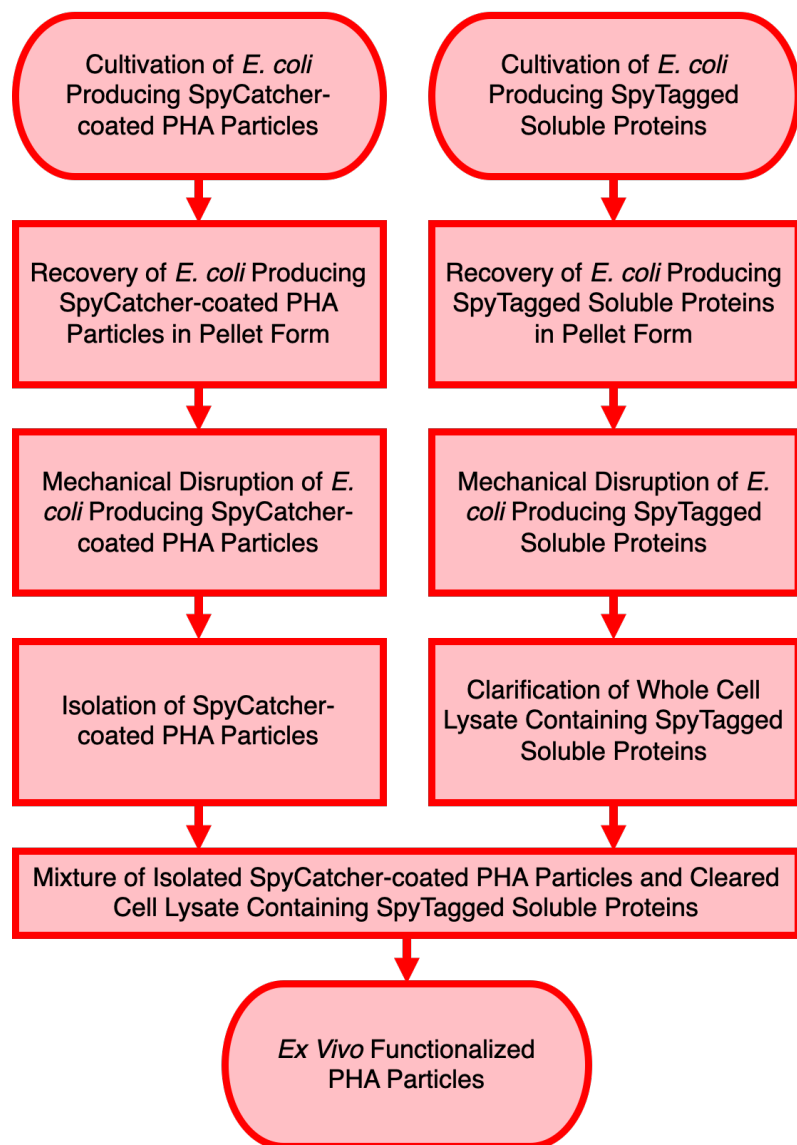


**Figure S2.** Flowchart of *ex vivo* functionalization of SpyCatcher-coated PHA particles using process 2.

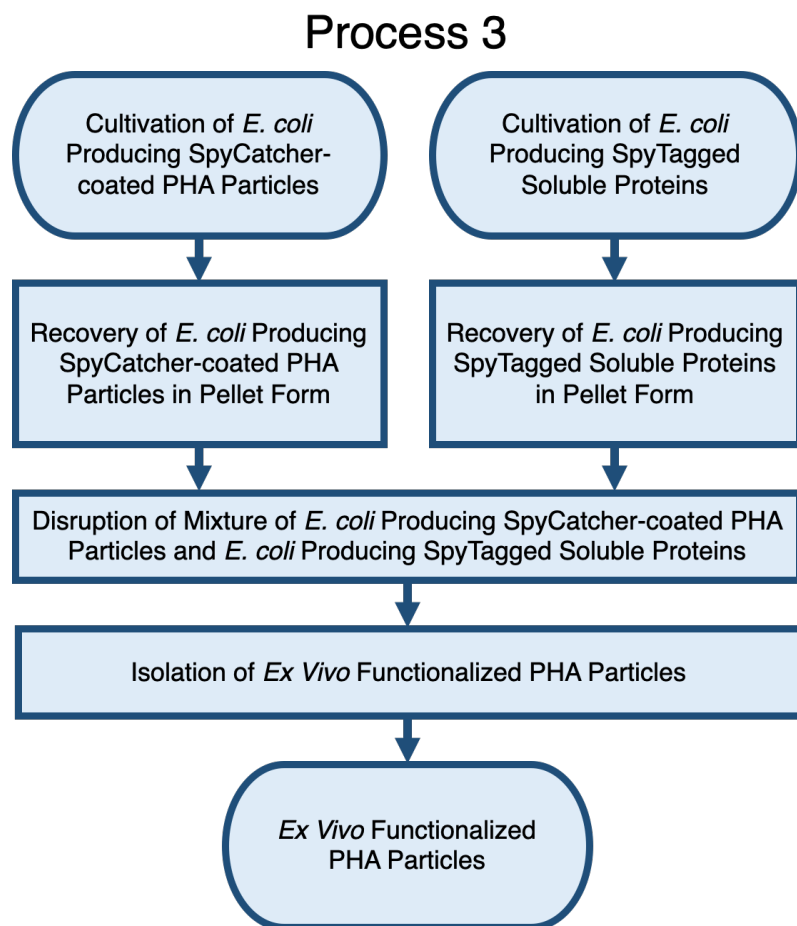


**Figure S3.** Flowchart of *ex vivo* functionalization of SpyCatcher-coated PHA particles using process 3.

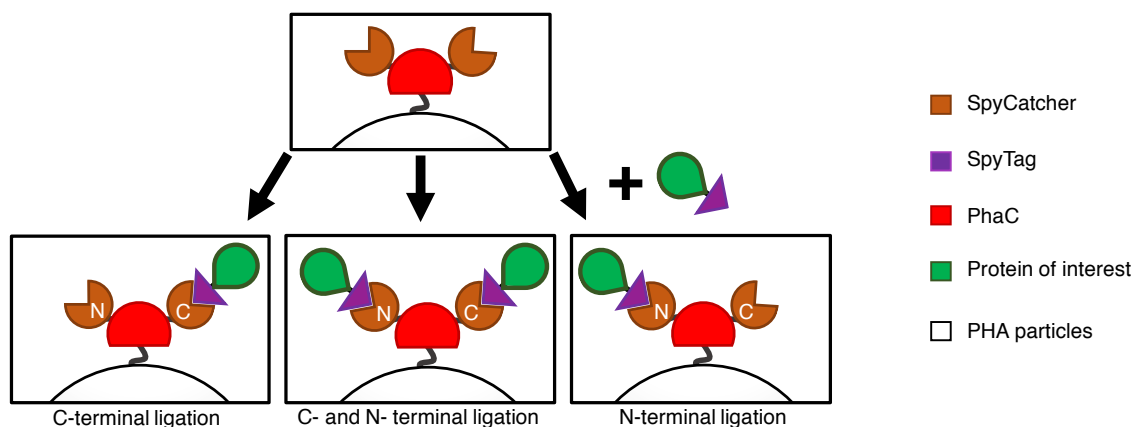


**Figure S4.** Three possible ligated products from functionalized SPS fusion protein-displaying PHA particles (SPS-P) (orange/brown) using SpyTagged proteins. Upon mixture of SPS-P with SpyTagged protein of interest (purple/green), SpyTagged proteins could immobilize on C- or/and N-terminal SpyCatcher domains.

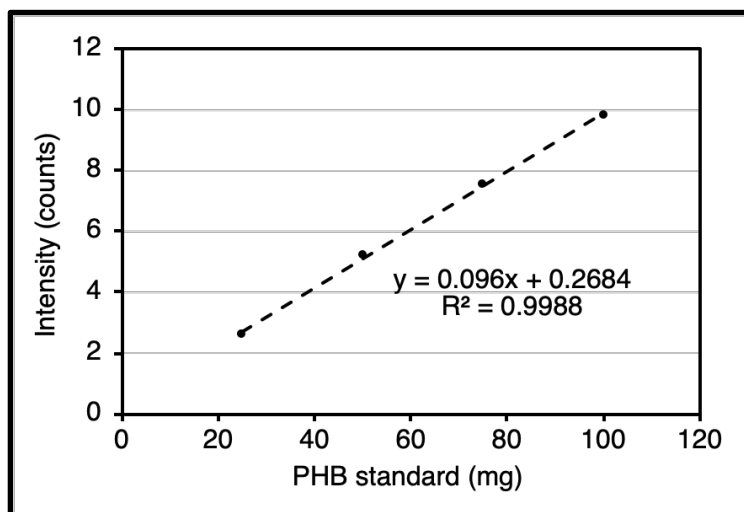


**Figure S5.** Poly(*R*)-3-hydroxybutyrate (PHB) standard curve obtained from GC–MS. Pure PHB as a standard for compositional analysis of SpyCatcher-coated PHA particles.

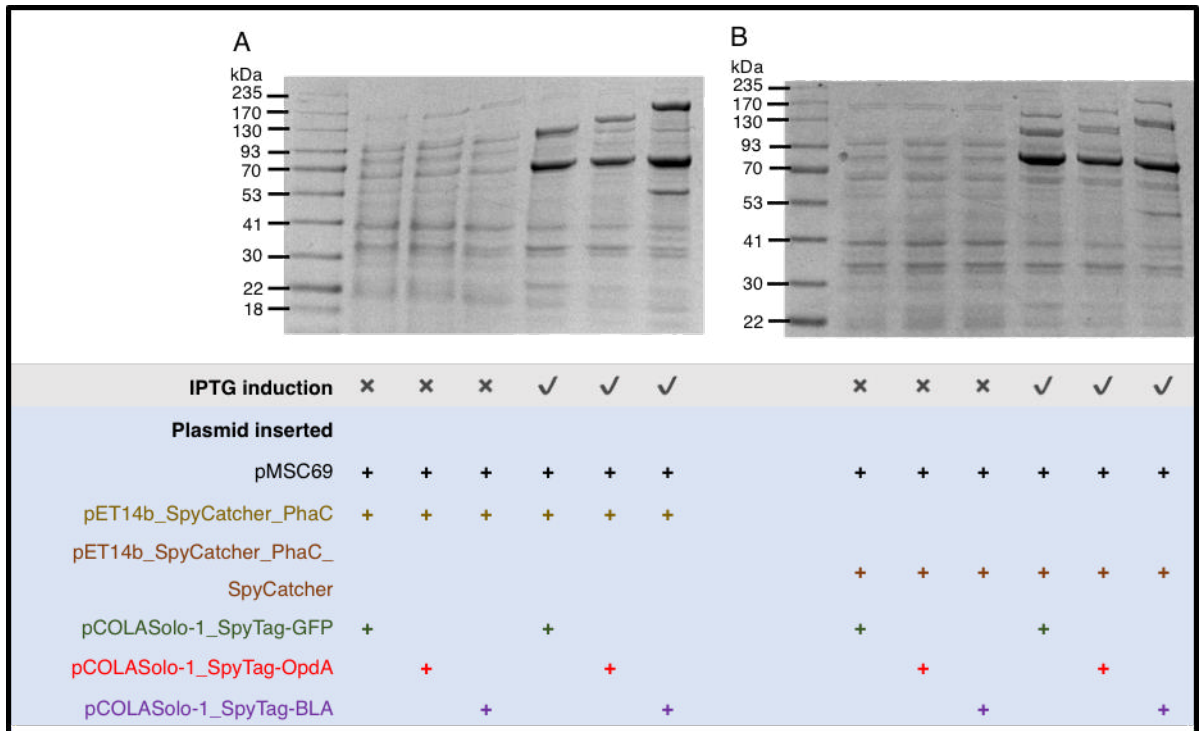


**Figure S6.** Whole cell lysate (WCL) of *E. coli* BL21(DE3) containing modular *in vivo* functionalized SpyCatcher-coated PHA particles (Process 1). **(A)** WCL of *E. coli* BL21(DE3) containing *in vivo* functionalized SP-Ps. **(B)** WCL of *E. coli* BL21(DE3) containing *in vivo* functionalized SPS-Ps. SP-P, SP-displaying PHA particles; SPS-P, SPS-displaying PHA particles.

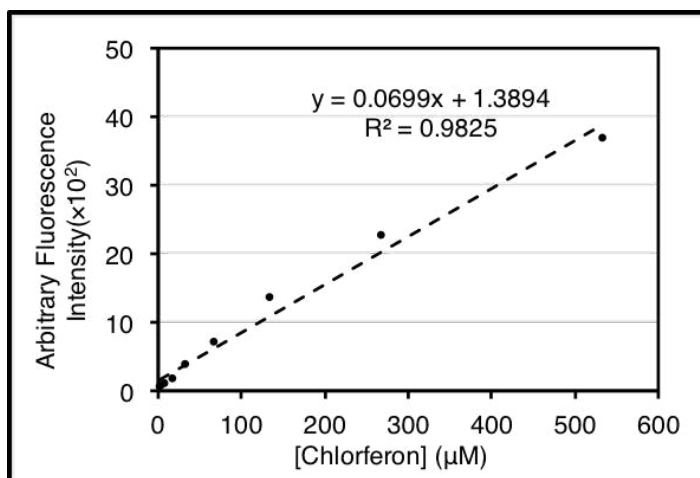


**Figure S7.** Chlorferon standard curve obtained from fluorescence spectroscopy for the OpdA activity assay.

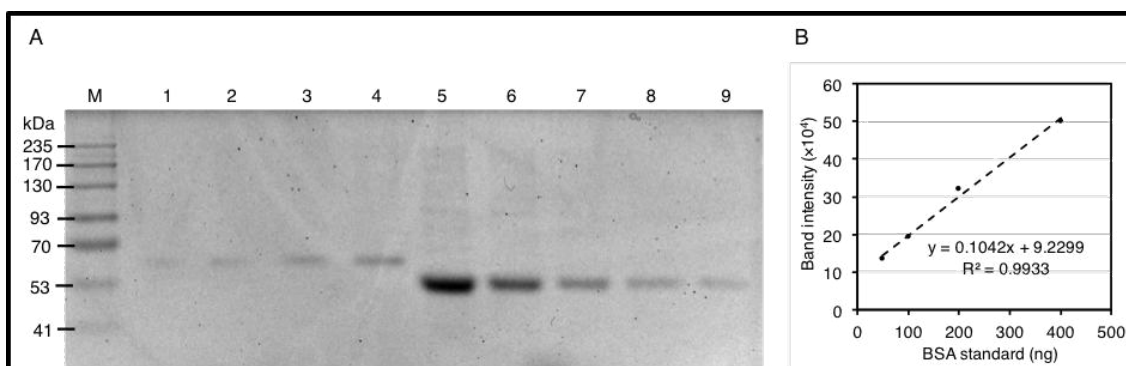


**Figure S8.** Densitometric protein quantification of wild-type PhaC (WT) on PHA particles relative to BSA standards. **(A)** SDS-PAGE analysis of WT at varying dilution factors. Lane M, Gangnam pre-stained protein marker; lane 1, BSA (50 ng); lane 2, BSA (100 ng); lane 3, BSA (200 ng); lane 4, BSA (400 ng); lane 5, WT (dilution factor of 6); lane 6, WT (dilution factor of 12); lane 7, WT (dilution factor of 24); lane 8, WT (dilution factor of 47); lane 9, WT (dilution factor of 94). **(B)** BSA standard curve obtained from SDS-PAGE densitometric analysis.

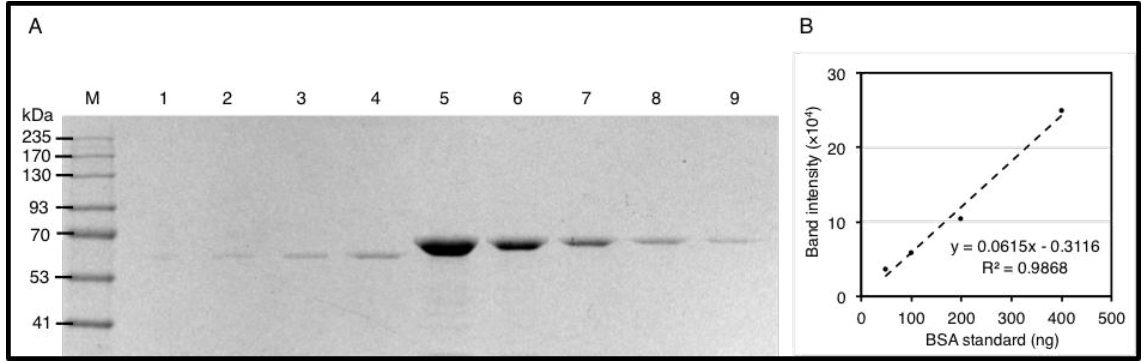


**Figure S9.** Densitometric protein quantification of SpyCatcher-PhaC (SP) fusion protein on PHA particles relative to BSA standards. **(A)** SDS-PAGE analysis of SP fusion protein at varying dilution factors. Lane M, Gangnam pre-stained protein marker; lane 1, BSA (50 ng); lane 2, BSA (100 ng); lane 3, BSA (200 ng); lane 4, BSA (400 ng); lane 5, SP fusion protein (dilution factor of 12); lane 6, SP fusion protein (dilution factor of 24); lane 7, SP fusion protein (dilution factor of 47); lane 8, SP fusion protein (dilution factor of 94); lane 9, SP fusion protein (dilution factor of 187). **(B)** BSA standard curve obtained from SDS-PAGE densitometric analysis.

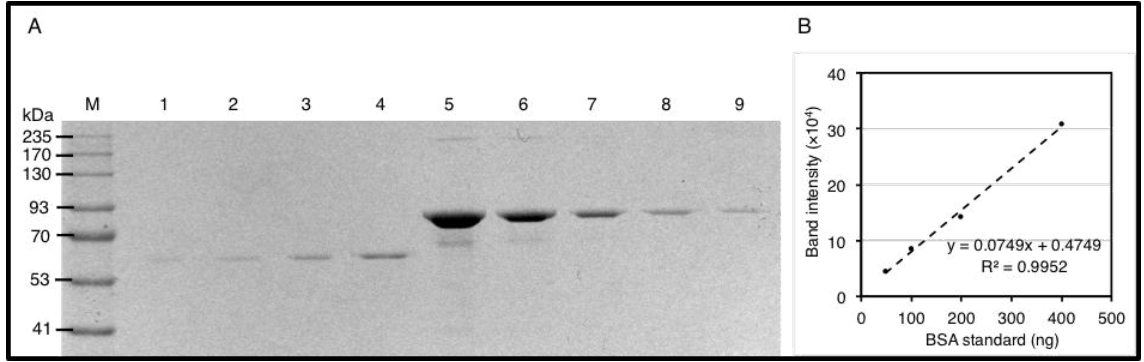


**Figure S10.** Densitometric protein quantification of SpyCatcher-PhaC-SpyCatcher (SPS) fusion protein on PHA particles relative to BSA standards. **(A)** SDS-PAGE analysis of SPS fusion protein at varying dilution factors. Lane M, Gangnam pre-stained protein marker; lane 1, BSA (50 ng); lane 2, BSA (100 ng); lane 3, BSA (200 ng); lane 4, BSA (400 ng); lane 5, SPS fusion protein (dilution factor of 12); lane 6, SPS fusion protein (dilution factor of 24); lane 7, SPS fusion protein (dilution factor of 47); lane 8, SPS fusion protein (dilution factor of 94); Lane 9, SPS fusion protein (dilution factor of 187). **(B)** BSA standard curve obtained from SDS-PAGE densitometric analysis.

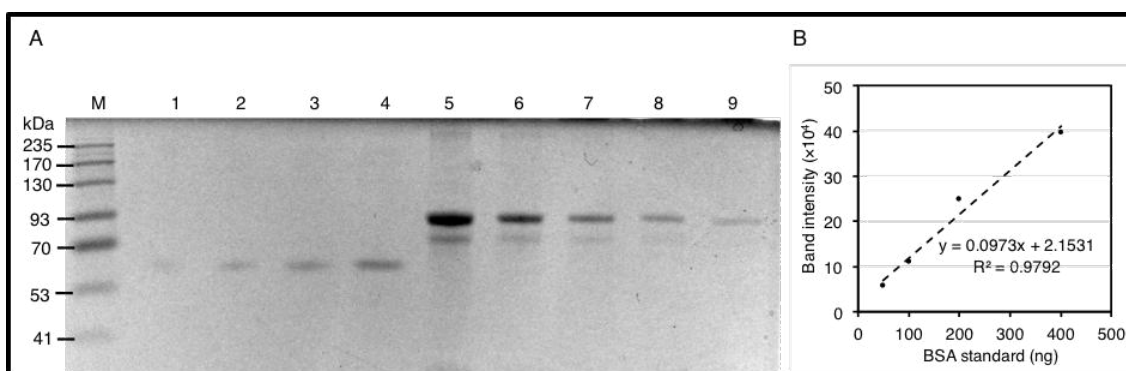


**Figure S11.** Densitometric protein quantification of PhaC-OpdA fusion protein on PHA particles relative to BSA standards. **(A)** SDS-PAGE analysis of PhaC-OpdA fusion protein at varying dilution factors. Lane M, Gangnam pre-stained protein marker; lane 1, BSA (50 ng); lane 2, BSA (100 ng); lane 3, BSA (200 ng); lane 4, BSA (400 ng); lane 5, PhaC-OpdA fusion protein (dilution factor of 6); lane 6, PhaC-OpdA fusion protein (dilution factor of 12); lane 7, PhaC-OpdA fusion protein (dilution factor of 24); lane 8, PhaC-OpdA fusion protein (dilution factor of 47); lane 9, PhaC-OpdA fusion protein (dilution factor of 94). **(B)** BSA standard curve obtained from SDS-PAGE densitometric analysis.

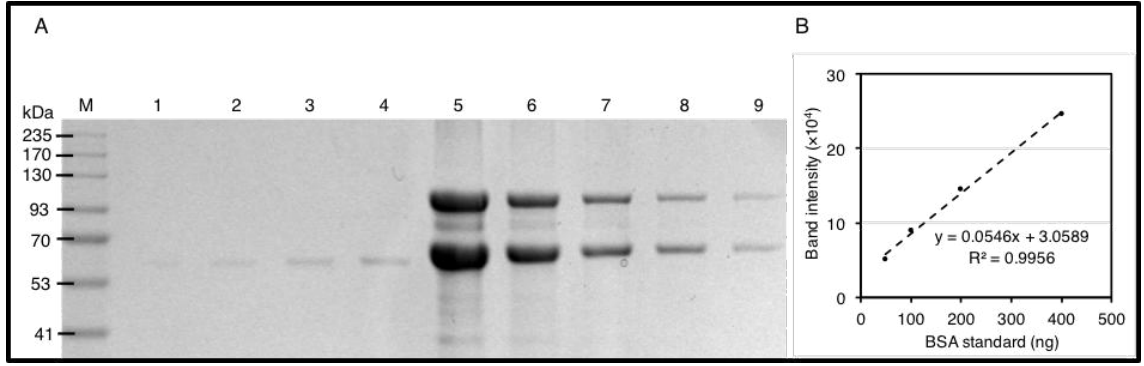


**Figure S12.** Densitometric protein quantification of SpOpdA-SP ligated protein (SpOpdA-SP-L) on PHA particles relative to BSA standards (Process 1). **(A)** SDS-PAGE analysis of SpOpdA-SP-L at varying dilution factors. Lane M, Gangnam pre-stained protein marker; lane 1, BSA (50 ng); lane 2, BSA (100 ng); lane 3, BSA (200 ng); lane 4, BSA (400 ng); lane 5, SpOpdA-SP-L (dilution factor of 6); lane 6, SpOpdA-SP-L (dilution factor of 12); lane 7, SpOpdA-SP-L (dilution factor of 24); lane 8, SpOpdA-SP-L (dilution factor of 47); lane 9, SpOpdA-SP-L (dilution factor of 94). **(B)** BSA standard curve obtained from SDS-PAGE densitometric analysis.

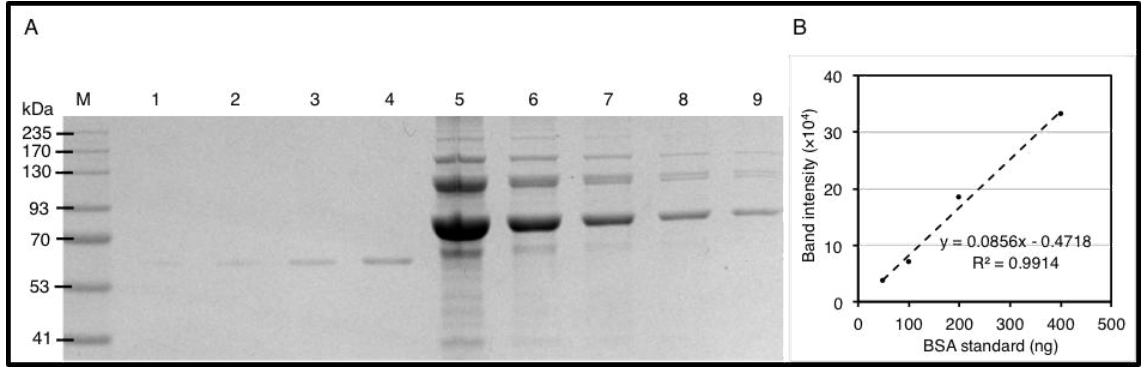


**Figure S13.** Densitometric protein quantification of SpOpdA-SPS ligated protein (SpOpdA-SPS-L) on PHA particles relative to BSA standards (Process 1). **(A)** SDS-PAGE analysis of SpOpdA-SPS-L at varying dilution factors. Lane M, Gangnam pre-stained protein marker; lane 1, BSA (50 ng); lane 2, BSA (100 ng); lane 3, BSA (200 ng); lane 4, BSA (400 ng); lane 5, SpOpdA-SPS-L (dilution factor of 6); lane 6, SpOpdA-SPS-L (dilution factor of 12); lane 7, SpOpdA-SPS-L (dilution factor of 24); lane 8, SpOpdA-SPS-L (dilution factor of 47); lane 9, SpOpdA-SPS-L (dilution factor of 94). **(B)** BSA standard curve obtained from SDS-PAGE densitometric analysis.

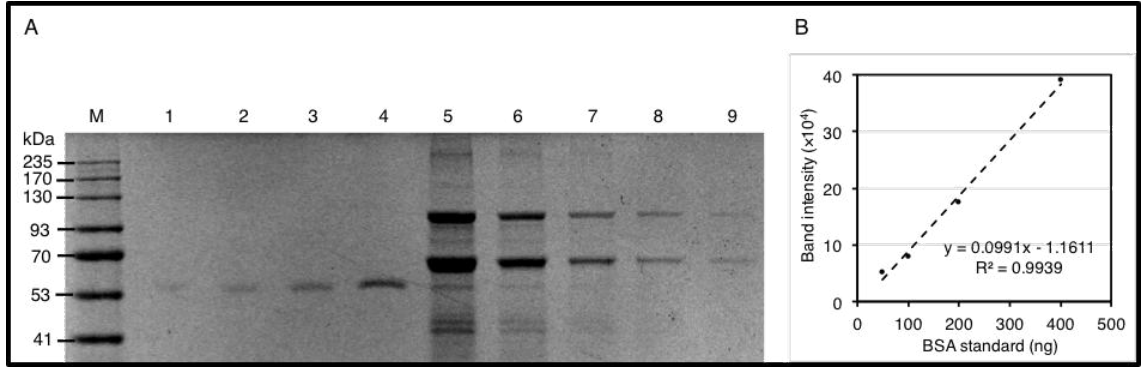


**Figure S14.** Densitometric protein quantification of SpOpdA-SP ligated protein (SpOpdA-SP-L) on PHA particles relative to BSA standards (Process 2). **(A)** SDS-PAGE analysis of SpOpdA-SP-L at varying dilution factors. Lane M, Gangnam pre-stained protein marker; lane 1, BSA (50 ng); lane 2, BSA (100 ng); lane 3, BSA (200 ng); lane 4, BSA (400 ng); lane 5, SpOpdA-SP-L (dilution factor of 12); lane 6, SpOpdA-SP-L (dilution factor of 24); lane 7, SpOpdA-SP-L (dilution factor of 47); lane 8, SpOpdA-SP-L (dilution factor of 94); lane 9, SpOpdA-SP-L (dilution factor of 187). **(B)** BSA standard curve obtained from SDS-PAGE densitometric analysis.

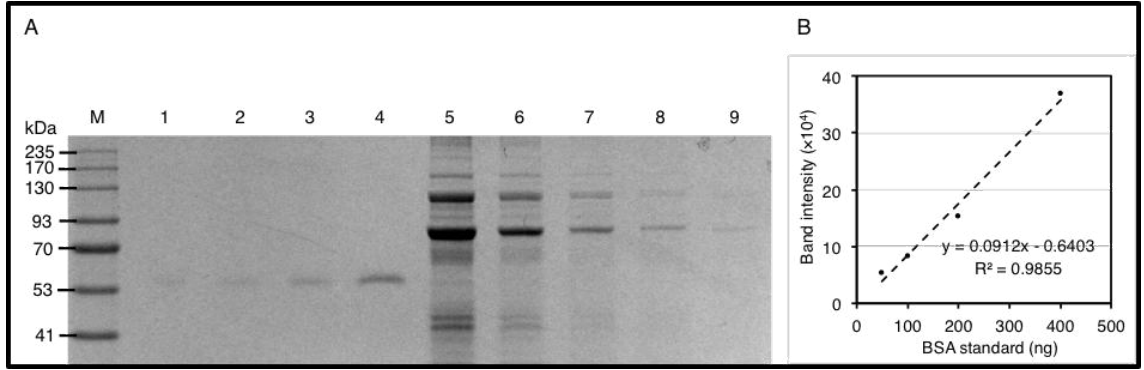


**Figure S15.** Densitometric protein quantification of SpOpdA-SPS ligated protein (SpOpdA-SPS-L) on PHA particles relative to BSA standards (Process 2). **(A)** SDS-PAGE analysis of OpdA-SPS-L at varying dilution factors. Lane M, Gangnam pre-stained protein marker; lane 1, BSA (50 ng); lane 2, BSA (100 ng); lane 3, BSA (200 ng); lane 4, BSA (400 ng); lane 5, SpOpdA-SPS-L (dilution factor of 12); lane 6, SpOpdA-SPS-L (dilution factor of 24); lane 7, SpOpdA-SPS-L (dilution factor of 47); lane 8, SpOpdA-SPS-L (dilution factor of 94); lane 9, SpOpdA-SPS-L (dilution factor of 187). **(B)** BSA standard curve obtained from SDS-PAGE densitometric analysis.

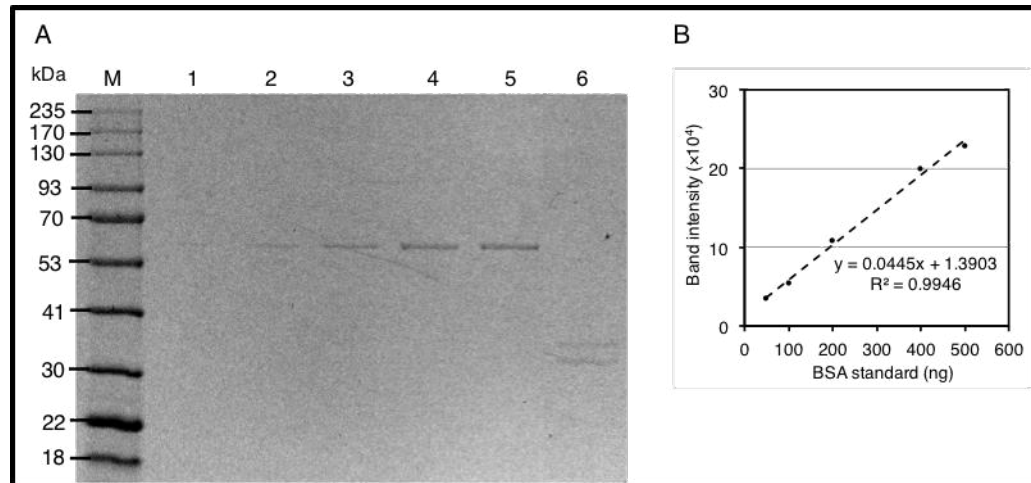


**Figure S16.** Densitometric protein quantification of N-terminally SpyTagged and C-terminally hexahistidine-tagged soluble OpdA (SpOpdA-H6). **(A)** SDS-PAGE analysis of SpOpdA-His6 and BSA standards. Lane M, Gangnam pre-stained protein marker; lane 1, BSA (50 ng); lane 2, BSA (100 ng); lane 3, BSA (200 ng); lane 4, BSA (400 ng); lane 5, BSA (400 ng); lane 6, SpOpdA-H6 (dilution factor of 24). **(B)** BSA standard curve obtained from SDS-PAGE densitometric analysis.

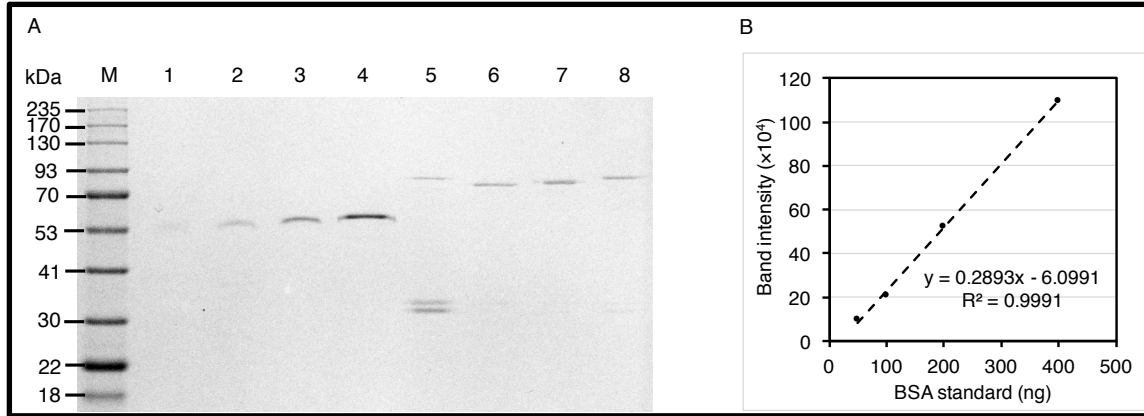


**Figure S17.** Densitometric protein quantification of various combinations of Catcher domains fused PhaC fusion proteins relative to BSA standards. **(A)** SDS-PAGE analysis of various Catcher domain pairs fused to PhaC fusion proteins at varying dilution factors. Lane M, Gangnam pre-stained protein marker; lane 1, BSA (50 ng); lane 2, BSA (100 ng); lane 3, BSA (200 ng); lane 4, BSA (400 ng); lane 5, NPD fusion protein (dilution factor of 94); lane 6, DPN fusion protein (dilution factor of 187); lane 7, PPN fusion protein (dilution factor of 187); lane 8, NPP fusion protein (dilution factor of 187). **(B)** BSA standard curve obtained from SDS-PAGE densitometric analysis.

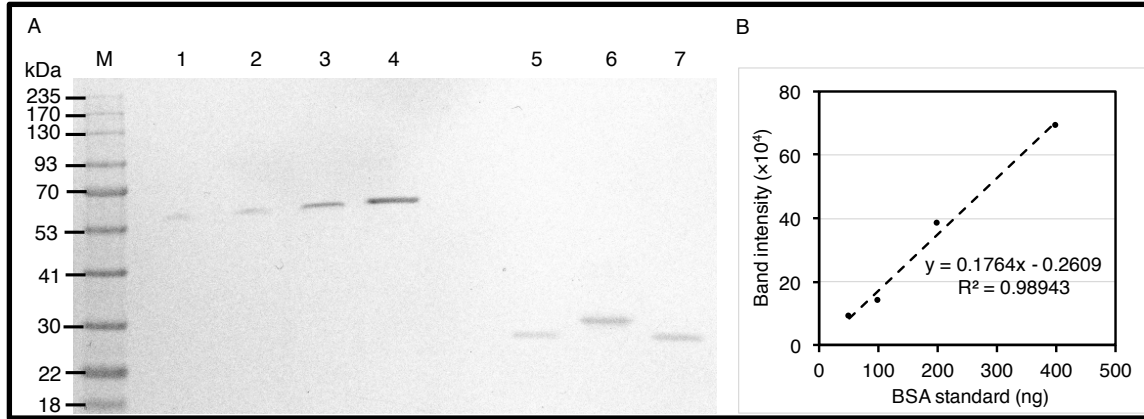


**Figure S18.** Densitometric protein quantification of various tagged GFP fusion proteins relative to BSA standards. **(A)** SDS-PAGE analysis of different tagged GFP fusion proteins at dilution factor of 38. Lane M, Gangnam pre-stained protein marker; lane 1, BSA (50 ng); lane 2, BSA (100 ng); lane 3, BSA (200 ng); lane 4, BSA (400 ng); lane 5, SpGFP-H6; lane 6, SnGFP-H6; lane 7, SdGFP-H6. **(B)** BSA standard curve obtained from SDS-PAGE densitometric analysis.

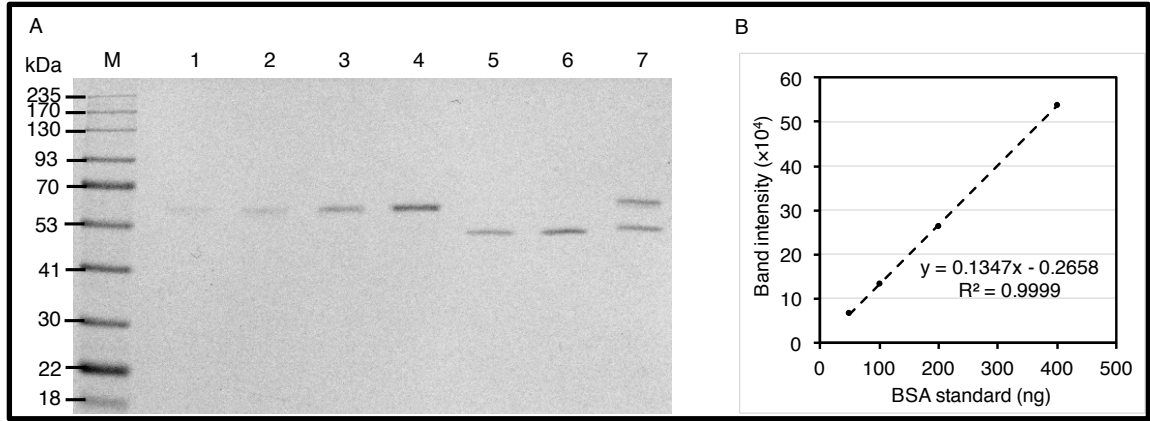


**Figure S19.** Densitometric protein quantification of different tagged BLA fusion proteins relative to BSA standards. **(A)** SDS-PAGE analysis of different tagged BLA fusion proteins at dilution factor of 38. Lane M, Gangnam pre-stained protein marker; lane 1, BSA (50 ng); lane 2, BSA (100 ng); lane 3, BSA (200 ng); lane 4, BSA (400 ng); lane 5, SpBLA-H6; lane 6, SnBLA-H6; lane 7, SdBLA-H6. **(B)** BSA standard curve obtained from SDS-PAGE densitometric analysis.

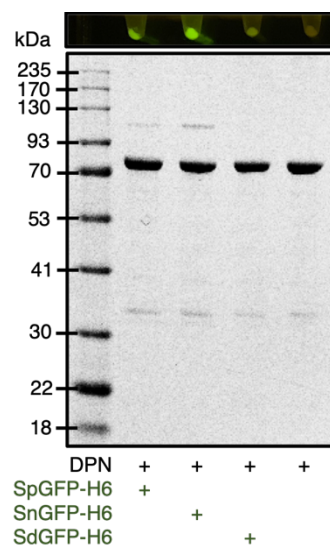


**Figure S20.** Modular functionalization of DPN fusion protein displaying PHA particles (DPN-P) *in vitro* using various tagged GFPs. Functionalized PHA particles were visualized by blue light exposure (top) and SDS-PAGE analysis (bottom).

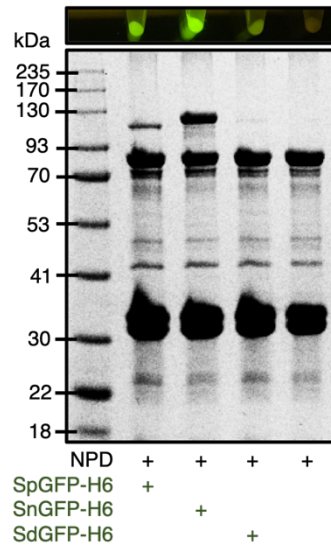


**Figure S21.** Modular functionalization of NPD fusion protein displaying PHA particles (NPD-P) *in vitro* using various tagged GFPs. Functionalized PHA particles were visualized by blue light exposure (top) and SDS-PAGE analysis (bottom).

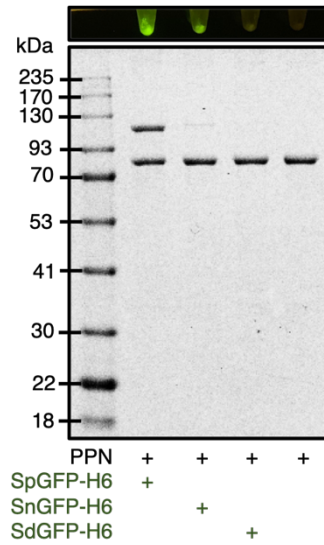


**Figure S22.** Modular functionalization of PPN fusion protein displaying PHA particles (PPN-P) *in vitro* using various tagged GFPs. Functionalized PHA particles were visualized by blue light exposure (top) and SDS-PAGE analysis (bottom).

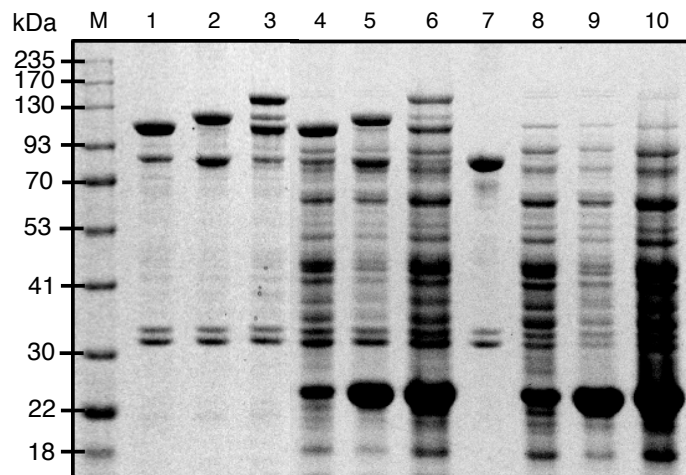


**Figure S23.** NPP fusion protein displaying PHA particles (NPP-P) could react with tagged proteins individually and simultaneously in complex environments *ex vivo* (Process 2). Lane M, Gangnam pre-stained protein marker; lane 1, functionalized NPP-P prepared using cleared lysate containing SpGFP-H6 after washing; lane 2, functionalized NPP-P prepared using cleared lysate containing SnGFP-H6 after washing; lane 3, functionalized NPP-P prepared using cleared lysate containing both SpGFP-H6 and SnGFP-H6 after washing; lane 4, mixture of NPP-P and cleared lysate containing SpGFP-H6 after incubation and before washing; lane 5, mixture of NPP-P and cleared lysate containing SnGFP-H6 after incubation and before washing; lane 6, mixture of NPP-P and cleared lysate containing both SpGFP-H6 and SnGFP-H6 after incubation and before washing; lane 7, plain NPP-P; lane 8, cleared lysate containing SpGFP-H6; lane 9, cleared lysate containing SnGFP-H6; lane 10, cleared lysate containing SpGFP-H6 and SnGFP-H6.

## Chapter 5

### General discussion and future works

This thesis presents efforts to modularize recombinant PHA particle technology for various applications, including industrial use, due to the inherent limitations as analyzed in chapter 2. Therefore, in order to address these issues, a new class of directed protein ligation systems, the Tag/Catcher systems were proposed to merge with the PHA particle technology to further expand the design space of this technology. Chapter 3 of this thesis demonstrated the design of the modular PHA scaffold mediated by the most established SpyTag/SpyCatcher system, where tunable immobilization of SpyTagged functional proteins onto the SpyCatcher-coated PHA particles was achieved *in vitro*. Several innovative streamlined processes to enable one-step recombinant PHA functionalization were presented in chapter 4 of the thesis. Meanwhile, chapter 4 of this thesis also covers the design of the bimodular PHA scaffold by incorporating alternative Tag/Catcher systems into consideration, such as SdyTag/SdyCatcher and SnoopTag/SnoopCatcher systems. A general summary of the research findings and future perspectives is also critically discussed in this chapter.

PHA particle technology based on the PhaC fusion approach represents a very versatile method to functionalize PHAs. The surface exposed arrangement of PhaC on PHA particles have been harnessed by genetically merging PhaC with a range of protein domains of industrial interest and clinically relevant uses (1-4). This one-step biosynthesis approach

enables better control of protein orientation upon immobilization on the PHA scaffolds when compared to the functionalization of chemically reactive PHAs. Either the N- or C-terminus of foreign proteins of interest can be translationally fused to the N- or C-terminus, or both termini of PhaC (5). However, since PhaC plays a crucial role in PHA polymerization, precaution needs to be taken to pinpoint the insertion location of proteins of interest to PhaC. Past studies have demonstrated that the N-terminus of PhaC is a flexible region exposed on the surface of PhaC, and not significant in affecting the synthase activity (6, 7). Also, although the C-terminus of PhaC contains the crucial catalytic triad responsible for polymerization activity of PHAs *in vivo*, it is suggested that the C-terminus of PhaC is still able to tolerate the incorporation of different foreign protein domains, by inserting a suitable peptide linker between the synthase and protein functions of interest (8). Therefore, to ensure the independent function of each protein domain using this approach, it is essential to ensure an adequate degree of movement and distance between the PhaC and functional proteins. Additional choice of rigid, flexible, and cleavable peptide linkers can be inserted in between the functional proteins and PhaC to satisfy different application purposes.

Despite numerous groups, including our group, have reported the oriented display of functional proteins on PHA particles using the PhaC fusion approach (9, 10), limitations in using this approach, as mentioned in chapter 2, could hinder the further progress of PHA particle technology beyond the proof-of-concept. Tuning the production yields, physico-chemical uniformity, and immobilized protein density of recombinant PHA particles are very important in making PHA particle technology as a generic toolbox for protein display.

However, recent studies have suggested that recombinant fusion of PhaC with different functional moieties show inconsistency in the charge state on the particle surface, particle size distribution and the compositional purity of the PHA materials (3, 11, 12). Furthermore, the density and functional performance of the immobilized proteins on recombinant PHA particles vary randomly when fused with a range of functional domains at different insertion sites of PhaC (1, 13, 14).

To circumvent these problems, we proposed to integrate a modular functionalization concept based on the Tag/Catcher protein ligation systems to the PHA particle technology, as described in chapter 3. We demonstrated that the most established pair among the Tag/Catcher systems, SpyTag/SpyCatcher pair showed decent compatibility with the PHA particle technology during the *in vitro* preparation steps (13). Moreover, we showed the potential of this approach to enable tunable immobilization of various SpyTagged proteins to SpyCatcher-coated PHA particles, which ultimately resulted in the sequential multifunctionalization of PHA particles (13). Upon successful functionalization of the modular PHA scaffold with various functional domains, the immobilized proteins exhibited retained or enhanced functionality and tolerance to extreme conditions in comparison to the soluble forms, while additionally enabling convenient recycling (13).

However, more efficient strategies need to be developed in order to achieve quicker and low-cost mass production of functionalized PHA particles based on this modular concept beyond *in vitro* reaction conditions. The *in vitro* modular approach presented in chapter 3

imparts better controllability of immobilized protein density and orientation, as well as the particle uniformity (13). Nevertheless, the use of highly purified soluble tagged proteins for subsequent *in vitro* immobilization of these functional domains could result in higher manufacturing duration and production costs. Therefore, we sought to implement several cost-effective innovative processes in pursuit of simpler SpyTag/SpyCatcher technology-based functionalization of our modular PHA scaffold, as demonstrated in chapter 4. Our proposed approaches using *in vivo* and *ex vivo* processes could functionalize the SpyCatcher-coated PHA particles with varying efficiency but without the need to purify the SpyTagged proteins, suggesting that the SpyTag/SpyCatcher interaction is very specific. Two of the proposed functionalization processes were considered successful, and the functionalized PHA particles overall remained stable during the enzymatic assays.

The bimodular design of the PHA scaffold by incorporating various combinations of Tag/Catcher systems with the PhaC-based PHA particle technology is presented in chapter 4. Though multi-functionalization of PHA particles can be achieved on the same scaffold by SpyCatcher-coated PHA particles using a sequential functionalization strategy as described in chapter 3. However, the step-by-step sequential approach requires rigorous optimization of the Tag/Catcher ratio for different moieties and therefore indicate inefficiency. Our preliminary screening of various combinations of Tag/Catcher pairs fused to PhaC suggested that fusion of SnoopCatcher to N-terminus of PhaC and SpyCatcher to C-terminus of PhaC could result in the simultaneous dual-functionalization of PHA particles in *in vitro* and *ex vivo* environments. This construct prevents the risk of inaccessibility of SnoopTagged proteins to SnoopCatcher, as demonstrated when SnoopCatcher was fused

to the C-terminus of PhaC. Additionally, this construct provides sufficient orthogonality towards the SpyCatcher domain. Our selected bimodular PHA particles also remain resilient over multiple cycles of freeze-thaw treatment, indicating that functionalized bimodular PHA scaffolds could be less prone to ruinous effects in the case of the interrupted cold chain. Subsequent functionality assays further revealed that the Tagged proteins immobilized on the selected bimodular PHA particles were functional.

Achieving programmable and highly consistent scaffolding characteristics has been the “holy grail” in the field of biomaterials. As the preceding parts of this thesis have presented, incorporating the concept of modularity to PHA particle technology introduces a certain extent of unprecedented particle uniformity. This thesis also outlined several attempts in achieving controllable surface functionalization of the recombinant PHA particles using the modular approach, which ultimately allows easy production of multifunctional PHA particles. Nevertheless, though significant progress has been achieved to date, numerous challenging barriers still need to be tackled for the use of this technology in real-world utilization. For instance, it would be useful to develop more stable cell lines in producing these recombinant PHA particles, by using the CRISPR-Cas9-mediated technology, to replace the current plasmid-based gene modification method. Several studies have reported that inserting a foreign plasmid into *E. coli* able to impose a range of metabolic burdens to the host cell (15-17). This probably explains the inconsistency of this technology in several aspects to date, as discussed in this thesis. CRISPR-Cas9 genome editing system is capable of integrating the genes required for *in vivo* PHA biosynthesis and assembly, *e.g.* *phaA*, *phaB*, and *phaC*, directly into the genome of *E. coli* strain to allow stable and improved

PHA production in these engineered microbial cell factories. It would also be desirable to achieve controllable PHA composition and several physicochemical properties of the PHA particles (*e.g.* shape, size, surface charge, and hydrophobicity). Recently, it was shown that the size of PHA particles can be controlled in halophilic bacterium *Halomonas bluephagenesis*, by the deletions of various combinations of PhaPs at the genome level (18). Kawashima *et al.* also reported that the composition of recombinant PHA copolymers can be altered by implementing a phasin replacement approach, *i.e.* by replacing phasin in *Cupriavidus necator* (PhaP<sub>1Re</sub>) with phasin from *Aeromonas caviae* (PhaP<sub>Ac</sub>) (19). Therefore, adaptation of phasins into the PhaC-based modular functionalization approach, if optimize well, could take this technology to a completely new level.

Interestingly, Lee's group recently reported a string of successful significant breakthroughs in the elucidation of the biosynthesis mechanism of *C. necator* PhaC (20, 21). In summary, the crystal structure of PhaC and the detailed molecular description of how PhaC polymerizes PHAs *in vivo* were reported (20). Then, the 3D reconstructed model of the whole PhaC was unraveled for the first time and followed by a series of biochemical studies (21). These groundbreaking findings could lead to a better understanding of the PHA biosynthesis mechanism and possibly, its relationship with the folding state of PhaC when fused with foreign proteins that have been puzzling molecular biologists for decades. Further fundamental understanding of the biology underlying the PHA particle assembly *in vivo* could bring the PHA particle technology to the next stage. By combining these discoveries with the reported crystal structures of the various Tag/Catcher protein complexes (22, 23), it is possible to create a library of generic modular PHA scaffolds with various characteristics

as mentioned using rational genetic engineering to serve for a range of working environments.

In summary, the findings in this thesis present the modular design of PHA scaffolds mediated by the Tag/Catcher protein ligation systems. This approach could address several of the limitations exhibited by the PHA particle technology without hampering its benefits. We can foresee that the established modular functionalization system will continue to expand the design space and evolve this technology toward an array of industrial applications.

## References

1. Hay ID, Du J, Reyes PR, Rehm BH. *In vivo* polyester immobilized sortase for tagless protein purification. *Microb. Cell Fact.* 2015;14(1):190.
2. Chen S, Parlane NA, Lee J, Wedlock DN, Buddle BM, Rehm BH. New skin test for detection of bovine tuberculosis on the basis of antigen-displaying polyester inclusions produced by recombinant *Escherichia coli*. *Appl. Environ. Microbiol.* 2014;80(8):2526-35.
3. Gonzalez-Miro M, Rodríguez-Noda LM, Fariñas-Medina M, Cedré-Marrero B, Madariaga-Zarza S, Zayas-Vignier C, et al. Bioengineered polyester beads co-displaying protein and carbohydrate-based antigens induce protective immunity against bacterial infection. *Sci. Rep.* 2018;8(1):1888.

4. Ran G, Tan D, Zhao J, Fan F, Zhang Q, Wu X, et al. Functionalized polyhydroxyalkanoate nano-beads as a stable biocatalyst for cost-effective production of the rare sugar D-allulose. *Bioresour. Technol.* 2019;289:121673.
5. Rehm FB, Chen S, Rehm B. Enzyme engineering for *in situ* immobilization. *Molecules.* 2016;21(10):1370.
6. Schubert P, Krüger N, Steinbüchel A. Molecular analysis of the *Alcaligenes eutrophus* poly (3-hydroxybutyrate) biosynthetic operon: identification of the N terminus of poly (3-hydroxybutyrate) synthase and identification of the promoter. *J. Bacteriol.* 1991;173(1):168-75.
7. Rehm BH. Polyester synthases: natural catalysts for plastics. *Biochem. J.* 2003;376(1):15-33.
8. Jahns AC, Rehm BH. Tolerance of the *Ralstonia eutropha* class I polyhydroxyalkanoate synthase for translational fusions to its C terminus reveals a new mode of functional display. *Appl. Environ. Microbiol.* 2009;75(17):5461-6.
9. Parlane NA, Gupta SK, Rubio-Reyes P, Chen S, Gonzalez-Miro M, Wedlock DN, et al. Self-assembled protein-coated polyhydroxyalkanoate beads: properties and biomedical applications. *ACS Biomater. Sci. Eng.* 2016;3(12):3043-57.

10. Moradali MF, Rehm BHA. Bacterial biopolymers: from pathogenesis to advanced materials. *Nat. Rev. Microbiol.* 2020;In press:In press.
11. Rubio-Reyes P, Parlane NA, Wedlock DN, Rehm BH. Immunogenicity of antigens from *Mycobacterium tuberculosis* self-assembled as particulate vaccines. *Int. J. Med. Microbiol.* 2016;306(8):624-32.
12. Gonzalez-Miro M, Radecker A-M, Rodríguez-Noda LM, Fariñas-Medina M, Zayas-Vignier C, Hernández-Cedeño M, et al. Design and biological assembly of polyester beads displaying pneumococcal antigens as particulate vaccine. *ACS Biomater. Sci. Eng.* 2018;4(9):3413-24.
13. Wong JX, Rehm BH. Design of modular polyhydroxyalkanoate scaffolds for protein immobilization by directed ligation. *Biomacromolecules.* 2018;19(10):4098-112.
14. Hooks DO, Blatchford PA, Rehm BHA. Bioengineering of bacterial polymer inclusions catalyzing the synthesis of *N*-acetylneuraminic acid. *Appl. Environ. Microbiol.* 2013;79(9):3116-21.
15. Hoffmann F, Rinas U. Stress Induced by Recombinant Protein Production in *Escherichia coli*. *Physiological Stress Responses in Bioprocesses.* Berlin, Heidelberg: Springer Berlin Heidelberg; 2004. p. 73-92.

16. Silva F, Queiroz JA, Domingues FC. Evaluating metabolic stress and plasmid stability in plasmid DNA production by *Escherichia coli*. *Biotechnol. Adv.* 2012;30(3):691-708.
17. Andersson L, Yang S, Neubauer P, Enfors S-o. Impact of plasmid presence and induction on cellular responses in fed batch cultures of *Escherichia coli*. *J. Biotechnol.* 1996;46(3):255-63.
18. Shen R, Ning Z-Y, Lan Y-X, Chen J-C, Chen G-Q. Manipulation of polyhydroxyalkanoate granular sizes in *Halomonas bluephagenesis*. *Metab. Eng.* 2019;54:117-26.
19. Kawashima Y, Orita I, Nakamura S, Fukui T. Compositional regulation of poly(3-hydroxybutyrate-co-3-hydroxyhexanoate) by replacement of granule-associated protein in *Ralstonia eutropha*. *Microb. Cell Fact.* 2015;14(1):187.
20. Kim J, Kim YJ, Choi SY, Lee SY, Kim KJ. Crystal structure of *Ralstonia eutropha* polyhydroxyalkanoate synthase C-terminal domain and reaction mechanisms. *Biotechnol. J.* 2017;12(1):1600648.
21. Kim Y-J, Choi SY, Kim J, Jin KS, Lee SY, Kim K-J. Structure and function of the N-terminal domain of *Ralstonia eutropha* polyhydroxyalkanoate synthase, and the proposed structure and mechanisms of the whole enzyme. *Biotechnol. J.* 2017;12(1):1600649.

22. Li L, Fierer JO, Rapoport TA, Howarth M. Structural Analysis and Optimization of the Covalent Association between SpyCatcher and a Peptide Tag. *J. Mol. Biol.* 2014;426(2):309-17.
23. Izoré T, Contreras-Martel C, El Mortaji L, Manzano C, Terrasse R, Vernet T, et al. Structural Basis of Host Cell Recognition by the Pilus Adhesin from *Streptococcus pneumoniae*. *Structure*. 2010;18(1):106-15.

# Appendix

DRC 16



## STATEMENT OF CONTRIBUTION DOCTORATE WITH PUBLICATIONS/MANUSCRIPTS

We, the candidate and the candidate's Primary Supervisor, certify that all co-authors have consented to their work being included in the thesis and they have accepted the candidate's contribution as indicated below in the *Statement of Originality*.

Name of candidate:	Jin Xiang, Wong	
Name/title of Primary Supervisor:	Professor David Harding	
Name of Research Output and full reference:		
Jin Xiang Wong, Kampachiro Ogura, Shuxiong Chen, and Bernd H. A. Rehm. (2020). Bioengineered Polyhydroxyalkanoates as Immobilized Enzyme Scaffolds for Industrial Applications. <i>Frontiers in Bioengineering and Biotechnology</i> , under review.		
In which Chapter is the Manuscript /Published work:	2	
Please indicate:		
<ul style="list-style-type: none"> <li>The percentage of the manuscript/Published Work that was contributed by the candidate:</li> </ul>	50	
and		
<ul style="list-style-type: none"> <li>Describe the contribution that the candidate has made to the Manuscript/Published Work:</li> </ul>		
For manuscripts intended for publication please indicate target journal:		
Frontiers in Bioengineering and Biotechnology		
Candidate's Signature:	Jin Xiang, Wong	Digitally signed by Jin Xiang, Wong Date: 2019.12.04 07:38:35 +08'00'
Date:	04/12/2019	
Primary Supervisor's Signature:	Dave Harding	Digitally signed by Dave Harding Date: 2019.12.05 10:01:12 +13'00'
Date:	05/12/2019	

(This form should appear at the end of each thesis chapter/section/appendix submitted as a manuscript/ publication or collected as an appendix at the end of the thesis)



## STATEMENT OF CONTRIBUTION DOCTORATE WITH PUBLICATIONS/MANUSCRIPTS

We, the candidate and the candidate's Primary Supervisor, certify that all co-authors have consented to their work being included in the thesis and they have accepted the candidate's contribution as indicated below in the *Statement of Originality*.

Name of candidate:	Jin Xiang, Wong	
Name/title of Primary Supervisor:	Professor David Harding	
Name of Research Output and full reference:		
Jin Xiang Wong and Bernd H. A. Rehm. (2018). Design of Modular Polyhydroxyalkanoate Scaffolds for Protein Immobilization by Directed Ligation. <i>Biomacromolecules</i> , 19 (10), 4098-4112.		
In which Chapter is the Manuscript /Published work:	3	
Please indicate:		
<ul style="list-style-type: none"> <li>The percentage of the manuscript/Published Work that was contributed by the candidate:</li> </ul>	90%	
and		
<ul style="list-style-type: none"> <li>Describe the contribution that the candidate has made to the Manuscript/Published Work:</li> </ul>		
For manuscripts intended for publication please indicate target journal:		
Biomacromolecules		
Candidate's Signature:	Jin Xiang, Wong	Digitally signed by Jin Xiang, Wong Date: 2019.12.04 07:39:43 +08'00'
Date:	04/12/2019	
Primary Supervisor's Signature:	Dave Harding	Digitally signed by Dave Harding Date: 2019.12.05 10:03:25 +13'00'
Date:	05/12/2019	

(This form should appear at the end of each thesis chapter/section/appendix submitted as a manuscript/ publication or collected as an appendix at the end of the thesis)



RightsLink®



Home



Help



Email Support



Sign in



Create Account

**Design of Modular Polyhydroxyalkanoate Scaffolds for Protein Immobilization by Directed Ligation**

Author: Jin Xiang Wong, Bernd H. A. Rehm

Publication: Biomacromolecules

Publisher: American Chemical Society

Date: Oct 1, 2018

Copyright © 2018, American Chemical Society

**PERMISSION/LICENSE IS GRANTED FOR YOUR ORDER AT NO CHARGE**

This type of permission/license, instead of the standard Terms & Conditions, is sent to you because no fee is being charged for your order. Please note the following:

- Permission is granted for your request in both print and electronic formats, and translations.
- If figures and/or tables were requested, they may be adapted or used in part.
- Please print this page for your records and send a copy of it to your publisher/graduate school.
- Appropriate credit for the requested material should be given as follows: "Reprinted (adapted) with permission from (COMPLETE REFERENCE CITATION). Copyright (YEAR) American Chemical Society." Insert appropriate information in place of the capitalized words.
- One-time permission is granted only for the use specified in your request. No additional uses are granted (such as derivative works or other editions). For any other uses, please submit a new request.

[BACK](#)[CLOSE WINDOW](#)



## STATEMENT OF CONTRIBUTION DOCTORATE WITH PUBLICATIONS/MANUSCRIPTS

We, the candidate and the candidate's Primary Supervisor, certify that all co-authors have consented to their work being included in the thesis and they have accepted the candidate's contribution as indicated below in the *Statement of Originality*.

Name of candidate:	Jin Xiang, Wong	
Name/title of Primary Supervisor:	Professor David Harding	
Name of Research Output and full reference:		
Jin Xiang Wong, Majela Gonzalez-Miro, Andrew J. Sutherland-Smith, and Bernd H. A. Hehm. (2020). Covalent Functionalization of Bioengineered Polyhydroxyalkanoate Particles directed by Specific Protein-Protein Interactions. <i>Frontiers in Bioengineering and Biotechnology</i> , under review.		
In which Chapter is the Manuscript /Published work:	4	
Please indicate:		
<ul style="list-style-type: none"> <li>The percentage of the manuscript/Published Work that was contributed by the candidate:</li> </ul>	70	
and		
<ul style="list-style-type: none"> <li>Describe the contribution that the candidate has made to the Manuscript/Published Work:</li> </ul>		
For manuscripts intended for publication please indicate target journal:		
Frontiers in Bioengineering and Biotechnology		
Candidate's Signature:	Jin Xiang, Wong	Digitally signed by Jin Xiang, Wong Date: 2019.12.04 07:40:14 +08'00'
Date:	04/12/2019	
Primary Supervisor's Signature:	Dave Harding	Digitally signed by Dave Harding Date: 2019.12.05 10:04:05 +13'00'
Date:	05/12/2019	

(This form should appear at the end of each thesis chapter/section/appendix submitted as a manuscript/ publication or collected as an appendix at the end of the thesis)